Lawrence Berkeley Laboratory
UNIVERSITY OF CALIFORNIA
EARTH SCIENCES DIVISION

THREE-DIMENSIONAL TERRAIN EFFECTS IN ELECTRICAL AND MAGNETOMETRIC RESISTIVITY SURVEYS

G.L. Oppliger
(Ph.D. Thesis)

September 1982

Prepared for the U.S. Department of Energy under Contract DE-AC03-76SF00098

DISCLAIMER

LBL-10145

THREE-DIMENSIONAL TERRAIN EFFECTS IN ELECTRICAL AND MAGNETOMETRIC RESISTIVITY SURVEYS

Gary Lee Oppliger
(Ph.D. Thesis)

Earth Sciences Division
Lawrence Berkeley Laboratory
and
Department of Materials Science and Mineral Engineering
University of California
Berkeley, California 94720

September 1982

This work was supported by the Assistant Secretary for Conservation and Renewable Energy, Office of Renewable Technology, Geothermal and Hydropower Technologies Division of the U.S. Department of Energy under Contract Number DE-AC03-76SF00098, an HEW Domestic Mining and Mineral and Mineral Fuel Conservation Fellowship, and Newmont Exploration Limited.

Three-Dimensional Terrain Effects in Electrical and Magnetometric Resistivity Surveys

by

Gary Lee Oppliger

THREE-DIMENSIONAL TERRAIN EFFECTS IN ELECTRICAL

AND MAGNETOMETRIC RESISTIVITY SURVEYS

Gary Lee Oppliger

Ph.D. Engineering Geoscience

H. F. Morrison, Chairman

Three-dimensional modeling of topographic effects in electrical resistivity and magnetometric resistivity surveys has been accomplished using the surface integral equation method. The technique provides a means for: 1) analyzing these effects on earth models of homogeneous conductivity and 2) removing terrain effects from field data.

A new method combining current source images with surface charge is developed to treat the air-earth interface electric field boundary conditions. The method uses an image of each subsurface current source positioned above the surface so as to induce a surface charge distribution which approximately cancels the charge distribution induced by the subsurface current source. The resulting total surface charge distribution varies more slowly spacially than either of the original charge distributions and hence may be represented more accurately on a coarsely segmented model surface with simple basis functions.

The topographic surface is modeled by a finite number of cells, each with constant slope and surface charge density. Charge values are obtained with an iterative solution technique. Surface elec-

tric fields are calculated from the surface charge distribution, current sources and images. The magnetic field is found by evaluating a surface integral involving surface slopes and electric fields. The numerical solution is verified by comparisons with dipole-dipole resistivity results from a two-dimensional finite element model of a valley and with analytic solutions for the magnetic fields over a dipping interface. Resistivity and magnetometric resistivity terrain effects are investigated by modeling a suite of 16 two- and three-dimensional terrain features. Finally, methods for removing terrain effects from apparent resistivity and magnetometric resistivity data are described and demonstrated with examples using actual field measurements.

The results of this study show that: 1) magnetic field and electric potential terrain effects occur with similar percentages over a given topographic feature, although their anomaly patterns are generally dissimilar, 2) electric and magnetic field terrain effects generally become significant on terrain features with slopes exceeding 10 degrees, and 3) the integral equation modeling technique provides an effective means of determining terrain corrections over realistically complex three-dimensional topography for both the electrical resistivity and magnetometric resistivity methods.

ACKNOWLEDGEMENTS

I am indebted to my dissertation committee members, Professor T. V. McEvilly, Professor H. F. Morrison, and Dr. M. N. Nabighian of Newmont Exploration Ltd. for their assistance and patience. I would especially like to thank Professor H. F. Morrison for obtaining the funding for this work and both Professor H. F. Morrison and Dr. M. N. Nabighian for their constructive suggestions and encouragement throughout the course of this study.

Special thanks are due to Mrs. Carrie Zwerg who carefully typed the final manuscript and to my wife, Yvonne, who helped prepare the illustrations.

Financial support for this work was provided by an HEW Domestic Mining and Mineral and Mineral Fuel Conservation Fellowship, the Department of Energy, and Newmont Exploration Limited.

TABLE OF CONTENTS

LIST OF FIGURES

LIST OF TABLES

CHAPTER 1

INTRODUCTION

The direct current electrical prospecting methods are powerful tools in mineral and geothermal exploration. This class of methods, which includes all of the electrical resistivity techniques and the relatively new magnetometric resistivity method, is used extensively to detect and delineate buried geologic structures which have electrical conductivities which contrast with the surrounding country rock. Much of this work is carried out in areas of rugged topography where terrain effects can produce misleading anomalies in the measured fields. Hence it is important to understand these effects and where necessary remove them from the measurements.

1-1 The Electrical Resistivity Method

The Electrical Resistivity Method (usually referred to as the Resistivity Method) employs a current transmitter which injects a low frequency (usually 1 Hz or less) alternating current into two electrodes imbedded in the ground. Low frequency currents are employed to eliminate electromagnetic induction effects and allow treatment of the fields assuming direct current conditions. Along the surface, measurements are made of the electric potential difference between a second pair of electrodes to detect distortions in the field due to subsurface zones of anomalous conductivity.

These potential difference measurements are reduced to apparent resistivity values. The apparent resistivity is defined as the theoretical resistivity that must be assigned to a uniform half-space earth model to produce a calculated potential difference equivalent to the measured value. The equation for the apparent resistivity is a function of the measured potential difference V_m, the applied current I, and a geometric factor G which is a function of the position of current and potential electrodes:

$$\rho_a = G\, V_m / I \ .$$

1-2 Terrain Effects in Electrical Resistivity Surveys

By definition, the apparent resistivity of a uniform half-space measured with any electrode configuration will be equal to the half-space's intrinsic resistivity. This concept of apparent resistivity may be extended to an earth having an irregular surface: apparent resistivities measured on a uniform earth with arbitrary terrain will equal the intrinsic resistivity of that earth. However, the application of this definition requires the calculation of the unique geometric factors for the specific topography and electrode geometries involved. Because of the difficulty of computing the appropriate geometric factors for an irregular earth surface, it has been standard practice to apply the more easily calculated flat-earth geometric factors irrespective of the type of topography the data were collected over. This inappropriate use of flat-earth geometric factors is the basic cause of terrain effects in apparent resistivity surveys.

The data in a typical resistivity survey will consist of several tens to several hundreds of potential measurements made with varing electrode positions and spacings. These data are generally plotted as apparent resistivities verses electrode separation and/or measurement location to form resistivity sounding or pseudo-section diagrams. Although these diagrams do not represent the actual distribution of earth resistivities, they are a means of organizing the data, so that patterns diagnostic of particular earth conductivity structures may be identified by comparison with model results. The effect of irregular terrain on these resistivity diagrams is to produce fictitious

patterns of anomalous resistivities which tend to obscure the anomalies created by subsurface geologic structures.

1-3 The Magnetometric Resistivity Method

The Magnetometric Resistivity (MMR) method was first patented by Jakosky (1933), but received little use until about 1970 when improvements in instrumentation made the method a viable exploration tool. The MMR method is similar to the Resistivity method in that both techniques employ a current transmitter unit which injects low frequency (non-inductive) alternating currents into the earth through a pair of electrodes. However, the Magnetometric Resistivity method differs from the resistivity method in that the potential measuring electrodes are replaced by a sensitive coil or magnetometer and a component of the magnetic field due to current flow in the earth is measured. The presence of a conductivity inhomogeneity redistributes the flow of current causing a perturbation in the normal magnetic field pattern. Conductive zones will generally have higher than average current densities resulting in increased horizontal component magnetic field readings over these zones.

1-4 Terrain Effects in Magnetometric Resistivity Surveys

Terrain effects occur in MMR surveys when measurements made over irregular terrain are reduced using half-space primary (normal) magnetic fields. The half-space primary magnetic field is the theoretical field produced by a current source imbedded in an electrically homogeneous half-space and is defined by a simple analytic expression. Reduction of MMR measurements is accomplished by subtracting this half-space field from each measured value; the residual quantity is the MMR anomaly, which is non-zero only when the normal half-space current flow pattern is disturbed by zones of anomalous conductivity. Terrain features also disturb this normal half-space current pattern -- generating MMR terrain anomalies. To prevent these terrain effects, it is necessary to calculate and remove the theoretical magnetic fields for a homogeneous earth model of the terrain in the survey area.

1-5 Terrain Effects in Electric and Magnetic Induced Polarization Surveys

The electric induced polarization (EIP or IP) response of a homogeneous earth is not affected by topography (Fox et al, 1980). The measured IP parameters, percent frequency effect, chargeability, and phase angle represent the ratio of polarization current to normal current and hence are unaffected by terrain effects, which distort normal and polarization currents to the same degree. However, the IP response of a finite body is altered by irregular topography because the polarization and normal currents are distorted by different amounts.

Topography has much the same effect on the magnetic induced polarization (MIP) method as it does on the EIP method. It is fundamental to the MIP method that a uniformly polarizable earth with an arbitrary surface produces no MIP response, and hence is free from MIP terrain effects. The way in which terrain influences MIP observations over a finite body depends on the method used to reduce the MIP measurements. If the MIP effect is calculated as the ratio of polarization magnetic fields to total measured magnetic fields, terrain effects result because topography distorts polarization and total fields in different proportions. (This method of calculation is analogous to that applied to EIP observations.) Alternatively, if the MIP effect is calculated as the ratio of polarization to anomalous magnetic fields, both of which are affected by terrain in the same way, MIP terrain effects are largely cancelled.

However, accurate determination of the anomalous magnetic field depends, first, on calculating the primary (normal) magnetic field, which can be significantly distorted by topography. For a description of the MIP method see Seigel (1974).

1-6 Previous Work on Electrical Methods Terrain Effects

The first description of terrain effects in a direct current electrical methods survey can be traced to the first full-scale field test of the equipotential (electric potential) technique, a method conceived and developed by Conrad Schlumberger in France in 1912 (Allaud and Martin, 1977). Schlumberger's technique is based on the measurement of the electric potential field in the vicinity of a pair of widely spaced grounded electrodes which inject a low frequency alternating current into the earth. Conrad Schlumberger noted that distortions of the equipotential lines near a particular steep slope were due to the geometry of the slope causing zones of diffused and concentrated current flow.

Due to the difficulty of evaluating terrain effects, they have until recently been largely ignored. Tank models and analytic solutions have provided insight to the problem but have not provided the flexibility required to treat real field data. The availability of high speed digital computers in the late 1960's made numerical modeling of electrical methods for exploration geophysics efficient and practical. Although there have been numerous resistivity numerical model studies for inhomogeneities beneath a flat earth surface, there have been only a handful of studies treating the effects of topography.

The published studies of topographic effects in resistivity surveys have employed a variety of numerical techniques. In most cases, the computer programs used for these studies were slightly

modified versions of programs used for flat-earth inhomogeneity studies: Jepsen (1969), using a finite difference program, modeled the surface electric field distortions produced by several 2-D terrain features in a uniform D. C. electric field. Coggon (1971) used a two-dimensional finite element program to model dipole-dipole and gradient array resistivity and induced polarization responses over a valley and hill. Hallof (1970) and Rijo (1977) have demonstrated terrain effects in resistivity surveys with a few two-dimensional models. Fox et al (1980) made a systematic model suite study of two-dimensional terrain effects in dipole-dipole resistivity surveys using a finite element program and presented a technique for terrain correcting field data. This is the most complete study of terrain effects available, but it is applicable only to dipole-dipole surveys over two-dimensional terrain. Papazian (1979) describes an approximate technique employing Schwarz-Christoffel transformations for modeling resistivity data collected over two-dimensional topography. Spiegel et al (1980) show how the approximate electric potential can be found on two-dimensional topography over a 3-D body by using the Schwarz-Christoffel transformation. Their method transforms the coordinates defining the irregular surface and buried body into a half-space, which can be modeled using a conventional flat surface 3-D numerical model. Note that the 2-D nature of the Schwarz-Christoffel transformation necessarily requires that line current sources are used.

This limits the usefulness of the two above techniques. Recently, Holcome, H. T. (1981) (draft copy) has developed a specialized finite element program capable of modeling resistivity surveys on three-dimensional terrain over three-dimensional inhomogeneities. With the exception of Holcome, H. T. (1981) and the present study, published work on terrain effects in resistivity surveys have been limited to two-dimensional topographic features.

Except for the present study, the topic of terrain effects in Magnetometric Resistivity surveys has not be investigated. The available flat-earth Magnetometric Resistivity studies consist basically of a collection of analytic solutions for several simple geometric shapes by Edwards et al (1978), and a two-dimensional integral equation numerical model study by Gomez-Trevino and Edwards (1979).

1-7 Objective of Research

Exploration geophysicists have long known topographic features to be the cause of false or misleading anomalies in D. C. electrical methods surveys. However, the evaluation and correction of these terrain effects is difficult, requiring the use of forward numerical model solutions for the electric and magnetic fields over arbitrary three-dimensional terrains. Up to now, there have been no model studies on the terrain effect in MMR surveys; and the available model studies on electrical resistivity terrain effects have been limited to two-dimensional topography. Hence, there is a definite need for a modeling technique which would enable the geophysicist to estimate and remove three-dimensional terrain effects in both electrical resistivity and magnetometric resistivity surveys.

The objectives of this research are, then, first, to develop a computer program capable of efficiently modeling the electric and magnetic field distortions produced by realistically complex three-dimensional terrains in electrical resistivity and magnetometric resistivity surveys; second, investigate the significance of these types of terrain effects; and third, develop practical methods for the removal of terrain effects from field data to facilitate unbiased interpretations of subsurface structures.

1-8 Scope of this Study

This work examines the application of the integral equation numerical modeling technique to the estimation of 3-D topographic effects for homogeneous earths in the Electrical Resistivity and Magnetometric Resistivity geophysical prospecting methods. A new and fundamentally powerful technique for applying current source images in combination with surface charges is developed and used to meet the boundary conditions on the air-earth interface. The integral equations required for the solution of the electric and magnetic fields are reformulated in terms of surface slopes. Verification of the accuracy of the numerical solution is made by comparisons with independent modeling techniques. Resistivity and magnetometric resistivity terrain effects are investigated by modeling a suite of two- and three-dimensional topographic features. The effect of terrain on uniform electric fields is examined. A computationally efficient method for estimating terrain caused vertical magnetic fields is developed and demonstrated. Finally, methods for correcting apparent resistivity and MMR data for terrain effects are described and demonstrated with examples using real field data.

CHAPTER 2

NUMERICAL MODELING TECHNIQUE

2-1 An Integral Equation Approach to the Terrain Problem

Three-dimensional topography is efficiently simulated with the surface integral-equation method since only the surface of the earth need be represented by model elements. The other principal numerical techniques, finite-difference and finite-element, require three-dimensional meshes of model elements which can become prohibitively large when used to model detailed three-dimensional terrains. However, it is recognized that the relative effectiveness of any modeling program will generally depend more on efficiency of the program code and the specific class of the problem modeled than it will on the type of numerical method on which it is based.

To treat the terrain problem, the standard integral equation method is modified by a technique for applying images in combination with surface charges; the resulting integral equation is formulated in terms of surface charges and terrain slopes. The terrain is divided into a grid of flat parallelogrammatic plates or elements on each of which the charge density is assumed to be uniform. An approximate solution to the surface integral equation is obtained using the "point matching" method to solve for the charge at the center of each element. The "point matching" method is a particular case of the method of moments (Harrington, 1968). The integral equation can thus be written as a set of simultaneous linear equa-

tions with surface charges as the unknowns. The large number of surface elements makes a matrix inversion solution of the equations impractical; but the system of equations is easily and rapidly solved by an iterative approach.

Once the surface charge distribution has been determined, the other electrical parameters are easily calculated. Electric potential is determined from an evaluation of the potential contributions produced by the surface charge distribution and the current sources and images. Apparent resistivities are then calculated directly from the potential. Surface electric fields, which are required for the calculation of the magnetic field, are determined by adding electric fields produced by the sources and images to the electric field due to the surface charge distribution. Finally, the magnetic field is found, not by a volume integration over current densities, but, by evaluating a surface integral equation involving terrain slopes and surface electric fields; an approximate separation of primary and secondary magnetic fields is used to reduce problems created by electric field singularities and the finite area of the model.

2-2 Properties of an Arbitrary Surface

Essential to the development of the integral equations for the terrain problem are the following basic analytical properties of an arbitrary surface. The formulations follow that of Bhattacharyya and Chan (1977). A rectangular cartesian coordinate system is used with the z-axis pointing down, the x-axis pointing north and the y-axis pointing east. Let (x, y, z) define a point on the surface. The surface can then be defined as a function of two variables and represented by $z = f(x, y)$. We assume $f(x, y)$ has continuous and finite partial first and second order derivatives at all points on the surface. The unit vector $\hat{n}$ normal to the surface is defined by the direction cosines (n_x, n_y, n_z), where

$$n_x = \frac{-f_x}{(1 + f_x^2 + f_y^2)^{\frac{1}{2}}} \quad ,$$

$$n_y = \frac{-f_y}{(1 + f_x^2 + f_y^2)^{\frac{1}{2}}} \quad , \qquad (2\text{-}2\text{-}1)$$

$$n_z = \frac{1}{(1 + f_x^2 + f_y^2)^{\frac{1}{2}}} \quad .$$

The variables f_x and f_y are the derivatives of $f(x, y)$ along the x and y directions respectively. The relation between a surface element ds and its projection on the (x, y)-plane dxdy is given by

$$ds = \frac{dxdy}{n_z} = (1 + f_x^2 + f_y^2)^{\frac{1}{2}}\, dxdy. \qquad (2\text{-}2\text{-}2)$$

The normal derivative of a function on the surface is defined by

the operator

$$\frac{\partial}{\partial n} = n_x \frac{\partial}{\partial x} + n_y \frac{\partial}{\partial y} + n_z \frac{\partial}{\partial z} \ . \qquad (2\text{-}2\text{-}3)$$

2-3 Combined Use of Images and Surface Charge

The first paper using the surface integral approach for solution of the DC resistivity problem was published by Alfano (1959, 1960, 1961). Other papers using this approach have been published by Dieter, Paterson and Grant (1969), Pratt (1972), Barnett (1972), and Snyder (1976). The basic equation used in the DC integral equation method (derived in Appendix 1) is given by

$$\frac{\rho(P)}{2\varepsilon} = k \left[\frac{I}{4\pi\sigma_1} \frac{\partial}{\partial n} \left(\frac{1}{r_{PC}}\right) + \frac{1}{2\pi} \int_{s'} \frac{\rho(M)}{2\varepsilon} \frac{\partial}{\partial n} \left(\frac{1}{r_{PM}}\right) dS \right] , \quad (2\text{-}3\text{-}1)$$

where the geometry is that of Figure 2-3-1, and

$\frac{\partial}{\partial n}$ is the derivative normal to the surface s,

$k = (\sigma_1 - \sigma_2)/(\sigma_1 + \sigma_2)$,

$\rho(P)$ is the surface charge density at P,

I is the strength of a current source located at C,

s is the surface between the zones of conductivities σ_1 and σ_2,

σ_1 and σ_2 are the conductivities of mediums 1 and 2,

ε is the permittivity,

and the prime on s indicates that the singularity at P is not included in the integration.

It is an established technique in flat earth integral equation modeling problems to apply equation (2-3-1) only to the surfaces of buried inhomogeneities and their images. Satisfaction of the electric field boundary condition (zero normal electric field) at the air-earth interface is achieved indirectly through electric field

symmetry created by images of the current sources and the surface charge on the inhomogeneities. This approach creates a charge free air-earth interface. Once a terrain feature is included in the model, the electric field symmetry across the earth's surface is lost, making the image method unsuitable for the solution of the surface boundary condition. Three alternate schemes for treating the surface boundary conditions for integral equation terrain models are described below.

There are two conventional techniques for including terrain features in integral equation models. The first simply treats the air as a semi-infinite inhomogeneity imbedded in a whole-space and relies on surface charges defined by the integral equation (2-3-1) to satisfy surface boundary conditions. This technique necessitates that a large portion of the surface be represented by model elements, even if much of the model surface is flat. A second technique employs an image of the terrain surface reflected across a plane of symmetry which lies above the highest surface feature. An example of this method applied to the hill model of Figure 2-3-2 is shown in Figure 2-3-3. Note that it is necessary to place the hill in a large topographic depression to create an image of finite size. This image technique is a direct extension of the standard method of using images of inhomogeneities in flat earth models to meet the air-earth interface electric field boundary conditions. The only advantage in using the surface image approach in a terrain problem is that where the plane of symmetry can be made to coincide with

the earth's surface there is no surface charge and hence no obligation to represent those areas with model elements.

A third technique for modeling terrain surfaces (the method used in this study) involves the combined use of current source images and surface charges. The technique is directed in particular at treating the extreme variations in surface charge density associated with buried or down hole current sources, as illustrated in Figure 2-3-4a. The problem of rapid charge variation also occurs on inhomogeneities in flat-earth models where it has been traditionally managed by the use of higher order basis functions to represent the charge on the elements or by increasing the density of elements in the problem area. In contrast, the new technique eliminates extreme charge variations by positioning a current source image, as shown in Figure 2-3-4c, above the surface opposite the current source. In this way, the source and image provide a first order solution to the boundary conditions, while surface charge handles the higher order detail of the solution.

To show the validity of this special use of images, we introduce an electric field annihilator surface charge distribution. This charge distribution completely shields the region it encloses from externally generated electric fields. The annihilator equation is easily derived by applying equation (2-3-1) to the surface geometry given in Figure 2-3-4b. By letting σ_1' become infinite, the electric field in medium 1 is forced to zero and the charge distribution ρ_2 becomes an electric field annihilator for medium 1.

Rewriting equation (2-3-1), this annihilator may be given as:

$$\frac{\rho_2(P)}{2\varepsilon} = \frac{I_Q}{4\pi\sigma_2'} \frac{\partial}{\partial n} \left(\frac{1}{r_{PQ}}\right) + \frac{1}{2\pi} \int_{S'} \frac{\rho_2(M)}{2\varepsilon} \frac{\partial}{\partial n} \left(\frac{1}{r_{PM}}\right) dS. \quad (2\text{-}3\text{-}2)$$

By applying the annihilator, we are given the freedom to place current sources above the surface without affecting the electric field intensity below the surface.

We next apply equation (2-3-1) to the standard problem of Figure 2-3-4a in which the current source is located below the surface. In this case, the surface charge distribution ρ_1 is found by rewriting equation (2-3-1) as

$$\frac{\rho_1(P)}{2\varepsilon} = k \left[\frac{I_C}{4\pi\sigma_1} \frac{\partial}{\partial n} \left(\frac{1}{r_{PC}}\right) + \frac{1}{2\pi} \int_{S'} \frac{\rho_1(M)}{2\varepsilon} \frac{\partial}{\partial n} \left(\frac{1}{r_{PM}}\right) \right] dS. \quad (2\text{-}3\text{-}3)$$

Next the following conditions are placed on equations (2-3-2) and (2-3-3): 1) The geometry of the surfaces S in both equations are identical. 2) The resistivity contrast coefficient k for equation (2-3-3) is one. This corresponds to medium 2 being highly resistive relative to medium 1, and includes the cases of an air-earth contact and of highly resistive buried inhomogeneities. 3) The conductivity of medium 2 in equation (2-3-2) is set equal to the medium 1 conductivity in equation (2-3-3). With these conditions met, we add equations (2-3-2) and (2-3-3) obtaining:

$$\frac{\rho_0(P)}{2\varepsilon} = \frac{I_C}{4\pi\sigma_1} \frac{\partial}{\partial n} \left(\frac{1}{r_{PC}}\right) + \frac{I_Q}{4\pi\sigma_1} \frac{\partial}{\partial n} \left(\frac{1}{r_{PQ}}\right) + \frac{1}{2\pi} \int_{S'} \frac{\rho_0(M)}{2\varepsilon} \frac{\partial}{\partial n} \left(\frac{1}{r_{PM}}\right) dS, \quad (2\text{-}3\text{-}4)$$

where ρ_0 is a new surface charge distribution defined as:

$$\rho_0 = \rho_1 + \rho_2.$$

Equation (2-3-4) has some interesting and important properties: 1) its structure is essentially the same as equation (2-3-1) for $k = 1$; 2) there is no difference in the treatment of current sources above or below the surface; 3) the application of the electric field annihilator assures us that a current source placed above the surface has no effect on the electric field solution below the surface; 4) where the surface is flat and an image current source is placed directly opposite a buried source, there will be no surface charge. This configuration corresponds to the standard image method applied to the solution of the surface boundary condition on a homogeneous earth.

The cancellation effect that results from the addition of the two surface charge distributions is illustrated in Figure 2-3-4c. The advantage provided by this method in a numerical model is fairly clear. The image may be positioned so that its charge distribution will approximately cancel the charge distribution associated with the source. The residual charge distribution is much more slowly varying than either of the original distributions and hence places fewer demands on the numerical model; that is, the charge may be represented accurately on a coarse grid with a simple basis function.

2-4 Formulation of the Surface Integral in Terms of Surface Slopes

To reform the basic surface charge integral equation in terms of surface slopes, we begin by writing equation (2-3-4) as

$$q(P) = t(P) + \frac{1}{2\pi} \int_{s'} q(M) \frac{\partial}{\partial n} \left(\frac{1}{r_{PM}}\right) dS , \qquad (2\text{-}4\text{-}1)$$

where t(p) is the normal component of wholespace electric field due to current sources and images, and

$$q(P) = \frac{\rho_0(P)}{2\varepsilon} . \qquad (2\text{-}4\text{-}2)$$

Next, let the locations M and P refer respectively to primed and unprimed locations in cartesian coordinates. Thus,

$$P = (x, y, z) \text{ and } M = (x', y', z'), \qquad (2\text{-}4\text{-}3)$$

$$\text{and } R = r_{PM} = \left[(x-x')^2 + (y-y')^2 + (z-z')^2\right]^{\frac{1}{2}} . \qquad (2\text{-}4\text{-}4)$$

Combining equations (2-2-2), (2-2-3) and (2-4-4) we obtain

$$\frac{\partial}{\partial n} \left(\frac{1}{R}\right) dS = - \left[(x-x')n_x + (y-y')n_y + (z-z')\right] \cdot \frac{1}{R^3} \cdot \frac{dx'dy'}{n_{z'}} , \qquad (2\text{-}4\text{-}5)$$

or in terms of surface slopes f_x, f_y

$$\frac{\partial}{\partial n} \left(\frac{1}{R}\right) dS = \left[(x-x') f_x + (y-y')f_y - (z-z')\right] \cdot \frac{(1 + f_{x'}^2 + f_{y'}^2)^{\frac{1}{2}}}{R^3 (1+f_x^2+f_y^2)^{\frac{1}{2}}} dx'dy' . \qquad (2\text{-}4\text{-}6)$$

We may now rewrite (2-4-1) in terms of surface normal vectors as

$$q(x,y) = t(x,y) - \frac{1}{2\pi} \iint_{S'} q(x', y') \cdot \left[(x-x')n_x + (y-y')n_y + (z-z')n_z\right] \frac{dx'dy'}{R^3 n_{z'}} . \qquad (2\text{-}4\text{-}7)$$

Alternately, using equation (2-4-6) we may write (2-4-1) in terms of surface slopes as $q(x,y) = t(x,y) + \frac{1}{2\pi}\iint_{S'} q(x', y') \cdot \left[(x-x')f_x + (y-y')f_y - (z-z')\right] \cdot \frac{(1 + f_{x'}^2 + f_{y'}^2)^{\frac{1}{2}}}{R^3(1 + f_x^2 + f_y^2)^{\frac{1}{2}}} dx'dy' .$

(2-4-8)

Equation (2-4-8) may be simplified by dividing the surface charge and normal component of primary electric field at each point by the vertical component of the surface normal vector. The area of an infinitesimal surface element is given by equation (2-2-2). The first term on the right hand side of this equation relates the area of the horizontal projection dxdy of a surface element to the true area of the element.

We next define two new functions Q and T by weighting the surface charge q and the normal component of primary electric field t by

$$\frac{1}{n_z} = (1 + f_x + f_y) . \qquad (2\text{-}4\text{-}9)$$

Thus Q and T are defined as

$$Q(x,y) = q(x,y)(1 + f_x^2 + f_y^2)^{\frac{1}{2}} , \qquad (2\text{-}4\text{-}10)$$

$$T(x,y) = t(x,y)(1 + f_x^2 + f_y^2)^{\frac{1}{2}} . \qquad (2\text{-}4\text{-}11)$$

multiplying equation (2-4-8) by (2-4-9) and substituting equations (2-4-10) and (2-4-11) in the result, we obtain the following integral equation involving weighted surface charge and surface slopes.

$$Q(x,y) = T(x,y) + \frac{f_x}{2\pi} \iint_{S'} \frac{Q(x',y')(x-x')}{R^3}\, dx'dy'$$

$$+ \frac{f_y}{2\pi} \iint_{S'} \frac{Q(x',y')(y-y')}{R^3} dx'dy' + \frac{1}{2\pi} \iint_{S'} \frac{Q(x',y')(z-z')}{R^3}\, dx'dy' \qquad (2\text{-}4\text{-}12)$$

2-5 Numerical Solution of the Surface Charge Integral Equation

The surface charge integral equation is solved by the method of "collocation" or "point-matching". Here the method is applied to a surface representing topography.

The model surface is divided into flat parallelogrammatic elements by laying out an equispaced N x N grid over the terrain. The resulting elements are tangent to the terrain surface at their centers and have areas which are inversely proportional to the vertical component of their surface normal vectors. Since the elements are planar, neighboring elements will not generally join at adjacent edges. However, the errors introduced by these gaps are not generally significant in the types of models considered here because the grid size is large and the surfaces are smoothly varying.

A more exact surface representation can be achieved with triangular elements; however, the program coding is more complex and program execution is slower.

The orientation of an element is determined from the surface slopes in the x and y directions at the center of the element. A simple technique for averaging surface gradients in the forward and reverse directions was found adequate for determing slopes. A bicubic spline was also used to find slopes but showed no advantage over the simpler technique.

An approximate solution to the surface charge integral equation, equation (2-4-12), may be obtained by solving its left hand side at the center of each surface element. Thus, the double

integral becomes a double summation of a series of integrals over smaller areas.

Equation (2-4-12) thus becomes:

$$Q(x_i, y_j) = T(x_i, y_j) + \frac{f_x(x_i, y_j)}{2\pi} \sum_{p=1}^{M} \sum_{q=1*}^{N} \iint_{A_{pq}} \frac{Q(x',y')(x_i-x')}{R^3}$$

$$\cdot dx'dy' + \frac{f_y(x_i,y_j)}{2\pi} \sum_{p=1}^{M} \sum_{q=1*}^{N} \iint_{A_{pq}} \frac{Q(x', y')(y_j-y')}{R^3} \, dx'dy'$$

$$+ \frac{1}{2\pi} \sum_{p=1}^{M} \sum_{q=1*}^{N} \iint_{A_{pq}} \frac{Q(x', y') \, [H(x_i,y_i)-H(x',y')]}{R^3} \, dx'dy', \quad (2\text{-}5\text{-}1)$$

where H(x, y) is the surface elevation array and * implies that the summation excludes (i, j) = (p, q).

A basis function must be selected to represent the variation of surface charge density over the surface element A_{pq}. Although it is possible to use higher order basis functions, we have chosen the zeroth order function because of the resulting simplified mathematics.

Barnett (1972) numerically evaluated the integrals in equation (2-5-1). However, satisfactory results for most terrains have been obtained by treating the surface charge as being concentrated at the center of each surface element.

This approximation allows the integral to be written as a product. For example, the first integral in equation (2-5-1)

becomes

$$\iint_{A_{pq}} \frac{Q(x',y')(x_i-x')}{R^3}\,dx'dy' = \frac{Q(x_p,\ y_q)(x_i-x_p)}{R^3}\,A_{pq}. \qquad (2\text{-}5\text{-}2)$$

This approximation is nearly exact when used to estimate the electric field coupling between widely separated surface elements. (Here, electric field coupling refers to the normal electric field at the center of a surface element due to charges on another element). However, when adjacent elements are considered, the approximation is in general much less accurate but not necessarily ineffective when applied to the topographic problem. This is so partly because the degree of electric field coupling between a pair of elements decreases as the charge carrying element approaches alignment with the plane containing the observation element.

In cases where the surface is represented with an adequate density of elements, so that it appears to be smoothly varying, adjacent elements will lie nearly in the same plane and will therefore tend to be coupled only to a small degree.

Substituting equation (2-5-2) into (2-5-1), we obtain the final numerical form of the integral equation for surface charge

$$Q(x_i, y_j) = T(x_i, y_j) + \frac{f_x(x_i, y_j)}{2\pi} \sum_{p=1}^{M} \sum_{q=1*}^{N} \frac{Q(x_p, y_q)(x_i - x_p)}{R^3} A_{pq}$$

$$+ \frac{f_y(x_i, y_j)}{2\pi} \sum_{p=1}^{M} \sum_{q=1*}^{N} \frac{Q(x_p, y_q)(y_j - y_q)}{R^3} A_{pq} \qquad (2\text{-}5\text{-}3)$$

$$+ \frac{1}{2\pi} \sum_{p=1}^{M} \sum_{q=1*}^{N} \frac{Q(x_p, y_q)\left[H(x_i, y_j) - H(x_p, x_q)\right]}{R^3} A_{pq} \ ,$$

where H(x,y) is an array containing surface elevations.

Solution Method:

Equation (2-5-3) represents a set of simultaneous linear equations which could be solved by a matrix inversion approach. However, since we are working with surface grids with well over a thousand elements, the corresponding matrix would contain over a million elements. Also, since the charge on each element generally couples into every other element, the matrix would be full. These factors, combined with computer limitations, make the direct matrix inversion approach impractical for this type of problem. Fortunately, equation (2-5-3) is easily solved by an iterative approach.

The unknown array Q is initially set to array T, then placed in the right hand side of equation (2-5-3). As each new value for array Q is calculated, it is used to update the array. The method differs from the Neumann series approach where the array Q is updated only after new values for Q have been calculated for all

values in the array.

Even though the resistivity reflection coefficient for the air-earth interface is unity, the iterative solution for charge generally converges to a satisfactory level of accuracy in two to three iterations. This rapid convergence may be attributed to the moderate degree of electrical coupling between surface elements on gently varying terrain.

2-6 Formulation of Normal Component of Primary Electric Field in Terms of Surface Slopes

The potential due to a current source of strength I located at point (x_0, y_0, z_0) in a homogeneous medium of conductivity σ is given by

$$\phi(x, y, z) = \frac{I}{4\pi\sigma R} , \tag{2-6-1}$$

where

$$R = \left[(x-x_0)^2 + (y-y_0)^2 + (z-z_0)^2\right]^{\frac{1}{2}} . \tag{2-6-2}$$

The normal component of electric field across a surface is

$$E_n = \frac{-I}{4\pi\sigma} \frac{\partial}{\partial n} \left(\frac{1}{R} \right) . \tag{2-6-3}$$

Using

$$\frac{\partial}{\partial n} = n_x \frac{\partial}{\partial x} + n_y \frac{\partial}{\partial y} + n_z \frac{\partial}{\partial z} , \tag{2-6-4}$$

we have

$$E_n(x,y,z) = \frac{I}{4\pi\sigma R^3} \left[(x-x_0)n_x + (y-y_0)n_y + (z-z_0)n_z\right] , \tag{2-6-5}$$

or in terms of surface slopes

$$E_n(x,y,z) = \frac{I \left[-(x-x_0)f_x - (y-y_0)f_y + (z-z_0)\right]}{4\pi\sigma R^3 \left(1 + f_x^2 + f_y^2\right)^{\frac{1}{2}}} . \tag{2-6-6}$$

2-7 Electric Potential Due to Current Sources and Images

In our formulation of the topographic problem, the total electric potential is composed of three parts: the potential due to the current source in the earth, the potential due to the current image source above the surface, and the potential due to the surface charge distribution. The potential ϕ_1 due to the current source and image is written as a summation of whole-space electric potential functions,

$$\phi_1 = \frac{I_s}{4\pi\sigma r_1} + \frac{I_i}{4\pi\sigma r_2} \quad , \qquad (2\text{-}7\text{-}1)$$

where r_1 and r_2 are the respective distances between the observation point and the current source I_s and the current image source I_i, and σ is the earth's conductivity.

2-8 Estimation of the Electric Potential Due to Surface Charges

This section describes the method used to estimate the surface potential due to the charge distribution on the model surface elements.

The potential ϕ due to a volume charge distribution $q(\bar{r})$ in a volume V_0 is

$$\phi(\bar{r}) = \frac{1}{4\pi\varepsilon} \int_{V_0} \frac{q(\bar{r}')}{|\bar{r}-\bar{r}'|} \, dV \, . \qquad (2\text{-}8\text{-}1)$$

When the charge is confined to a surface S, as it is in our terrain model, the above equation reduces to

$$\phi(\bar{r}) = \frac{1}{4\pi\varepsilon} \int_{S} \frac{q(\bar{r}')}{|\bar{r}-\bar{r}'|} \, dS \, , \qquad (2\text{-}8\text{-}2)$$

where $q(\bar{r}')$ is surface charge density.

Equation (2-8-2) must be evaluated over the constant charge density on each surface element. Although it is possible to perform this integration analytically over each of the arbitrarily oriented surface elements, the following approximations have proven satisfactory for the types of model surfaces considered in this work: First, charge on elements which are three or more elements distant from the point of observation may be treated as point concentrations of charge. Second, the angular orientation of surface elements may be ignored when the integration is performed over neighboring elements, that is, the elements are treated as if they are contained in and lying parallel to a single plane. This approximation eliminates the need to evaluate the integral in equation (2-8-2)

for each unique set of orientations of surface elements and observations.

The integral (2-8-2) is evaluated analytically only once for each of a small number of element geometries (Figure 2-8-2) surrounding a general observation point. A table of geometric correction factors is computed by normalizing these integrations by the corresponding values obtained by concentrating the charges at the centers of the elements.

From the perspective of the computer algorithm, the potential is computed by first assuming the charges are concentrated at the centers of the elements. Then, when an element is identified as lying within a three element radius of the observation point, the appropriate geometric correction factor is applied. The singularity at the observation point is treated separately as an analytic calculation.

The correction factors and singularity are evaluated in the following section.

2-8.1 Analytic Integration of the Potential Function Over Square Surface Elements

The following integral evaluation technique is used both for estimating the magnetic field contribution due to electric field on surface elements and for estimating the contribution to potential due to charge on surface elements.

The integral to be evaluated, in both cases, excluding constants, is of the form

$$P(\bar{r}') = \iint_{\text{element}} \frac{dxdy}{|\bar{r}-\bar{r}'|} , \qquad (2\text{-}8\text{-}3)$$

where

$$\bar{r} = \hat{i}x + \hat{j}y + \hat{k}z . \qquad (2\text{-}8\text{-}4)$$

Let the observation point be located at the origin. Then, in cylindrical coordinates, equation (2-8-3) becomes

$$P = \iint_{\text{element}} d\theta dr . \qquad (2\text{-}8\text{-}5)$$

To demonstrate the method used, the singular element is evaluated. Referencing Figure 2-8-1, the symmetry of the singular element requires that the integration be performed over only 1/8th of the element, i.e., the shaded portion. Equation (2-8-5) then becomes

$$P_0 = 8 \int_{\theta_1}^{\theta_2} \int_{0}^{r_1 = \frac{a}{2}\sec\theta} d\theta dr , \qquad (2\text{-}8\text{-}6)$$

where

$$\theta_2 = 45.0^0 ,$$

$$\theta_1 = 0.0^0 .$$

Thus

$$P_0 = 8\int_{\theta_1}^{\theta_2} \frac{a}{2} \sec\theta d\theta , \qquad (2\text{-}8\text{-}7)$$

$$P_0 = 4a\log \left[\tan\left(\frac{\pi}{4} + \frac{\theta}{2}\right)\right]\Big|_{\theta_1}^{\theta_2} ,$$

$$P_0 = 3.525494a . \qquad (2\text{-}8\text{-}8)$$

Calculations in cylindrical coordinates for element geometries of types 1, 2 and 3, as defined in Figure 2-8-2, can be carried out in a similar fashion.

Let the contribution from element type i be P_i. Then

$$P_1 = 1.03805a ,$$

$$P_2 = 0.724697a ,$$

$$P_3 = 0.50509a . \qquad (2\text{-}8\text{-}9)$$

If the above P_i are normalized by the corresponding values obtained by treating the surface charge or E field as concentrated at the center of each element, the following correction constants C_i are obtained:

$$C_1 = 1.03805 ,$$

$$C_2 = 1.02488 ,$$

$$C_3 = 1.01018 . \qquad (2\text{-}8\text{-}10)$$

2-8.2 Charge on an Outer Surface Grid

The model surface surrounding the main N x N grid area is assumed to be flat and have surface electric fields which are very close to half-space field values. These assumptions do not exclude the possibility that significant surface charge may be present on the flat surface surrounding the topography. If the current sources and images are arranged symmetrically about the flat outer surface, as shown in Figure 2-8-3a, there is no charge on the outer surface (assuming effects of topography on the electric field do not extend to this outer surface). However, where current sources and images are asymmetrically positioned about the outer surface, as in Figure 2-8-3b, there can be significant charge on the outer surface.

To obtain accurate estimates of the potential on the inner model grid, it is necessary to include the potential contribution made by charges on the outer flat surface. This is accomplished by coarsely griding the outer surface and using the normal component of primary electric field at the center of each element (due to current sources and images) to determine the surface charge density for that element. This outer grid charge distribution is included in the integral for the potential (equation (2-8-2)).

2-9 Tangential Surface Electric Fields from Surface Potentials

The tangential surface electric field due to charge on the model surface is found by taking the gradient of the surface potential. The gradient of this surface potential is first computed treating the potential fields as if impressed on a horizontal surface. The x and y components of this pseudo-grandient are multiplied respectively by

$$(1 + f_x^2)^{-\frac{1}{2}} \text{ and } (1 + f_y^2)^{-\frac{1}{2}} \qquad (2\text{-}9\text{-}1)$$

to correct for the sloping terrain surface. The x, y, and z components of the resulting tangential surface electric field are written as

$$E_x = E_{FX} \frac{1}{1 + f_x^2} ,$$

$$E_y = E_{FY} \frac{1}{1 + f_y^2} ,$$

$$E_z = E_{FX} \frac{f_x}{1 + f_x^2} + E_{FY} \frac{f_y}{1 + f_y^2} , \qquad (2\text{-}9\text{-}2)$$

where E_{FX} and E_{FY} are the negative x and y components of the gradient of the potential distribution impressed on a horizontal surface, and f_x and f_y are terrain slopes.

This technique is applied only to the potential due to surface charges to prevent the problem of computing gradients near singularities. The total tangential electric field is found by adding the easily calculated electric fields of the current sources and images to the electric fields derived from the potential due to surface charges.

2-10 Determination of the Magnetic Field from Surface Electric Fields and Surface Slopes

The magnetic field at any point on, above, or below the surface may be found by evaluation of an integral involving surface electric fields and surface slopes. To derive this integral equation, we start with the modified Biot-Savart Law for solenoidal current flow as given by Edwards et al (1978) and derived in Appendix III.

$$\bar{B}(\bar{r}) = \frac{\mu}{4\pi} \int_S \frac{\nabla'\phi(\bar{r}') \times \nabla'\sigma(\bar{r}')}{|\bar{r} - \bar{r}'|} dS' \quad , \tag{2-10-1}$$

where $\bar{B}(\bar{r})$ is the magnetic field,

$\phi(\bar{r})$ is the electric potential,

$\sigma(\bar{r})$ is the conductivity of the earth at r,

μ is the vacuum permeability,

and S is the set of all surfaces across which the conductivity changes. The gradient of the potential yields the electric field from

$$\bar{E} = -\nabla\phi(\bar{r}'). \tag{2-10-2}$$

The gradient of the conductivity (Gomez-Trevino, 1978) can be written as

$$\nabla'\sigma(\bar{r}') = (\sigma_1 - \sigma_2)\hat{n}\delta(S) \quad , \tag{2-10-3}$$

where $\hat{n}$ is the unit vector outward normal to the surface S, σ_1 and σ_2 are the conductivities of the two mediums separated by surface S, and $\delta(S)$ is a Dirac delta function which becomes non-zero only on S.

Using (2-10-2) and (2-10-3), the magnetic field may be rewritten as

$$\bar{B}(\bar{r}) = \frac{-\mu(\sigma_1-\sigma_2)}{4\pi} \int_S \frac{\bar{E} \times \hat{n}}{|\bar{r}-\bar{r}'|} \, dS' , \qquad (2\text{-}10\text{-}4)$$

where

$$\bar{E} \times \hat{n} = \hat{i}(E_y n_z - E_z n_y) - \hat{j}(E_x n_z - E_z n_x) + \hat{k}(E_x n_y - E_y n_x) . \qquad (2\text{-}10\text{-}5)$$

Thus, the components of magnetic field are given by

$$B_x(\bar{r}') = \frac{-\mu(\sigma_1-\sigma_2)}{4\pi} \iint_S \frac{(E_y n_z - E_z n_y)}{|\bar{r}-\bar{r}'|} \, dS ,$$

$$B_y(\bar{r}') = \frac{-\mu(\sigma_1-\sigma_2)}{4\pi} \iint_S \frac{(E_z n_x - E_x n_z)}{|\bar{r}-\bar{r}'|} \, dS ,$$

$$B_z(\bar{r}') = \frac{-\mu(\sigma_1-\sigma_2)}{4\pi} \iint_S \frac{(E_x n_y - E_y n_x)}{|\bar{r}-\bar{r}'|} \, dS . \qquad (2\text{-}10\text{-}6)$$

Applying equations (2-2-2) and (2-2-3) to (2-10-6) the magnetic field may be written in terms of surface slopes as

$$B_x(\bar{r}') = \frac{-\mu(\sigma_1-\sigma_2)}{4\pi} \iint_S \frac{(E_y + E_z f_y)}{|\bar{r}-\bar{r}'|} \, dxdy ,$$

$$B_y(\bar{r}') = \frac{+\mu(\sigma_1-\sigma_2)}{4\pi} \iint_S \frac{(E_z f_x + E_x)}{|\bar{r}-\bar{r}'|} \, dxdy ,$$

$$B_z(\bar{r}') = \frac{+\mu(\sigma_1-\sigma_2)}{4\pi} \iint_S \frac{(E_x f_y - E_y f_x)}{|\bar{r}-\bar{r}'|} \, dxdy . \qquad (2\text{-}10\text{-}7)$$

Note that when the surface S is the air-earth interface, as in the topographic problem, medium 2 represents the air; thus $\sigma_2 = 0$.

2-10.1 Total Surface Electric Field

The surface electric field may be separated into components normal to and tangential to the surface. Thus, we can write

$$\bar{E}_T = \bar{E}_n + \bar{E}_t \ , \qquad (2\text{-}10\text{-}8)$$

where

$\bar{E}_T$ is the total surface electric field;

$\bar{E}_n$ is the electric field normal to the surface;

$\bar{E}_t$ is the electric field tangential to the surface.

Further, it can be shown that

$$\bar{E}_T \times \hat{n} = \bar{E}_t \times \hat{n} \ . \qquad (2\text{-}10\text{-}9)$$

This implies that the surface electric field used in the magnetic field equation (2-10-7) need not include the electric field normal to the surface. Therefore, for computational convenience, the total electric field in equation (2-10-7) is replaced by the sum of the total surface electric field due to current sources and images and the tangential electric field due to the surface charge distribution.

2-10.2 Estimation of the Magnetic Field due to Electric Fields on Model Elements

The magnetic field integrals in equation (2-10-7) are evaluated using the same techniques applied to the electric potential integral in section 2-8. The following approximations are employed in the magnetic field integrals: (1) Electric fields and surface slopes are treated as constants over each surface element; (2) Electric fields on elements which are three or more elements distant from the observation point are treated as point concentrations of electric field; (3) The angular orientation of nearby elements is disregarded, that is, nearby elements are treated as though they lie in the plane containing the observation element.

The procedures used to treat the singularity and elements lying within a three element radius of the observation point are described in section 2-8.

2-11 An Approximate Separation of Primary and Secondary Magnetic Fields

In flat earth integral equation problems, it is possible to separate primary and secondary electric fields on the earth's surface for the purpose of evaluating the magnetic field (Gomez-Trevino, 1978). Since the magnetic field due to the primary electric field on a flat earth surface is expressible in a simple analytic form, the integration in equation (2-10-4) need be carried out only over the secondary electric field. Calculation of the magnetic field by this technique has two important advantages over an integration over the total electric field: first, it avoids the problems associated with numerical integration over electric field singularities produced by current sources; and second, because the secondary electric field falls off more rapidly than the primary, the extent of the area of integration may be reduced. Clearly it is not possible to apply this electric field separation technique to the general topographic problem because there exists no simple relation between a primary electric field defined on an irregular earth surface and its corresponding magnetic field. However, it is possible to devise an approximation to the flat earth electric field separation technique which may be applied to the topographic problem.

One method of obtaining the total magnetic field over a terrain model is to integrate the total electric field E_T over the complete earth surface S. This could be written as

$$\bar{B}_T = K \int_S \frac{\bar{E}_T \times \hat{n}}{|\bar{r}-\bar{r}'|} \, dS \,, \qquad (2\text{-}11\text{-}2)$$

where

$$K = \frac{-\mu(\sigma_1-\sigma_2)}{4\pi} \,.$$

However, the use of (2-11-2) requires that the integration be preformed over a relatively large area surrounding the section of terrain being modeled and that special treatment be given to the integral near the current source. These problems may be avoided if outside the central zone of terrain the surface is flat and the E fields there are approximated well by their half-space values. Then, referring to Figure 2-11-1, the magnetic field may be rewritten as

$$\bar{B}_T = K \int_{S_T} \frac{\bar{E}_T \times \hat{n}}{|\bar{r}-\bar{r}'|} \, dS + K \int_{S_o} \frac{\bar{E}_p \times \hat{n}}{|\bar{r}-\bar{r}'|} \, dS \,, \qquad (2\text{-}11\text{-}3)$$

where

$\bar{E}_T$ is total electric field,

$\bar{E}_p$ is half-space electric field,

S_T is the central surface with terrain, and

S_o is the outer horizontal surface.

Let

$$K \int_{S_o+S_I} \frac{\bar{E}_p \times \hat{n}}{|\bar{r}-\bar{r}'|} \, dS = \bar{A} \,, \qquad (2\text{-}11\text{-}4)$$

where

$\bar{A}$ is the analytic expression for the magnetic field due

to a current source imbedded in a uniform half-space, and S_I is an inner horizontal surface in the plane of S_o. Then equation (2-11-3) may be rewritten as

$$\bar{B}_T = K\int_{S_T} \frac{\bar{E}_T \times \hat{n}}{|\bar{r}-\bar{r}'|}\, dS + \bar{A} - K\int_{S_I} \frac{\bar{E}_p \times \hat{n}}{|\bar{r}-\bar{r}'|}\, dS. \qquad (2\text{-}11\text{-}5)$$

In a numerical problem, the integrals over surfaces S_T and S_I in equation (2-11-5) become double summations over an N x N grid of surface elements. The horizontal coordinates of elements on surfaces S_T and S_I are identical. Surfaces S_T and S_I should intersect directly above the current source, and surface current sources should be positioned at the center of a surface element.

There are two advantages provided through use of equation (2-11-5). First, it allows calculation of the total magnetic field without performing an integration over the electric fields outside the central N x N grid area. Second, systematic errors accumulated by the numerical integration over surface S_T are effectively cancelled by the subtraction of the integral over surface S_I. The effect achieved through use of equation (2-11-5) is similar to that produced by separating the primary and secondary electric fields to remove the electric field singularity in the integral.

Note that when the earth's surface is flat, surfaces S_T and S_I coincide so that the integrals in equation (2-11-5) may be combined into a single integral over the secondary electric field. Equation (2-11-5), so modified, is equivalent in form to the equa-

tion used by Gomez-Trevino (1978) for determining the contribution to magnetic field from electric fields on the earth's surface.

2-12 Operational Considerations for the Numerical Modeling Program

This article reviews the capabilities and limitations of the terrain modeling program developed for this investigation. The terrain modeling program's basic function is to evaluate the electric potential and magnetic fields produced by direct current flow in an electrically homogeneous earth with arbitrary topography. The formulations employed are for an earth having a uniform electrical conductivity of arbitrary value and free space electric permittivity and magnetic permeability values.

2-12.1 Model Surfaces

In their analytic form, the equations developed apply to arbitrary terrains, excluding only those surfaces with discontinuous second derivatives and overhangs (i.e., non-single valued surfaces). However, some of the approximations used in the numerical solution of the terrain problem make accurate modeling of the electric and magnetic responses of some types of topographic features uncertain. To be avoided are terrains with slope angles exceeding fifty degrees or slope angle changes greater than five to ten degrees between adjacent elements. The rate of inter-element slope angle change may be decreased by smoothing the surface or increasing the model grid density. As an additional practical restriction, the maximum surface feature height should be less than 20 percent of the model width.

Further, the outer edges of the terrain model surface should connect smoothly with the surrounding infinite horizontal surface. This condition can usually be met by applying a linear taper to the outer 10 percent of the model surface. Under certain modeling conditions, e.g., where the current source and field measurement locations indicate that edge effects will be insignificant, the edges of the terrain model surface may be left unmodified.

Typical terrain model surfaces will be composed of uniformly spaced surface elements layed out on grids 41 x 41 to 61 x 61 elements in size.

2-12.2 Current Sources and Images

The primary electric field source for the terrain model may be either uniform field (produced by a very distant point current source) or polar (local point current sources). Current sources lying within a distance of 1.5 model elements of the surface must be positioned directly beneath the nearest model element for acceptable model results. Deeper current sources may be placed without restriction.

Where subsurface current sources are used, the position and strength of their corresponding images is not critical. The image is manually positioned so that it represents the approximate reflection of the current source (electrode) across the nearest section of surface elements; and the image strength is usually set to the current source strength.

Where surface current electrodes are modeled, the current images must be superimposed on their corresponding current sources, and the surface must generally be smooth for a radius of 2 model elements around the electrode. However, if a current electrode lies on the apex of a conical or ridge-like feature in the terrain, smoothing of the surface may not be necessary, provided the image strength is adjusted to satisfy the near source field behavior resulting from the solid angle formed by the surface around the electrode.

2-12.3 Estimation of Electric Potentials and Magnetic Fields

The program estimates electric potential at the center of each surface element and will optionally determine apparent resistivity values, computed with flat earth resistivity geometric factors, relative to an arbitrarly positioned potential reference electrode.

Magnetic field components are calculated on an observation grid surface which shares horizontal coordinates with the topographic surface model grid. Usually the observation surface is equated to the topographic surface thereby simulating surface magnetic field measurements; however, observation surfaces above or below the terrain surface may be specified.

Electric and magnetic field values at locations between grid locations may be found by interpolation.

2-12.4 Computer Requirements

Computer requirements for the terrain program are not excessive given the complexity of the terrain problem. On a CDC 7600 computer, a typical 41 x 41 element model with a single current electrode arrangement requires approximately 60 seconds to compute potentials and resistivities at all surface elements and an additional 20 seconds to compute vector magnetic fields at one-fourth of the surface elements. The required core or direct access data storage ranges between 6 to 12 times the number of model surface elements depending on the choice of trade-offs made between data storage and program execution time.

CHAPTER 3

NUMERICAL RESULTS

3-1 Verification of the Numerical Solution

Verification of the resistivity terrain numerical model was made by a comparison with 2-D finite element resistivity model results from Fox et al (1980). The 3-D integral equation terrain program was used to model a dipole-dipole survey line across a symmetric two-dimensional valley with 10 degree slope angles (Fox et al (1980), model case: V-SL6.0-SA10). The integral equation valley model was constructed from a simple 41 x 41 grid of surface elements. To accommodate current sources in the model surface, image strengths were adjusted to satisfy the near source electric field behavior resulting from the solid angles formed by the surface around the electrodes. Agreement between the integral equation and finite element model results is fairly good as shown in the apparent resistivity psudeo-sections in Figure 3-1-1.

Checks on the reciprocity of the potential fields for this model show a maximum error of 1.8 percent around the surface inflection at the base of the valley and an average error of 0.5 percent for all points calculated. This error can be further reduced by smoothing the surface and increasing the number of model elements near the surface inflection.

Verification of the magnetometric resistivity portion of the numerical model was made by comparisons with results from analytic

magnetic field expressions for a hemispherical depression and a dipping air-earth interface from Edwards et al (1978). Although the hemispherical depression with its near vertical sides and right angle break in slope at the rim is outside the class of problems intended for the terrain program, it still serves as a basic order-of-magnitude model check. The model for the hemispherical depression consists of a 41 x 41 square element grid as shown in Figure 3-1-2. The hemisphere is 14 model elements in diameter with a current source I positioned at the surface one diameter from the depression's center. To remove the abrupt slope change at the rim of the depression, the surface was smoothed. Figure 3-1-3 compares model and analytic expression results for the vertical magnetic field on lines A, B and C. In spite of the limitations of this particular model, the comparison is quite good.

Analytic expressions for MMR anomalies over a dipping interface, from Edwards et al (1978), provided checks on both the vertical and horizontal magnetic fields for the numerical model. Plan and section views of the 41 x 41 element dipping interface model are given in Figure 3-1-4. An electrode I is imbedded at the contact, and the interface dips at an angle of 11.25 degrees. The resistivity of the upper wedge ρ_2 was set to infinity in the analytic expressions to approximate air, and all field values were calculated along the horizontal surface Z = 0 on line A. The numerical model and analytic results are plotted together in Figures 3-1-5 and 3-1-6 as percent MMR anomaly. Agreement of the results is excellent. Maximum error

in the model results for vertical and horizontal components is less than one percent of the total magnetic field.

Other checks on the author's numerical model consist of comparisons of resistivity and magnetic field results for fine and coarse model grids and comparisons with flat earth cases.

3-2 Terrain Correction Technique for Apparent Resistivity Data

When properly calculated, the measured apparent resistivity of a homogeneous earth will always be equal to that earth's intrinsic resistivity; terrain effects result simply from the application of inappropriate geometric factors in computing the apparent resistivity.

For any resistivity array on any shape earth, the apparent resistivity ρ_a may be defined by:

$$\rho_a = G \frac{V}{I} , \qquad (3\text{-}2\text{-}1)$$

where V is the measured potential difference, I is the applied current, and G is the geometric factor, which depends on the shape of the earth's surface and the electrode configuration. The key to removing terrain effects is the determination of the correct geometric factors, which in turn depends upon defining the theoretical electric field in the vicinity of the current electrodes. On a flat, homogeneous earth, the electric field is expressible as a simple analytic function. However, on an irregular surface, the electric field cannot be expressed by analytic functions and must therefore be computed numerically.

An effective means of correcting resistivity data for terrain effects is to use a numerical terrain model to model the resistivity survey measurements (Fox et al, 1980). The model is assigned a homogeneous resistivity of 100 ohm-meters, and the program is set up to calculate apparent resistivities using flat-earth geometric

factors. The model apparent resistivities are then used as percent correction factors on the original apparent resistivities calculated from the field data. For example, a model apparent resistivity of 120 ohm-meters indicates that the terrain has elevated the potential between the measurement electrodes 20 percent above the corresponding flat-earth value. Thus, to remove the terrain effect, the measured potential or apparent resistivity is divided by 1.20.

Fox et al (1980) have demonstrated the effectiveness of this apparent resistivity terrain-correction scheme for 2-D earth's. Their results showed the terrain-correction method capable of stripping the effects of terrain from apparent resistivity data while not significantly disturbing the anomalies due to subsurface structures. Once terrain corrected, apparent resistivity data can, to a high degree of accuracy, be interpreted assuming a flat earth. Only small errors result from the distorted distances between buried structures and electrodes caused by the non-horizontal surface.

3-3 Resistivity Terrain Correction Example

To demonstrate the 3-D resistivity terrain correction technique, we present the results of a mise-a-la-masse resistivity survey conducted in an area of significant topographic relief. The objective of the survey was to locate extensions of a highly conductive sulfide interval intersected by a drill hole at a depth of 170 to 230 meters.

The survey area topography and drill hole location are shown in Figure 3-3-1. The energizing current electrode was placed in the sulfide zone, 220 meters below the surface (Figure 3-3-2), and the return current electrode was placed on the surface 1300 meters north of the drill hole. Surface electric potentials were measured (relative to a distant reference electrode) at some 200 points, and an apparent resistivity contour map (Figure 3-3-3) was calculated from the potentials using flat earth geometric factors and straight line distances between electrodes.

A fair degree of correlation is apparent between high and low apparent resistivity anomalies and high and low topographic features. An apparent resistivity anomaly high of 168 ohm-meters is centered on the hill just to the west of the drill hole, and apparent resistivity lows of 85 and 84 ohm-meters are located in topographic lows to the north and south of the drill hole.

To evaluate the contribution of topography to these anomalies, the mise-a-la-masse survey was modeled with the 3-D terrain resistivity program. Apparent resistivity model results for a uniform

model resistivity of 100 ohm-meters are shown in Figure 3-3-4.

A comparison of measured (Figure 3-3-3) and model (Figure 3-3-4) apparent resistivities shows a rough correlation of high and low anomalies. The model high of 119 ohm-meters (19 percent) on the hill to the west of the drill hole corresponds spatially to the measured high of 168 ohm-meters. And the model lows of 80 and 87 ohm-meters, north and south of the drill hole, correspond roughly with the measured lows of 84 and 85 ohm-meters.

Terrain effects were stripped from the measured data by normalizing the measured apparent resistivities by the model apparent resistivities. The resulting terrain corrected apparent resistivities are shown in Figure 3-3-5.

The terrain correction produced the following changes in the measured apparent resistivities. The measured 85 ohm-meter low north of the drill hole has been increased to 100 ohm-meters. The measured high of 168 ohm-meters west of the drill hole has been reduced to 150 ohm-meters, and the strike direction of the elongate anomaly associated with this 168 ohm-meter high has been changed by 30 degrees. In the terrain corrected data, this elongate anomaly has a distinct form which extends 250 meters due west and 100 meters due east of the drill hole collar and is bounded to the north and south by low resistivity anomalies of 100 and 86 ohm-meters. Overall the terrain corrected apparent resistivity anomalies show only a mild correlation with topography.

Interpretation of mise-a-la-masse apparent resistivity data is based on the association of high apparent resistivity anomalies with proximity to extensions of the conductive body contacted by the current electrode. A qualitative interpretation of the terrain corrected apparent resistivities based on this principle is shown in Figure 3-3-6. The shape of the elongate high anomaly suggests the conductive body has a horizontal dimension of 350 meters and an east-west strike direction. The narrow width (150 meters) of the anomaly indicates the top of the conductive body is no deeper than about 75 meters. The available geologic data also suggest the body is thin (a few meters thick), tabular and steeply dipping to the north.

3-4 Terrain-Correction Technique for Magnetometric Resistivity Data

By definition a homogeneous earth with an arbitrary surface will not produce an MMR anomaly. True MMR anomalies can result only from inhomogeneities imbedded in the earth. However, false anomalies or terrain effects will be observed when measurements taken over irregular terrain are reduced using flat-earth normal (primary) magnetic fields.

In the general case, the MMR anomaly is given by

$$B_c^a = B_c^m - B_c^n \,, \qquad (3\text{-}4\text{-}1)$$

where B_c^a is the anomalous part of the c component of magnetic field, B_c^m is the measured c component, and B_c^n is the theoretical c component for a homogeneous earth.

Essential to the removal of MMR terrain effects is the determination of the true value for the normal magnetic field B_c^n at each measurement location. When a flat homogeneous earth is assumed, the normal magnetic field is a simple analytic function. However, the normal magnetic field on an arbitrary surface cannot be represented by an analytic function and therefore must be computed numerically. Removal of MMR terrain effects is accomplished by using a numerical terrain model to calculate the normal magnetic field for a homogeneous earth at each measurement location. Equation (3-4-1) is then used to find the anomalous field. The magnetic field due to current flow in cables connecting the electrodes to the current transmitter is included in the data reduction as a separate calculation. This

calculation, based on the Biot-Savart Law, requires accurate definition of the path of the current carrying cables over the terrain. The terrain corrected MMR data will more accurately show the response of the subsurface resistivity structure, making qualitative and quantitative interpretations more valid.

It should be understood that this type of topographic correction serves only to remove the effect of current flow within the terrain and does not reduce the measurements to a horizontal plane. Where it is considered necessary, terrain corrected MMR measurements may be reduced to a horizontal plane using an approach developed by Bhattacharyya and Chan (1977). Although their technique was originally developed for the reduction of conventional magnetic data, it may be applied without modification to 3-D MMR data. It is the author's experience that the reduction of MMR data to a horizontal surface is of secondary importance compared to applying the basic terrain correction. Thus, terrain corrected data can usually be interpreted ignoring the elevation differences of the measurement stations or by treating the effects qualitatively.

3-5 Magnetometric Resistivity Terrain Correction Example

To illustrate the application of the MMR terrain correction, we present the results of an MMR survey conducted in an area having substantial topographic relief. This survey was carried out over the same ground and in search of the same target described in the resistivity terrain correction example. Again, the objective was to search for lateral extensions of a highly conductive sulfide zone intersected in a drill hole.

Figures 3-5-1 and 3-5-2, respectively, show plan and section views of the terrain and drill hole with current electrodes and intersected sulfide zone. Placing the return (or negative) current electrode at the bottom of the drill hole, rather than at a point on the surface, eliminates some of the difficulties associated with making magnetic field measurements near a current carrying wire. The pair of wires in the upper 220 meters of the drill hole carry currents flowing in opposing directions and therefore in combination produce no measurable magnetic field. Only the section of wire between 220 and 1000 meters must be considered when correcting the measured magnetic fields for effects of the wire.

Another advantage of this down-hole electrode configuration results from the near cancellation of the primary magnetic fields of current sources and wires. It can be shown that no magnetic field is produced on or above the surface when a current electrode pair with associated current carrying cables is placed in a vertical drill hole in a homogeneous half-space. In situations where the

surface has relief and the drill hole is a few degrees off from vertical, as is the case for this survey, only a partial cancellation of primary magnetic fields results.

In this survey, the two horizontal magnetic field components were measured at each station while the transmitter supplied the electrodes with a low frequency (3 Hz) squarewave current of 2 amperes. The measured fields, normalized by transmitter current strength, are plotted as vectors in Figure 3-5-3, and show a maximum strength of 105 milligammas per ampere.

To evaluate the contribution of terrain to the measured magnetic fields, computer models were run for both the actual topography and a half-space. Figure 3-5-1 shows the central portion (41 X 41 elements) of the 61 X 61 element terrain model surface. The terrain model horizontal magnetic fields due to topography, current sources, and current carrying wires (Figure 3-5-4) have a maximum strength of 56 milligammas per ampere. In contrast, the half-space horizontal fields (Figure 3-5-5) for an identical electrode and wire configuration have a maximum strength of only 19 milligammas per ampere, approximately one-third the maximum produced by the terrain model.

The standard MMR data reduction method subtracts the half-space fields from the measured fields to remove the effects of current flow in the earth and wires. In this case, the half-space fields are of relatively low strength (about 18 percent) compared to the

measured fields so that their subtraction produces little change in the measured fields.

In contrast, the MMR terrain correction technique subtracts the terrain model fields (Figure 3-5-4) from the measured fields (Figure 3-5-3) to create terrain corrected magnetic fields (Figure 3-5-6). In this case, the correction is relatively large, averaging roughly 50 percent of the measured field values. The effect of this correction on the measured fields is most noticeable in the areas to the north and south of the drill hole.

The terrain corrected magnetic fields can be interpreted qualitatively by identifying the magnetic field patterns produced by zones of concentrated current flow. Specifically, a lateral extension of the highly conductive zone intersected in the drill hole would provide a major channel for current flow from the positive electrode and would be indicated in the surface data by an area of clockwise (relative to the drill hole collar) horizontal vectors, via the right hand rule for magnetic fields. At the other extreme, resistive rock units would reduce current flow and would be indicated by counterclockwise field vectors. Since the terrain corrected fields must be consistent with Ampere's law applied to integration paths around the drill hole, areas of counterclockwise and clockwise vectors will have equivalent weights. (This is strictly true over irregular terrain only if the vertical field is included in the integration.)

An interpretation of the terrain corrected fields based on these principles is given in Figure 3-5-7. In this figure, the magnetic fields indicate two broad zones of relatively high resistivities to the north and south of the drill hole. Sandwiched between these resistive zones are two narrow conductive zones, (possibly the sulfide body) extending roughly east and west of the drill hole. The sparse data coverage obtained over these conductive zones does not allow accurate definition of their extent and depth. However, the terrain corrected mise-a-la-masse resistivity data is in general agreement with this interpretation.

The MMR terrain correction has improved our ability to resolve the resistive and conductive zones. The uncorrected measured data (Figure 3-5-3) over-emphasize the northern resistive zone and show no evidence of the southern resistive zone or of the conductive zones to the east and west.

3-6 Analysis of the Numerical Model Solution for the Terrain Correction Example

The calculation of magnetic fields for the terrain model in the previous section depended upon first solving for the intermediate model parameters of surface charge density, electric potential, electric fields, and the individual contributions to the magnetic field produced by current flow in the wires and current flow in the earth. This section examines these intermediate model solutions with the aim of clarifying their role in the calculation of the final magnetic field results.

The model surface used in the terrain correction example is composed of an equispaced 61 x 61 element surface grid. A contour plot of this surface is given in Figure 3-6-1. Note that there is no tapering of the edges of the model surface.

Since this model included down-hole current electrodes, current source images were positioned above the surface (Figure 3-6-2) to reduce the charge density on the surface. The exact location of these images is unimportant to the final model solutions, since the surface charge distribution adjusts itself to maintain the correct boundary conditions. In this case, the images were given horizontal coordinates identical to their associated down hole current electrodes and elevations above the drill hole collar equivalent to the depth of the electrodes below the collar. The images were assigned amplitudes and polarities equal to the corresponding down hole current sources.

A stable solution for charge density on the surface elements (Figure 3-6-3) was obtained in two iterations. A third iteration produced changes in the model's electric and magnetic field results of less than 0.2 percent. The detailed variation of charge density in the central one-third of the model can be studied from the enlargement of this 21 x 21 element area given in Figure 3-6-4.

The total electric potential on the model surface (relative to a reference electrode at infinity), shown in Figure 3-6-5, is composed of contributions produced by the surface charge distribution and the current sources and images. The percentage of the total potential solution due to surface charge, shown in Figure 3-6-6, ranges between -28 and +11 percent. The remainder of the potential solution is due, in roughly equal proportions, to the current sources and to their images. Had current source images not been used in this model, the contribution of surface charge to the potential solution would have been raised to the 60 percent level.

Whereas it is difficult to see relationships between the equipotential lines in Figure 3-6-5 and the model topography, conversion of the electric potential data to apparent resistivities (Figure 3-6-7) using flat earth geometric factors makes this relationship readily apparent. There is a general correlation of apparent resistivity highs and lows with respective topographic highs and lows. In terms of percentages, the apparent resistivities and potentials have been distorted by the terrain by as much as +19 to -22 percent.

Magnetic fields measured in an MMR survey can be separated into two parts: 1) fields due to current flow in the insulated wires which connect the current transmitter to the current electrodes and 2) fields due to current flow within the earth. Since the layout of the current carrying wires is known, their contribution to the magnetic field may be determined at any location through the Biot-Savart Law (Appendix II). Figures 3-6-8 and 3-6-9, respectively, show the model calculated horizontal and vertical surface magnetic field vectors created by current flow in the wire in the drill hole. Note the slightly skewed, counterclockwise, circular pattern in the horizontal field and the straight line formed by the zero field contour of the vertical component.

The terrain model determines the magnetic fields due to current flow in the earth by evaluating a surface integral involving only surface electric fields and terrain slopes. Figures 3-6-10 and 3-6-11, respectively, show horizontal and vertical fields calculated by this method. The total magnetic field on the model surface, Figures 3-6-12 and 3-6-13, is found by summing the fields produced by current flow in the wire and in the earth. The horizontal field vectors in Figures 3-6-12 are reduced to their x (north) and y (east) components in Figures 3-6-14 and 3-6-15.

To verify that the surface of the model under study has been represented with an adequate density of surface elements and that the resulting field solutions are stable, a second model was run

using the same terrain represented by 30 percent fewer elements (i.e., 51 x 51 elements). Figures 3-6-16 and 3-6-17, respectively, show the apparent resistivity and magnetic field x component data for this lower element density model. A comparison of these figures with their respective counterparts for the 61 x 61 element model in (Figures 3-6-7 and 3-6-14) shows the solutions to be in excellent agreement. Differences in the apparent resistivity data (and hence the potentials they were derived from) is everywhere less than 0.5 percent. Differences in the x component magnetic fields are less than 1.5 percent relative to the total horizontal field due to current flow in the earth. Part of this 1.5 percent disagreement can be attributed to shifting of field evaluation points due to the change in surface grid density.

It is instructive to compare the magnetic field patterns of the terrain model, Figure 3-6-18, with model results obtained for a flat horizontal surface, Figure 3-6-19, and a flat dipping surface, Figure 3-6-20, all employing identical configurations of current electrodes and wires. These figures show combined plots of horizontal field vectors and vertical magnetic field contours and are presented at the same horizontal scale. The flat horizontal model surface has a maximum horizontal field strength of only 19 milligammas/amp compared to a maximum of 56 milligammas/amp for the terrain model. However, the dipping model surface, which was given a dip similar to the terrain model topography near the drill hole collar, has field strengths and patterns very similar to the terrain model

results for the area near the drill hole collar. Similarities can also be seen in the positions of the zero crossings of the vertical magnetic field contours for the dipping surface and terrain models. All of this suggests that the average dip of the surface in the vicinity of the current electrodes has substantial influence on the measured magnetic fields.

3-7 Terrain Features in Uniform Electric Fields

Modeling the electrical response of terrain features in uniform primary electric fields has relevance to the telluric method and to situations where electrical resistivity and magnetometric resistivity measurements are made at distances from the current electrodes which are large compared to anomaly wave lengths. It should be noted, however, that direct current modeling of electromagnetically induced telluric fields is an approximation.

Uniform primary electric fields were created in the terrain models by locating a current source a large distance outside the main model area. Two 41 x 41 surface element terrain features were modeled: a 2-D ridge with 30 degree slopes, Figure 3-7-1, and a 3-D hill with 20 degree slopes, Figure 3-7-3.

The electric potential and magnetic field patterns over the terrain features are featureless because the terrain effect anomalies are super-imposed on the much larger background primary field created by the distant current source. This loss of anomaly resolution is a consequence of the rapid $1/r^2$ decrease in the anomaly inducing primary electric field relative to the slower $1/r$ fall off of the primary electric potential and magnetic fields. In contrast, electric field anomalies are resolvable in the background primary electric field because they are induced in direct proportion to the primary electric field strength.

Figures 3-7-2 and 3-7-4, respectively, show the percentage change in the surface electric field x component relative to the primary

electric field for the 2-D ridge and 3-D hill models. (The effect of the finite strike length of the 2-D ridge can be seen at the edges of the electric field solution as a loss of the 2-D character of the contours. However, a few model elements away from the edges, the solution becomes highly two dimensional.) As one might expect, the maximum reductions in electric field strength, 62 and 39 percent, occurred at the respective crests of the ridge and hill, while the maximum increases of 40 and 25 percent were located in narrow zones at the bases of the ridge and hill.

3-8 Magnetometric Resistivity and Electrical Resistivity Terrain Effects Over Two- and Three-Dimensional Features

The author has studied terrain effect magnetometric resistivity and electrical resistivity anomalies by investigating several basic two-and three-dimensional terrain features: a valley, ridge, hill, and sink. Homogeneous intrinsic resistivities of 100 ohm-meters were used for all models; terrain slope angles were set to 10, 20, and 30 degrees; and the current source was alternately placed at the crest, base, and mid-flank of each terrain feature. Apparent resistivity (pole-pole) and percent magnetic field anomalies were computed over the model surfaces, and the results contoured. The model results are presented in a format similar to that used for MMR and mise-a-la-masse surveys employing distant potential reference and current return electrodes and hence may be used directly as terrain effect interpretive aids for these survey methods.

Figures 3-8-1 through 3-8-8 show plan and section views of the eight terrain features modeled. Each terrain feature was modeled with an equispaced 41 x 41 grid of surface elements and given a homogeneous model resistivity of 100 ohm-meters. The models and model results are identified by case labels (e.g., R-SA10-1B) encoded in the following way: the first letter represents the type of terrain feature: R for ridge (2-D), V for valley (2-D), M for mound or hill (3-D), and S for sink (3-D). The letters SA are followed by the slope angle of the terrain feature in degrees. The final pair of letters indicates current electrode position A, B, or

C for crest, mid-flank, or base of the terrain feature, respectively. Table 3-8-1 lists the 16 models run for this study.

A word of caution: since finite length features were used to represent the two-dimensional surfaces, solution accuracy is degraded near the edges of these features.

TERRAIN MODEL CASES

TERRAIN TYPE		SLOPE (DEGREES)		CURRENT ELECTRODE
R	-	SA10	-	IB
R	-	SA20	-	IA
R	-	SA20	-	IB
R	-	SA20	-	IC
R	-	SA30	-	IB
V	-	SA20	-	IA
V	-	SA20	-	IB
V	-	SA20	-	IC
M	-	SA10	-	IB
M	-	SA20	-	IA
M	-	SA20	-	IB
M	-	SA20	-	IC
M	-	SA30	-	IB
S	-	SA20	-	IA
S	-	SA20	-	IB
S	-	SA20	-	IC

TERRAIN TYPES:
R RIDGE 2-D
V VALLEY 2-D
M HILL 3-D
S SINK 3-D

TABLE 3-8-1

3-8.1 Apparent Resistivity Model Results

Figures 3-8-9 through 3-8-24 show the resistivity model results for the pole-pole electrode configuration. The potential reference and current return electrodes are at infinity. Apparent resistivities are calculated at the center of each surface element using flat earth geometric factors and straight line distances between current and potential electrodes. Since the homogeneous background resistivity is 100 ohm-meters, the apparent resistivity results can be easily converted to percent resistivity or electric potential terrain effect.

The fundamental physical cause of terrain effects in electric potential fields is induced electric charge on the surface. This surface charge is the physical analog of the numerical integral equation charge solution obtained with the modeling program. Associated with the surface charge are anomalous potential fields which are basically the potential terrain effect. Assuming the current source is positive, positive surface charge elevates the electric potential causing anomalously high apparent resistivities; negative surface charge produces the opposite effect. Positive surface charge results from electric field vectors, due principally to the current source (although the surface charge makes contributions), impinging on the underside of the surface, while negative charge results from vectors impinging from above the surface. With the above considerations in mind, it is not difficult to understand the relations between resistivity anomalies, surface shape, and current locations for the terrain models in this suite.

Table 3-8-2 lists the high and low apparent resistivity anomalies produced for each of the model cases.

A review of the model results revealed the following:

1) The models show a general correlation of apparent resistivity highs with convex surfaces (e.g., tops of hills and ridges) and an association of resistivity lows with concave surfaces (e.g., sinks, valleys, and near the bases of hills and ridges).

2) Terrain features with slope angles as small as 10 degrees produce resistivity terrain effects exceeding 10 percent (e.g., Case M-SA10-IB has 17 percent anomaly). The maximum anomaly produced for 30 degree slope angles was 68 percent, Case M-SA30-IB.

3) The magnitude of the anomaly patterns for a given topographic shape bear an approximate linear relation to the terrain feature's height.

4) The anomalies on the 3-D hills are 30 to 60 percent larger than the corresponding 2-D ridge models with identical slope angles, suggesting that 3-D terrain may, in general, cause more severe terrain effects than 2-D terrain. However, the two depression terrain forms, the 2-D valley and 3-D sink, do not produce resistivity anomalies which differ significantly.

In an actual survey, the significance of these terrain effect anomalies depends on the amplitude of the anomalies one wishes to resolve in measured data. In the majority of resistivity surveys, a 10 percent terrain effect would not significantly alter interpretation of the data. However, where terrain effects exceed 20 percent,

TERRAIN MODEL

APPARENT RESISTIVITY MAXIMA AND MINIMA

CASE	OHM-METERS MAX	MIN
R-SA10-IB	113	95
R-SA20-IA	118	100
R-SA20-IB	127	90
R-SA20-IC	116	92
R-SA30-IB	143	86
V-SA20-IA	100	85
V-SA20-IB	112	77
V-SA20-IC	110	84
M-SA10-IB	117	97
M-SA20-IA	129	102
M-SA20-IB	139	94
M-SA20-IC	122	92
M-SA30-IB	168	92
S-SA20-IA	100	81
S-SA20-IB	108	76
S-SA20-IC	108	84

TABLE 3-8-2

as they do on models with slopes of 20 degrees or more, application of the resistivity terrain correction scheme described in section 3-2 should improve the accuracy of the interpretation.

3-8.2 Magnetic Field Model Results

Magnetic field anomalies on the surfaces of the terrain features (Figures 3-8-25 through 3-8-72) were computed as percent magnetic field anomalies, B_c^{pa}, using the following equation

$$B_c^{pa}(\bar{r}) = 100(B_c^M(\bar{r}) - B_c^N(\bar{r}))/B^N(\bar{r}) ,$$

where

$B^N(\bar{r}) = \frac{\mu I}{4\pi r}$ is the total normal (half-space) magnetic field,

$\bar{r} = x\hat{i} + y\hat{j}$ is the horizontal distance from the current source I, and

C = x, y, or z component.

The sign of the contoured magnetic field anomaly B_c^{pa} defines the polarity of anomalous field rather than an increase or decrease in field strength relative to the total normal field B^N. Positive vertical magnetic field anomalies denote vectors pointing into the figures. Since the contoured magnetic anomalies are derived from fields calculated at every other model grid point, the contours may not accurately represent extreme variations in the fields at certain locations. Table 3-8-3 lists the maximum percent magnetic field anomalies produced for each of the model cases.

The magnetic field model results do not indicate a simple relationship between topographic highs and lows, but rather a complex relationship involving terrain slopes and the surface electric field vectors. However, for a given topographic form, there is an

TERRAIN MODEL

MAXIMUM PERCENT MAGNETIC FIELD ANOMALIES

CASE	Bx	By	Bz
R-SA10-IB	5.4	6.6	15.0
R-SA20-IA	11.9	14.5	14.6
R-SA20-IB	10.0	14.7	30.3
R-SA20-IC	10.2	22.5	19.0
R-SA30-IB	15.5	24.7	45.0
V-SA20-IA	13.2	21.5	10.3
V-SA20-IB	12.5	15.8	30.1
V-SA20-IC	6.2	14.8	22.3
M-SA10-IB	10.4	9.9	14.0
M-SA20-IA	25.0	25.0	0.0
M-SA20-IB	23.1	21.4	28.0
M-SA20-IC	9.1	18.7	18.2
M-SA30-IB	40.1	36.5	41.9
S-SA20-IA	27.1	27.1	0.0
S-SA20-IB	19.1	19.2	27.6
S-SA20-IC	8.3	7.7	21.0

TABLE 3-8-3

approximate linear relation between the amplitude of the anomaly patterns (in all field components) and the terrain feature's height. Terrain features with slope angles as small as 10 degrees produce maximum magnetic field anomalies ranging from 5 to 15 percent. In the model suite, maximum x component anomalies range between 5.4 (Case R-SA10-IB) and 40 percent (Case M-SA30-IB); y component anomalies between 6.6 (Case R-SA10-IB) and 36.5 percent (Case M-SA30-IB); and z component anomalies between 0.0 (Case M-SA30-IA) and 45 percent (Case R-SA30-IB).

When one considers that many subsurface geologic structures produce maximum MMR anomalies of 30 percent or less, it is easy to see how uncorrected terrain effects can lead to inaccurate geophysical interpretations.

3-9 An Approximate Method for Estimating Vertical Magnetic Field Terrain Effects

The full numerical solution of magnetic field terrain effects requires that the direct current boundary value problem be solved. The magnetic field components are then found by evaluating surface integrals involving surface electric fields and terrain slopes. These integrals (taken from equations (2-10-7)) are given below:

$$B_x(\bar{r}') = \frac{-\mu(\sigma_1-\sigma_2)}{4\pi} \iint_S \frac{(E_y + E_z f_y)}{|\bar{r}-\bar{r}'|}\, dxdy \qquad (3\text{-}9\text{-}1)$$

$$B_y(\bar{r}') = \frac{+\mu(\sigma_1-\sigma_2)}{4\pi} \iint_S \frac{(E_z f_x + E_x)}{|\bar{r}-\bar{r}'|}\, dxdy \qquad (3\text{-}9\text{-}2)$$

$$B_z(\bar{r}') = \frac{+\mu(\sigma_1-\sigma_2)}{4\pi} \iint_S \frac{(E_x f_y - E_y f_x)}{|\bar{r}-\bar{r}'|}\, dxdy \qquad (3\text{-}9\text{-}3)$$

Since most of the computational effort of obtaining magnetic fields is expended in the solution of the surface electric fields, it is desirable to find schemes which speed this aspect of the computations. One such scheme developed by the author gives an approximate solution to the vertical magnetic field terrain effect by substituting the easily calculated half-space electric fields for the true horizontal electric fields in equation (3-9-3). This approach produces results of reasonable accuracy due to the relation between electric field and slope terms in the integrand. The value of the integrand is controlled predominately by the terrain slopes; errors in the vertical magnetic field estimate will not be greater than the

maximum difference between the true horizontal electric fields on the terrain and the half-space electric fields (an amount which is usually 10 to 20 percent). In practice, however, the averaging which results from the integration generally produces less error.

Figure 3-9-1 shows a comparison of vertical magnetic field anomalies calculated using the full numerical solution and using the approximate technique described above. The profile, from model Case R-SA30-IB, was taken perpendicular to the 2-D ridge, 4 model elements down strike of the current source. The approximation has an error which is everywhere less than 10 percent of the peak anomaly value. Tests on other terrain features showed similar accuracies.

CHAPTER 4

SUMMARY AND CONCLUSIONS

The Electrical Resistivity and Magnetometric Resistivity (MMR) direct current prospecting methods are powerful and highly versatile tools for the detection of conductivity inhomogeneities associated with geologic structures. Exploration geophysicists have long known topographic features to be the cause of misleading anomalies in these survey methods. However, the evaluation and correction of terrain effects is generally difficult, requiring the use of forward numerical model solutions for the electric and magnetic fields over arbitrary three-dimensional terrains. Until now there have been no model studies on the terrain effect in MMR surveys; and the available model studies on electrical resistivity terrain effects have been limited to two-dimensional topography. Hence, there is need for modeling techniques which enable the geophysicist to estimate and remove three-dimensional effects in both electrical resistivity and magnetometric resistivity surveys.

This work examined the application of the integral equation numerical modeling technique to the estimation of 3-D topographic effects for homogeneous earths in the Electrical Resistivity and Magnetometric Resistivity geophysical prospecting methods. A new and fundamentally powerful technique for applying current source images in combination with surface charge was developed and used

to meet the boundary conditions on the air-earth interface. The integral equations required for the solution of the electric and magnetic fields were reformed in terms of surface slopes. Verification of the accuracy of the numerical solutions were made by comparisons with independent modeling techniques. The effect of terrain on uniform electric fields was examined. A small suite of models were run to investigate resistivity and magnetometric resistivity terrain effects over two- and three-dimensional topographic features. A computationally efficient method for estimating the vertical magnetic field was developed and demonstrated. Finally, methods for correcting apparent resistivity and MMR data for terrain effects were described and demonstrated with examples using real field data.

The terrain problem is treated by modifying the standard integral equation method with a technique for applying images in combination with surface charge; the resulting integral equation is formulated in terms of surface charge and terrain slopes. The terrain is divided into a grid of flat plates or elements on each of which the charge density is assumed to be uniform. An approximate solution to the surface integral equation is obtained using the "point matching" method to solve for the charge at the center of each element. The integral equation is thus written as a set of simultaneous linear equations with surface charge as unknowns. This system of equations is easily and rapidly solved by an iterative approach.

Once the surface charge distribution has been solved, the other electrical parameters are easily calculated. Electric potential is determined from an evaluation of the potential contributions produced by the surface charge distribution and the current sources and images. Apparent resistivities are then calculated directly from the potential. Surface electric fields, which are required for the calculation of the magnetic field, are determined by adding electric fields produced by the sources and images to the electric field due to the surface charge distribution. Finally, the magnetic field is found by evaluating a surface integral equation involving terrain slopes and surface electric fields; an approximate separation of primary and secondary magnetic fields is used to reduce problems created by electric field singularities and the finite area of the model.

The new technique for applying current source images in combination with surface charges is directed at treating the extreme variations in surface charge density associated with buried or down hole current sources. The technique eliminates these extreme charge variations by the placement of a current source image above the surface opposite the current source. In this way, the current source and image provide a first order solution to the surface boundary conditions, while surface charge handles the higher order detail of the solution. Since the resulting surface charge distribution is much more slowly varying than it would have been without the image, it may be represented accurately on a coarse model grid with a simple

basis function.

This thesis has shown that the integral equation numerical modeling technique can be efficiently used to treat realistically complex three-dimensional topography for both the resistivity and magnetometric resistivity methods. Generally requiring only 2 to 3 iterations for adequate solution convergence, the iterative solution of the surface integral equation is a rapid means of obtaining the charge on the model surface. Since it is necessary to solve for surface charge for each current electrode configuration used, the iterative solution approach is best suited to the modeling of the mise-a-la-masse and MMR methods, which typically employ a small number of current electrode locations and a large number of field observation locations.

Computer requirements for the terrain program are not excessive given the complexity of the terrain problem. On a CDC 7600 series computer, a typical 41 x 41 element model with a single current electrode arrangement requires approximately 60 seconds to compute potentials and resistivities at all surface elements, and an additional 20 seconds to compute vector magnetic fields at one-fourth of the surface elements. The required core or direct access data storage ranges between 6 to 12 times the number of model surface elements, depending on the choice of trade-offs made between data storage requirements and program execution time.

The basic drawback of all integral equation formulations for electric potential is that the solution is poorly behaved at sharp

corners in the model surface, making it necessary to smooth the corners and increase the density of surface elements in those areas. Consequently, where surface current electrodes are modeled, care must be taken to smooth the surface near these electrodes. Subsurface current sources two or more model elements deep, however, may be used without special treatment of the surface. The new technique of applying current source images in combination with surface charge has greatly reduced the surface element density requirements on the model surface above these buried current sources.

The fundamental physical cause of electric potential terrain effects is induced electric surface charges. This surface charge is the physical analog of the numerical integral equation charge solution obtained with the modeling program. The application of flat earth data reduction procedures to resistivity and MMR measurements acquired over irregular terrain ignores these anomalous surface charge accumulations and hence causes terrain effect anomalies.

When correctly calculated, the measured apparent resistivity of a homogeneous earth will always be equal to the earth's intrinsic resistivity; terrain effects result simply from the application of inappropriate geometric factors in computing the apparent resistivity.

A simple procedure for removing terrain effects from existing apparent resistivity data consists of using the resistivity terrain effect program to model the survey, assigning a homogeneous resistivity of 1 ohm-meter to the model, and calculating model apparent resistivities using flat-earth geometric factors. The model apparent

resistivities are then divided into the field measured apparent resistivity values to remove the terrain effects. Fox et al (1980) have shown this terrain correction scheme to be effective in stripping the terrain effects from 2-D apparent resistivity data while not significantly altering the anomalies due to subsurface structures. Once terrain corrected, apparent resistivity data can be interpreted assuming a flat earth. Only small errors result from the distortion of distances between buried bodies and electrodes caused by the irregular surface.

In this thesis, the terrain correction scheme was successfully applied to a set of mise-a-la-masse apparent resistivity data acquired in an area of rugged three-dimensional terrain.

By definition a homogeneous earth with arbitrary topography will not produce an MMR anomaly. True MMR anomalies result only from inhomogeneities imbedded in the earth. However, terrain effect anomalies result when measurements taken over irregular terrain are reduced by subtracting half-space normal (primary) magnetic fields rather than the true normal magnetic fields for the area under study. The normal magnetic field is the theoretical magnetic field which would be observed over the survey area if the earth was of homogeneous resistivity.

Removal of MMR topographic effects is accomplished by using the numerical terrain model to calculate the normal magnetic fields for a homogeneous earth at each field measurement location. The

model fields are then subtracted from the measured fields to give the terrain corrected anomalous fields. Compensation for the magnetic fields caused by current flow in the cables connecting the electrodes to the current transmitter is included in the data reduction as a separate calculation using the Biot-Savart Law. Terrain corrected MMR data more accurately show the response of the subsurface resistivity structures, making qualitative and quantitative interpretations more valid.

Terrain effect magnetometric resistivity and electrical resistivity anomalies have been studied by investigating several basic two- and three-dimensional terrain features: a valley, ridge, hill, and sink. Homogeneous intrinsic resistivities of 100 ohm-meters were used for all models; terrain slope angles were set to 10, 20, and 30 degrees; and the current source was alternately placed at the crest, base, and mid-flank of each terrain feature. Apparent resistivity (pole-pole) and percent magnetic field anomalies were computed over the model surfaces, and the results contoured. The model results are presented in a format similar to that used for MMR and mise-a-la-masse surveys employing distant potential reference and current return electrodes and hence may be used directly as terrain effect interpretive aids for these survey methods.

These model results represent the first numerical simulation of magnetic field terrain effect anomalies due to direct current flow. The results show magnetic field terrain effects to be comparable in severity to electric potential terrain effects. Both

electric potential and magnetic field terrain effects become significant when terrain slopes exceed 10 degrees. The maximum electric potential and magnetic field terrain effect anomalies observed over homogeneous topographic features with 10 degree slopes were 13 and 15 percent, respectively, while topographic features with 20 degree slopes had respective electric potential and magnetic field anomalies of 27 and 30 percent.

The terrain modeling program developed in this thesis treats only earth models of homogeneous electrical conductivity. However, a simple extension of the theory will allow the inclusion of three-dimensional inhomogeneities. Following the technique developed in this thesis for the use of current source images in combination with surface charges, the approach would be to place, above the terrain surface, an image of the charge on the subsurface inhomogeneity. The image of the inhomogeneity need not be as detailed as its subsurface source because the image and source pair serve only as an approximate solution to the surface boundary conditions with the remainder of the solution absorbed by surface charge on the terrain.

Another potential area of application of the combined image surface charge technique occurs where a current source is placed in close proximity to a very highly resistive inhomogeneity. In this case it may be possible to reduce the variation of charge and hence reduce the number of model elements on the inhomogeneity by placing a current source image inside the body.

REFERENCES

Alfano, L., 1959, Introduction to the interpretation of resistivity measurements for complicated structural conditions; GEOPHYSICAL PROSPECTING, v. 7, p. 311-366.

Alfano, L., 1960, The influence of surface formations on the apparent resistivity values in electrical prospecting: GEOPHYSICAL PROSPECTING, v. 8, p. 575-606.

Alfano, L., 1961, The influence of surface formations on the apparent resistivity values in electrical prospecting, Part II: GEOPHYSICAL PROSPECTING, v. 9, p. 213-241.

Allaud, L. A., and Martin, M.H., Schlumberger the history of a technique: John Wiley & Sons, New York.

Barnett, C. T., 1972, Theoretical modeling of induced polarization effects due to arbitrarily shaped bodies: unpublished Ph.D. thesis, Colorado School of Mines.

Bhattacharyya, B. K., and Chan, K. C., 1977, Reduction of magnetic and gravity data on an arbitrary surface acquired in a region of high topographic relief: GEOPHYSICS, v. 42, p. 1411-1430.

Coggon, J. H., 1971, Electromagnetic and electrical modeling by the finite-element method: GEOPHYSICS, v. 36, p. 132-155.

Dieter, K., Paterson, N. R., and Grant, F. S., 1969, IP and resistivity type curves for three-dimensional bodies: GEOPHYSICS, v. 34, p. 615-632.

Edwards, R. N., Lee, H., and Nabighian, M. N., 1978, On the theory of magnetometric resistivity (MMR) methods: GEOPHYSICS, v. 43, p. 1176-1203.

Fox, R. C., Hohmann, G. W., Killpack, T. J., and Rijo, L., 1980, Topographic effects in resistivity and induced-polarization surveys: GEOPHYSICS, v. 45, p. 75-93.

Gomez-Trevino, E., and Edwards, R. N., 1979, Magnetometric resistivity (MMR) anomalies of two-dimensional structures: GEOPHYSICS, v. 44, p. 947-958.

Hallof, P. G., 1970, Theoretical induced polarization and resistivity studies, scale model cases, phase III: McPhar Geophysics Ltd.

Harrington, R. F., 1968, Field computation by moment methods: MacMillan Company, New York.

Jakosky, J. J., 1933, Method and apparatus for determining underground structure: U. S. patent no. 1,906,271.

Jepsen, A. F., 1969, Numerical modeling in resistivity prospecting: Ph.D. thesis, University of California, Berkeley.

Keller, G. V., and Frischknecht, F. C., 1966, Electrical methods in geophysical prospecting: Pergamon Press.

Papazian, P. B., 1979, Topographic modeling of resistivity surveys using the Schwartz Christoffel transformation: M.Sc. thesis, Colorado School of Mines.

Pratt, D. A., 1972, The surface integral approach to the solution of the 3D resistivity problem: Australian SEG, v. 3, p. 33-50.

Rijo, L., 1977, Modeling of electric and electromagnetic data: Ph.D. thesis, University of Utah.

Siegel, H. O., 1974, The magnetic induced polarization (MIP) method: GEOPHYSICS, v. 39, p. 321-339.

Snyder, D. D., 1976, A method for modeling the resistivity and induced polarization responses of two-dimensional bodies: GEOPHYSICS, v. 41, p. 997-1015.

Spiegel, R. J., Sturdivant, V. R., and Owen, T. E., 1980, Modeling resistivity anomalies from localized voids under irregular terrain: GEOPHYSICS, v. 45, p. 1164-1183.

APPENDIX I

DERIVATION OF THE INTEGRAL EQUATION FOR THE ELECTRIC POTENTIAL BOUNDARY VALUE PROBLEM

This derivation is similar in many respects to the development of the integral equation problem as given by Pratt (1972).

We begin with Ohm's law:

$$\bar{J} = \sigma\bar{E} \ , \qquad (I\text{-}1)$$

where $\bar{J}$ = current density,

σ = conductivity, and

$\bar{E}$ = electric field.

Taking the divergence of both sides of the equation (I-1), we have

$$\nabla\cdot\bar{J} = \nabla\cdot(\sigma\bar{E}), \qquad (I\text{-}2)$$

or

$$\nabla\cdot\bar{E} = \frac{\nabla\cdot\bar{J}}{\sigma} - \frac{\nabla\sigma\cdot\bar{E}}{\sigma} \ . \qquad (I\text{-}3)$$

Since

$$\bar{E} = -\nabla\phi \ , \qquad (I\text{-}4)$$

where ϕ is the electric potential, we obtain

$$\nabla^2\phi = \frac{-\nabla\cdot\bar{J}}{\sigma} + \frac{\nabla\sigma\cdot\bar{E}}{\sigma} \ . \qquad (I\text{-}5)$$

Equation (I-5) has the form of Poissons equation which has the solution

$$\phi = \int_V \left(\frac{\nabla\cdot\bar{J}}{4\pi r\sigma} - \frac{\nabla\sigma\cdot\bar{E}}{4\pi r\sigma}\right) dV, \qquad (I\text{-}6)$$

where r is the distance between the observation point for ϕ and the integration point. Since the strength of the current source I is given by

$$I = \int_V \nabla\cdot J \, dV \ , \tag{I-7}$$

equation (I-6) may be written as

$$\phi = \frac{I}{4\pi\sigma r} - \int_V \frac{\nabla\sigma\cdot\bar{E}}{4\pi\sigma r} \, dV. \tag{I-8}$$

Next from Maxwell's equations, we have

$$\nabla \times \bar{H} = \sigma\bar{E}. \tag{I-9}$$

Taking the divergence on both sides of (I-9) we obtain

$$\nabla\cdot\nabla \times \bar{H} = \nabla\cdot(\sigma\bar{E}). \tag{I-10}$$

Since $$\nabla\cdot\nabla \times \bar{H} \equiv 0 \ , \tag{I-11}$$

we are led to

$$\nabla\cdot(\sigma\bar{E}) = 0 \ , \tag{I-12}$$

which can be written as

$$\nabla\sigma\cdot\bar{E} + \sigma\nabla\cdot\bar{E} = 0 \ . \tag{I-13}$$

Next, Poisson's equation for the electrostatic scalar potential in a homogeneous, isotropic medium is:

$$\nabla^2\phi = -\frac{\rho}{\varepsilon} \ , \tag{I-14}$$

where ρ is charge density and ε is the permittivity of the medium. We may rewrite equation (I-14) as

$$\nabla\cdot\bar{E} = \frac{\rho}{\varepsilon} \ . \tag{I-15}$$

Substituting (I-15) into (I-13), we obtain

$$\frac{\rho}{\varepsilon} = \frac{-\nabla\sigma\cdot\bar{E}}{\sigma} \ , \tag{I-16}$$

and substituting (I-16) into (I-8), we have

$$\phi = \frac{I}{4\pi\sigma r} + \frac{1}{4\pi}\int_V \frac{\rho dV}{\varepsilon r} \ . \tag{I-17}$$

In this thesis the gradient of the conductivity will be nonzero only on surfaces. Thus, (I-17) becomes a surface integral

$$\phi = \frac{I}{4\pi\sigma r} + \frac{1}{4\pi}\int_S \frac{\rho\, dS}{\varepsilon r} \qquad (I\text{-}18)$$

The solution of the charge density distribution function ρ is determined by a consideration of the boundary conditions at the surface of the body. Referring to Figure 2-3-1, the conditions that must be met are:

(i) The normal component of current density must be continuous across all surfaces, i.e.,

$$\sigma_1 \frac{\partial \phi_1}{\partial n} = \sigma_2 \frac{\partial \phi_2}{\partial n} \quad . \qquad (I\text{-}19)$$

(ii) The difference in normal electric field across a surface is equal to ρ/ε.

Using the divergence theorem on (I-15), we obtain the following relation between electric fields crossing a conductivity discontinuity.

$$(E_{n_1} - E_{n_2})_S = \frac{\rho}{\varepsilon} \quad , \qquad (I\text{-}20)$$

or

$$\frac{-\partial \phi_1}{\partial n}\bigg|_S + \frac{\partial \phi_2}{\partial n}\bigg|_S = \frac{\rho}{\varepsilon} \quad . \qquad (I\text{-}21)$$

Substituting (I-19) into (I-21) gives us

$$\frac{-\partial \phi_1}{\partial n}\bigg|_S + \frac{\sigma_1}{\sigma_2}\frac{\partial \phi_1}{\partial n}\bigg|_S = \frac{\rho}{\varepsilon} \quad , \qquad (I\text{-}22)$$

or $$\left.\frac{\partial \phi_1}{\partial n}\right|_s = \frac{\rho}{\varepsilon}\left(\frac{\sigma_2}{\sigma_1 - \sigma_2}\right) . \qquad (I\text{-}23)$$

Referring again to Figure 2-3-1, we take the normal derivative of the righthand side of equation (I-18) at point P and equate the result to the righthand side of equation (I-23) to obtain

$$\frac{\rho(P)}{\varepsilon}\left(\frac{\sigma_2}{\sigma_1-\sigma_2}\right) = \frac{I}{4\pi\sigma_1}\frac{\partial}{\partial n}\left(\frac{1}{r_{PC}}\right) + \frac{1}{4\pi}\int_s \frac{\rho(M)}{\varepsilon}\frac{\partial}{\partial n}\left(\frac{1}{r_{PM}}\right)dS . \qquad (I\text{-}24)$$

This is a Freldholm integral equation of the second kind. Note that the equation has the units of electric field strength.

We next evaluate the singularity in the integral. The integrand gives the electric field at P due to charge at M. Recognizing this,we may evaluate the singularity by determining the electric field at M due to charge at M. Referring back to boundary condition (ii) and equation (I-20), we have

$$\left(E_{n_1} - E_{n_2}\right)\Big|_s = \frac{\rho}{\varepsilon} . \qquad (I\text{-}25)$$

The electric field due to the charge at the singularity is symmetric about the surface. Thus,

$$E_{n_1} = -E_{n_2} , \qquad (I\text{-}26)$$

and

$$E_{n_1} = \frac{\rho}{2\varepsilon} . \qquad (I\text{-}27)$$

Equation (I-27) gives the value of the singularity as:

$$\frac{\rho}{2\varepsilon} . \qquad (I\text{-}28)$$

By removing the singularity from the integral in equation (I-24), we obtain

$$\frac{\rho(P)}{2\varepsilon} = k\left[\frac{I}{4\pi\sigma_1}\frac{\partial}{\partial n}\left(\frac{1}{r_{PC}}\right) + \frac{1}{2\pi}\int_{S'}\frac{\rho(M)}{2\varepsilon}\frac{\partial}{\partial n}\left(\frac{1}{r_{PM}}\right)\right]dS \quad , \qquad (I\text{-}29)$$

where the prime on s indicates that the singularity at P is not included in the integration and where $k = (\sigma_1-\sigma_2)/(\sigma_1+\sigma_2)$.

APPENDIX II

MAGNETIC FIELD OF A FINITE CURRENT FILAMENT

The magnetic field produced by current flow in an arbitrarily oriented, straight length of insulated wire, can be found by applying the Biot-Savart Law.

If, as shown in Figure II-1, a current of strength I flows in a straight wire from P_1 to P_2 the magnitude of the magnetic field at P_0 can be shown to be given by

$$B = \frac{\mu I(\cos\phi_1 - \cos\phi_2)}{4\pi R_1 \sin\phi_1} \qquad (II\text{-}1)$$

To express this magnetic field as a vector in rectangular coordinates, we use the following relations:

$$P_0 = (x_0, y_0, z_0)$$

$$P_1 = (x_1, y_1, z_1)$$

$$P_2 = (x_2, y_2, z_2)$$

$$R_1 = |\bar{P}_1 - \bar{P}_0| = \sqrt{(x_1-x_0)^2 + (y_1-y_0)^2 + (z_1-z_0)^2}$$

$$P_{12} = |\bar{P}_1 - \bar{P}_2| = \sqrt{(x_1-x_2)^2 + (y_1-y_2)^2 + (z_1-z_2)^2}$$

$$\cos\phi_1 = \frac{(x_1-x_0)(x_1-x_2) + (y_1-y_0)(y_1-y_2) + (z_1-z_0)(z_1-z_2)}{R_1 P_{12}}$$

$$\sin\phi = \sqrt{1 - \cos^2\phi_1}$$

$$R_2 = |\bar{P}_2 - \bar{P}_0| = \sqrt{(x_2-x_0)^2 + (y_2-y_0)^2 + (z_2-z_0)^2}$$

$$\cos\phi_2 = \frac{(x_2-x_0)(x_1-x_2) + (y_2-y_0)(y_1-y_2) + (z_2-z_0)(z_1-z_2)}{R_2 P_{12}}$$

The unit vector $\hat{u}$ perpendicular to the plane containing vectors $\bar{P}_{12}$ and $\bar{R}_1$ is given by

$$\hat{u} = \frac{\bar{U}}{|\bar{P}_{12} \times \bar{R}_1|} ,$$

where $\bar{U} = \bar{P}_{12} \times \bar{R}_1$,

and
$$U_x = \hat{i}\,[(y_2-y_1)(z_1-z_0) - (z_2-z_1)(y_1-y_0)] ,$$
$$U_y = -\hat{j}[(x_2-x_1)(z_1-z_0) - (z_2-z_1)(x_1-x_0)] ,$$
$$U_z = \hat{k}\,[(x_2-x_1)(y_1-y_0) - (y_2-y_1)(x_1-x_0)] ,$$
$$L = |\bar{P}_{12} \times \bar{R}_1 = \sqrt{U_x^2 + U_y^2 + U_z^2} .$$

Then
$$u_x = \frac{U_x}{L} ,$$
$$u_y = \frac{U_y}{L} ,$$
$$u_z = \frac{U_z}{L} .$$

And finally,

$$B = (\hat{i}u_x + \hat{j}u_y + \hat{k}u_z)\,\frac{\mu I(\cos\phi_2 - \cos\phi_1)}{4\pi R_1 \sin\phi_1} . \qquad (II\text{-}2)$$

The magnetic field of a curved wire is found by approximating the curved path of the wire with a number of straight wire segments and summing the fields produced by each segment.

APPENDIX III

DERIVATION OF THE MODIFIED BIOT-SAVART LAW FOR SOLENOIDAL CURRENT FLOW

The following development of an integral equation for the magnetic field in terms of the cross product of electric field and gradient of conductivity follows that of Edwards et al (1978).

The magnetic field $\bar{B}(\bar{r})$ external to a volume V containing a distribution of current $\bar{J}(\bar{r}')$ may be written as

$$\bar{B}(\bar{r}) = \frac{\mu}{4\pi}\int_V \bar{J}(\bar{r}') \times \nabla' \left(\frac{1}{|\bar{r}-\bar{r}'|}\right) dv' \ . \qquad \text{(III-1)}$$

Applying the vector identity

$$\nabla' \times (\phi\bar{A}) = \phi\nabla' \times \bar{A} - \bar{A} \times \nabla'\phi \ , \qquad \text{(III-2)}$$

where $\bar{A}$ is a vector and ϕ a scalar, and Stokes theorem,

$$\int_V \nabla' \times \bar{A} dv' = \oint_S \hat{n} \times \bar{A} ds' \ , \qquad \text{(III-3)}$$

where S is the surface bounding the volume V and $\hat{n}(\bar{r}')$ is the unit vector outward normal to S, the magnetic field may be rewritten in the form

$$\bar{B}(\bar{r}) = \frac{\mu}{4\pi}\int_V \frac{\nabla' \times \bar{J}(\bar{r}')}{|\bar{r}-\bar{r}'|} dV' - \frac{\mu}{4\pi}\oint_S \hat{n} \times \left\{\frac{\bar{J}(\bar{r}')}{|\bar{r}-\bar{r}'|}\right\} dS' . \qquad \text{(III-4)}$$

Consider the volume V to be the half-space z>0, on and beneath the surface of the earth, where the current density $\bar{J}(\bar{r}')$ is generated by flow from a current electrode in V.

The boundaries of the surface S are selected to be a plane just above the earth's surface and a hemisphere of large radius R which in the limit completely encloses V. The surface integral over S vanishes on the plane boundary where $\bar{J} = 0$; it also vanishes on the hemispherical surface provided that $\bar{J}(\bar{r})$ falls off at a rate greater than 1/R. Whence,

$$\bar{B}(\bar{r}) = \frac{\mu}{4\pi} \int_V \frac{\nabla' \times \bar{J}(\bar{r}')}{|\bar{r}-\bar{r}'|} \, dV' \ . \qquad \text{(III-5)}$$

Everywhere within the earth, we define an electric potential $\phi(\bar{r}')$ related to current density through the local conductivity $\sigma(\bar{r}')$ by

$$\bar{J}(\bar{r}') = -\sigma(\bar{r}')\nabla'\phi(\bar{r}'). \qquad \text{(III-6)}$$

Using the vector identity (III-2) and observing that $\nabla' \times \nabla'\phi \equiv 0$, we obtain

$$\bar{B}(\bar{r}) = \frac{\mu}{4\pi} \int_V \frac{\nabla'\phi(\bar{r}') \times \nabla'\sigma(\bar{r}')}{|\bar{r}-\bar{r}'|} \, dV' \ . \qquad \text{(III-7)}$$

When the conductivity changes only across surfaces, equation (III-7) takes the final form

$$\bar{B}(\bar{r}) = \frac{\mu}{4\pi} \int_S \frac{\nabla'\phi(\bar{r}') \times \nabla'\sigma(\bar{r}')}{|\bar{r}-\bar{r}'|} \, dS'. \qquad \text{(III-8)}$$

APPENDIX IV

TERRAIN PROGRAM LISTING

```
C************************  PROGRAM  MTDPO  ********************************
C
C          *****    VERSION 1.0    9 SEPT 1979    *****
C          ***** LAST MODIFICATION  23 MARCH 1982 *****
C
C  AUTHOR      GARY  L. OPPLIGER
C              ENGINEERING GEOSCIENCE DEPT.
C              UNIV. OF CALIF. BERKELEY
C
C  PURPOSE     CALCULATES ELECTRIC POTENTIAL, RESISTIVITY, AND MAGNETIC
C              FIELDS DUE TO DIRECT CURRENT FLOW IN AN EARTH WITH
C              ARBITRARY 3-D TOPOGRAPHY AND UNIFORM CONDUCTIVITY.
C
C  REFERENCE   OPPLIGER, G. L., 1982, THREE-DIMENSIONAL TERRAIN EFFECTS
C              IN ELECTRICAL AND MAGNETOMETRIC RESISTIVITY SURVEYS: PH.D.
C              THESIS, UNIVERSITY OF CALIFORNIA, BERKELEY.
C
C  NUMERICAL TECHNIQUE
C              THE SURFACE CHARGE INTEGRAL EQUATION TECHNIQUE IS USED
C              TO SOLVE THE DIRECT CURRENT BOUNDARY PROBLEM AND OBTAIN
C              SOLUTIONS FOR ELECTRIC POTENTIAL AND ELECTRIC FIELDS.
C              MAGNETIC FIELDS ARE FOUND BY EVALUATING A SURFACE INTEGRAL
C              INVOLVING SURFACE ELECTRIC FIELDS AND SURFACE SLOPES.
C
C  UNITS OF CALCULATED FIELDS
C              POTENTIAL                =   VOLTS
C              APPARENT RESISTIVITY     =   OHM-METERS
C              MAGNETIC FIELD           =   MILLIGAMMAS
C
C************************************************************************
C
C
C                 DESCRIPTION OF PARAMETER CARDS
C
C                   ***** PARAMETER CARD 1 *****
C PARAMETER
C   NAME       FIELD         FORMAT
C
C   NPL      COL 7-10        INTEGER
C            SPECIFIES ROW AND COL SIZE OF THE MAIN MODEL GRID AREA.
C            NPL CANNOT BE LARGER THAN THE N*N ARRAY SIZE DEFINED BY
C            DIMENSION STATEMENTS. A TYPICAL VALUE FOR NPL IS 41.
C
C   NT       COL 17-20       INTEGER
C            SPECIFIES ROW AND COL DIMENSION OF THE OUTER SURFACE GRID
C            SURROUNDING THE MAIN MODEL GRID.(THIS OUTER SURFACE IS USED
C            ONLY FOR SURFACE CHARGE.) A TYPICAL VALUE FOR NT IS 20.
C
C   NPIN     COL 27-30       INTEGER
C            SPECIFIES THE NUMBER OF ROWS (AND COLS) OF THE OUTER GRID
C            WHICH ARE CONTAINED WITHIN THE MAIN MODEL GRID.
C            ***NOTE*** (NT-NPIN) MUST BE AN EVEN INTEGER. A TYPICAL
C            VALUE FOR NPIN IS 6.
C
C   MTIME    COL 37-40       INTEGER
C            SPECIFIES THE NUMBER OF TIMES THE SURFACE CHARGE SOLUTION
C            IS RELAXED. TYPICAL VALUES FOR MTIME ARE 2 AND 3.
C
C   NPUQ     COL 47-50       INTEGER
C            CONTROLS CREATION OF PUNCHED CARD OUTPUT OF SURFACE CHARGE
C            SOLUTION. NPUQ = 0   FOR NO PUNCHED CARDS
C                      NPUQ = 1   FOR PUNCHED CARDS
C
```

```
C   FLATZ   COL 51-60       FLOATING
C           SPECIFIES THE ELEVATION IN MAP UNITS (FEET OR METERS) OF
C           THE HORIZONTAL SURFACE USED FOR THE SEPARATION OF HALF-SPACE
C           AND TOTAL (TERRAIN) MAGNETIC FIELDS. FLATZ IS USUALLY SET TO
C           THE MODEL SURFACE ELEVATION AT OR ABOVE THE CENTRAL OR MAIN
C           CURRENT ELECTRODE.
C
C   EFLATZ  COL 61-70       FLOATING
C           SPECIFIES THE ELEVATION IN MAP UNITS OF THE HORIZONTAL OUTER
C           GRID SURFACE SURROUNDING THE MAIN MODEL AREA. SURFACE CHARGE
C           IS INDUCED ON THIS SURFACE GRID ONLY BY CURRENT SOURCES AND
C           IMAGES. THE MAIN MODEL SURFACE GRID SHOULD HAVE ITS
C           BOUNDARIES TAPERED TO CONNECT SMOOTHLY WITH THE OUTER
C           SURFACE SPECIFIED BY EFLATZ. GRIDDING OF THIS OUTER SURFACE
C           IS CONTROLLED BY PARAMETERS NT AND NPIN.
C
C
C                   ***** PARAMETER CARD 2 *****
C PARAMETER
C   NAME      FIELD         FORMAT
C
C   NSRC    COL 7-10        INTEGER
C           SPECIFIES THE NUMBER OF CURRENT SOURCES (ELECTRODES) PRESENT
C           IN THE MODEL.
C
C   NSRCIM  COL 17-20       INTEGER
C           SPECIFIES THE TOTAL NUMBER OF CURRENT SOURCES AND IMAGES
C           USED FOR THE MODEL.
C
C   NSEG    COL 27-30       INTEGER
C           SPECIFIES THE NUMBER OF CURRENT CARRYING STRAIGHT WIRE
C           SEGMENTS USED FOR THE MODEL.
C
C   SCALE   COL 31-40       FLOATING
C           SPECIFIES THE INTERVAL IN METERS BETWEEN MODEL GRID POINTS.
C
C   SIGMA   COL 41-50       FLOATING
C           SPECIFIES CONDUCTIVITY OF THE EARTH MODEL IN MHOS/METER.
C
C   FTMT    COL 51-60       FLOATING
C           FACTOR TO CONVERT UNITS OF ALL INPUT COORDINATES (EXCEPT
C           MODEL SURFACE ELEVATIONS) TO UNITS OF METERS. FOR EXAMPLE
C           FTMT = 0.3048 IF COORDINATES WERE GIVEN IN FEET AND
C           FTMT = 1.0    IF COORDINATE WERE GIVEN IN METERS.
C
C   ATTN    COL 61-70       FLOATING
C           FACTOR TO CONVERT MODEL SURFACE ELEVATIONS TO METERS.
C           FOR EXAMPLE,  ATTN = 0.3048 IF SURFACE ELEVATIONS WERE
C           GIVEN IN FEET, AND  ATTN = 1.0 IF SURFACE ELEVATIONS WERE
C           GIVEN IN METERS.
C
C
C                   ***** PARAMETER CARD 3 *****
C PARAMETER
C   NAME      FIELD         FORMAT
C
C   IW(1)   COL 7-10        INTEGER
C           SPECIFIES THE RADIUS (IN TERMS OF THE NUMBER OF ROWS OR
C           COLUMNS) OF INFLUENCE OF THE SURFACE CHARGE RELAXATION
C           PROCESS. THE MAXIMUM AREA OF INFLUENCE IS OBTAINED BY
C           SETTING IW(1) = NPL-1. THIS IS THE SAFEST VALUE FOR IW(1).
C           SMALLER VALUES MAY BE SPECIFIED TO SAVE COMPUTATION TIME
C           ONLY IF IT CAN BE DETERMINED THAT THE EXCLUDED DISTANT
C           ELEMENTS ARE UNIMPORTANT TO THE CHARGE RELAXATION PROCESS.
C
C   IW(2)   COL 17-20       INTEGER
```

```
C           SPECIFIES THE MAXIUM DISTANCE (IN TERMS OF THE NUMBER OF
C           ROWS OR COLUMNS) FROM THE CENTER OF THE MODEL SURFACE AT
C           WHICH MAGNETIC FIELD VALUES WILL BE CALCULATED. SET
C           IW(2) = (NPL-1)/2  TO CALCULATE MAGNETIC FIELD VALUES OVER
C           THE COMPLETE MODEL GRID.
C
C   IW(3)   COL 27-30       INTEGER
C           CONTROLS THE EXTENT OF INTEGRATION OVER SURFACE CHARGE TO
C           DETERMINE THE POTENTIAL. FOR BEST RESULTS IW(3) = NPL-1 .
C
C   NSKPX   COL 37-40       INTEGER
C   NSKPY   COL 47-50       INTEGER
C           CONTROLS THE SKIPPING OF ROWS (NSKPX) AND COLUMNS (NSKPY)
C           IN THE CALCULATION OF MAGNETIC FIELDS ON THE MODEL SURFACE.
C           NSKPX=1 AND NSKPY=1 CAUSES THE MAGNETIC FIELDS TO BE
C           DETERMINED AT ALL GRID POINTS. NSKPX=2 AND NSKPY=2 CAUSES
C           THE MAGNETIC FIELDS TO BE DETERMINED AT EVERY 4TH GRID
C           POINT. ETC..
C
C
C                 ***** PARAMETER CARD 4 *****
C
C           THE PARAMETERS ON CARD 4 CONTROL THE CREATION OF PRINTER,
C           PLOTTER, AND PUNCHED CARD OUTPUT FOR THE CALCULATED
C           ELECTRIC AND MAGNETIC FIELD VALUES.
C           DEFINITIONS OF CONTROL VALUES -
C                0.0  FIELDS ARE NOT CALCULATED OR OUTPUT.
C                1.0  FIELDS ARE PRINTED AND PLOTTED.
C                2.0  FIELDS ARE PRINTED PLOTTED AND PUNCHED.
C
C PARAMETER
C   NAME      FIELD          FORMAT
C
C   BWOW    COL 7-10        FLOATING
C           FOR OUTPUT OF MAGNETIC B FIELDS DUE ONLY TO CURRENT FLOW
C           IN THE EARTH MODEL, DOES NOT INCLUDE FIELDS DUE TO
C           CURRENT FLOW IN THE WIRE SEGMENTS.
C
C   RBF     COL 17-20       FLOATING
C           FOR OUTPUT OF HALF-SPACE REDUCED MAGNETIC B FIELDS. I.E.
C           THE ABOVE BWOW FIELDS WITH THE HALF-SPACE NORMAL FIELDS
C           SUBTRACTED. THIS IS THE ANOMALOUS MAGNETIC FIELD DUE TO
C           THE TOPOGRAPHY.
C
C   BWW     COL 27-30       FLOATING
C           FOR OUTPUT OF TOTAL MAGNETIC B FIELD. THIS FIELD INCLUDES
C           CONTRIBUTIONS DUE TO CURRENT FLOW IN THE EARTH AND IN THE
C           WIRE SEGMENTS.
C
C   BANM    COL 37-40       FLOATING
C           FOR OUTPUT OF THE PERCENT MAGNETIC FIELD TERRAIN ANOMALY.
C           THE PERCENTAGE IS CALCULATED RELATIVE TO THE MAGNITUDE OF
C           HALF-SPACE NORMAL MAGNETIC FIELD.
C
C   EPOT    COL 47-50       FLOATING
C           FOR OUTPUT OF ELECTRIC POTENTIAL CALCULATED RELATIVE TO
C           A REFERENCE POTENTIAL ELECTRODE AT INFINITY.
C
C   APPR    COL 57-60       FLOATING
C           FOR OUTPUT OF APPARENT RESISTIVITIES CALCULATED RELATIVE
C           TO A REFERENCE POTENTIAL ELECTRODE AT INFINITY.  THIS
C           CALCULATION USES FLAT EARTH GEOMETRIC FACTORS AND STRAIGHT
C           LINE DISTANCES BETWEEN ELECTRODES. THE RESULT IS PROPERLY
C           CALLED THE TERRAIN EFFECT APPARENT RESISTIVITY ANOMALY.
C
C
```

```
C                    ***** PARAMETER CARD 5 *****
C PARAMETER
C   NAME       FIELD          FORMAT
C
C  GREFX     COL 11-20        FLOATING
C            NORTHING (X) OF ORIGIN OF MODEL SURFACE GRID
C            IN MAP UNITS (FEET OR METERS).
C
C  GREFY     COL 21-31        FLOATING
C            EASTING (Y) OF ORIGIN OF MODEL SURFACE GRID
C            IN MAP UNITS (FEET OR METERS).
C
C
C
C               ***** CURRENT SOURCE AND IMAGE CARDS *****
C
C            THESE PARAMETERS SPECIFY THE COORDINATES AND STRENGTHS OF
C            THE CURRENT SOURCES AND IMAGE SOURCES USED IN THE MODEL.
C            ONE CARD IS REQUIRED FOR EACH CURRENT SOURCE OR IMAGE.
C             **NOTE**  CURRENT SOURCE CARDS MUST BE GROUPED TOGETHER
C            AND READ BEFORE THE IMAGE SOURCE CARDS.
C
C PARAMETER
C   NAME          FIELD         FORMAT
C
C SOURCE(M,1)  COL 11-20     FLOATING
C            NORTHING OR X COORDINATE OF M TH CURRENT SOURCE OR IMAGE,
C            SPECIFIED IN MAP UNITS (FEET OR METERS).
C
C SOURCE(M,2)  COL 21-30     FLOATING
C            EASTING OR Y COORDINATE OF M TH CURRENT SOURCE OR IMAGE,
C            SPECIFIED IN MAP UNITS (FEET OR METERS).
C
C SOURCE(M,3)  COL 31-40     FLOATING
C            ELEVATION OR Z COORDINATE OF M TH CURRENT SOURCE OR IMAGE,
C            IN MAP UNITS (FEET OR METERS) RELATIVE TO THE DATUM USED
C            FOR THE MODEL TOPOGRAPHY.
C
C SOURCE(M,4)  COL 41-50     FLOATING
C            STRENGTH AND POLARITY OF CURRENT SOURCE OR IMAGE SOURCE
C            SPECIFIED IN AMPERES.
C
C
C                    ***** WIRE SEGMENT CARDS *****
C
C            TWO CARDS ARE REQUIRED TO SPECIFY EACH WIRE SEGMENT.
C            THE FIRST CARD IN EACH PAIR SPECIFIES THE STARTING POINT OF
C            THE WIRE SEGMENT. THE SECOND CARD SPECIFIES THE END POINT.
C            UP TO 40 WIRE SEGMENTS MAY BE SPECIFIED.
C            THE PROGRAM ASSUMES A POSITIVE CURRENT OF WAMP(N) AMPERES
C            FLOWS FROM THE FIRST END POINT, ENDP(K,1,N), TO THE SECOND
C            END POINT,  ENDP(K,2,N), SPECIFIED IN EACH CARD PAIR.
C            COORDINATES ARE GIVEN IN MAP UNITS (FEET OR METERS).
C            THE ELEVATION IS GIVEN RELATIVE TO THE DATUM USED FOR
C            THE MODEL SURFACE.
C
C PARAMETER
C   NAME          FIELD         FORMAT
C
C     FIRST CARD IN PAIR
C
C ENDP(1,1,N)  COL 11-20    FLOATING
C            NORTHING OR X COORDINATE OF STARTING LOCATION FOR THE
C            N TH WIRE SEGMENT IN MAP UNITS.
C
C ENDP(2,1,N)  COL 21-30    FLOATING
```

```
C            EASTING OR Y COORDINATE OF STARTING LOCATION FOR THE
C            N TH WIRE SEGMENT IN MAP UNITS.
C
C ENDP(3,1,N)  COL 31-40   FLOATING
C            ELEVATION OR Z COORDINATE OF STARTING LOCATION FOR THE
C            N TH WIRE SEGMENT IN MAP UNITS.
C
C WAMP(N)       COL 41-50   FLOATING
C            CURRENT FLOWING IN WIRE SEGMENT N FROM POINT 1 TO 2.
C            GIVEN IN +/-  AMPERES.
C
C     SECOND CARD IN PAIR
C
C ENDP(1,2,N)  COL 11-20   FLOATING
C            NORTHING OR X COORDINATE OF END LOCATION FOR THE N TH
C            WIRE SEGMENT IN MAP UNITS.
C
C ENDP(2,2,N)  COL 21-30   FLOATING
C            EASTING OR Y COORDINATE OF END LOCATION FOR THE N TH
C            WIRE SEGMENT IN MAP UNITS.
C
C ENDP(3,2,N)  COL 31-40   FLOATING
C            ELEVATION OR Z COORDINATE OF END LOCATION FOR THE N TH
C            WIRE SEGMENT IN MAP UNITS.
C
C WAMP(N)       COL 41-50   FLOATING
C            CURRENT FLOWING IN WIRE SEGMENT N FROM POINT 1 TO 2.
C            GIVEN IN +/- AMPERES.
C
C
C****************** END OF PARAMETER CARDS ************************

C*** JOB CONTROL CARDS FOR LAWRENCE BERKELEY LABORATORY  CDC7600  ***

MMR,12,300.801077,OPPLIGER
*HOLDOUT
*USERPR
FTN4,OPT=2,R=2,PL=9000.
FETCHPS,GARYO,TAPE2,DATA15.
FETCHPS,IDDS,ULIB,ULIBX.
FETCHPS,GPACBN7,GPAC,SCBN.
LINK,F=LGO,P=ULIB,F=GPAC,X.
REWIND,FILM.
COPY,FILM,FILM1.
REWIND,FILM,FILM1.
DISPOSE,FILM1=3M,M=ME.
DISPOSE,FILM=MF,M=ME.
EXIT.
DUMP,0.

      PROGRAM MTOPO(FILM,TAPE2,OUTPUT,PUNCH,TAPE6=OUTPUT,TAPE8=PUNCH)
      COMMON/IGSZZZ/Z(200)
      DIMENSION DAT(41,41),DATY(41,41),ENDP(3,2,40),WAMP(40),AA(3)
      DIMENSION ELV(41,41),FX(41,41),FY(41,41),PFN(41,41),Q(41,41)
      DIMENSION PRVQ(41,41),POT(41,41),EX(41,41),EY(41,41),EZ(41,41)
      DIMENSION BFLD(41,41,3),EFX(41,41),EFY(41,41),SOURCE(10,4)
      DIMENSION APR(41,41),POTQ(41,41),FXY(41,41),SELV(41,41)
      DIMENSION AEX(41,41),AEY(41,41),IW(4)
      EQUIVALENCE (FX(1,1),AEX(1,1))
      EQUIVALENCE (FY(1,1),AEY(1,1))
      EQUIVALENCE (DAT(1,1),FXY(1,1))
      EQUIVALENCE (PFN(1,1),POT(1,1),EX(1,1))
      EQUIVALENCE (PRVQ(1,1),EFY(1,1),BFLD(1,1,1))
      EQUIVALENCE (Q(1,1),EFX(1,1),BFLD(1,1,2))
      EQUIVALENCE (APR(1,1),BFLD(1,1,3))
      EQUIVALENCE (ELV(1,1),SELV(1,1))
```

```
C EQUIVALENCE OF SELV AND ELV SHOULD BE REMOVED WHEN THEY REPRESENT
C DIFFERENT SURFACES.

C INITIALIZE CONTOUR PLOT PARAMETERS
C THE FOLLOWING 3 CALLS ARE TO LBL BERKELEY PLOT SUBROUTINES.
      A2=10HMMR PLOTS
C     CALL MODESG(Z,6,A2)
C     CALL SETSMG(Z,19,100.0)
C     CALL SETSMG(Z,20,100.0)

C   *******       BEGIN READING PARAMETER CARDS        *******

C READ CARD 1 PARAMETERS
      READ(2,180)NPL,NT,NPIN,MTIME,NPUQ,FLATZ,EFLATZ
  180 FORMAT(5(6X,I4),2F10.2)
C READ CARD 2 PARAMETERS
      READ(2,182)NSRC,NSRCIM,NSEG,SCALE,SIGMA,FTMT,ATTN
  182 FORMAT(3(6X,I4),F10.4,2F10.6,F12.7)
C READ CARD 3 PARAMETERS
      READ(2,190)IW(1),IW(2),IW(3),NSKPX,NSKPY
  190 FORMAT(5(6X,I4))
C READ CARD 4 PARAMETERS
      READ(2,184) BWOW,RBF,BWW,BANM,EPOT,APPR
  184 FORMAT(6X,F4.0,5F10.0)
C READ CARD 5 PARAMETERS
      READ(2,186) GREFX, GREFY
  186 FORMAT(10X,2F10.0)
C
      WRITE(6,200)(NPL,NT,NPIN,MTIME,NPUQ,FLATZ,EFLATZ)
  200 FORMAT(1H1,5X,*NPL=*,I4,4X,*NT=*,I4,4X,*NPIN=*,I4,
     C 4X,*MTIME=*,I2,4X,*NPUQ=*,I2,4X,*FLATZ=*,F14.6,4X,
     C *EFLATZ=*,F14.6)
      WRITE(6,210)NSRC,NSRCIM,NSEG,SCALE,SIGMA,FTMT,ATTN
  210 FORMAT(3X,*NSRC=*,I3,3X,*NSRCIM=*,I3,3X,*NSEG=*,I3,
     C 3X,*SCALE=*,F14.6,3X,*SIGMA=*,F14.9,3X,*FTMT=*,F14.9,
     C 3X,*ATTN=*,F14.9)
      WRITE(6,220)IW(1),IW(2),IW(3),NSKPX,NSKPY
  220 FORMAT(5X,*IW(1)=*,I3,4X,*IW(2)=*,I3,4X,
     C *IW(3)=*,I3,4X,*NSKPX=*,I3,4X,*NSKPY=*,I3)
      WRITE(6,212)BWOW,RBF,BWW,BANM,EPOT,APPR
  212 FORMAT(5X,*BWOW=*,F3.1,4X,*RBF=*,F3.1,4X,*BWW=*,F3.1,4X,
     C *BANM=*,F3.1,4X,*EPOT=*,F3.1,4X,*APPR=*,F3.1)
      WRITE(6,214) GREFX, GREFY
  214 FORMAT(5X,*COORDINATES OF GRID POINT (1,1) IN MAP UNITS*,
     C * NORTH= *,F12.2,* EAST= *,F12.2)
C
      DO 15 M=1,NSRCIM
C READ CURRENT SOURCE AND IMAGE CARDS
   15 READ(2,110)(SOURCE(M,N),N=1,4)
  110 FORMAT(10X,4F10.2)
      DO 225 M=1,NSRCIM
  225 WRITE(6,230)(SOURCE(M,N),N=1,4)
  230 FORMAT(2X,*SOURCE/IMAGE MAP COORDINATES  NORTH,  EAST,  *,
     C   *ELEVATION,  AMPERES*,/,4(2X,F16.6))
      IF(NSEG.EQ.0)GO TO 231
      DO 113 I=1,NSEG
      DO 113 M=1,2
C READ WIRE SEGMENT CARDS
      READ(2,111) ((ENDP(N,M,I),N=1,3),WAMP(I))
  111 FORMAT(10X,4F10.2)
  113 WRITE(6,116) ((ENDP(N,M,I),N=1,3),WAMP(I))
  116 FORMAT(2X,*WIRE END POINT MAP COORDINATES NORTH,  EAST,  *,
     C  *ELEVATION,  AMPERES*,/,4(2X,F16.6))
  231 CONTINUE

C READ GRID OF ELEVATION VALUES
```

```
C      DO 20 N=1,NPL
C   20 READ(2,100)(ELV(M,N),M=1,NPL)
  100 FORMAT(12F6.0)

C OR CREATE A MODEL SURFACE BY CALLING SUBROUTINE CSURFS
       CALL CSURFS(NPL,ELV,SCALE,SELV)

C    *******         END READING PARAMETER CARDS        *******

C    *******      SCALE COORDINATES AND ELEVATIONS      *******

C CALCULATE MEAN ELEVATION
       AVG=0.0
       DO 21 M=1,NPL
       DO 21 N=1,NPL
    21 AVG=ELV(M,N)+AVG
       AVG=AVG/FLOAT(NPL*NPL)
C SCALE AND CHANGE SIGN OF ELEVATIONS (Z AXIS IS + DOWNWARD)
       CC = - ATTN/SCALE
       DO 22 M=1,NPL
       DO 22 N=1,NPL
    22 ELV(M,N)=CC*ELV(M,N)

C WHEN ELV AND SELV ARE EQUIVALENCED SELV SHOULD NOT BE SCALED BY CC
C      DO 23 M=1,NPL
C      DO 23 N=1,NPL
C   23 SELV(M,N)=CC*SELV(M,N)

       AVG=ATTN*AVG
       WRITE(6,27)AVG
    27 FORMAT(3X,'AVERAGE ELEVATION IN METERS IS ',G14.6)
       FLATZ =  - FTMT*FLATZ/SCALE
       EFLATZ =  - FTMT*EFLATZ/SCALE
       DO 17 M=1,NSRCIM
       SOURCE(M,1) = FTMT*( SOURCE(M,1)-GREFX )/SCALE + 1.0
       SOURCE(M,2) = FTMT*( SOURCE(M,2)-GREFY )/SCALE + 1.0
    17 SOURCE(M,3) = - FTMT*SOURCE(M,3)/SCALE
       DO 227 M=1,NSRCIM
   227 WRITE(6,232)(SOURCE(M,N),N=1,4)
   232 FORMAT(2X,'SOURCE/IMAGE COORDINATES IN GRID UNITS RELATIVE',
      C    ' TO (0,0)   NORTH, EAST, ELEVATION',/,3(2X,F14.6))
       IF(NSEG.EQ.0)GO TO 233
       DO 119 I=1,NSEG
       DO 119 NP=1,2
       ENDP(1,NP,I) = FTMT*( ENDP(1,NP,I)-GREFX )/SCALE + 1.0
       ENDP(2,NP,I) = FTMT*( ENDP(2,NP,I)-GREFY )/SCALE + 1.0
   119 ENDP(3,NP,I) = - FTMT*ENDP(3,NP,I)/SCALE
       DO 124 I=1,NSEG
       DO 124 M=1,2
   124 WRITE(6,126)(ENDP(N,M,I),N=1,3)
   126 FORMAT(2X,'WIRE END POINT COORDINATES IN GRID UNITS RELATIVE',
      C    ' TO (0,0)   NORTH, EAST, ELEVATION',/,3(2X,F14.6))
   233 CONTINUE
C PRINT AND PLOT ELEVATIONS
       A1=10H ELV
       CALL PRNTAL(NPL,ELV,A1)
       CALL PLOTAL(ELV,NPL,A1,DAT)

C    *******   CALCULATE SLOPES OF SURFACE ELEMENTS   *******

       CALL SLOPE(NPL,ELV,FX,FY)
C      A1=10HSURFACE FX
C      CALL PRNTAL(NPL,FX,A1)
C      A1=10HSURFACE FY
C      CALL PRNTAL(NPL,FY,A1)
```

```
C    *******  CALCULATE PRIMARY NORMAL COMPONENTS OF  *******
C    *******        ELECTRIC FIELD ON THE SURFACE     *******

      CALL NORMPE(NPL,ELV,SOURCE,PFN,Q,FX,FY,SIGMA,NSRCIM)
C THE E FIELDS ARE WEIGHTED BY THE AREA OF THE ELEMENT.
C THE NORMAL E FIELDS ARE USED AS STARTING VALUES IN THE

C    *******          RELAX SURFACE CHARGES           *******

      CALL RLXARY(NPL,PFN,Q,PRVQ,ELV,FX,FY,PRECHG,IW,MTIME)
C PRINT AND PLOT SURFACE CHARGE
      A1=10HCHARGE
      CALL PRNTAL(NPL,Q,A1)
      CALL PLOTAL(Q,NPL,A1,DAT)
      IF(NPUQ.EQ.0)GO TO 251
      WRITE(8,250)((Q(M,N),M=1,NPL),N=1,NPL)
  250 FORMAT(8E10.4)
  251 CONTINUE

C    ******* CALCULATE SURFACE POTENTIAL DUE TO SURFACE *******
C    *******      CHARGES, CURRENT SOURCES AND IMAGES   *******

      CALL POTENT(NPL,Q,ELV,POT,SOURCE,NSRCIM,SIGMA,IW,POTQ)

C    ******* ADD POTENTIAL DUE TO PRIMARY CHARGE ON THE *******
C    *******          COARSE OUTER MODEL GRID           *******

      CALL AUXPOT(NPL,POT,SIGMA,ELV,EFLATZ,NT,NPIN,SOURCE,NSRCIM,POTQ)
      DO 130 M=1,NPL
      DO 130 N=1,NPL
  130 POT(M,N)=POT(M,N)/SCALE
C PRINT POTENTIAL
      IF(EPOT.EQ.0.0)GO TO 35
      A1=10HPOTENTIAL
      CALL PRNTAL(NPL,POT,A1)
      CALL PLOTAL(POT,NPL,A1,DAT)
      IF(EPOT.NE.2.0)GO TO 35
      WRITE(8,250)((POT(M,N),M=1,NPL),N=1,NPL)
   35 CONTINUE
      IF(APPR.EQ.0.0)GO TO 38

C    ******* CALCULATE TERRAIN EFFECT APPARENT RESISTIVITY  *******
C    ******* (IN OHM-METERS) USING TOTAL MODEL E POTENTIAL, *******
C    ******* FLAT EARTH GEOMETRIC FACTORS, STRAIGHT LINE    *******
C    ******* DISTANCES, AND REFERENCE ELECTRODE AT INFINITY. *******

      CALL APRES(NPL,ELV,SOURCE,NSRC,POT,APR,SCALE)
      A1=10HAPP RESIS
      CALL PRNTAL(NPL,APR,A1)
      CALL PLOTAL(APR,NPL,A1,DAT)
      IF(APPR.NE.2.0)GO TO 38
      WRITE(8,250)((APR(M,N),M=1,NPL),N=1,NPL)
   38 CONTINUE

C    *******    CALCULATE PERCENT ELECTRIC FIELD ANOMALY    *******

C     CALL EPER(NPL,SOURCE,NSRC,POT,APR,EFX,EFY,FLATZ,SIGMA,SCALE)
C     A1=10HEX PER ANM
C     CALL PRNTAL(NPL,EFX,A1)
C     CALL PLOTAL(EFX,NPL,A1,DAT)
C     A1=10HEY PER ANM
C     CALL PRNTAL(NPL,EFY,A1)
C     CALL PLOTAL(EFY,NPL,A1,DAT)

      IF(BWOW+RBF+BWW+BANM.EQ.0.0)GO TO 65
```

```
C    *******     CALCULATE E FIELD ON MODEL SURFACE      *******

      CALL TEFLD(NPL,POTQ,EX,EY,EZ,FX,FY,EFX,EFY,FXY,
     C ELV,SOURCE,NSRCIM,SIGMA)
C E FIELD DUE TO SURFACE CHARGE IS FOUND FROM SLOPES OF POTENTIAL.
C E FIELD DUE TO SOURCES AND IMAGES IS CALCULATED FROM ANALYTIC FORMULA


C    ******* CALCULATE THE MAGNETIC FIELD (MILLIGAMMAS) DUE TO *******
C    ******* CURRENT FLOW IN THE EARTH BY AN INTEGRATION OVER  *******
C    *******   SURFACE ELECTRIC FIELDS AND TERRAIN SLOPES      *******

      CALL BFIELD(NPL,EX,EY,EZ,BFLD,SIGMA,SCALE,ELV,FX,FY,IW,NSKPX,NSKPY
     C,SELV)
C ROUTINE BFIELD INTEGRATES OVER TOTAL E FIELDS ON MAIN MODEL SURFACE

      CALL AUXB2(NPL,BFLD,SIGMA,SCALE,SELV,IW,FLATZ,AEX,AEY,
     C SOURCE,NSRC,NSKPX,NSKPY)
C ROUTINE AUXB2 ADDS EFFECT OF INTEGRATION OVER E OUTSIDE MODEL GRID
C BY SUBTRACTING AN INTEGRATION OVER HALF-SPACE E FIELDS ON THE MODEL
C GRID FROM THE THEORTICAL HALF-SPACE MAGNETIC FIELDS.
      NCTR=INT(FLOAT(NPL)/2.0) +1
      CALL WINDOW(NCTR,NCTR,IFX,ILX,IFY,ILY,NPL,2,IW)
      NK=0
      DO 320 I=IFX,ILX,NSKPX
  320 NK=NK+1
      AA(1)=10HBX W/O WR
      AA(2)=10HBY W/O WR
      AA(3)=10HBZ W/O WR
      IF(BWOW.EQ.0.0)GO TO 46
      DO 45 KK=1,3
      CALL PRINTA(BFLD(1,1,KK),IFX,ILX,IFY,ILY,NSKPX,NSKPY,AA(KK))
      IF(BWOW.NE.2.0)GO TO 45
      WRITE(8,250)((BFLD(M,N,KK),M=IFX,ILX,NSKPX),N=IFY,ILY,NSKPY)
   45 CALL GPLOT1(BFLD(1,1,KK),NPL,AA(KK),DAT,IFX,ILX,NSKPX,
     C IFY,ILY,NSKPY)
      A1=10HBWOW HORIZ
      CALL GPLOT3(BFLD(1,1,1),BFLD(1,1,2),NK,A1,DAT,DATY,
     C IFX,ILX,NSKPX,IFY,ILY,NSKPY)
   46 CONTINUE
      NFLAT=1
      IF(RBF+BANM.EQ.0.0)GO TO 52

C    ******* CALCULATE THE MAGNETIC FIELD TERRAIN EFFECT (IE  *******
C    ******* THE REDUCED FIELD) BY REMOVING THE HALF-SPACE OR *******
C    ******* NORMAL MAGNETIC FIELD FROM THE TOTAL FIELD.      *******

      CALL NORMB(IFX,ILX,NSKPX,IFY,ILY,NSKPY,SELV,BFLD,SOURCE,
     C NSRC,SCALE,-1.0,NFLAT,FLATZ)
      AA(1)=10HBX REDUCED
      AA(2)=10HBY REDUCED
      AA(3)=10HBZ REDUCED
      IF(RBF.EQ.0.0)GO TO 57
      A1=10HB HORIZ
      CALL GPLOT3(BFLD(1,1,1),BFLD(1,1,2),NK,A1,DAT,DATY,
     C IFX,ILX,NSKPX,IFY,ILY,NSKPY)
      DO 50 KK=1,3
      CALL PRINTA(BFLD(1,1,KK),IFX,ILX,IFY,ILY,NSKPX,NSKPY,AA(KK))
      CALL GPLOT1(BFLD(1,1,KK),NPL,AA(KK),DAT,IFX,ILX,NSKPX,
     C IFY,ILY,NSKPY)
      IF(RBF.NE.2)GO TO 50
      WRITE(8,250)((BFLD(M,N,KK),M=IFX,ILX,NSKPX),N=IFY,ILY,NSKPY)
   50 CONTINUE
   57 IF(BANM.EQ.0.0)GO TO 56

C    ******* CALCULATE PERCENT B FIELD ANOMALY NORMALIZED  *******
```

```
C    ******* BY TOTAL NORMAL (HALF-SPACE) FIELD MAGNITUDES *******

      CALL BANOMT(IFX,ILX,NSKPX,IFY,ILY,NSKPY,SELV,BFLD,SOURCE,
     C NSRC,SCALE,1.0)
      AA(1)=10HBX PER AMT
      AA(2)=10HBY PER AMT
      AA(3)=10HBZ PER AMT
      DO 310 KK=1,3
      CALL PRINTA(BFLD(1,1,KK),IFX,ILX,IFY,ILY,NSKPX,NSKPY,AA(KK))
  310 CALL GPLOT1(BFLD(1,1,KK),NPL,AA(KK),DAT,IFX,ILX,NSKPX,
     C IFY,ILY,NSKPY)
C CONVERT PER ANOM NORMALIZED BY TOTAL BACK TO REDUCED B FIELD.
      CALL BANOMT(IFX,ILX,NSKPX,IFY,ILY,NSKPY,SELV,BFLD,SOURCE,
     C NSRC,SCALE,-1.0)
   56 CONTINUE
C ADD BACK NORMAL B FIELD
      CALL NORMB(IFX,ILX,NSKPX,IFY,ILY,NSKPY,SELV,BFLD,SOURCE,NSRC,
     C SCALE,1.0,NFLAT,FLATZ)
   52 CONTINUE

      IF(BWW.EQ.0.0)GO TO 65
      IF(NSEG.EQ.0)GO TO 65

C    ******* ADD MAGNETIC FIELD DUE TO CURRENT FLOW IN WIRES *******
C    ******* TO MAGNETIC FIELD DUE CURRENT FLOW IN THE EARTH *******

      CALL BWIRE(NPL,SELV,BFLD,ENDP,NSEG,SCALE,NSKPX,NSKPY,IW,WAMP)
      AA(1)=10HBX TOTAL
      AA(2)=10HBY TOTAL
      AA(3)=10HBZ TOTAL
      A1=10HB T HORIZ
      CALL GPLOT3(BFLD(1,1,1),BFLD(1,1,2),NK,A1,DAT,DATY,IFX,ILX,
     C NSKPX,IFY,ILY,NSKPY)
      DO 55 KK=1,3
      CALL PRINTA(BFLD(1,1,KK),IFX,ILX,IFY,ILY,NSKPX,NSKPY,AA(KK))
      IF(BWW.NE.2.0)GO TO 55
      WRITE(8,250)((BFLD(M,N,KK),M=IFX,ILX,NSKPX),N=IFY,ILY,NSKPY)
   55 CALL GPLOT1(BFLD(1,1,KK),NPL,AA(KK),DAT,IFX,ILX,NSKPX,
     C IFY,ILY,NSKPY)

C PLOTING COMPLETE.  CALL LBL BERKELEY PLOTTING EXIT.
   65 CALL EXITG(Z)
      STOP
      END



      SUBROUTINE CSURF5(NPL,ELV,SCALE,SELV)
C CREATES A SMOOTH 2-D TERRAIN FEATURE
C THIS ROUTINE USED TO CREATE THESIS MODEL R-SA20
      DIMENSION ELV(41,41),SELV(41,41)
      SIGN=-1.0
C SIGN=-1.0 FOR HILLS , SIGN=1.0 FOR VALLEYS
      DEG=20.0
C DEG IS SLOPE OF TERRAIN FEATURE IN DEGREES
      A1=4.686117
      A2=4.640621
      A3=4.549633
      A4=5.459553
      A5=0.36397023
      A6=0.181985
      B1=0.045496
      B2=0.0909925
      B3=0.181985
      B4=0.36397023
      B5=0.181985
```

```
      B6=0.0909925
      PI=3.1415927
      C1=50.0/FLOAT(NPL-1)
      ANG1=PI*20.0/180.0
      ANG2=PI*DEG/180.0
      C2=C1*TAN(ANG1)/TAN(ANG2)
C C1 IS HORIZONTAL SCALE, C2 IS VERTICAL SCALE
      CNTRX=FLOAT(INT(FLOAT(NPL)/2.0)+1)
      DO 40 M=1,NPL
      X=ABS(FLOAT(M)-CNTRX)*C1
      Z=A1-B1*X
      IF(X.GT.1.0)Z=A2-B2*(X-1.0)
      IF(X.GT.2.0)Z=A3-B3*(X-2.0)
      IF(X.GT.3.0)Z=A4-B4*X
      IF(X.GT.14.0)Z=A5-B5*(X-14.0)
      IF(X.GT.15.0)Z=A6-B6*(X-15.0)
      IF(X.GT.16.0)Z=0.0
      Z=SIGN*SCALE*Z/C2
C Y IS STRIKE DIRECTION FOR 2-D MODELS
      DO 40 N=1,NPL
   40 ELV(M,N)=Z
      RETURN
      END



      SUBROUTINE NORMPE(NPL,ELV,SOURCE,PFN,Q,FX,FY,SIGMA,NSRCIM)
C CALCULATES PRIMARY NORMAL ELECTRIC FIELD DUE TO SOURCES
C AND IMAGES  AND INITALIZES Q(M,N) TO PFN(M,N)
C Q AND PFN ARE SCALED BY TRUE SURFACE AREA OF EACH ELEMENT
C TRUE AREA IS A FCN OF Z COMPONENT OF SURFACE NORMAL VECTOR
      DIMENSION ELV(41,41),PFN(41,41),Q(41,41),FX(41,41),FY(41,41)
      DIMENSION SOURCE(10,4)
C CON=1.0/4*PI*SIGMA
      CON=1.0/(12.5663706*SIGMA)
      DO 10 M=1,NPL
      DO 10 N=1,NPL
      EEX=0.0
      EEY=0.0
      EEZ=0.0
      DO 5 I=1,NSRCIM
      PX=SOURCE(I,1)
      PY=SOURCE(I,2)
      PZ=SOURCE(I,3)
      AMP=SOURCE(I,4)
      DX=FLOAT(M)-PX
      DY=FLOAT(N)-PY
      DZ=ELV(M,N)-PZ
      R1=SQRT(DX*DX+DY*DY+DZ*DZ)
      IF(R1.GT.0.05)GO TO 3
      R1=1.0
      AMP=0.0
    3 CR32=-AMP*CON/(R1*R1*R1)
      EEX=DX*CR32+EEX
      EEY=DY*CR32+EEY
    5 EEZ=DZ*CR32+EEZ
      PFN(M,N)=-EEX*FX(M,N)-EEY*FY(M,N)+EEZ
   10 Q(M,N)=PFN(M,N)
      RETURN
      END

      SUBROUTINE RLXARY(NPL,PFN,Q,PRVQ,ELV,FX,FY,PRECHG,IW,MTIME )
C ROUTINE FOR RELAXING SURFACE CHARGE ARRAY Q(M,N)
      DIMENSION PFN(41,41),Q(41,41),PRVQ(41,41),ELV(41,41)
      DIMENSION FX(41,41),FY(41,41)
      DIMENSION IW(4)
```

```
      PI2=6.2831853
      IIW=IW(1)
      NOI=0
    5 IF(NOI.GE.MTIME) RETURN
      NOI=NOI+1
C SAVE CHARGE FROM LAST ITERATION
      DO 10 M=1,NPL
      DO 10 N=1,NPL
   10 PRVQ(M,N)=Q(M,N)
      DO 20 M=1,NPL
      IFX=M-IIW
      IF(IFX.LT.1) IFX=1
      ILX=M+IIW
      IF(ILX.GT.NPL) ILX=NPL
      DO 20 N=1,NPL
      HGT=ELV(M,N)
      IFY=N-IIW
      IF(IFY.LT.1) IFY=1
      ILY=N+IIW
      IF(ILY.GT.NPL) ILY=NPL
      EEX=0.0
      EEY=0.0
      EEZ=0.0
      DO 15 I=IFX,ILX
      IX=M-I
      DX=FLOAT(IX)
      IXX=IX*IX
      DO 15 J=IFY,ILY
      IY=N-J
      DZ=HGT-ELV(I,J)
      R3=SQRT(FLOAT(IXX+IY*IY)+DZ*DZ)
      R3=R3*R3*R3
      IF(R3.LT..0000001) GO TO 15
C SKIP SINGULARITY
      QR3=Q(I,J)/R3
      EEX=EEX+DX*QR3
      EEY=EEY+FLOAT(IY)*QR3
      EEZ=EEZ-DZ*QR3
   15 CONTINUE
   20 Q(M,N)=PFN(M,N)+(FX(M,N)*EEX+FY(M,N)*EEY+EEZ)/PI2
      CALL CHANGE(PRVQ,Q,NOI,NPL)
      GO TO 5
      END

      SUBROUTINE CHANGE(PRVQ,Q,NOI,NPL)
C FINDS ABSOLUTE VALUE OF TOTAL CHARGE AND ABSOLUTE OF CHANGE IN
C CHARGE AFTER EACH ITERATION.
      DIMENSION Q(41,41),PRVQ(41,41)
      ABQ=0.0
      ABQP=0.0
      DO 10 M=1,NPL
      DO 10 N=1,NPL
      ABQ=ABQ+ABS(Q(M,N))
   10 ABQP=ABQP+ABS(Q(M,N)-PRVQ(M,N))
      IF(NOI.EQ.1)WRITE(6,20)
   20 FORMAT(1H1,5X,*ITERATION NO.    ABSOLUTE CHARGE TOTAL    *,
     C *ABSOLUTE CHANGE IN CHARGE*)
      WRITE(6,100)NOI,ABQ,ABQP
  100 FORMAT(13X,I2,12X,G15.9,12X,G15.9)
      RETURN
      END

      SUBROUTINE WINDOW(M,N,IFX,ILX,IFY,ILY,NPL,K,IW)
C SETS INTEGRATION WINDOW SIZE
      DIMENSION IW(4)
      IFX=M-IW(K)
```

```
      ILX=M+IW(K)
      IFY=N-IW(K)
      ILY=N+IW(K)
      IF(IFX.LT.1) IFX=1
      IF(ILX.GT.NPL) ILX=NPL
      IF(IFY.LT.1) IFY=1
      IF(ILY.GT.NPL) ILY=NPL
      RETURN
      END

      SUBROUTINE POTENT(NPL,Q,ELV,POT,SOURCE,NSRCIM,SIGMA,IW,POTQ)
C CALCULATES POTENTIAL FROM SURFACE CHARGES, CURRENT SOURCES
C AND IMAGES.
C POT IS TOTAL POTENTIAL.   POTQ IS POTENTIAL DUE TO SURFACE CHARGE
      DIMENSION Q(41,41),POTQ(41,41),ELV(41,41),POT(41,41)
      DIMENSION IW(4),SOURCE(10,4)
      CON1=1.0/(12.5663706*SIGMA)
      CON2=0.15915494
C CON2=1/(2*PI)
      IIW=IW(3)
      DO 40 M=1,NPL
      IFX=M-IIW
      ILX=M+IIW
      IF(IFX.LT.1) IFX=1
      IF(ILX.GT.NPL) ILX=NPL
      XM=FLOAT(M)
      DO 40 N=1,NPL
C SET INTEGRATION WINDOW SIZE
      IFY=N-IIW
      ILY=N+IIW
      IF(IFY.LT.1) IFY=1
      IF(ILY.GT.NPL) ILY=NPL
      HGT=ELV(M,N)
      YN=FLOAT(N)
      POTL=0.0
      DO 20 I=IFX,ILX
      IX=M-I
      IXX=IX*IX
      DO 20 J=IFY,ILY
      IY=N-J
      DZ=HGT-ELV(I,J)
      R=SQRT(FLOAT(IXX+IY*IY)+DZ*DZ)
      IF(R.GT.2.99)GO TO 13
      IF(R.GT.1.80)GO TO 15
      IF(R.GT.1.10)GO TO 17
      IF(R.GT.0.30)GO TO 19
C FOR SINGULARITY
      POTL=POTL+Q(I,J)*3.52549
      GO TO 20
C NEXT FOR DIAGONAL SURFACE ELEMENTS
   17 POTL=POTL+Q(I,J)*1.0249/R
      GO TO 20
C NEXT FOR ADJACENT ELEMENTS
   19 POTL=POTL+Q(I,J)*1.03805/R
      GO TO 20
C FOR NEXT DISTANT RING OF ELEMENTS
   15 POTL=POTL+Q(I,J)*1.010/R
      GO TO 20
C NEXT FOR DISTANT ELEMENTS
   13 POTL=POTL+Q(I,J)/R
   20 CONTINUE
C CALCULATE POTENTIAL DUE TO SOURCES AND IMAGES
      PPOT=0.0
      DO  5 I=1,NSRCIM
      PX=SOURCE(I,1)
      PY=SOURCE(I,2)
```

```
      PZ=SOURCE(I,3)
      AMP=SOURCE(I,4)
      DX=XM-PX
      DY=YN-PY
      DZ=HGT-PZ
    5 PPOT=PPOT+AMP/(SQRT(DX*DX+DY*DY+DZ*DZ)+1.0E-20)
      POTQ(M,N)=POTL*CON2
   40 POT(M,N)=POTL*CON2+PPOT*CON1
      RETURN
      END

      SUBROUTINE AUXPOT(NPL,POT,SIGMA,ELV,FLATZ,NT,NPIN,SOURCE,
     C NSRCIM,POTQ)
C ADDS POTENTIAL DUE TO CHARGES ON THE COARSE OUTER MODEL GRID
      DIMENSION ELV(41,41),SOURCE(10,4),X(35),Y(35),AEZ(35,35)
      DIMENSION POT(41,41),POTQ(41,41)
C NT IS LENGTH OF OUTER GRID
C NPIN IS NO. OF POINTS INSIDE INNER GRID
C (NT-NPIN) MUST BE AN EVEN NO.
C SD IS POINT SPACING ON OUTER GRID
      SD=FLOAT(NPL)/FLOAT(NPIN)
      NNN=NT-NPIN
      X(1)=0.5-(FLOAT(NNN)/2.0 -0.5)*SD
      Y(1)=0.5-(FLOAT(NNN)/2.0 -0.5)*SD
      DO 30 I=2,NT
      X(I)=X(1)+FLOAT(I-1)*SD
   30 Y(I)=Y(1)+FLOAT(I-1)*SD
C THE AREA OF EACH ELEMENT IS AE
      AE=SD*SD
C NOW CALCULATE ELECTRIC FIELD ON OUTER GRID
C DUE TO CURRENT SOURCES AND IMAGES.
      CON1=1.0/(4.0*3.14159265*SIGMA)
      CON2=1.0/(2.0*3.14159265)
      DO 10 M=1,NT
      DO 10 N=1,NT
      EEZ=0.0
      DO 15 I=1,NSRCIM
      PX=X(M)-SOURCE(I,1)
      PY=Y(N)-SOURCE(I,2)
      PZ=FLATZ-SOURCE(I,3)
      AMP=SOURCE(I,4)
      CR=1.0/SQRT(PX*PX+PY*PY+PZ*PZ)
      CRA=-CR*CR*CR*AMP*CON1
   15 EEZ=EEZ+PZ*CRA
C WEIGHT BY AREA AE
   10 AEZ(M,N)=EEZ*AE
C NEXT SET E FIELDS IN CENTRAL SECTION OF GRID TO ZERO
C THE FIRST POINT INSIDE INNER GRID IS (M,N) WHERE
C M=N=(NNN/2 +1)
      NF=NNN/2 +1
      NL=NF+NPIN-1
      DO 60 I=NF,NL
      DO 60 J=NF,NL
   60 AEZ(I,J)=0.0
C NEXT CALCULATE POTENTIAL FIELD DUE TO E FIELD ON OUTER GRID.
      DO 40 M=1,NPL
      FM=FLOAT(M)
      DO 40 N=1,NPL
      PP=0.0
      FN=FLOAT(N)
      PZ=ELV(M,N)-FLATZ
      PZZ=PZ*PZ
      DO 20 I=1,NT
      PX=FM-X(I)
      PXX=PX*PX
      DO 20 J=1,NT
```

```
      PY=FN-Y(J)
      R=SQRT(PXX+PY*PY+PZZ)
      IF(R.LE.0.001)GO TO 20
      PP=PP+AEZ(I,J)/R
   20 CONTINUE
      POTQ(M,N)=POTQ(M,N)+PP*CON2
   40 POT(M,N)=POT(M,N)+PP*CON2
      RETURN
      END

      SUBROUTINE APRES(NPL,ELV,SOURCE,NSRC,POT,APR,SCALE)
C CALCULATES TERRAIN EFFECT APPARENT RESISTIVITY (IN OHM-METERS)
C USING TOTAL E POTENTIAL, FLAT EARTH GEOMETRIC FACTORS, STRAIGHT
C LINE DISTANCES, AND A REFERENCE ELECTRODE AT INFINITY.
      DIMENSION ELV(41,41),POT(41,41),APR(41,41)
      DIMENSION SOURCE(10,4)
      CON=6.28318531*SCALE
      DO 20 M=1,NPL
      SX=FLOAT(M)
      DO 20 N=1,NPL
      GMF=0.0
      SY=FLOAT(N)
      SZ=ELV(M,N)
      DO 10 KK=1,NSRC
      DX=SX-SOURCE(KK,1)
      DY=SY-SOURCE(KK,2)
      DZ=SZ-SOURCE(KK,3)
      AMP=SOURCE(KK,4)
   10 GMF=GMF+AMP/(SQRT(DX*DX+DY*DY+DZ*DZ)+1.0E-20)
   20 APR(M,N)=CON*POT(M,N)/GMF
C NOTE SCALE FACTORS IN POT AND GMF CANCEL
      RETURN
      END


      SUBROUTINE TEFLD(NPL,POTQ,EX,EY,EZ,FX,FY,EFX,EFY,FXY,
     C ELV,SOURCE,NSRCIM,SIGMA)
C CALCULATES E FIELD TANGENTIAL TO SURFACE FROM POTENTIAL DISTRIBUTION
C ON SURFACE. USES SLOPE ROUTINE ON POTENTIALS DUE TO CHARGE DIST..
C E FIELD DUE TO SOURCES AND IMAGES IS COMPUTED FROM ANALYTIC FORM.
      DIMENSION FX(41,41),FY(41,41),POTQ(41,41),EFX(41,41),EFY(41,41)
      DIMENSION EX(41,41),EY(41,41),EZ(41,41)
      DIMENSION FXY(41,41),ELV(41,41),SOURCE(10,4)
C CON=1.0/4*PI*SIGMA
      CON=1.0/(12.5663706*SIGMA)
      CALL SLOPE(NPL,POTQ,EFX,EFY)
      DO 50 M=1,NPL
      DO 50 N=1,NPL
      EEX=0.0
      EEY=0.0
      EEZ=0.0
      DO 5 I=1,NSRCIM
      PX=SOURCE(I,1)
      PY=SOURCE(I,2)
      PZ=SOURCE(I,3)
      AMP=SOURCE(I,4)
      DX=FLOAT(M)-PX
      DY=FLOAT(N)-PY
      DZ=ELV(M,N)-PZ
      R1=SQRT(DX*DX+DY*DY+DZ*DZ)
      IF(R1.GT.0.05)GO TO 3
C TREAT SOURCE AS THOUGH IT WERE ON SURFACE IF R1 < 0.05 .
      R1=1.0
      AMP=0.0
    3 CR32=AMP*CON/(R1*R1*R1)
      EEX=DX*CR32+EEX
```

```
      EEY=DY*CR32+EEY
    5 EEZ=DZ*CR32+EEZ
      FXX=FX(M,N)
      C1=1.0/(1.0+FXX*FXX)
      FYY=FY(M,N)
      C2=1.0/(1.0+FYY*FYY)
      EEFX=EFX(M,N)
      EEFY=EFY(M,N)
      EX(M,N)=-EEFX*C1+EEX
      EY(M,N)=-EEFY*C2+EEY
   50 EZ(M,N)=-EEFX*C1*FXX-EEFY*C2*FYY+EEZ
      RETURN
      END

      SUBROUTINE BFIELD(NPL,EX,EY,EZ,BFLD,SIGMA,SCALE,ELV,FX,FY,IW,
     C NSKPX,NSKPY,SELV)
C CALCULATES MAGNETIC FIELD ON SURFACE FROM SURFACE ELECTRIC FIELDS
C AND SURFACE SLOPES. INTEGRATES ONLY OVER MAIN MODEL GRID.
C BFLD IS IN MILLIGAMMAS.
      DIMENSION ELV(41,41),FX(41,41),FY(41,41),BFLD(41,41,3)
      DIMENSION EX(41,41),EY(41,41),EZ(41,41)
      DIMENSION IW(4), SELV(41,41)
      CON3=(1.0E-7)*(1.0E+12)*SIGMA/SCALE
      NCTR=INT(FLOAT(NPL)/2.0) +1
      CALL WINDOW(NCTR,NCTR,IFX,ILX,IFY,ILY,NPL,2,IW)
      DO 40 M=IFX,ILX,NSKPX
      DO 40 N=IFY,ILY,NSKPY
      HGT=SELV(M,N)
      BX=0.0
      BY=0.0
      BZ=0.0
      DO 20 I=1,NPL
      IX=M-I
      IXX=IX*IX
      DO 20 J=1,NPL
      IY=N-J
      DZ=HGT-ELV(I,J)
      EEX=EX(I,J)
      EEY=EY(I,J)
      EEZ=EZ(I,J)
      FFX=FX(I,J)
      FFY=FY(I,J)
      R=SQRT(FLOAT(IXX+IY*IY)+DZ*DZ)
      IF(R.GT.2.99)GO TO 13
      IF(R.GT.1.80) GO TO 15
      IF(R.GT.1.10) GO TO 17
      IF(R.GT.0.3 ) GO TO 19
C FOR SINGULARITY
      BX=BX-(EEY+EEZ*FFY)*3.525494
      BY=BY+(EEZ*FFX+EEX)*3.525494
      BZ=BZ+(EEX*FFY-EEY*FFX)*3.525494
      GO TO 20
C NEXT FOR DIAGONAL SURFACE ELEMENTS
   17 CR=1.02487760/R
      BX=BX-(EEY+EEZ*FFY)*CR
      BY=BY+(EEZ*FFX+EEX)*CR
      BZ=BZ+(EEX*FFY-EEY*FFX)*CR
      GO TO 20
C NEXT FOR ADJACENT ELEMENTS
   19 CR=1.03805/R
      BX=BX-(EEY+EEZ*FFY)*CR
      BY=BY+(EEZ*FFX+EEX)*CR
      BZ=BZ+(EEX*FFY-EEY*FFX)*CR
      GO TO 20
C NEXT FOR NEXT RING OF ELEMENTS
   15 CR=1.010/R
```

```
      BX=BX-(EEY*EEZ*FFY)*CR
      BY=BY+(EEZ*FFX+EEX)*CR
      BZ=BZ+(EEX*FFY-EEY*FFX)*CR
      GO TO 20
C NEXT FOR DISTANT ELEMENTS
   13 CR=1.00/R
      BX=BX-(EEY+EEZ*FFY)*CR
      BY=BY+(EEZ*FFX+EEX)*CR
      BZ=BZ+(EEX*FFY-EEY*FFX)*CR
   20 CONTINUE
      BFLD(M,N,1)=BX*CON3
      BFLD(M,N,2)=BY*CON3
   40 BFLD(M,N,3)=BZ*CON3
      RETURN
      END

      SUBROUTINE BWIRE(NPL,SELV,BFLD,ENDP,NSEG,SCALE,NSKPX,
     C NSKPY,IW,WAMP)
C ROUTINE CALCULATES MAGNETIC FIELD RESPONSE IN MILLIGAMMMAS
C DUE TO A NUMBER OF STRAIGHT WIRE SEGMENTS CARRYING WAMP AMPERES.
C NSEG IS NO. OF SEGMENTS
C ENDP ARE THE COORDS OF THE END POINTS OF THE WIRE SEGMENTS
C CURRENT FLOWS FROM ENDP(K,1,I) TO ENDP(K,2,I)
C OBS  ARE THE COORDS OF THE MAGNETIC FIELD OBSERVATION POINT
       DIMENSION SELV(41,41),BFLD(41,41,3),WAMP(40),U(3),IW(4)
       DIMENSION ENDP(3,2,40),OBS(3),P10(3),P12(3),P20(3)
CCCCC     CON4 IS MU/4PI *1.0E+12
      CON4=1.0E+5
      CON5=CON4/SCALE
      NCTR=INT(FLOAT(NPL)/2.0) +1
      CALL WINDOW(NCTR,NCTR,IFX,ILX,IFY,ILY,NPL,2,IW)
      DO 40 M=IFX,ILX,NSKPX
      OBS(1)=FLOAT(M)
      DO 40 N=IFY,ILY,NSKPY
      OBS(2)=FLOAT(N)
      OBS(3)=SELV(M,N)
      DO 40 I=1,NSEG
      DO 10 K=1,3
      P10(K)=ENDP(K,1,I)-OBS(K)
      P12(K)=ENDP(K,1,I)-ENDP(K,2,I)
   10 P20(K)=ENDP(K,2,I)-OBS(K)
      R1=SQRT(P10(1)**2+P10(2)**2+P10(3)**2) + 1.0E-40
      RP12=SQRT(P12(1)**2+P12(2)**2+P12(3)**2)
      R2=SQRT(P20(1)**2+P20(2)**2+P20(3)**2) + 1.0E-40
      COSP1=(P10(1)*P12(1)+P10(2)*P12(2)+P10(3)*P12(3))
     C /(R1*RP12)
      COSP2=(P20(1)*P12(1)+P20(2)*P12(2)+P20(3)*P12(3))/(R2*RP12)
      SINP1=SQRT(1.0 - COSP1**2)
      SINP2=SQRT(1.0-COSP2*COSP2)
C SELECT MOST ACCURATE ESTIMATE OF RR
      RR=R1*SINP1
      IF(SINP1.LT.SINP2)RR=R2*SINP2
C PREVENT DIVISION BY ZERO
      CC=COSP1-COSP2
C IF OBSERVATION POINT IS VERY NEAR THE AXIS OF THE WIRE, SET B TO 0
      IF(SINP1+SINP2.LT.1.0E-6)CC=0.0
      U(1)=P12(2)*P10(3)-P12(3)*P10(2)
      U(2)=P12(3)*P10(1)-P12(1)*P10(3)
      U(3)=P12(1)*P10(2)-P12(2)*P10(1)
      UM=SQRT( U(1)**2+U(2)**2+U(3)**2 )
      IF(UM.EQ.0.0)UM=1.0E-40
      ABSB=WAMP(I)*CON5*CC/RR
      DO 40 J=1,3
   40 BFLD(M,N,J)=ABSB*U(J)/UM+BFLD(M,N,J)
      RETURN
      END
```

```
      SUBROUTINE AUXB2(NPL,BFLD,SIGMA,SCALE,SELV,IW,FLATZ,AEX,AEY,
     C SOURCE,NSRC,NSKPX,NSKPY)
C ADDS EFFECT OF INTEGRATION OF OVER E FIELD OUTSIDE MAIN MODEL
C GRID BY SUBTRACTING AN INTEGRATION OVER HALF-SPACE E FIELDS
C ON THE MODEL GRID FROM THE THEORTICAL HALF-SPACE MAGNETIC FIELDS.
C ARRAY BFLD IS IN MILLIGAMMAS.
      DIMENSION SELV(41,41),BFLD(41,41,3),IW(4)
      DIMENSION SOURCE(10,4)
      DIMENSION AEX(41,41),AEY(41,41)
C NOW CALCULATE ELECTRIC FIELD ON GRID
C DUE TO CURRENT SOURCES .
      CON1=1.0/(2.0*3.14159265*SIGMA)
      DO 10 M=1,NPL
      FM=FLOAT(M)
      DO 10 N=1,NPL
      EEX=0.0
      EEY=0.0
      FN=FLOAT(N)
      DO 5 I=1,NSRC
      PX=FM-SOURCE(I,1)
      PY=FN-SOURCE(I,2)
      PZ=FLATZ-SOURCE(I,3)
      AMP=SOURCE(I,4)
      R1=SQRT(PX*PX+PY*PY+PZ*PZ)
      IF(R1.GT.0.05)GO TO 3
C TREAT SOURCE AS THOUGH IT WERE ON THE SURFACE IF R1 < 0.05 .
C AND E FIELD DUE TO SOURCE IS SET TO ZERO AT SOURCE POINT.
      R1=1.0
      AMP=0.0
    3 CRA=AMP*CON1/(R1*R1*R1)
      EEX=EEX+PX*CRA
    5 EEY=EEY+PY*CRA
      AEX(M,N)=EEX
   10 AEY(M,N)=EEY
      CON3=(1.0E-7)*(1.0E+12)*SIGMA/SCALE
      NCTR=INT(FLOAT(NPL)/2.0) +1
      CALL WINDOW(NCTR,NCTR,IFX,ILX,IFY,ILY,NPL,2,IW)
      DO 40 M=IFX,ILX,NSKPX
      DO 40 N=IFY,ILY,NSKPY
      HGT=SELV(M,N)
      BX=0.0
      BY=0.0
      DO 20 I=1,NPL
      IX=M-I
      IXX=IX*IX
      DO 20 J=1,NPL
      IY=N-J
      R=SQRT(FLOAT(IXX+IY*IY))
      IF(R.GT.2.99)GO TO 13
      IF(R.GT.1.80) GO TO 15
      IF(R.GT.1.10) GO TO 17
      IF(R.GT.0.3 ) GO TO 19
C FOR SINGULARITY
      BX=BX-AEY(I,J)*3.525494
      BY=BY+AEX(I,J)*3.525494
      GO TO 20
C NEXT FOR DIAGONAL SURFACE ELEMENTS
   17 CR=1.02487760/R
      BX=BX-AEY(I,J)*CR
      BY=BY+AEX(I,J)*CR
      GO TO 20
C NEXT FOR ADJACENT ELEMENTS
   19 CR=1.03805/R
      BX=BX-AEY(I,J)*CR
```

```
      BY=BY+AEX(I,J)*CR
      GO TO 20
C NEXT FOR NEXT RING OF ELEMENTS
   15 CR=1.010/R
      BX=BX-AEY(I,J)*CR
      BY=BY+AEX(I,J)*CR
      GO TO 20
C NEXT FOR DISTANT ELEMENTS
   13 CR=1.00/R
      BX=BX-AEY(I,J)*CR
      BY=BY+AEX(I,J)*CR
   20 CONTINUE
      BFLD(M,N,1)=BFLD(M,N,1)-BX*CON3
   40 BFLD(M,N,2)=BFLD(M,N,2)-BY*CON3
      CALL NORMB(IFX,ILX,NSKPX,IFY,ILY,NSKPY,SELV,BFLD,SOURCE,
     C NSRC,SCALE,1.0,1,FLATZ)
      RETURN
      END


      SUBROUTINE NORMB(IFX,ILX,NSKPX,IFY,ILY,NSKPY,SELV,BFLD,
     C SOURCE,NSRC,SCALE,SIGN,NFLAT,FLATZ)
C REMOVES OR ADDS *NORMAL* MAGNETIC FIELD
C THE *NORMAL* FIELD IS THAT DUE TO A SEMI-INFINITE VERTICAL
C WIRE BEGINNING AT THE CURRENT SOURCE
C SIGN =-1.0 CAUSES SUBTRACTION OF FIELD,  1.0 FOR ADDITION
C NFLAT=1 CAUSES ELEVATION ARRAY SELV TO BE IGNORED AND THE
C VALUE FLATZ IS USED FOR OBSERVATION ELEVATION.
C ARRAY BFLD MAGNETIC FIELD IN MILLIGAMMAS.
      DIMENSION BFLD(41,41,3),SELV(41,41),SOURCE(10,4)
      CON3=1.0E-7*1.0E+12/SCALE
      DO 10 M=IFX,ILX,NSKPX
      FM=FLOAT(M)
      DO 10 N=IFY,ILY,NSKPY
      FN=FLOAT(N)
      DO 10 I=1,NSRC
      PX=FM-SOURCE(I,1)
      PY=FN-SOURCE(I,2)
      PZ=SELV(M,N)-SOURCE(I,3)
      IF(NFLAT.EQ.1)PZ=FLATZ-SOURCE(I,3)
      AMP=SOURCE(I,4)
      PXPY=PX*PX+PY*PY
      R1=SQRT(PXPY+PZ*PZ)
      IF(PXPY.EQ.0.0)GO TO 2
      IF(R1.GT.0.05)GO TO 3
    2 R1=1.0
      PXPY=1.0
      AMP=0.0
    3 CR=1.0/R1
      CB=SIGN*AMP*CON3*(1.0+PZ*CR)/PXPY
      BFLD(M,N,1)=BFLD(M,N,1)-PY*CB
   10 BFLD(M,N,2)=BFLD(M,N,2)+PX*CB
      RETURN
      END


      SUBROUTINE BANOM(IFX,ILX,NSKPX,IFY,ILY,NSKPY,SELV,BFLD,
     C SOURCE,NSRC,SCALE,FORWRD)
C THIS ROUTINE CALCULATES PERCENT MMR ANOMALY FOR ONE OR TWO
C ELECTRODES. IF TWO ELECTRODES ARE USED THE LINE CONNECTING
C THEM MUST BE PARALLEL TO THE Y AXIS.
C THE INPUT PARAMETER BFLD MUST BE THE ANOMALOUS(IE REDUCED)B FIELD.
C IF THE PARAMETER FORWRD = 1.0 THE ROUTINE FUNCTIONS AS DESCRIBED
C ABOVE, IF FORWRD =-1.0 THE ROUTINE WILL PERFORM THE REVERSE
C OPERATION ON BFLD CONVERTING IT FROM PERCENT MMR ANOMALLY TO REDUCED
C B FIELD.
```

```
      DIMENSION BFLD(41,41,3),SELV(41,41),SOURCE(10,4)
      CON3=1.0E-7*1.0E+12/SCALE
      DO 10 N=IFY,ILY,NSKPY
      FN=FLOAT(N)
      BXREF=0.0
      DO 5 II=1,NSRC
      PY=FN-SOURCE(II,2)
      PX=0.0
      AMP=SOURCE(II,4)
      R2=PX*PX+PY*PY
      IF(R2.GT.0.0025)GO TO 3
      R2=1.0
      AMP=0.0
    3 CB=AMP*CON3/R2
    5 BXREF=BXREF-PY*CB
C NEXT CARD FOR CONTROL OF DYNAMIC RANGE OF PLOTS
      IF(ABS(BXREF).LE.1.0E-15)BXREF=1.0E+40
      DO 10 M=IFX,ILX,NSKPX
      DO 10 I=1,3
      IF(FORWRD.EQ.-1.0)BFLD(M,N,I)=BXREF*BFLD(M,N,I)/100.0
  10  IF(FORWRD.EQ. 1.0)BFLD(M,N,I)=100.0*BFLD(M,N,I)/BXREF
      RETURN
      END


      SUBROUTINE BANOMT(IFX,ILX,NSKPX,IFY,ILY,NSKPY,SELV,BFLD,
     C SOURCE,NSRC,SCALE,FORWRD)
C CALCULATES PERCENT ANOMALY NORMALIZED BY TOTAL FIELD
C IF FORWRD=1.0 ROUTINE FUNCTIONS AS DESCRIBED ABOVE.
C IF FORWRD=-1.0 ROUTINE WILL PERFORM THE REVERSE OPERATION
      DIMENSION BFLD(41,41,3),SELV(41,41),SOURCE(10,4)
      CON3=(1.0E-7)*(1.0E+12)/SCALE
      DO 10 M=IFX,ILX,NSKPX
      FM=FLOAT(M)
      DO 10 N=IFY,ILY,NSKPY
      FN=FLOAT(N)
      BX=0.0
      BY=0.0
      DO 5 II=1,NSRC
      PX=FM-SOURCE(II,1)
      PY=FN-SOURCE(II,2)
    9 AMP=SOURCE(II,4)
      R2=PX*PX+PY*PY
      IF(R2.GT.0.0025)GO TO 3
      R2=1.0
      AMP=0.0
    3 CB=AMP*CON3/R2
      BX=BX-PY*CB
    5 BY=BY+PX*CB
      BT=SQRT(BX*BX+BY*BY)
C NEXT CARD FOR CONTROL OF DYNAMIC RANGE OF PLOTS
      IF(BT.LE.1.0E-15)BT=1.0E+40
      DO 10 I=1,3
      IF(FORWRD.EQ.-1.0)BFLD(M,N,I)=BT*BFLD(M,N,I)/100.0
   10 IF(FORWRD.EQ. 1.0)BFLD(M,N,I)=100.0*BFLD(M,N,I)/BT
      RETURN
      END

      SUBROUTINE EPER(NPL,SOURCE,NSRC,POT,APR,EFX,EFY,FLATZ,SIGMA,
     C SCALE)
C COMPUTES PERCENT E FIELD (POTENTIAL DIFFERENCE) NORMALIZED
C BY TOTAL E FIELD.
      DIMENSION POT(41,41),APR(41,41),EFX(41,41),EFY(41,41)
      DIMENSION SOURCE(10,4)
C NEXT 14 LINES COMPUTE THEORETICAL POTENTIAL IN ARRAY APR.
      CON=1.0/(6.28318531*SIGMA*SCALE)
```

```
      DO 20 M=1,NPL
      SX=FLOAT(M)
      DO 20 N=1,NPL
      GMF=0.0
      SY=FLOAT(N)
      SZ=FLATZ
      DO 10 KK=1,NSRC
      DX=SX-SOURCE(KK,1)
      DY=SY-SOURCE(KK,2)
      DZ=SZ-SOURCE(KK,3)
      AMP=SOURCE(KK,4)
   10 GMF=GMF+AMP/(SQRT(DX*DX+DY*DY+DZ*DZ)+1.0E-40)
   20 APR(M,N)=CON*GMF
      DO 40 M=1,NPL
      M3=M+1
      IF(M.EQ.NPL)M3=NPL
      DO 40 N=1,NPL
      N3=N+1
      IF(N.EQ.NPL)N3=NPL
      EX=APR(M3,N)-APR(M,N)
      EY=APR(M,N3)-APR(M,N)
      ET=SQRT(EX*EX+EY*EY)
      IF(ET.EQ.0.0)ET=1.0E-40
      EFX(M,N)=-100.0*(POT(M3,N)-POT(M,N))/ET
   40 EFY(M,N)=-100.0*(POT(M,N3)-POT(M,N))/ET
      RETURN
      END

      SUBROUTINE SLOPE(NPL,F,FX,FY)
C CALCULATES SLOPES ON SURFACE F
C AVERAGES SLOPES FROM ELEMENTS ON EITHER SIDE OF EACH POINT.
      DIMENSION F(41,41),FX(41,41),FY(41,41)
      DO 40 M=1,NPL
      M1=M-1
      M3=M+1
      IF(M.EQ.1)M1=1
      IF(M.EQ.NPL)M3=NPL
      DO 40 N=1,NPL
      N1=N-1
      N3=N+1
      IF(N.EQ.1)N1=1
      IF(N.EQ.NPL)N3=NPL
      FX(M,N)=(-F(M1,N)+F(M3,N))/2.0
   40 FY(M,N)=(-F(M,N1)+F(M,N3))/2.0
      RETURN
      END


      SUBROUTINE PRINTA(DATA,IFX,ILX,IFY,ILY,NSKX,NSKY,A1)
C GENERAL ROUTINE FOR PRINTING ARRAYS
      DIMENSION DATA(41,41)
      PRINT 105,A1
  105 FORMAT(1H1,20X,,*THE FOLLOWING DATA ARRAY IS *,A10)
      PRINT 108,IFX,ILX,NSKX,IFY,ILY,NSKY
      DO 40 M=IFX,ILX,NSKX
      PRINT 100,M
   40 PRINT 110,((DATA(M,N)),N=IFY,ILY,NSKY)
  100 FORMAT(5X,,*X COORDINATE IS*,I5)
  110 FORMAT(10(1X,G11.5))
  108 FORMAT(4X,,*FIRSTX=*,I3,,* ,LASTX=*,I3,,* ,SKIPX=*,I3,,* ,FIRSTY=*,
     CI3,,* ,LASTY=*,I3,,* ,SKIPY=*,I3)
      RETURN
      END

      SUBROUTINE PRNTAL(NPL,DATA,A1)
C PRINTS ALL ELEMENTS IN THE ARRAY DATA
```

```
      DIMENSION DATA(41,41)
      IFX=1
      ILX=NPL
      NSKX=1
      IFY=1
      ILY=NPL
      NSKY=1
      CALL PRINTA(DATA,IFX,ILX,IFY,ILY,NSKX,NSKY,A1)
      RETURN
      END

      SUBROUTINE PLOTAL(DATA,NPL,A1,DAT)
C CONTOUR PLOTING ROUTINE FOR PLOTING ALL POINTS IN DATA
      COMMON/IGSZZZ/Z(200)
      DIMENSION DATA(41,41),DAT(NPL,1),LAB(4)
C REPACK DATA INTO DAT
      DO 10 M=1,NPL
      DO 10 N=1,NPL
C M AND N ARE SWITCHED TO ACCOMMODATE PLOT ROUTINES.
   10 DAT(N,M)=DATA(M,N)
C SET UP LABEL
      ENCODE(40,100,LAB)A1
  100 FORMAT(*TOPOGRAPHIC EFFECTS *,A10)
C THE FOLLOWING ARE LBL BERKELEY PLOT SUBROUTINES.
      CALL EZCNTR(DAT,NPL,NPL)
      CALL SETSMG(Z,14,3.0)
      CALL LEGNDG(Z,38.0,97.5,30,LAB)
      CALL SETSMG(Z,14,0.0)
      CALL PAGEG(Z,0,1,1)
      RETURN
      END

      SUBROUTINE GPLOT1(DATA,NPL,A1,DAT,IFX,ILX,NSKPX,IFY,ILY,NSKPY)
C ROUTINES GPLOT1 AND GPLOT2 WORK TOGETHER TO PLOT SPARSE ARRAYS
      DIMENSION DATA(41,41),DAT(41,41)
      NK=0
      DO 10 I=IFX,ILX,NSKPX
   10 NK=NK+1
      CALL GPLOT2(DATA,NK,A1,DAT,IFX,ILX,NSKPX,IFY,ILY,NSKPY)
      RETURN
      END

      SUBROUTINE GPLOT2(DATA,NK,A1,DAT,IFX,ILX,NSKPX,IFY,ILY,NSKPY)
C ROUTINES GPLOT1 AND GPLOT2 WORK TOGRTHER TO PLOT SPARSE ARRAYS
      COMMON/IGSZZZ/Z(200)
      DIMENSION DATA(41,41),DAT(NK,1),LAB(4)
      M=0
      DO 10 I=IFX,ILX,NSKPX
      M=M+1
      N=0
      DO 10 J=IFY,ILY,NSKPY
      N=N+1
   10 DAT(N,M)=DATA(I,J)
C SET UP LABEL FOR PLOT
      ENCODE(30,100,LAB)A1
  100 FORMAT(*TOPOGRAPHIC EFFECTS *,A10)
C THE FOLLOWING ARE LBL BERKELEY PLOT SUBROUTINES.
      CALL EZCNTR(DAT,NK,NK)
      CALL SETSMG(Z,14,3.0)
      CALL LEGNDG(Z,38.0,97.5,30,LAB)
      CALL SETSMG(Z,14,0.0)
      CALL PAGEG(Z,0,1,1)
      RETURN
      END

      SUBROUTINE GPLOT3(DATAX,DATAY,NK,A1,DATX,DATY,IFX,ILX,NSKPX,
```

```
     C IFY,ILY,NSKPY)
C PLOTS HORIZONTAL FIELD VECTORS AS ARROWS
      COMMON/IGSZZZ/Z(200)
      DIMENSION DATAX(41,41),DATAY(41,41),DATX(NK,1),DATY(NK,1),LAB(4)
      M=0
      DO 10 I=IFX,ILX,NSKPX
      M=M+1
      N=0
      DO 10 J=IFY,ILY,NSKPY
      N=N+1
      DATY(N,M)=DATAY(I,J)
   10 DATX(N,M)=DATAX(I,J)
C SET UP LABEL FOR PLOT
      ENCODE(30,100,LAB)A1
  100 FORMAT('TOPOGRAPHIC EFFECTS ',A10)
C THE FOLLOWING ARE LBL BERKELEY PLOT SUBROUTINES.
      CALL EZVEC(DATY,DATX,NK,NK)
      CALL SETSMG(Z,14,3.0)
      CALL LEGNDG(Z,38.0,97.5,30,LAB)
      CALL SETSMG(Z,14,0.0)
      CALL PAGEG(Z,0,1,1)
      RETURN
      END

C***  SAMPLE CARD DECK FOR 2-D RIDGE MODEL WITH 20 DEGREE SLOPES  ***
C***     THE MODEL SUFRACE IS CREATED BY SUBROUTINE CSURF5        ***
C***        MODEL IS EQUIVALENT TO THESIS MODEL R-SA20-IB         ***
C
C---+----1----+----2----+----3----+----4----+----5----+----6----+----7

CARD1    41         20          6          1          0     21.839        0.0
CARD2     1          2          0       10.0      0.010        1.0        1.0
CARD3    35         20         40          2          2
CARD4   1.0        1.0        0.0        1.0        1.0        1.0
CARD5               10.0       10.0
SOURCE             260.0      200.0     21.838        1.0
IMAGE              260.0      200.0     21.838        1.0
```

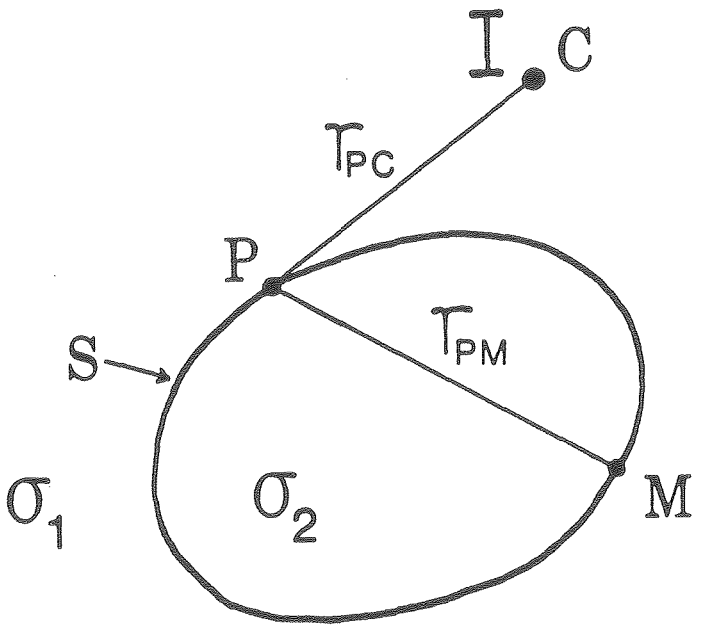

Figure 2-3-1. An inhomogeneity of conductivity σ_2 imbedded in a whole-space of conductivity σ_1 with a current source I located at C.

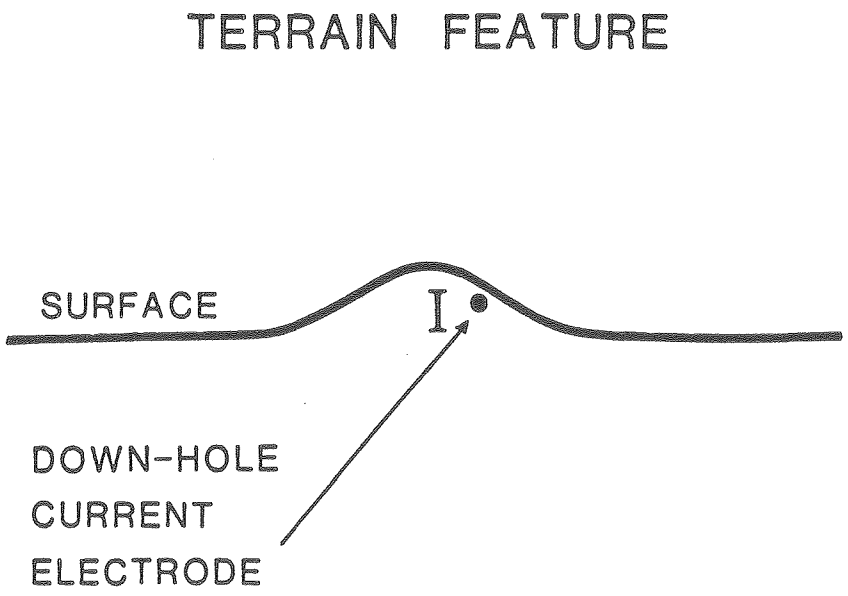

Figure 2-3-2. A subsurface current source imbedded in a hill.

TRADITIONAL APPROACH

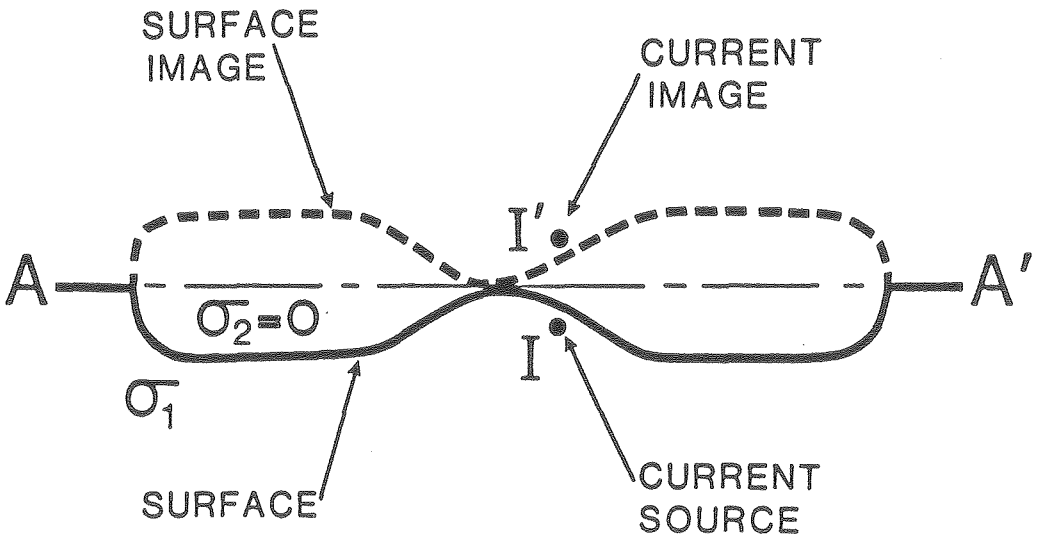

Figure 2-3-3. Integral equation approach employing an image of the topography and current source.

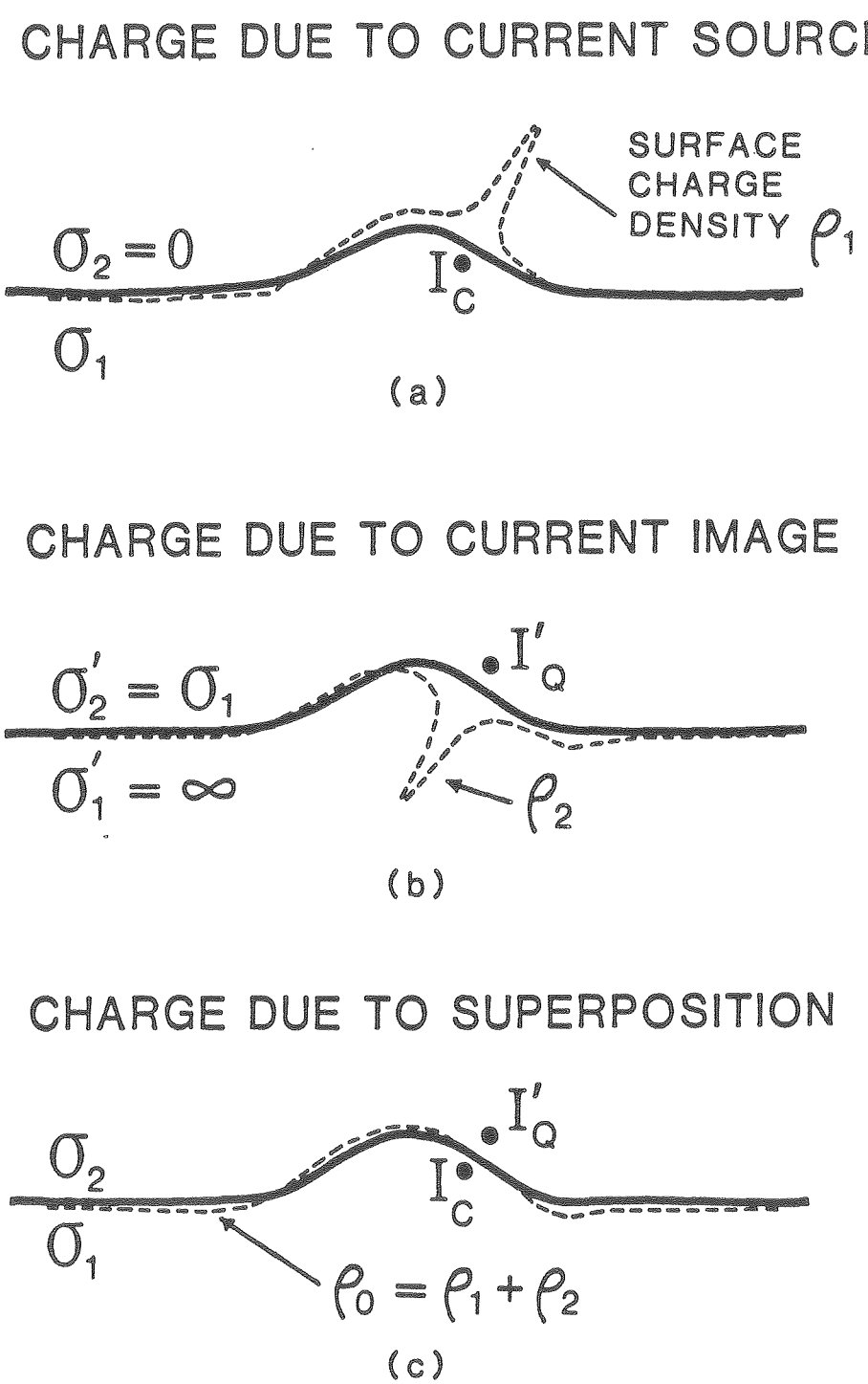

Figure 2-3-4. Schematic representations of the surface charge distributions due to: (a) a subsurface current source; (b) a current source image above a perfectly conducting earth; and (c) the superposition of the charge distributions in (a) and (b).

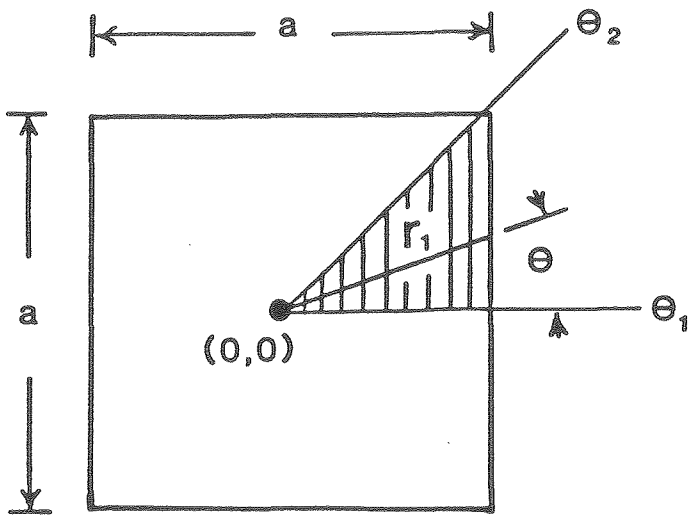

Figure 2-8-1. Geometry for the evaluation of the potential at the center of a surface element carrying a uniform charge density. The integration over charge is carried out over the shaded portion of the element.

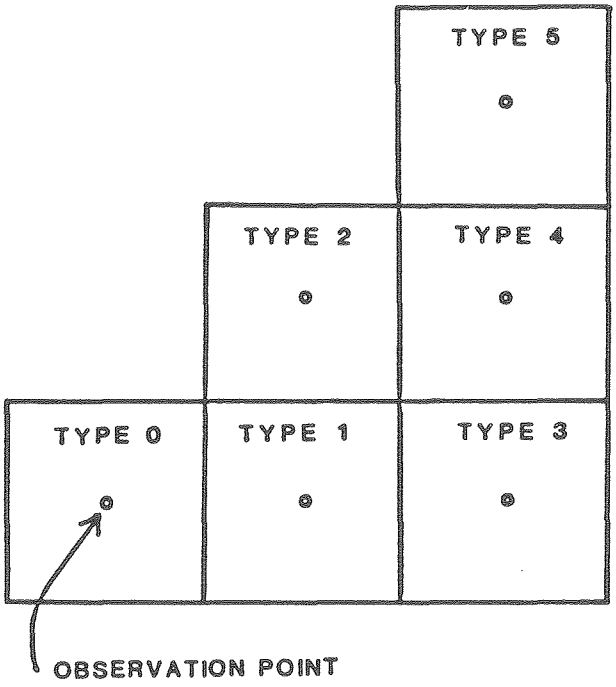

Figure 2-8-2. Surface element geometric types for elements surrounding an observation point. The potential at the observation point due to charge on a neighboring element is determined by analytic integration.

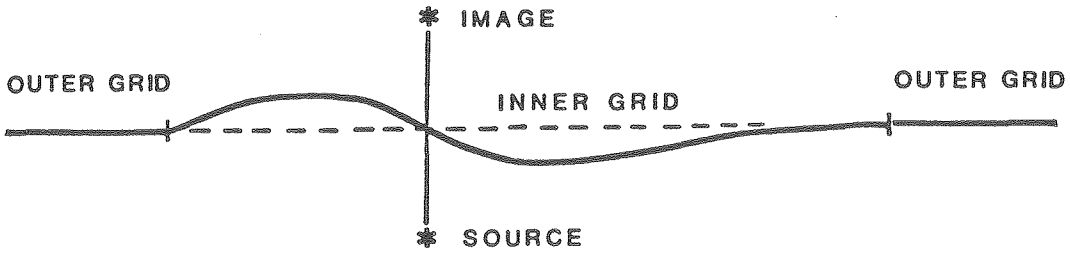

(a)

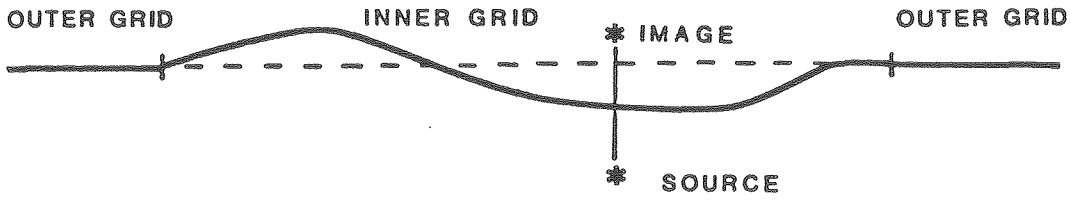

(b)

Figure 2-8-3. (a) Geometry of model surfaces when the current source and image are symmetric about the plane of the outer grid.

(b) Geometry of surfaces when symmetry of source and image does not exist with the outer grid.

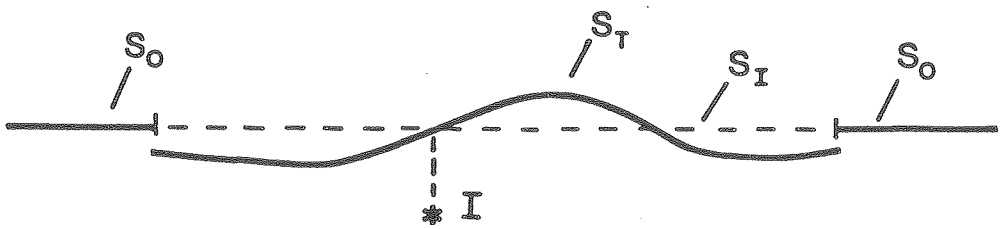

Figure 2-11-1. Surfaces used for the calculation of the total magnetic field. Surfaces S_T and S_I intersect directly above the current source I. Surface S_T is the model topography; S_O is the outer horizontal surface surrounding S_T; and S_I is the inner horizontal surface.

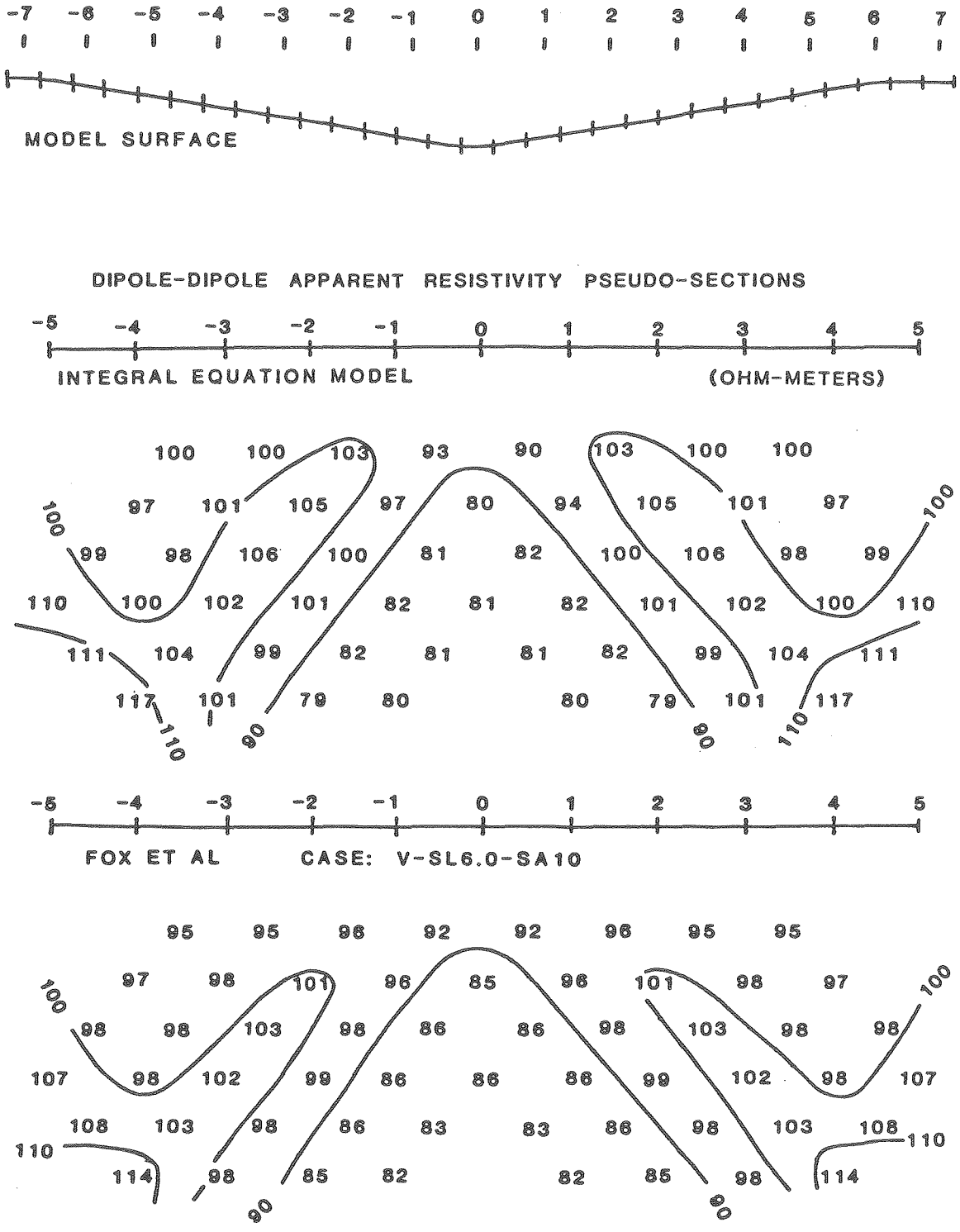

Figure 3-1-1. Comparison of integral equation (author's) and finite element (Fox et al, 1980) dipole-dipole apparent resistivity model psudeo-sections computed for a 2-D valley with 10° slopes.

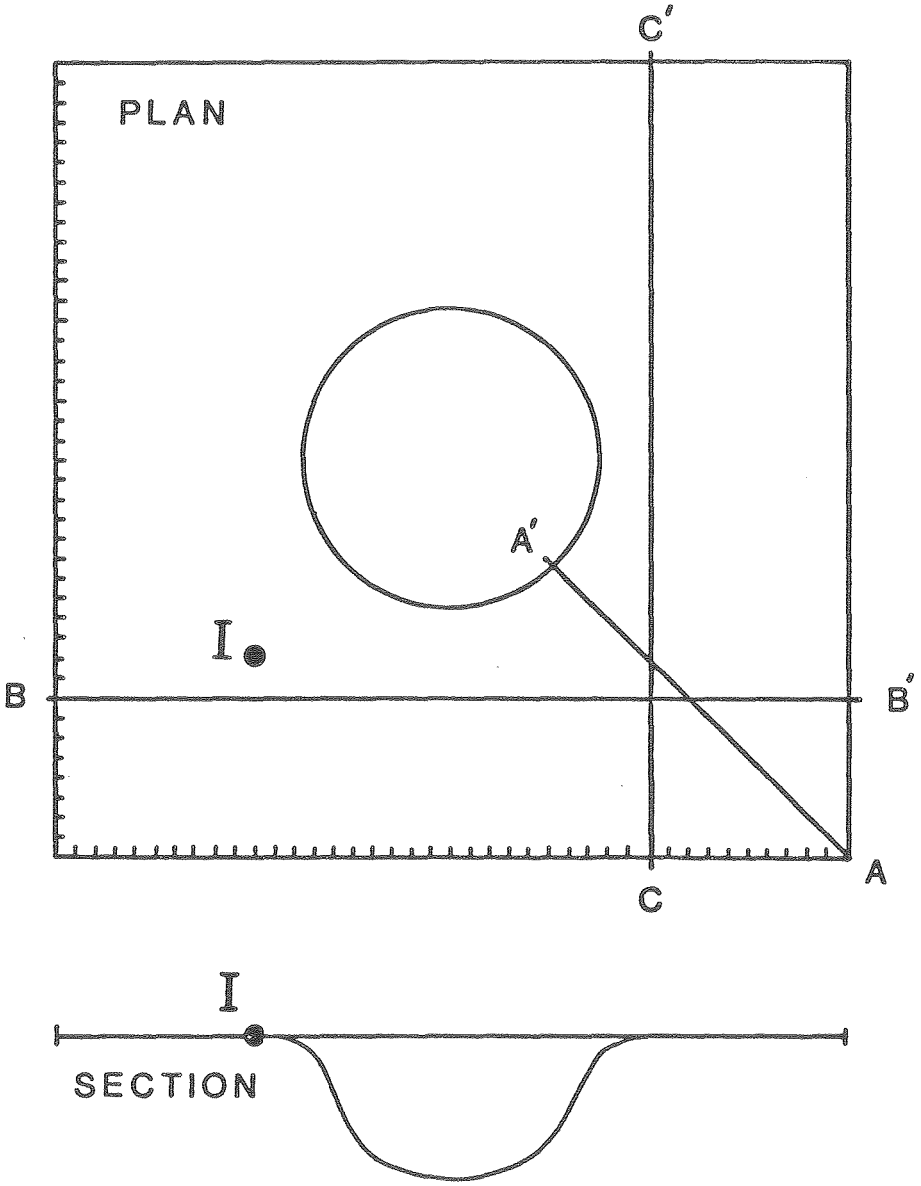

Figure 3-1-2. 41 x 41 element model surface used to represent a hemispherical depression. A current source is located at I and the fields are measured along lines A, B, and C.

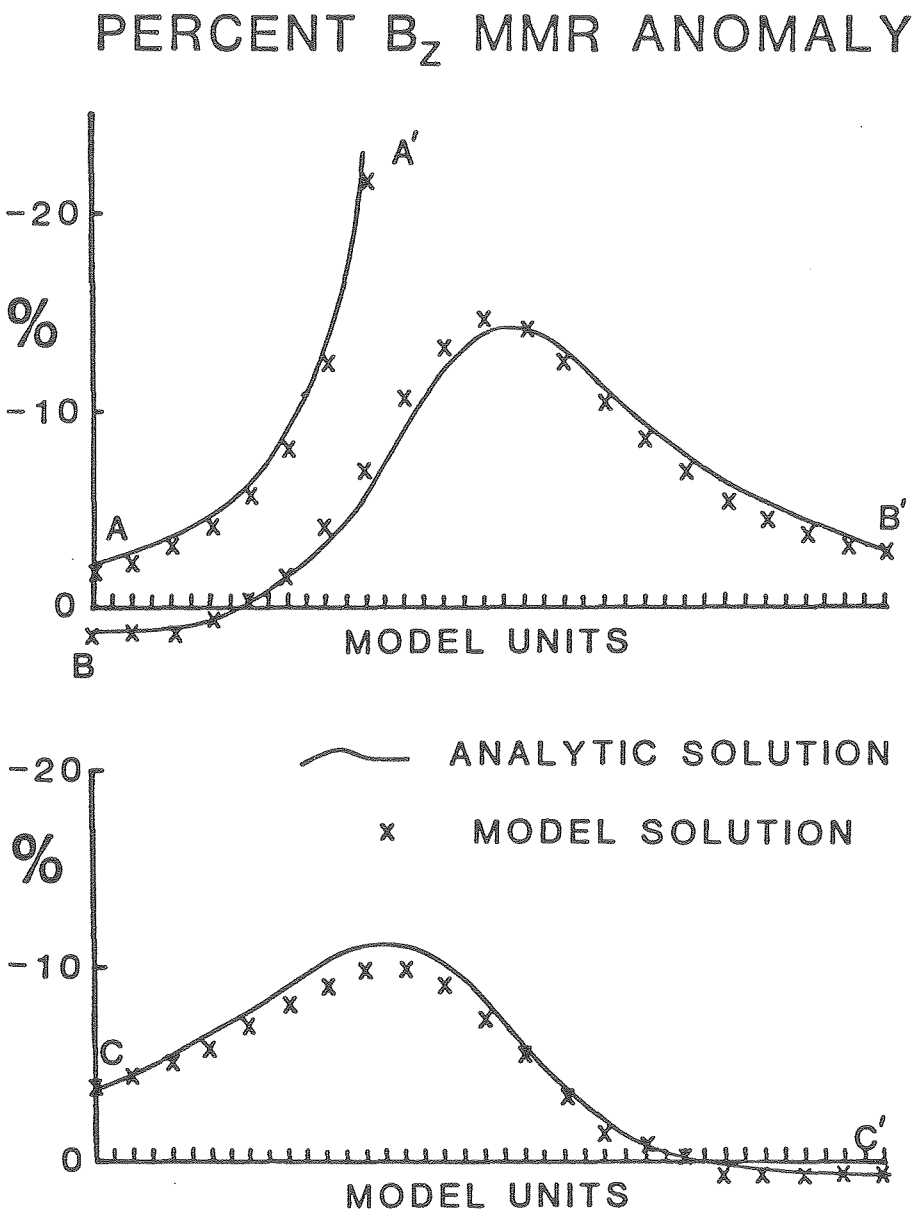

Figure 3-1-3. Comparison of analytic equation and integral equation model solutions for the vertical magnetic field anomalies over a hemispherical depression.

SECTION

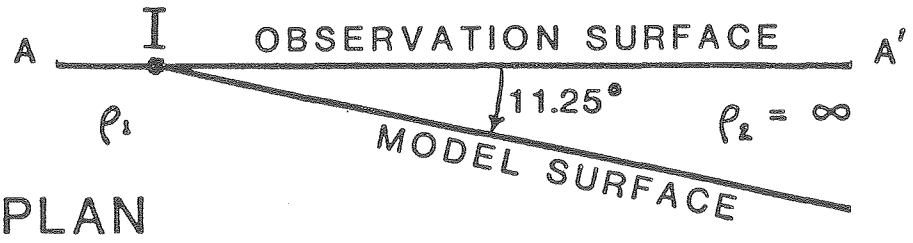

PLAN

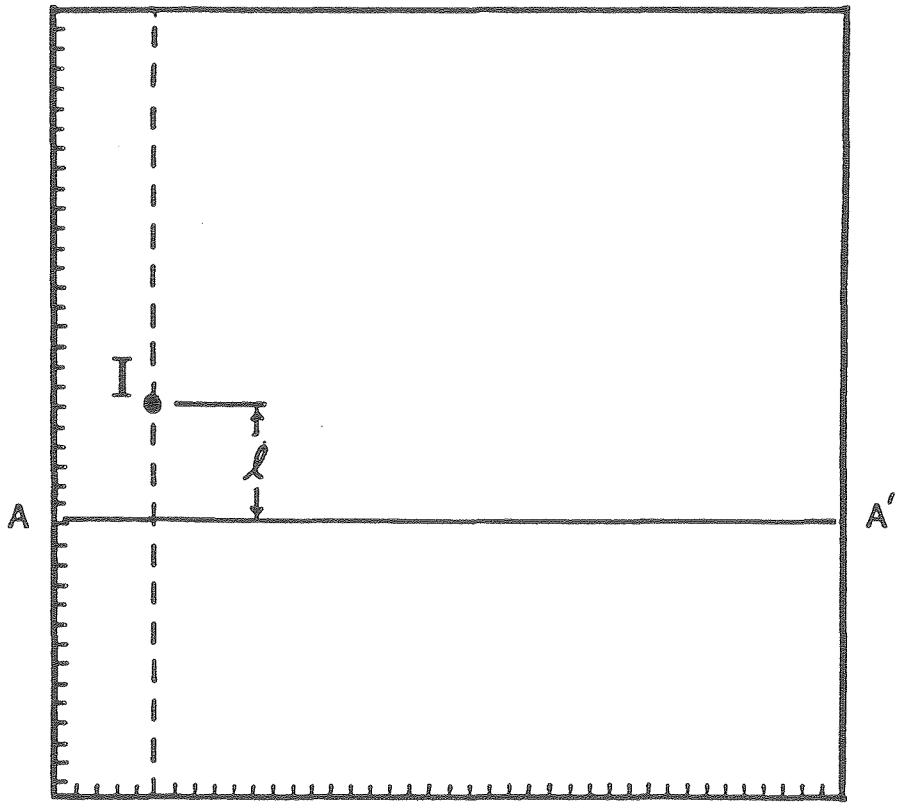

Figure 3-1-4. 41 x 41 element model surface used to represent a dipping interface (sloping terrain surface). A current source is located at I. The magnetic fields are measured along line A.

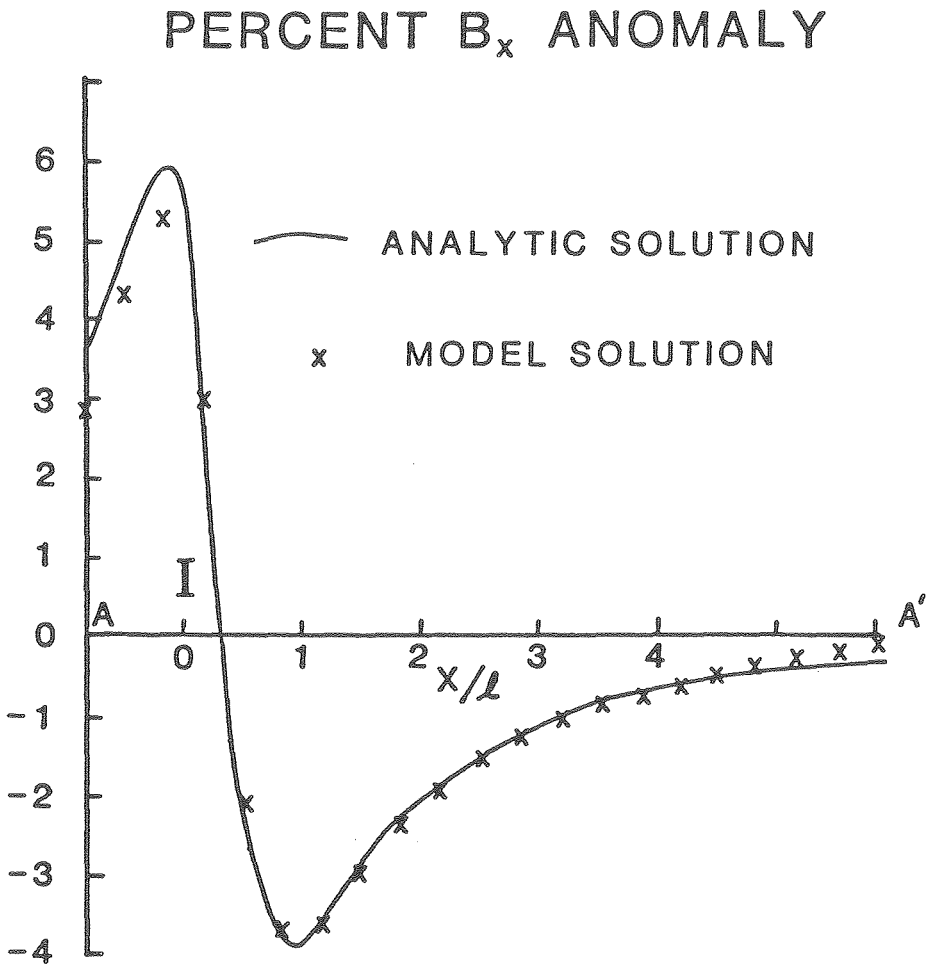

Figure 3-1-5. Comparison of analytic equation and integral equation model solutions for the horizontal magnetic field anomaly over an interface dipping at 11.25°.

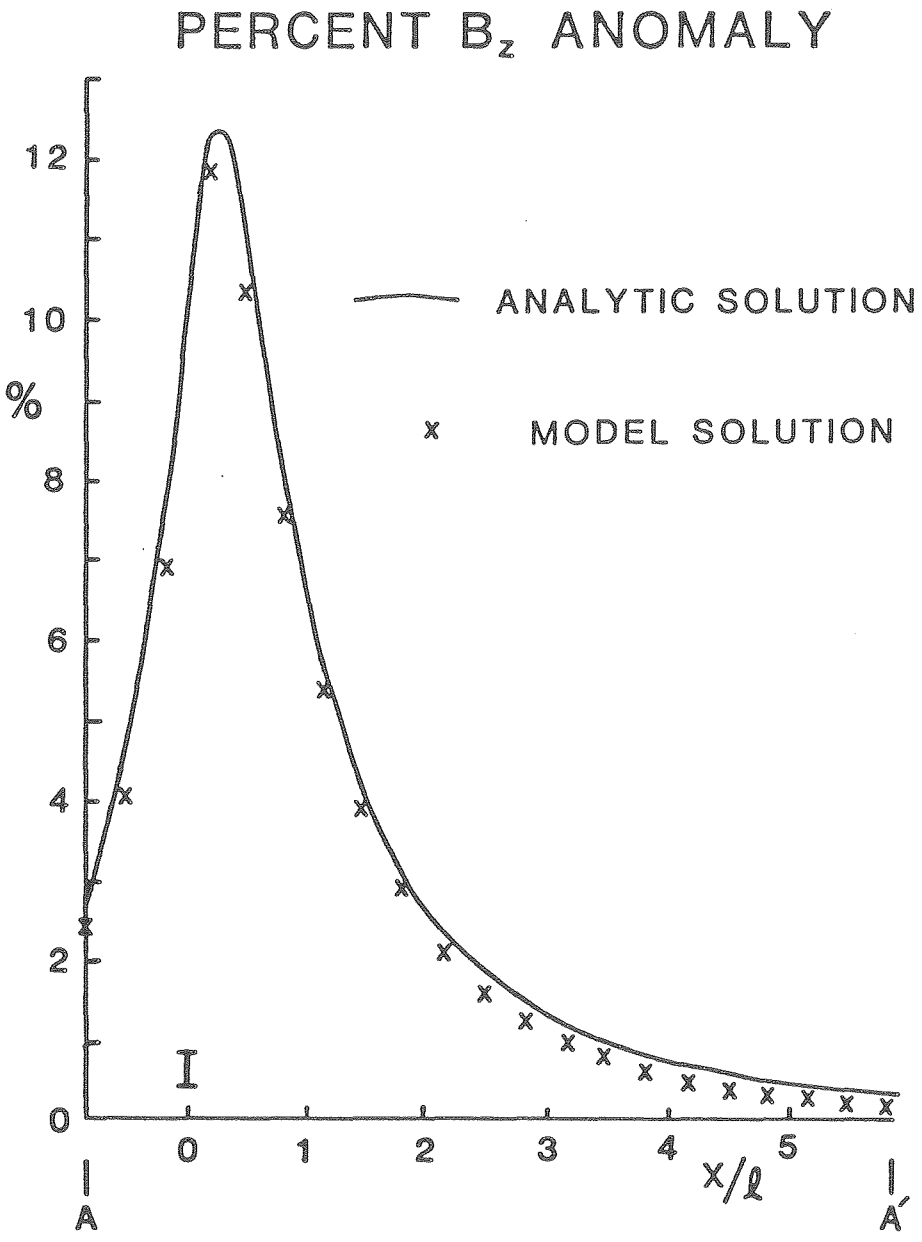

Figure 3-1-6. Comparison of analytic equation and integral equation model solutions for the vertical magnetic field anomaly over an interface dipping at 11.25°.

TOPOGRAPHY

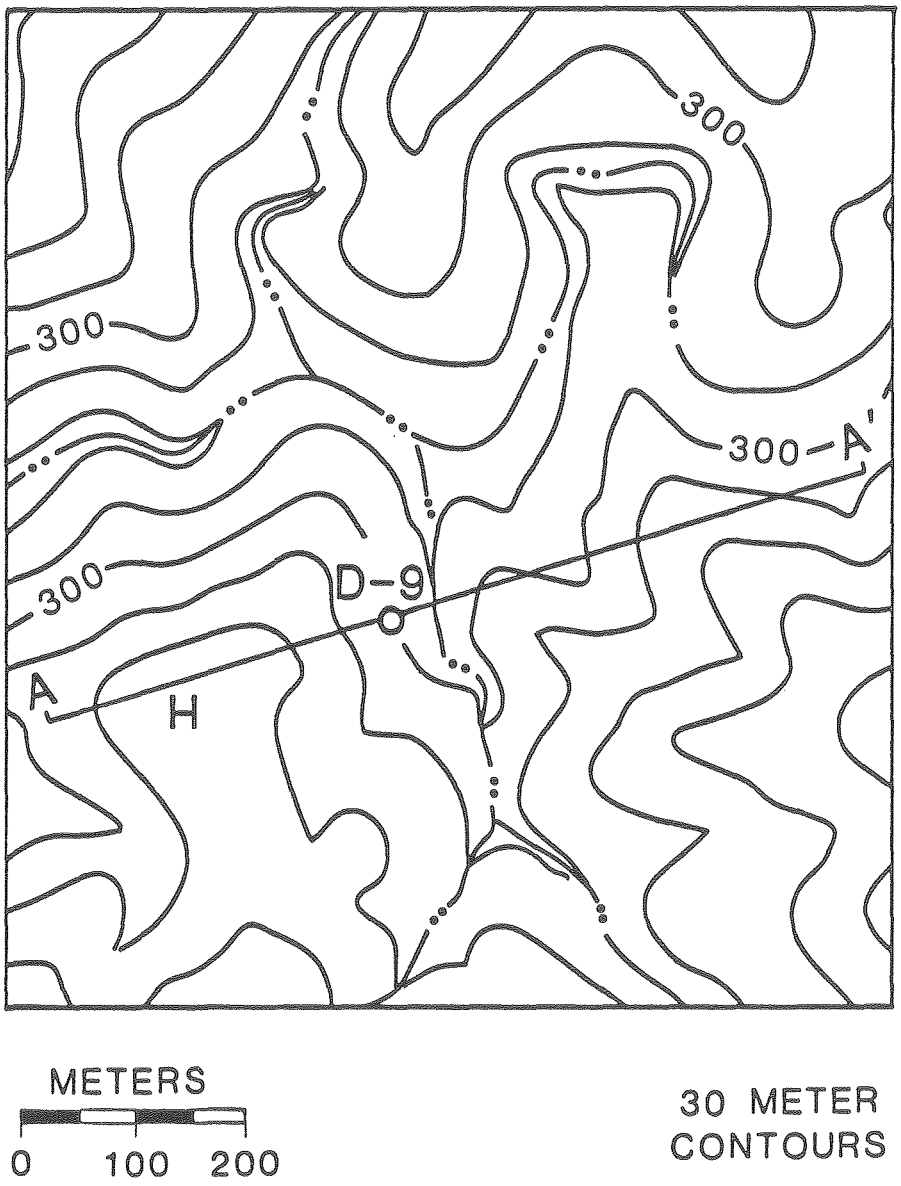

Figure 3-3-1. Topography in the resistivity survey area around test drill hole D-9. The area shown corresponds to the central 41 x 41 elements of a 61 x 61 element terrain model.

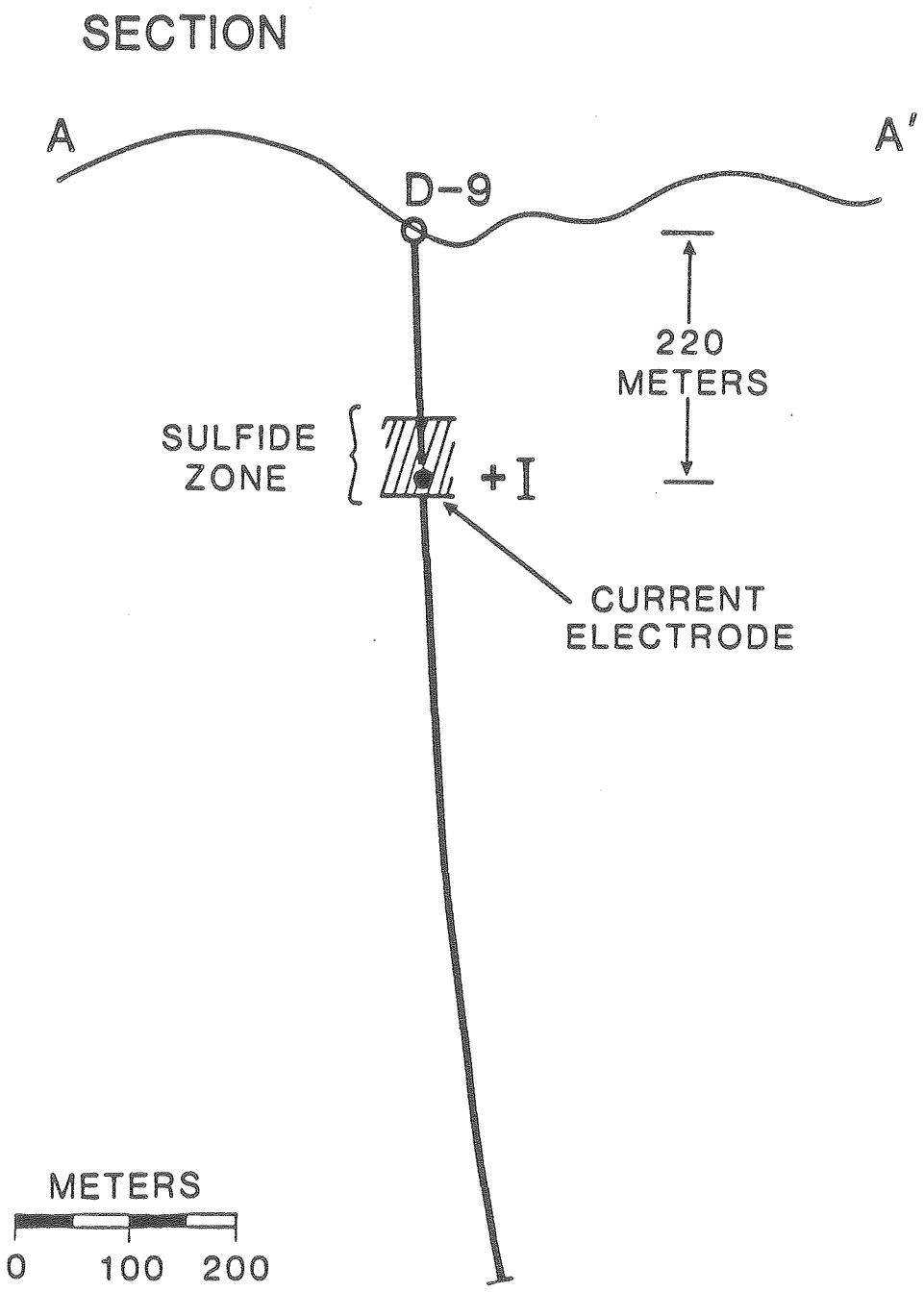

Figure 3-3-2. Current electrode configuration used for the mise-a-la-masse resistivity survey in the area around drill hole D-9.

MEASURED APPARENT RESISTIVITIES

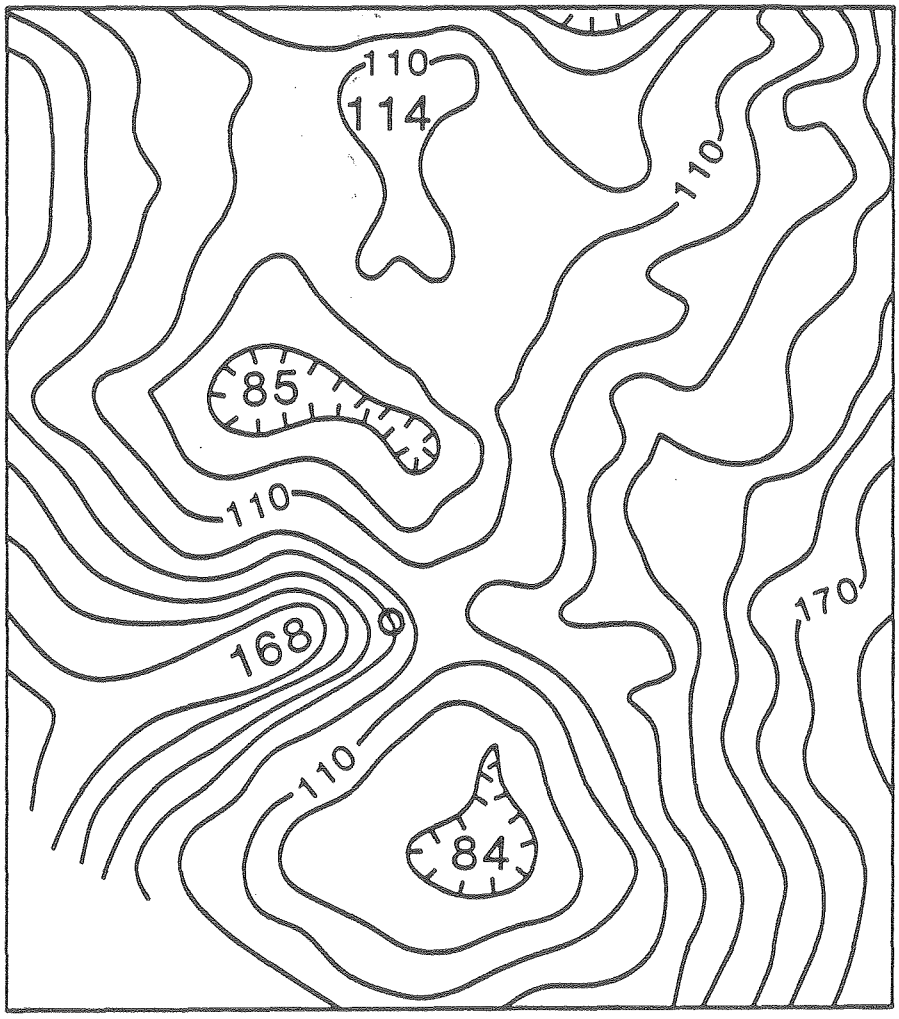

Figure 3-3-3. Actual mise-a-la-masse apparent resistivities measured on the surface around drill hole D-9.

TERRAIN MODEL
APPARENT RESISTIVITIES

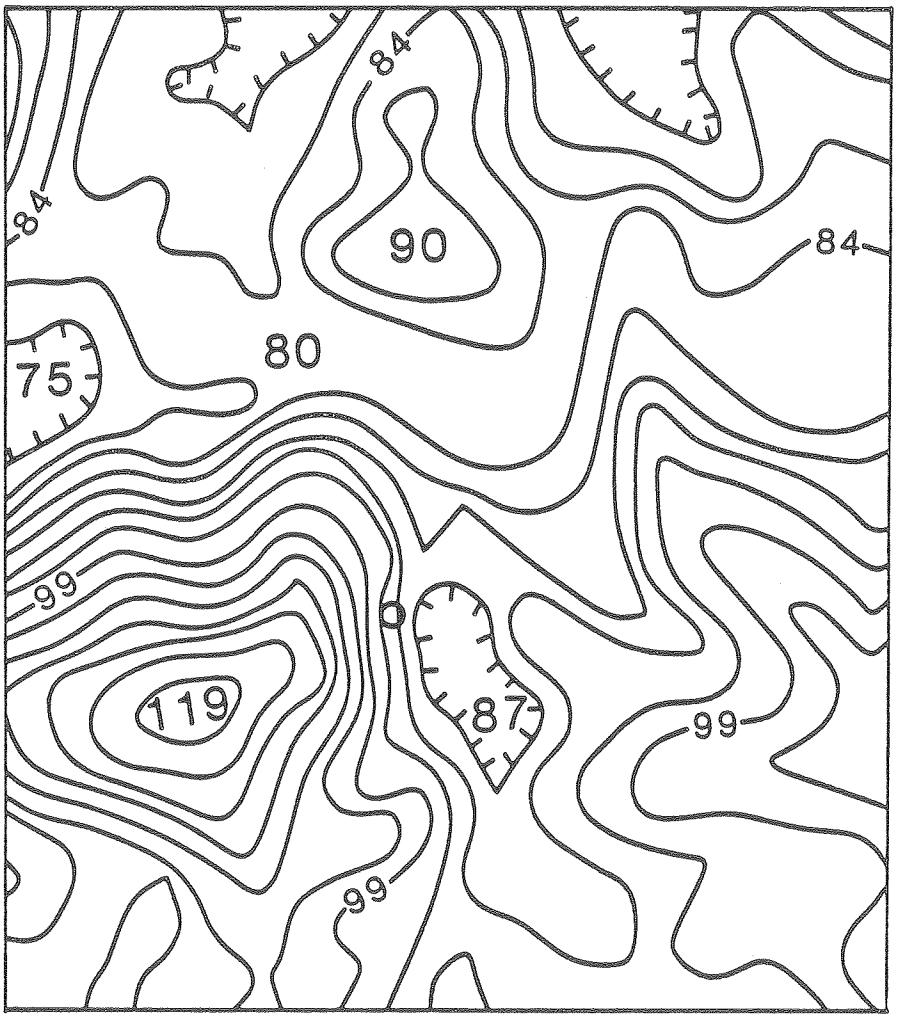

Figure 3-3-4. Terrain model mise-a-la-masse apparent resistivities computed on the surface around drill hole D-9.

TERRAIN CORRECTED APPARENT RESISTIVITIES

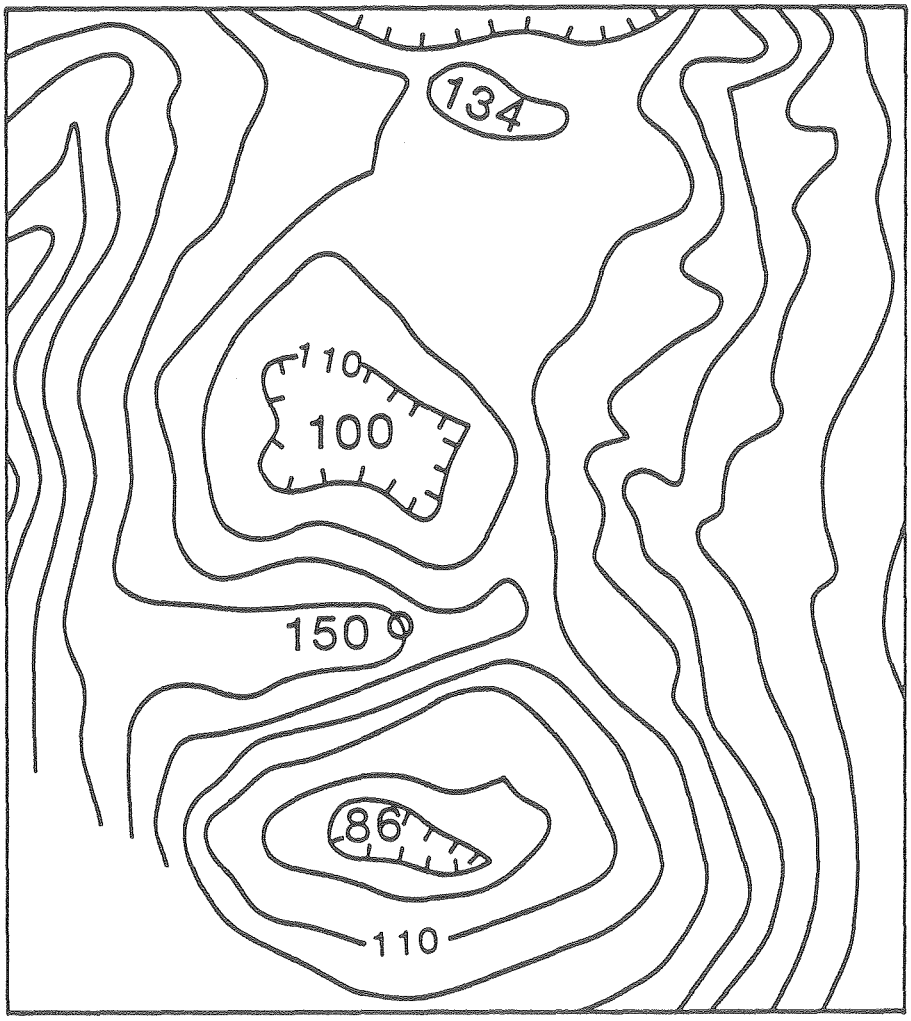

Figure 3-3-5. Terrain corrected mise-a-la-masse apparent resistivities for the area around drill hole D-9.

INTERPRETATION

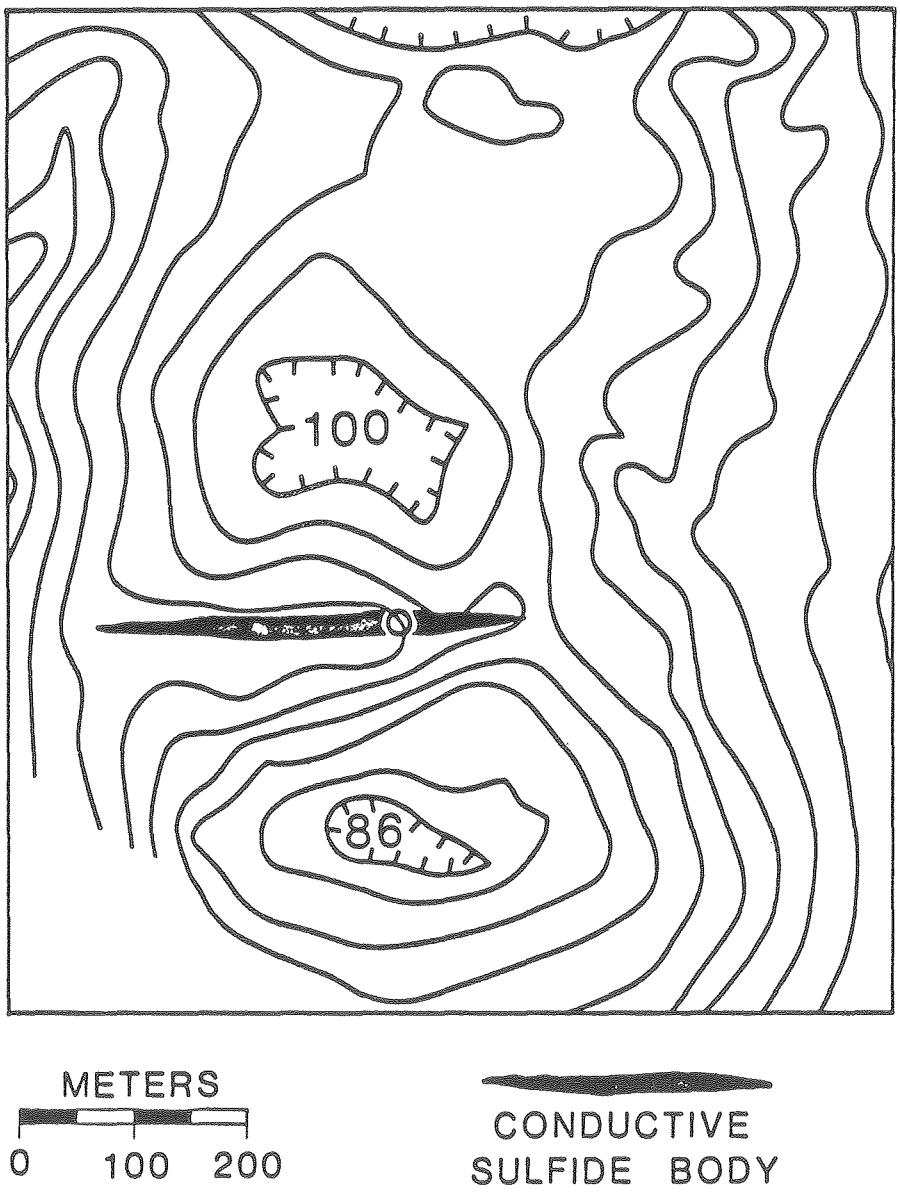

Figure 3-3-6. Qualitative interpretation of the terrain corrected mise-a-la-masse apparent resistivities in the vicinity of drill hole D-9.

TOPOGRAPHY

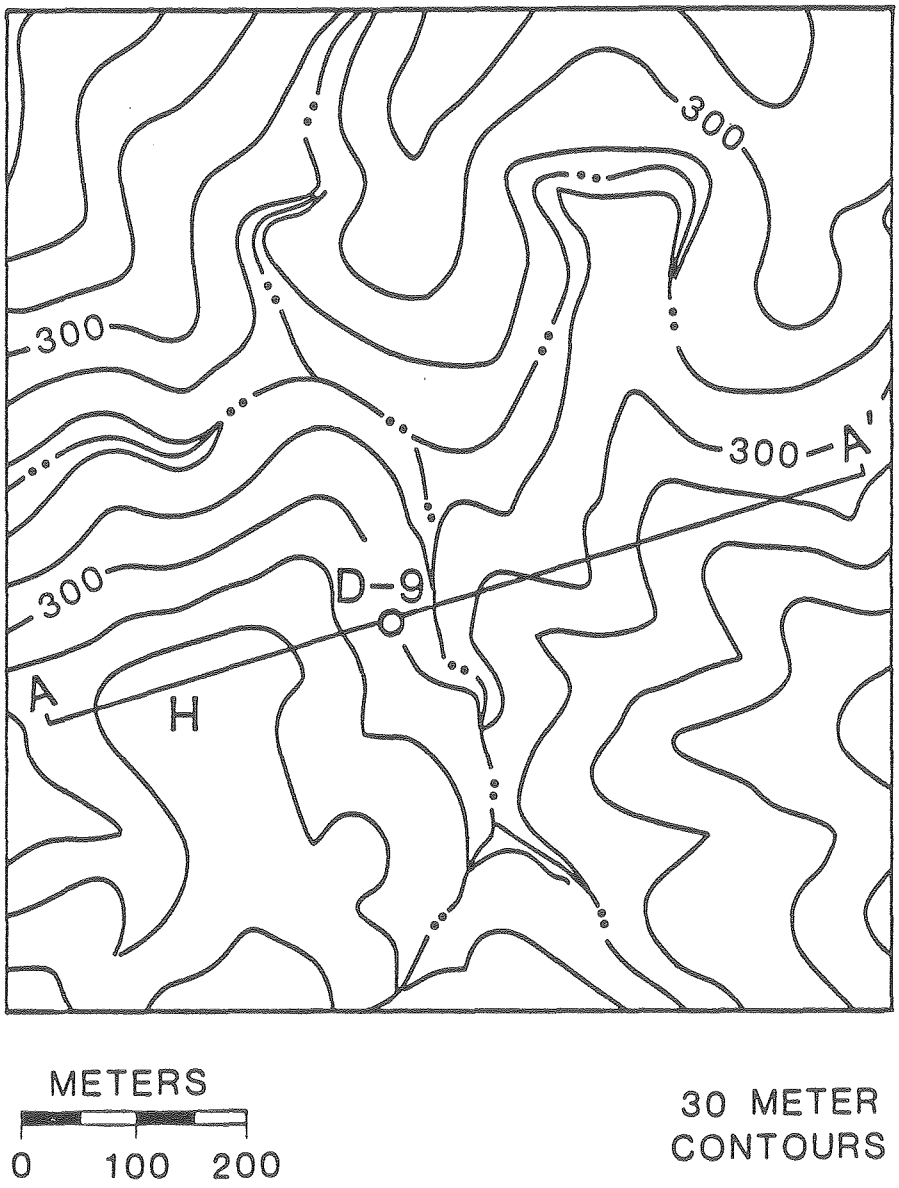

Figure 3-5-1. Topography of the MMR survey area around drill hole D-9. The area shown corresponds to the central 41 x 41 element of a 61 x 61 element terrain model.

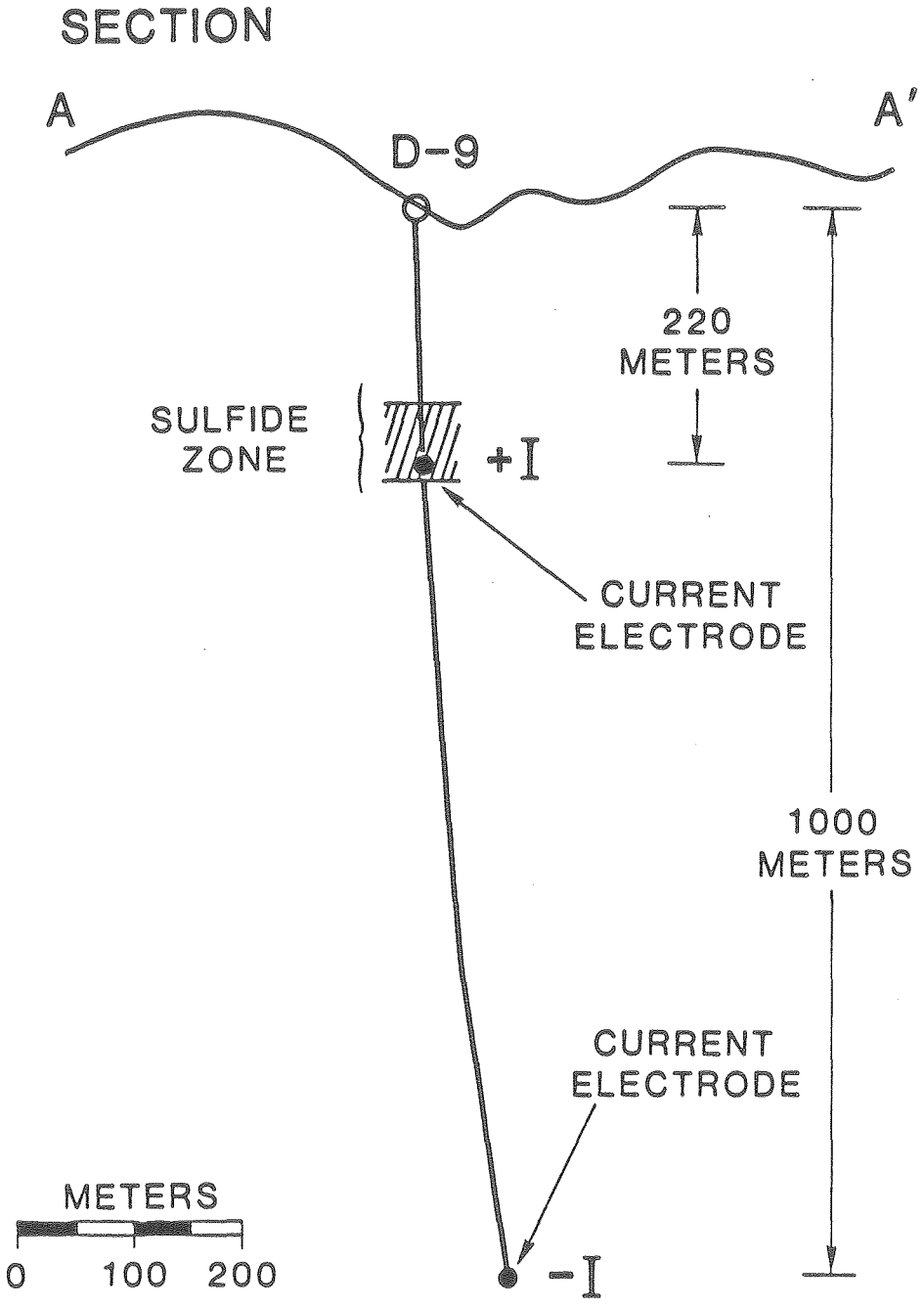

Figure 3-5-2. Current electrode configuration used for the MMR survey in the area of drill hole D-9.

MEASURED MAGNETIC FIELDS

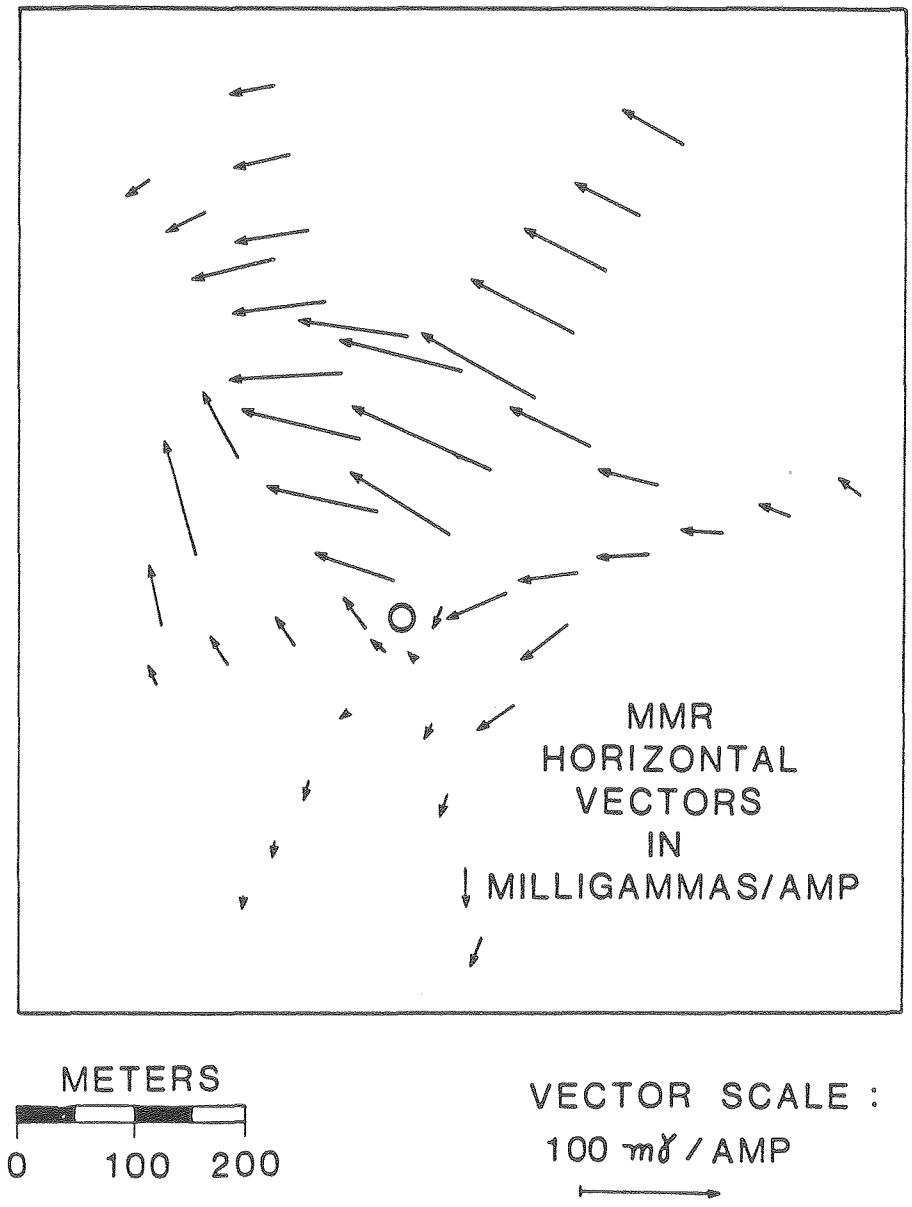

Figure 3-5-3. Actual MMR magnetic fields measured on the surface around drill hole D-9.

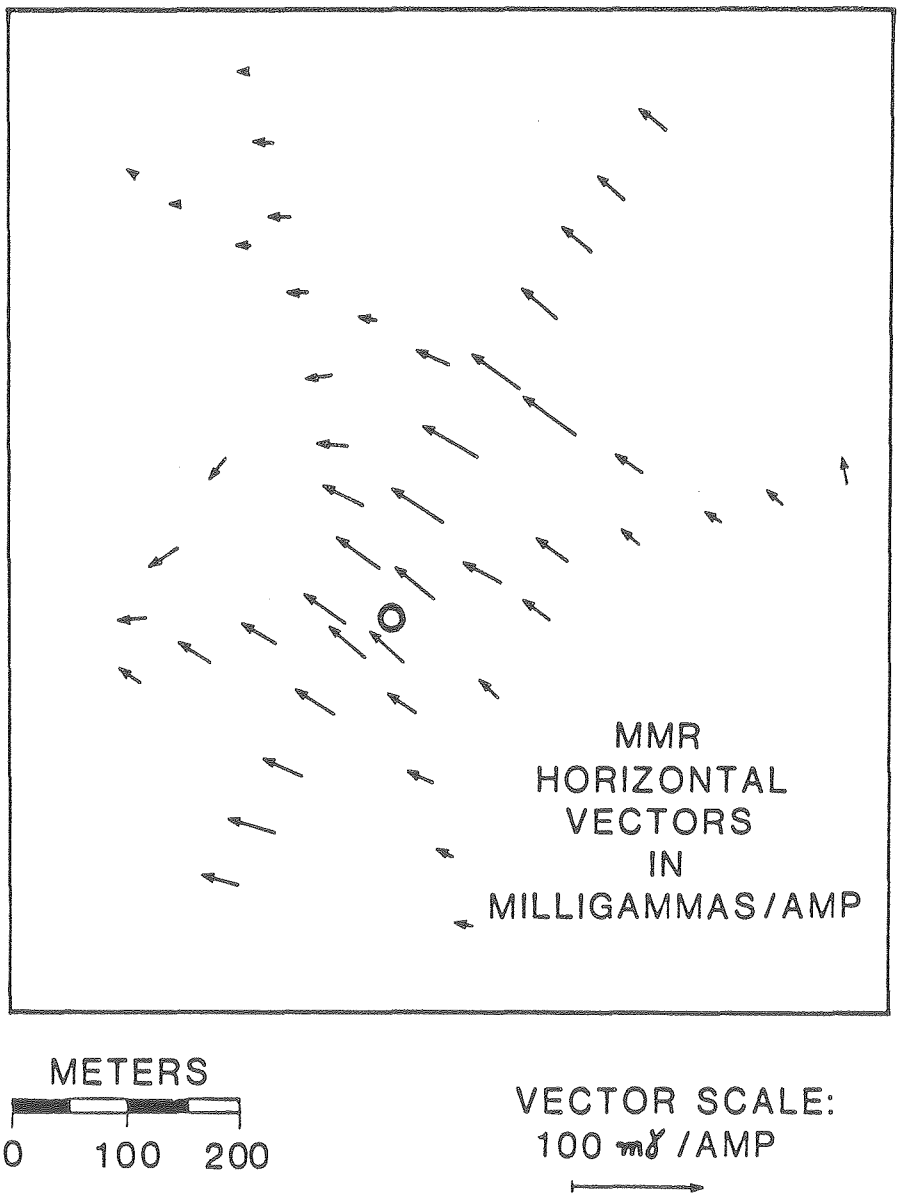

Figure 3-5-4. Terrain model MMR magnetic fields computed on the surface around drill hole D-9.

HALF-SPACE MAGNETIC FIELDS

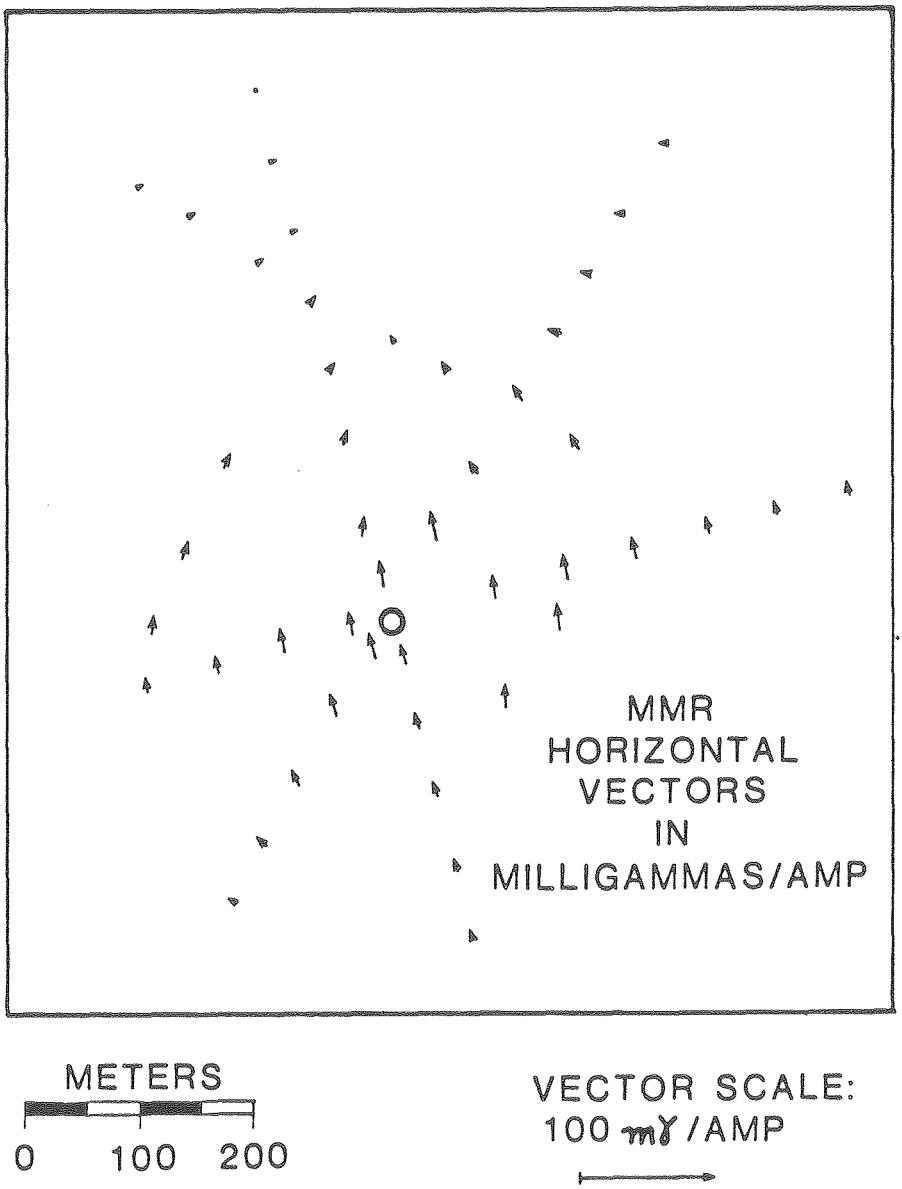

Figure 3-5-5. Half-space surface MMR magnetic fields computed in the vicinity of drill hole D-9.

TERRAIN CORRECTED MAGNETIC FIELDS

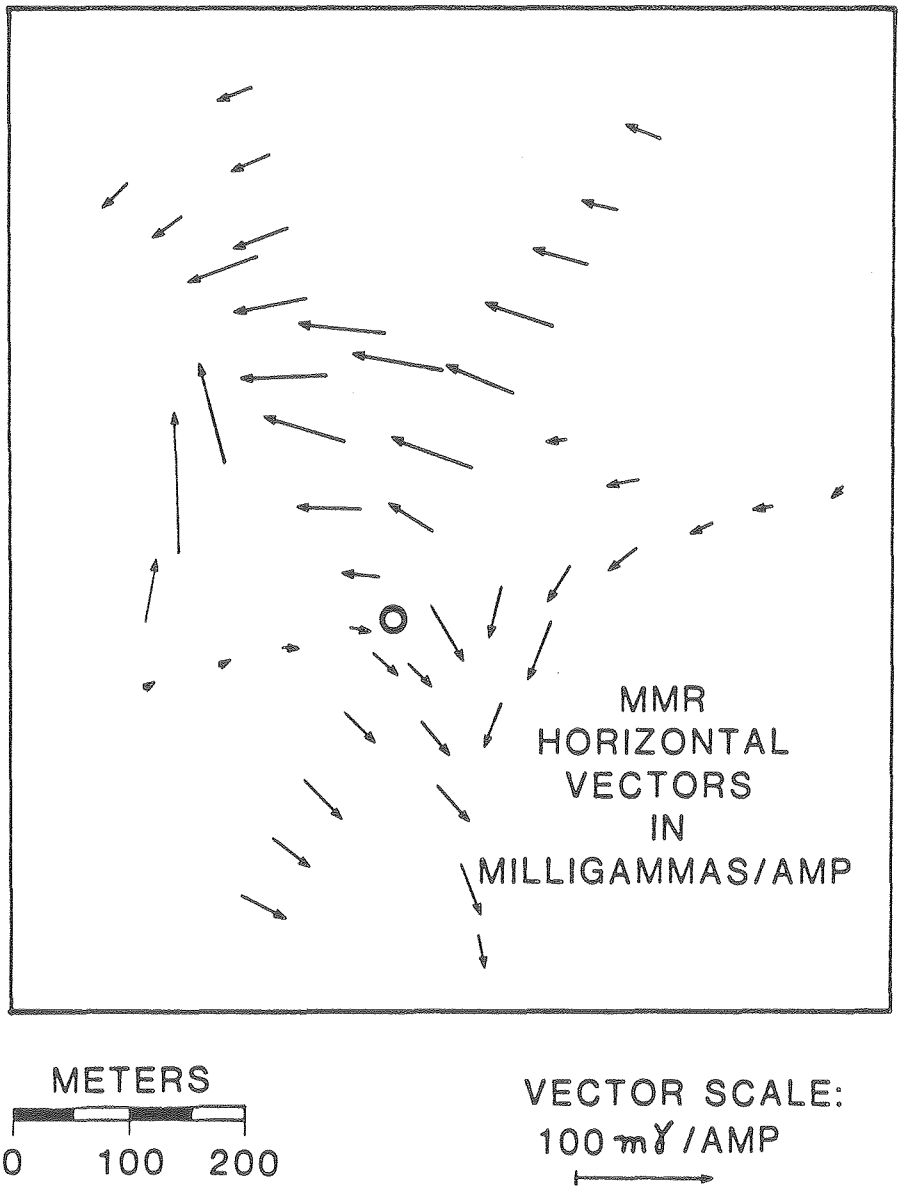

Figure 3-5-6. Measured MMR magnetic fields with terrain model fields removed, i.e., terrain corrected fields.

INTERPRETATION

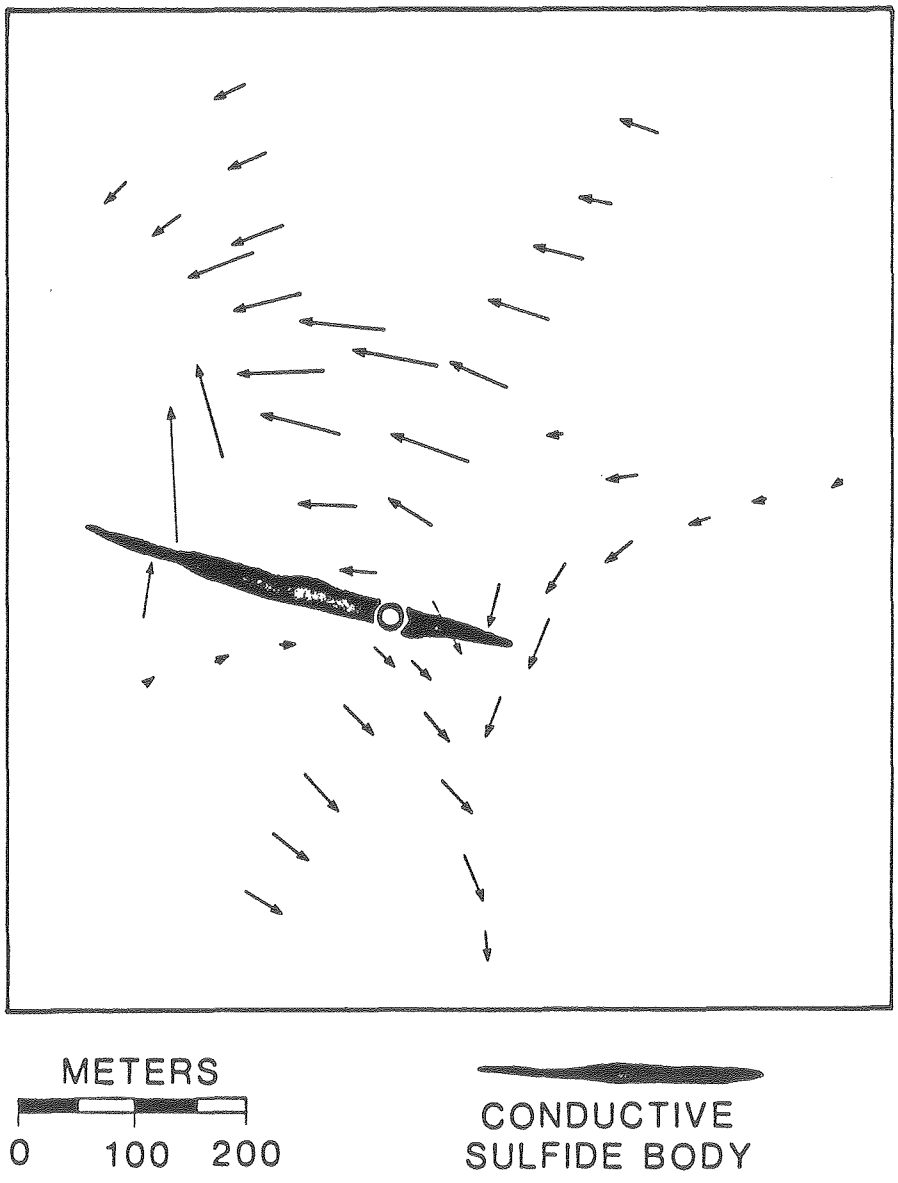

Figure 3-5-7. Qualitative interpretation of the terrain corrected magnetic field in the vicinity of drill hole D-9.

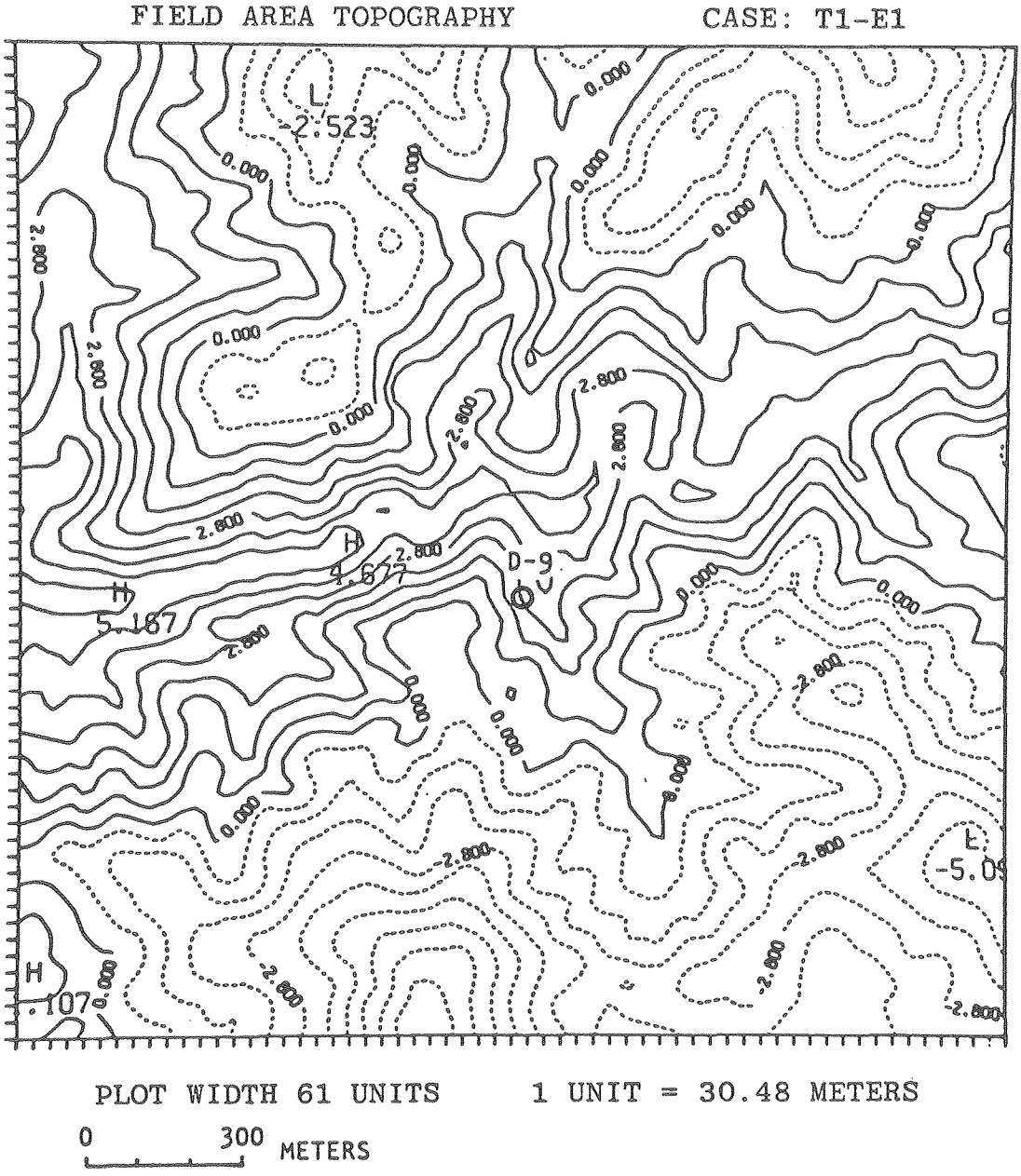

Figure 3-6-1. Model topography. Complete 61 x 61 element model surface used to model the mise-a-la-masse and MMR surveys in the vicinity of drill hole D-9. Contour interval of 0.7 model units (or 21 meters). Increasing elevations indicated by decreasing contour values.

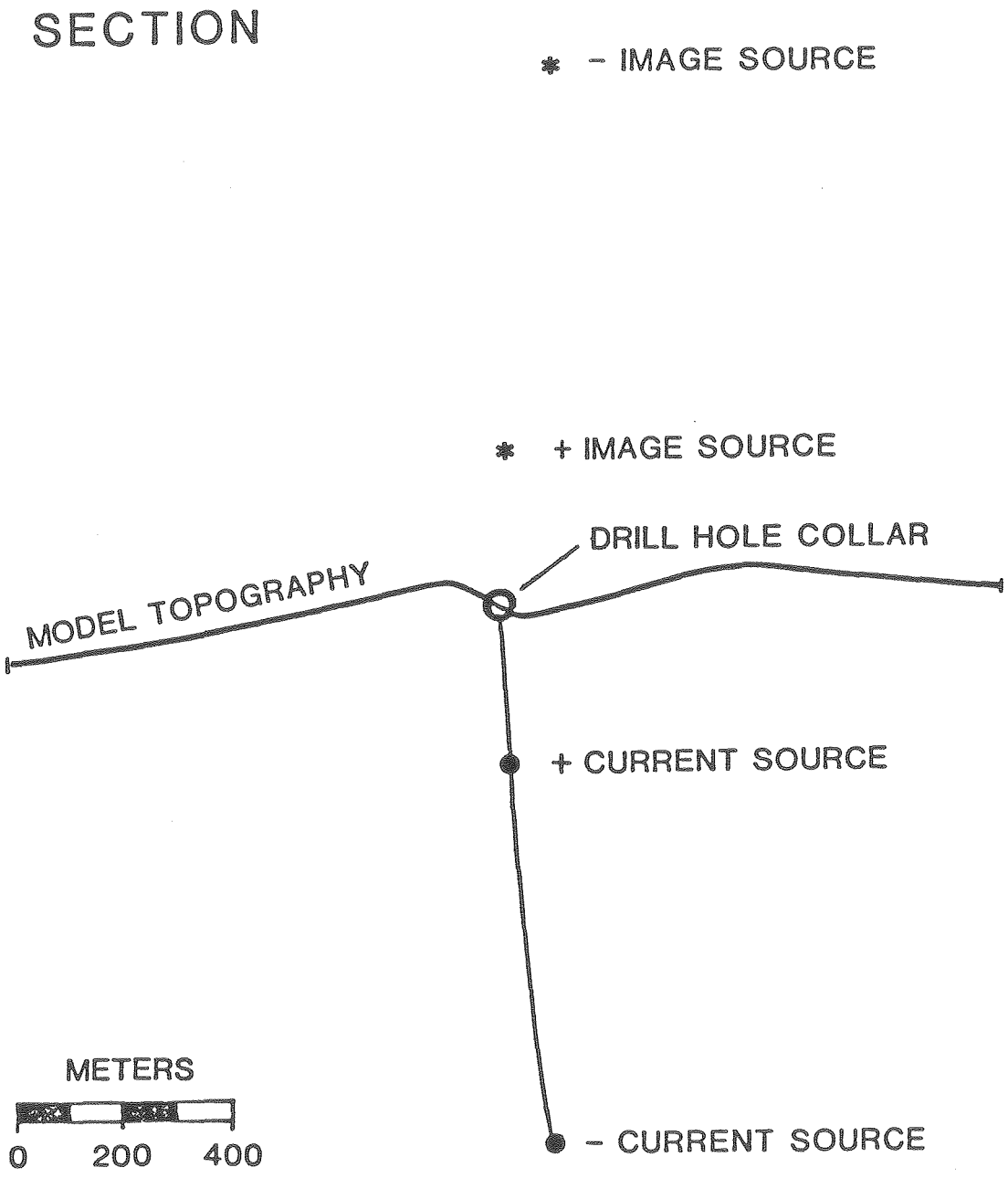

Figure 3-6-2. West-east section through the model topography and drill hole D-9 showing the locations of down-hole current sources and above-surface current source images.

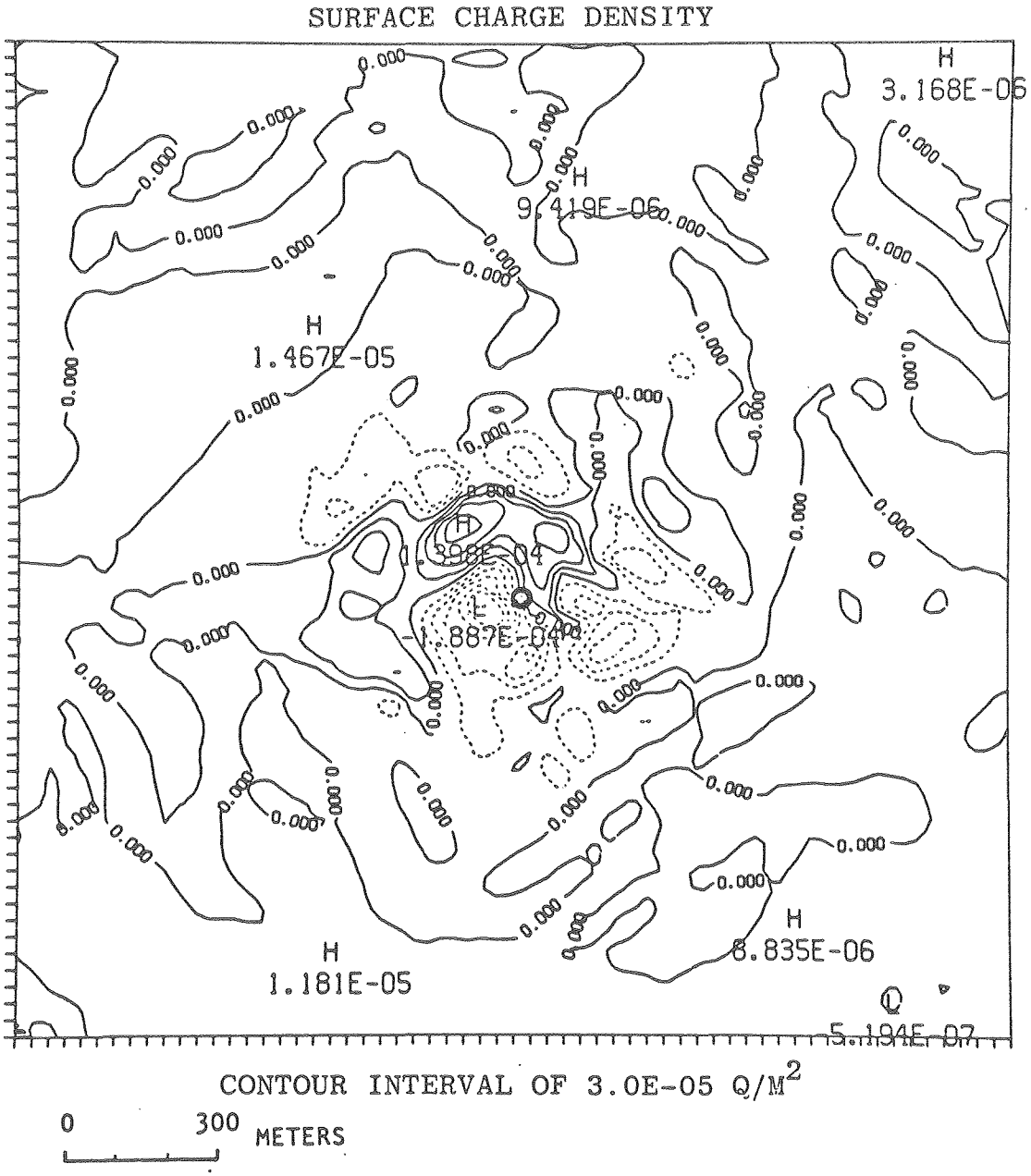

Figure 3-6-3. Surface charge density on the 61 x 61 element model surface.

ENLARGEMENT OF CENTER SECTION OF MODEL GRID

SURFACE CHARGE DENSITY

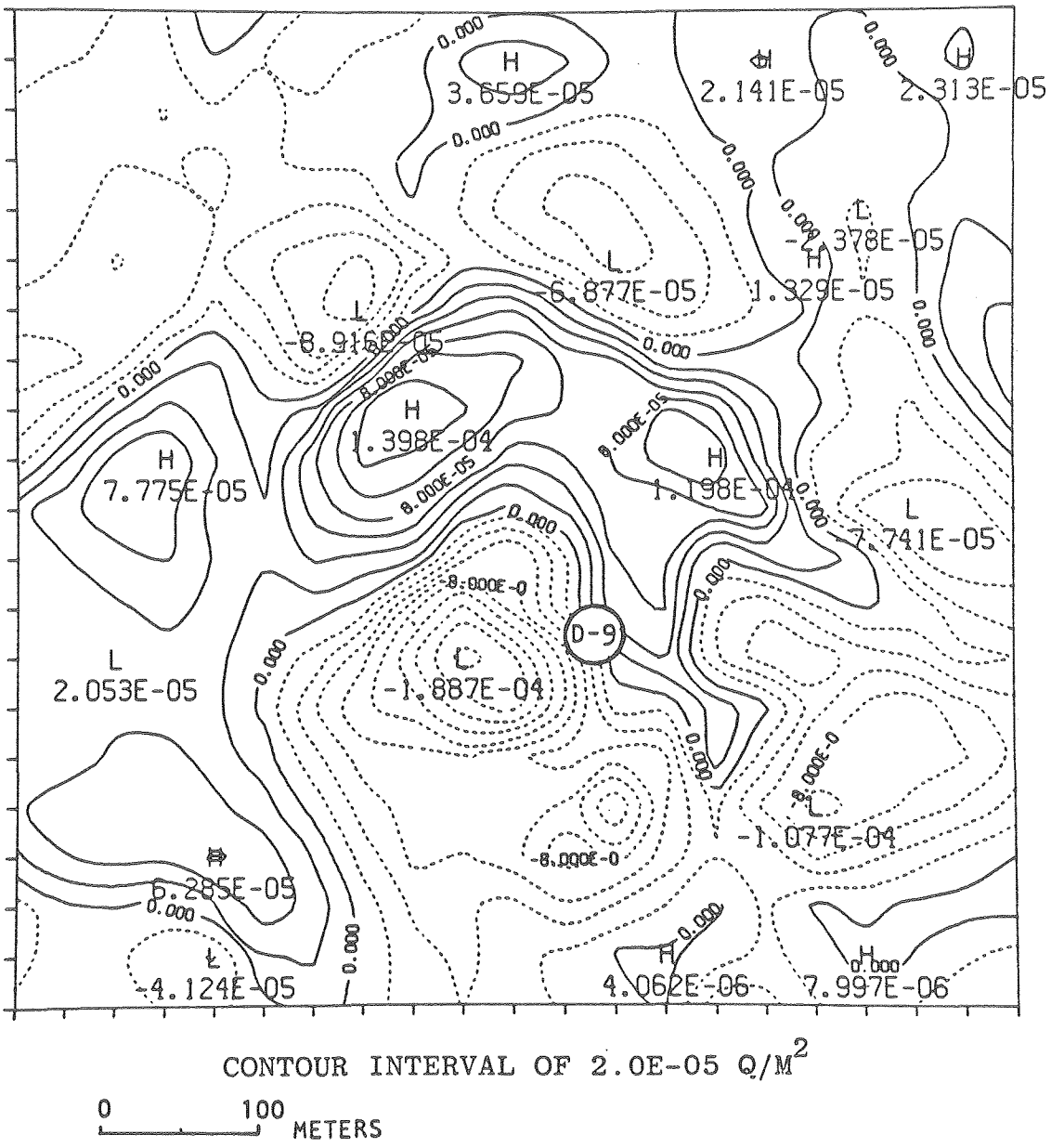

CONTOUR INTERVAL OF 2.0E-05 Q/M^2

Figure 3-6-4. Detail of surface charge density on the central 21 x 21 elements of the model surface.

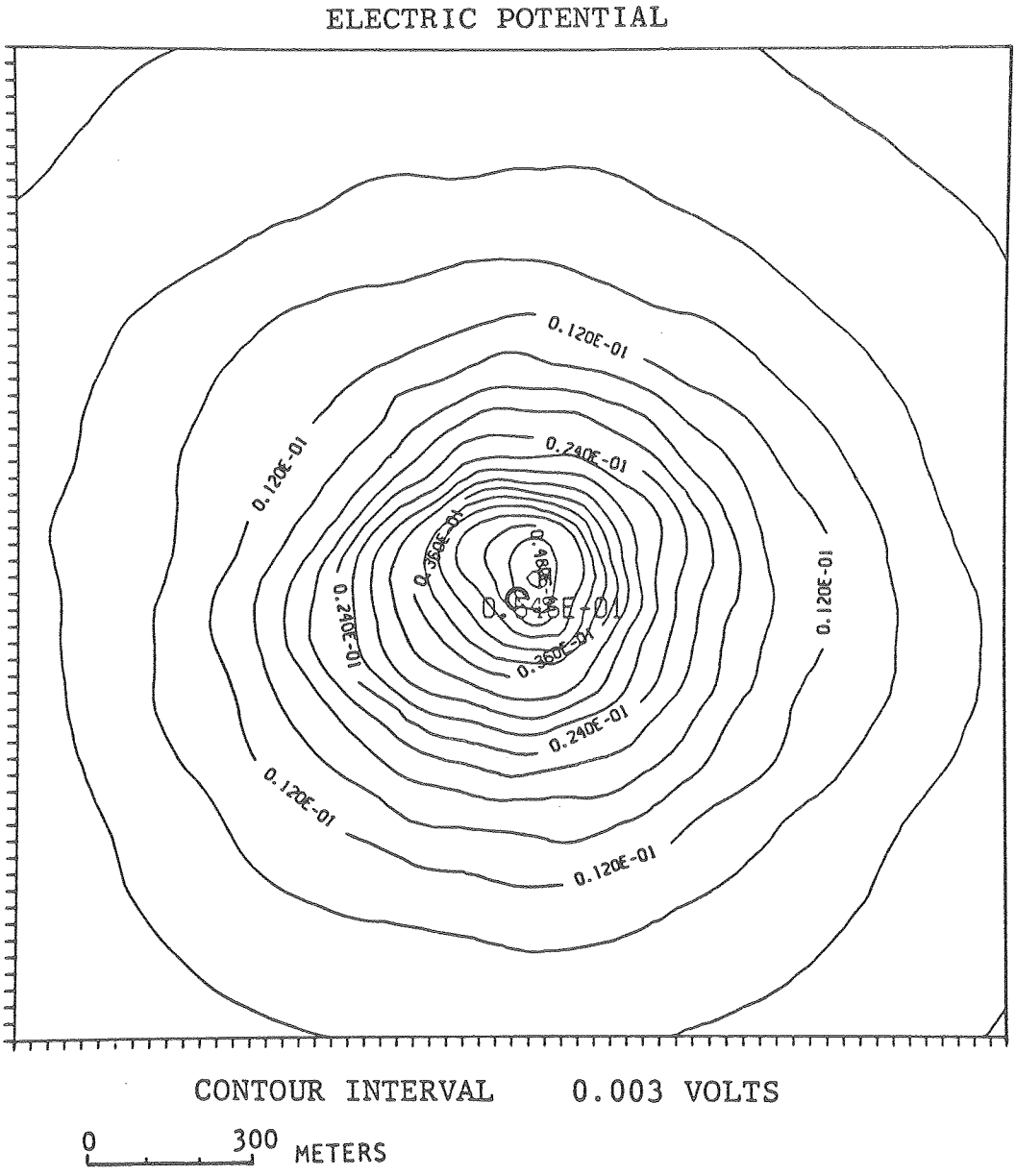

Figure 3-6-5. Electric potential on the model surface relative to a reference potential electrode at infinity.

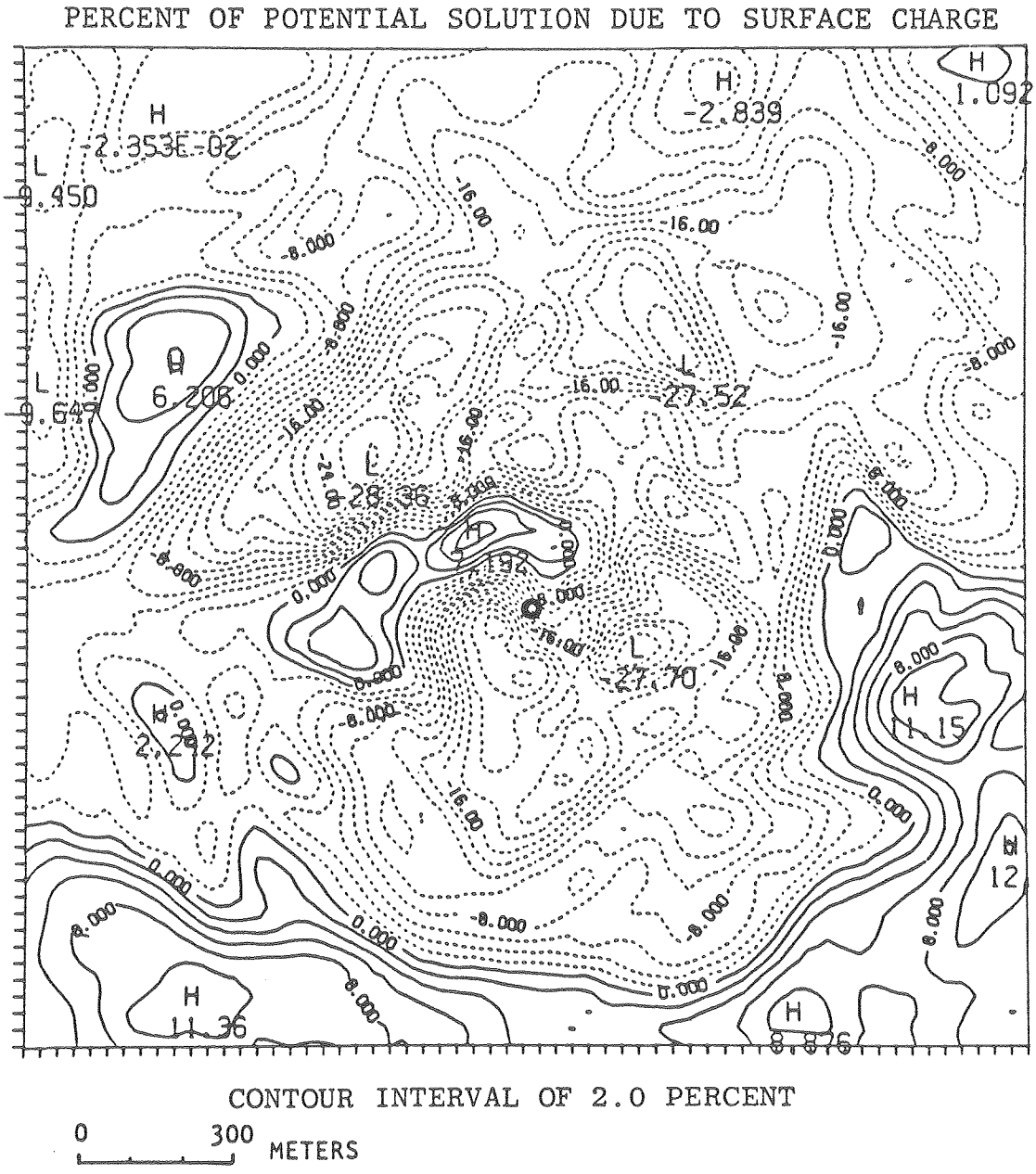

Figure 3-6-6. Percentage of the total potential model solution due to surface charge.

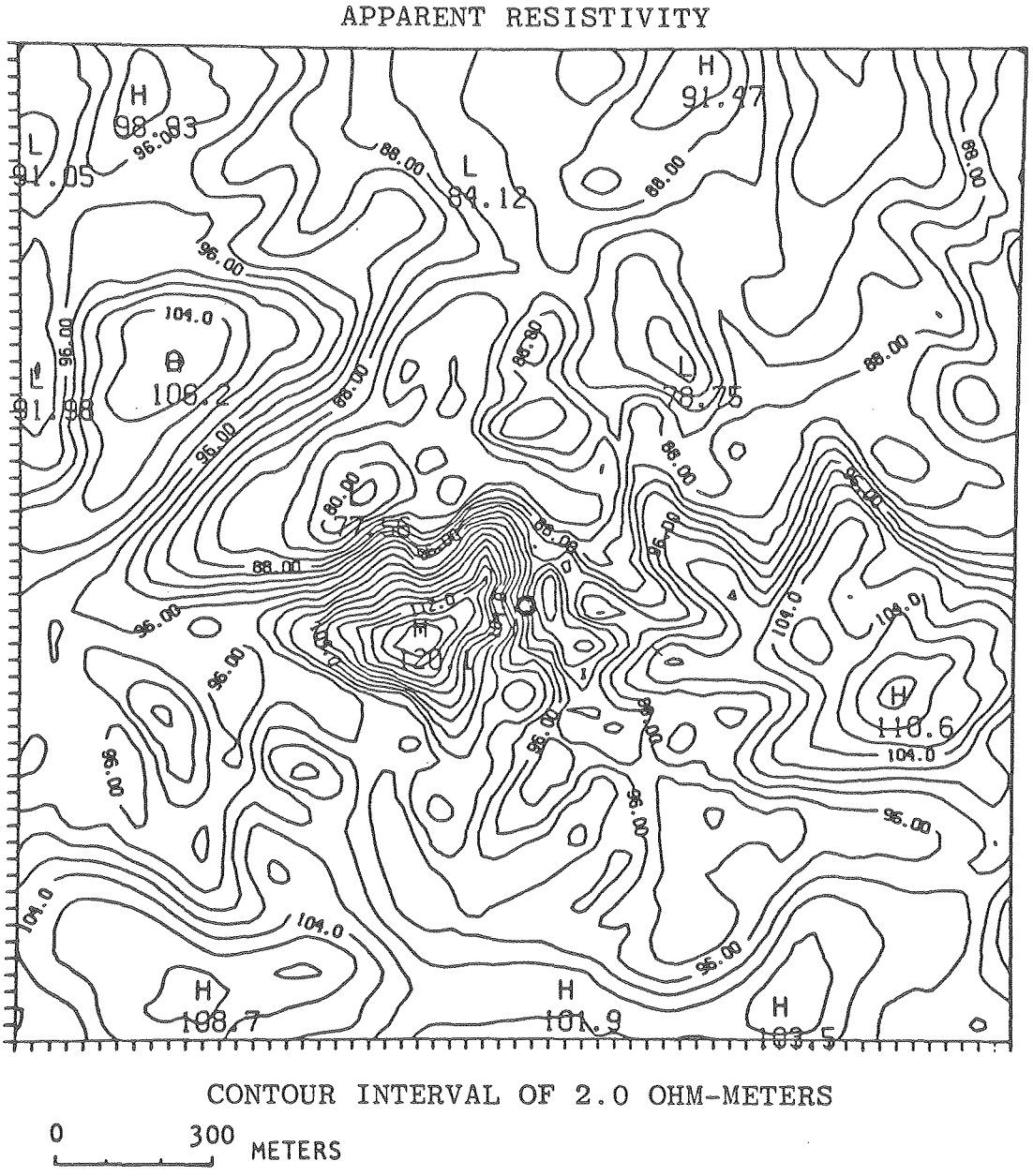

Figure 3-6-7. Model apparent resistivities computed from the total potential using flat earth geometric factors and straight lines distances between electrodes. (61 x 61 element model surface).

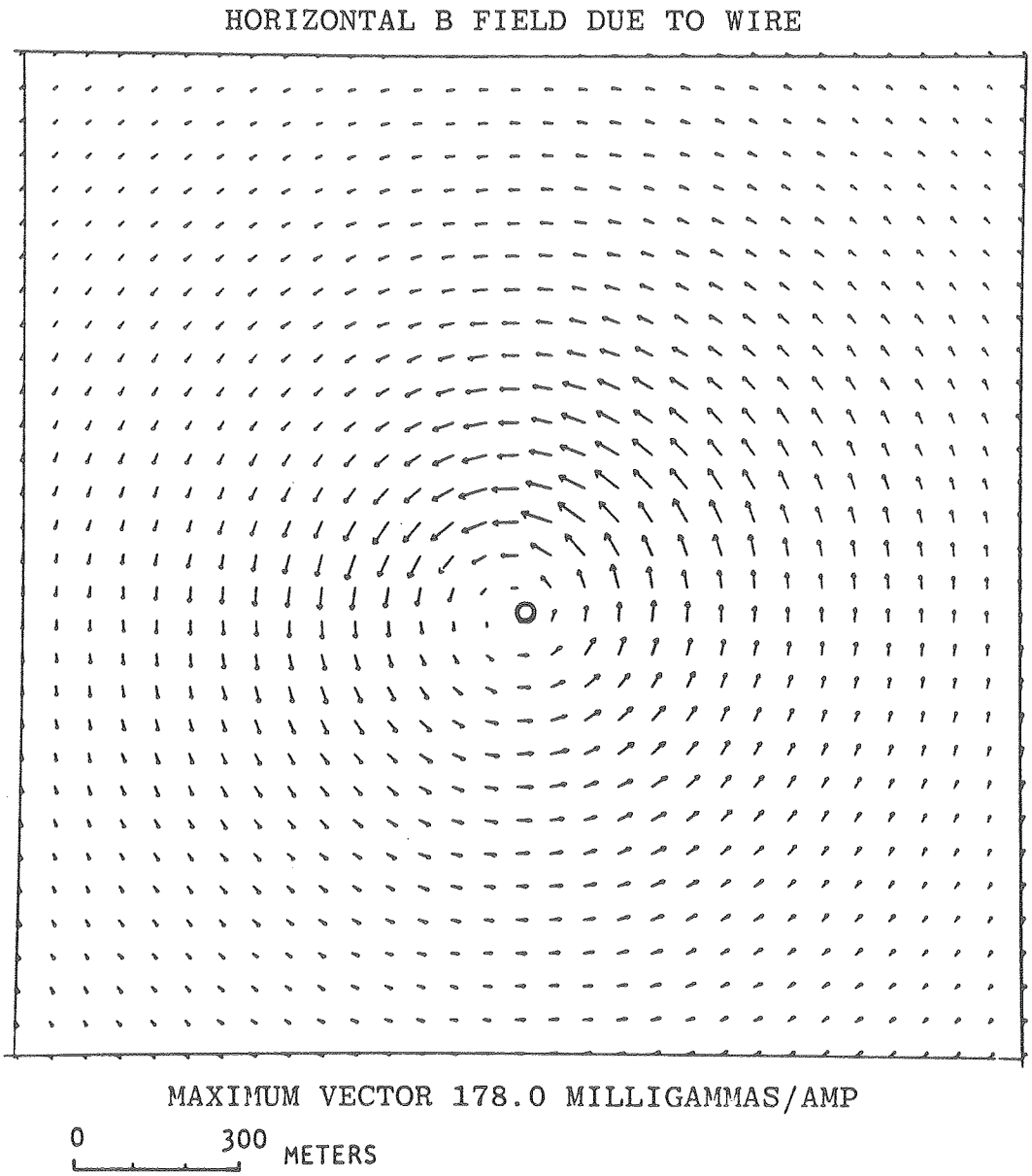

Figure 3-6-8. Horizontal vector magnetic fields on the model surface due to current flow in the wires connected to the down-hole current electrodes.

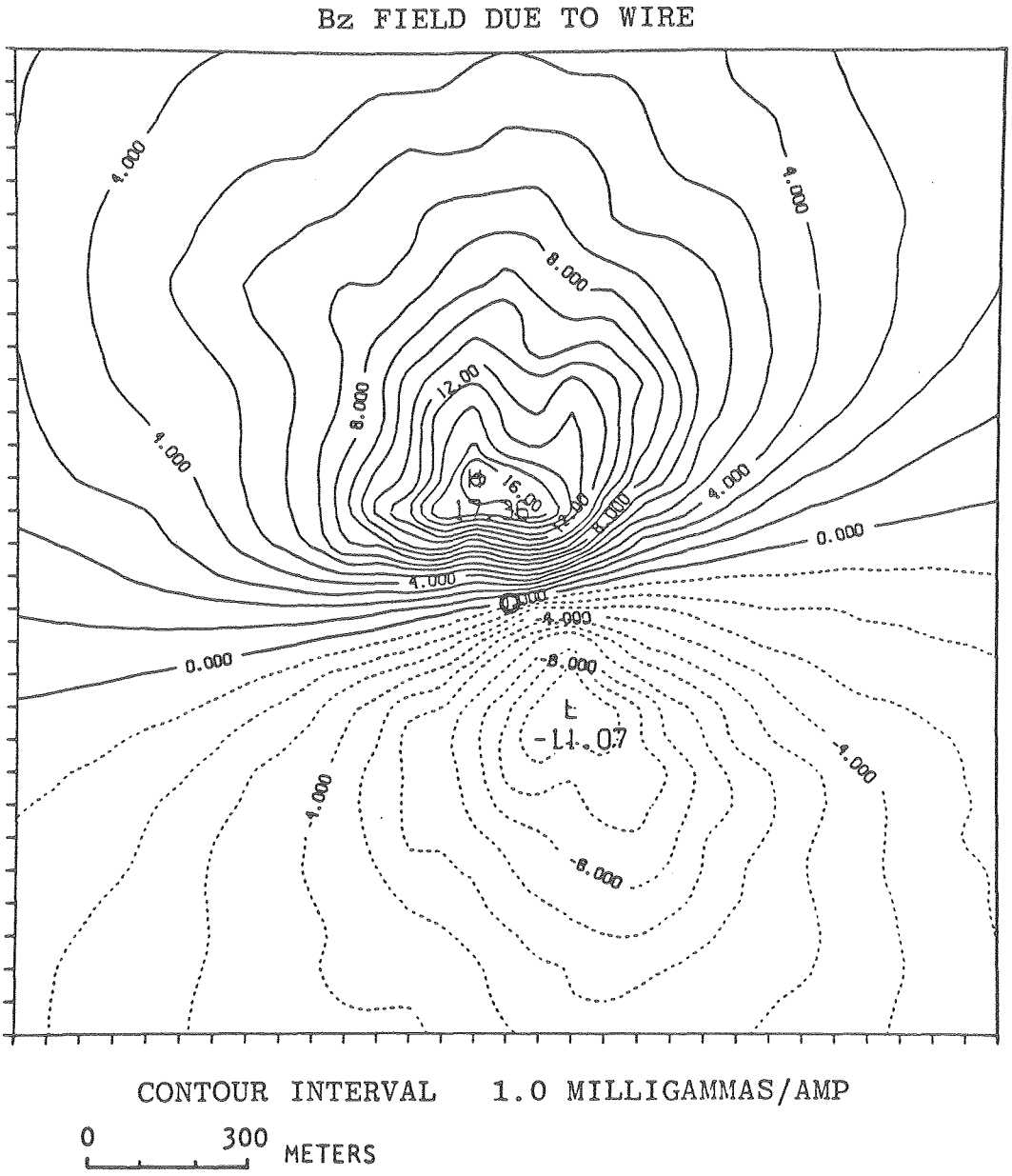

Figure 3-6-9. Vertical magnetic field on the model surface due to current flow in the wires connected to the down-hole current electrodes.

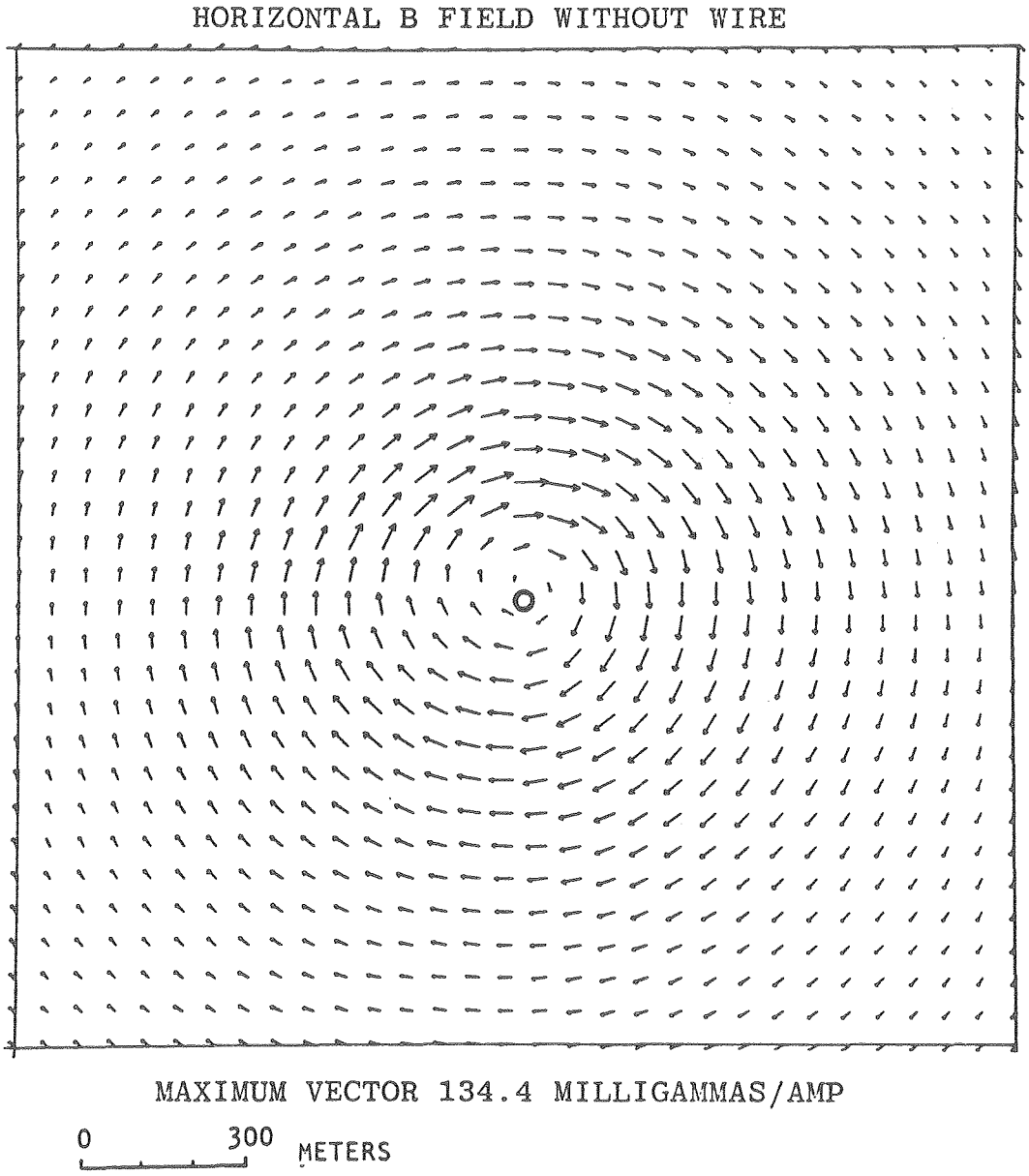

Figure 3-6-10. Horizontal vector magnetic fields on the model surface due to current flow (from the down-hole electrodes) in the homogeneous earth model.

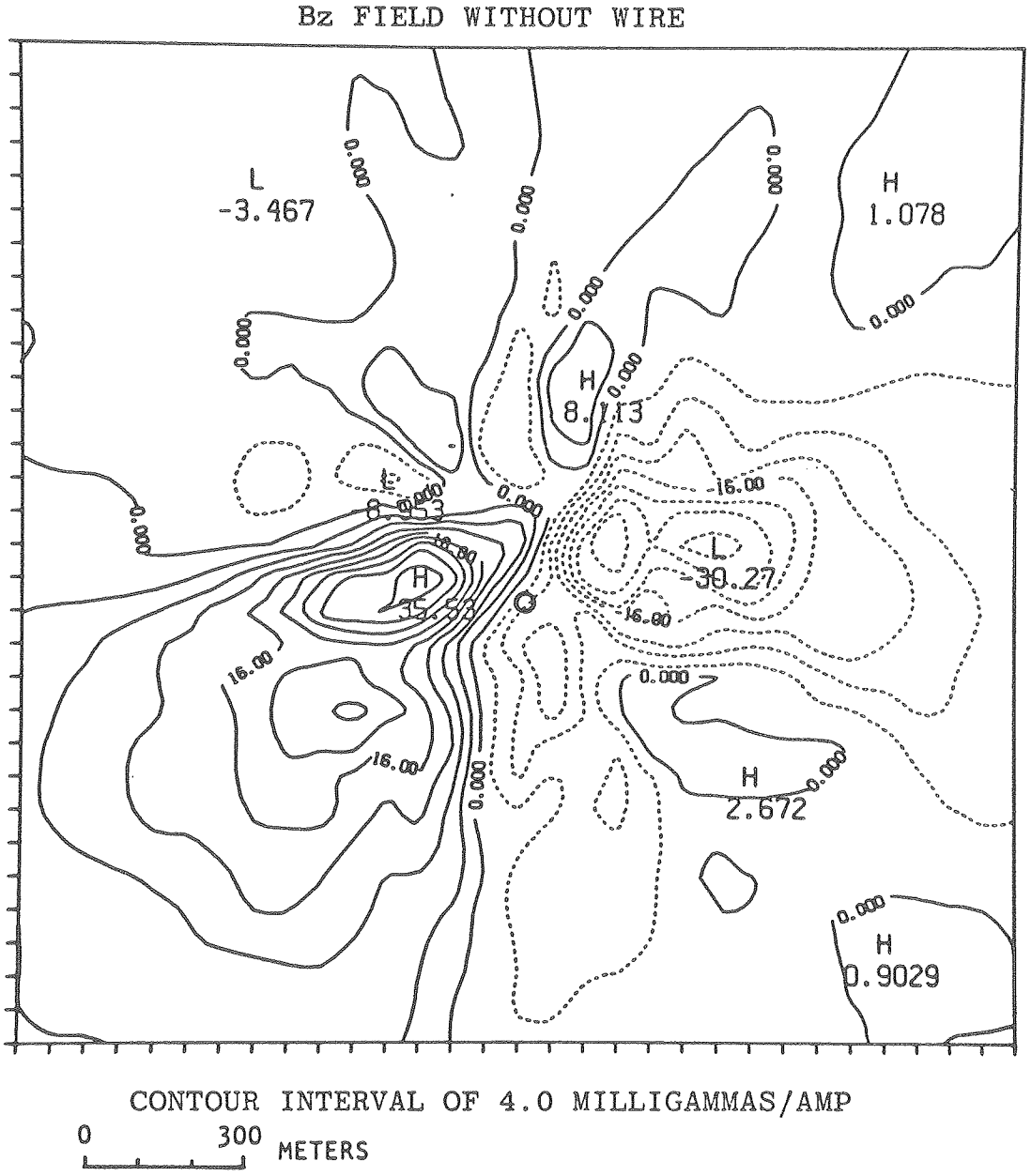

Figure 3-6-11. Vertical magnetic field on the model surface due to current flow (from the down-hole electrodes) in the homogeneous earth model.

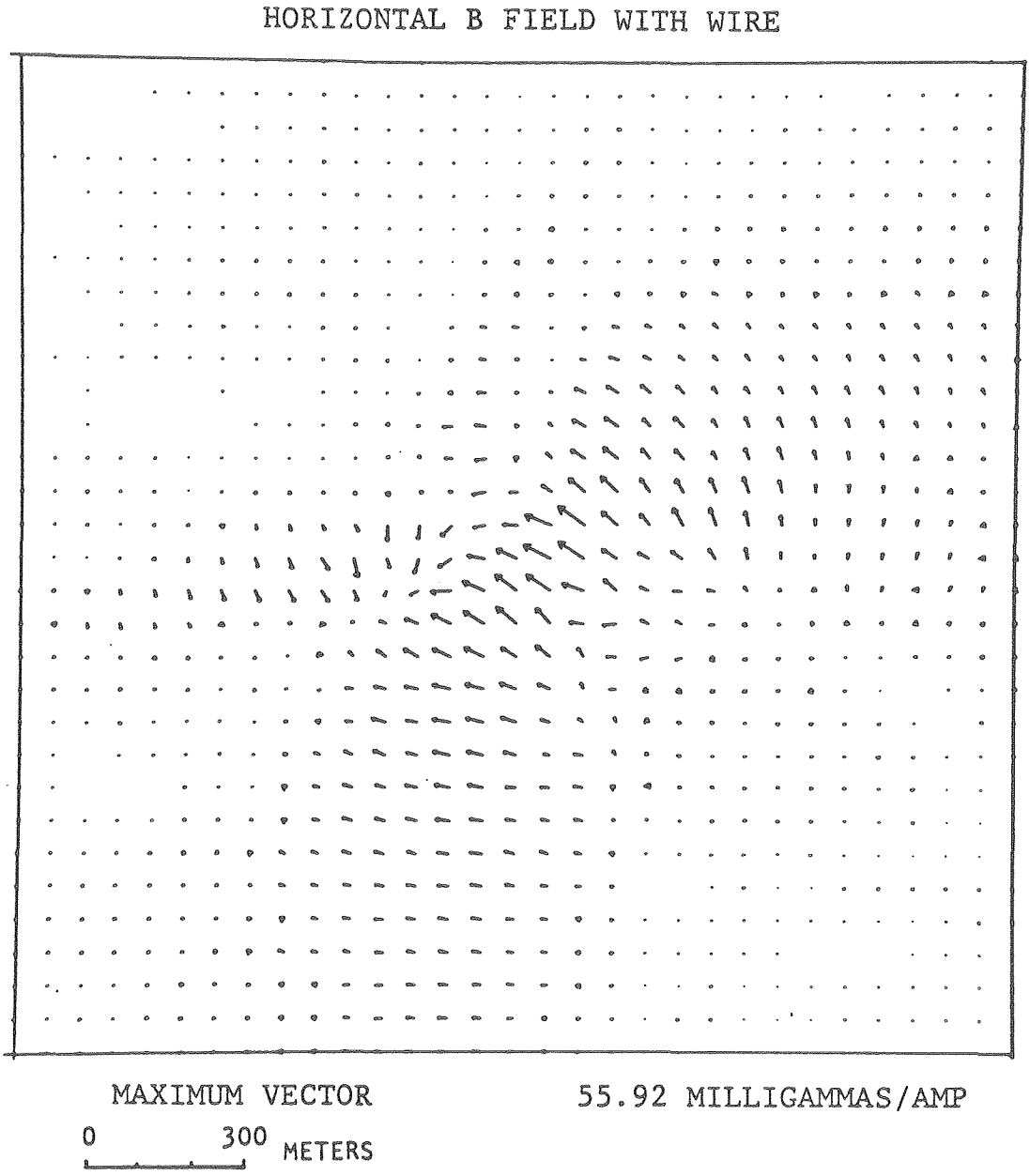

Figure 3-6-12. Horizontal magnetic field vectors on the model surface due to current flow in the wires and in the earth.

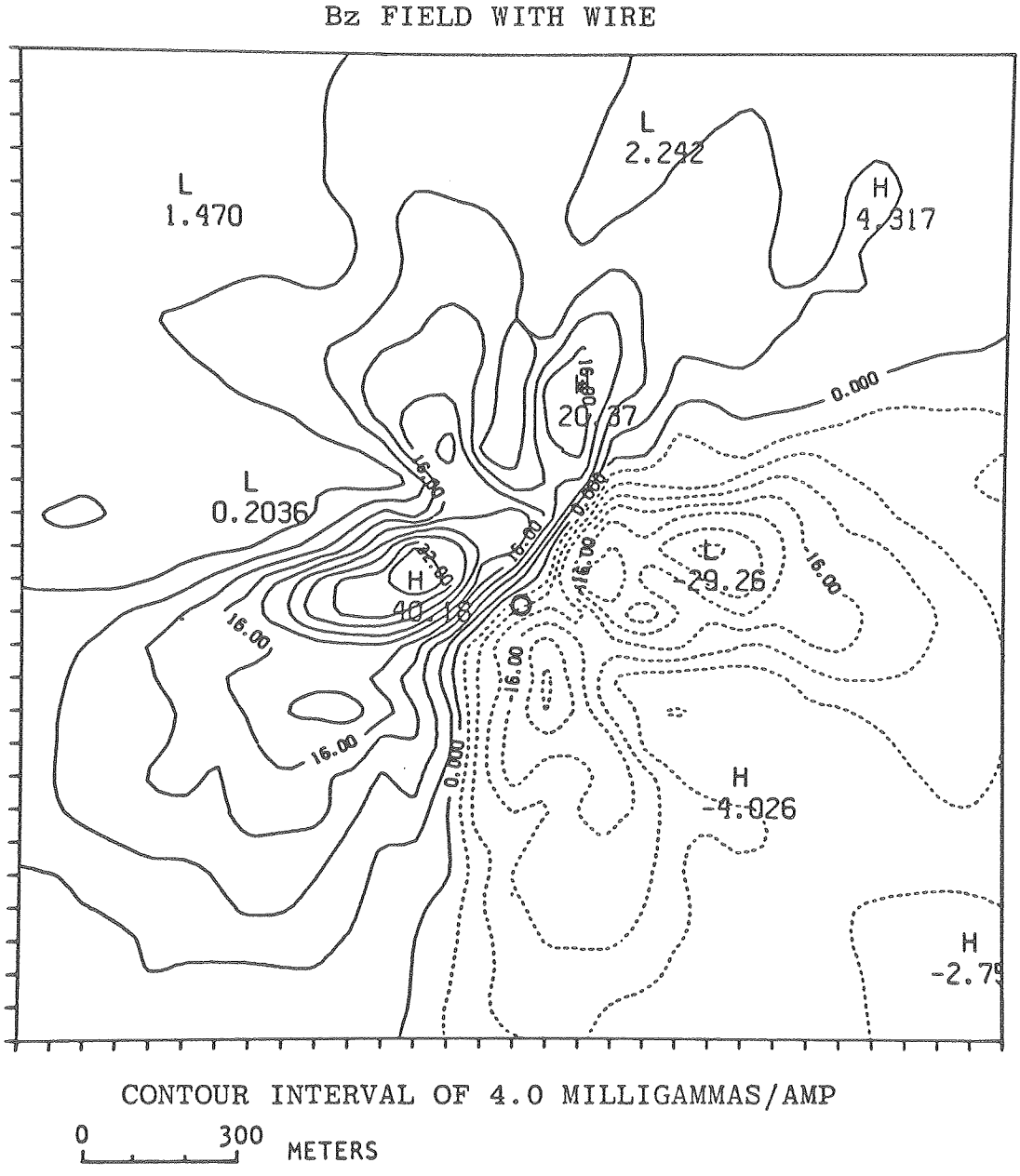

Figure 3-6-13. Vertical magnetic field on the model surface due to current flow in the wires and in the earth.

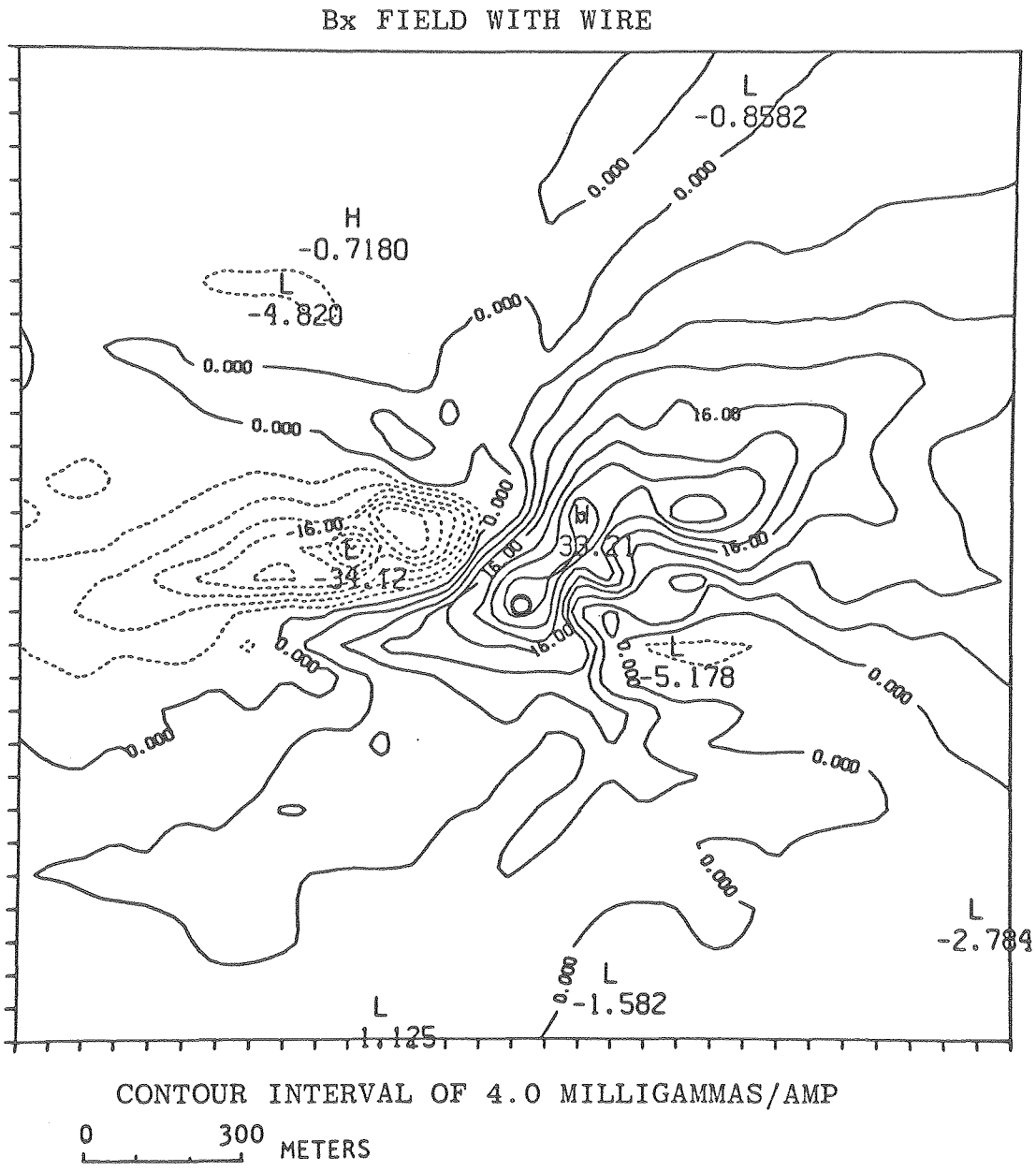

Figure 3-6-14. Magnetic field x (north) component on the model surface due to current flow in the wires and in the earth. (61 x 61 element model surface).

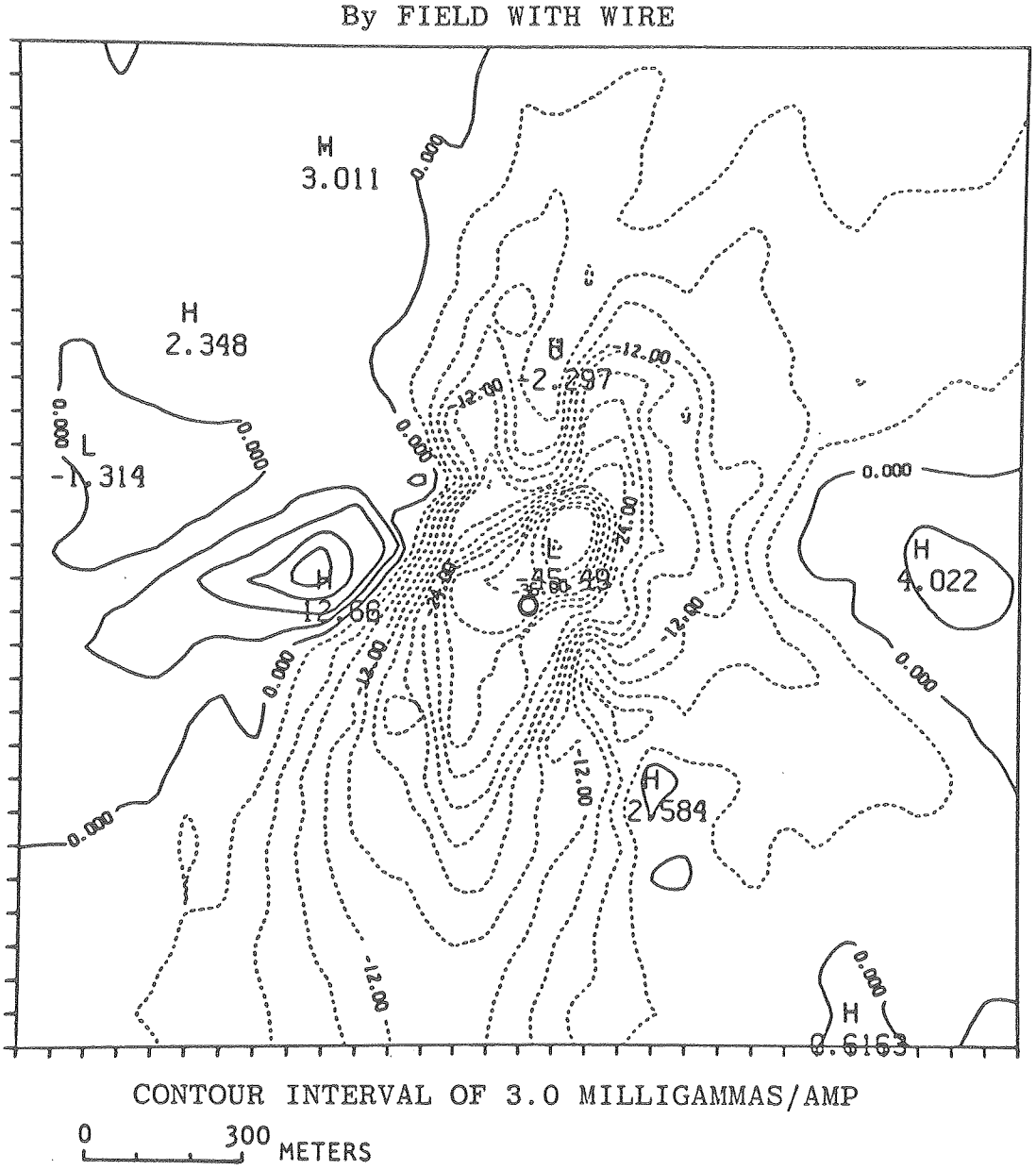

Figure 3-6-15. Magnetic field y (east) component on the model surface due to current flow in the wires and in the earth. (61 x 61 element model surface).

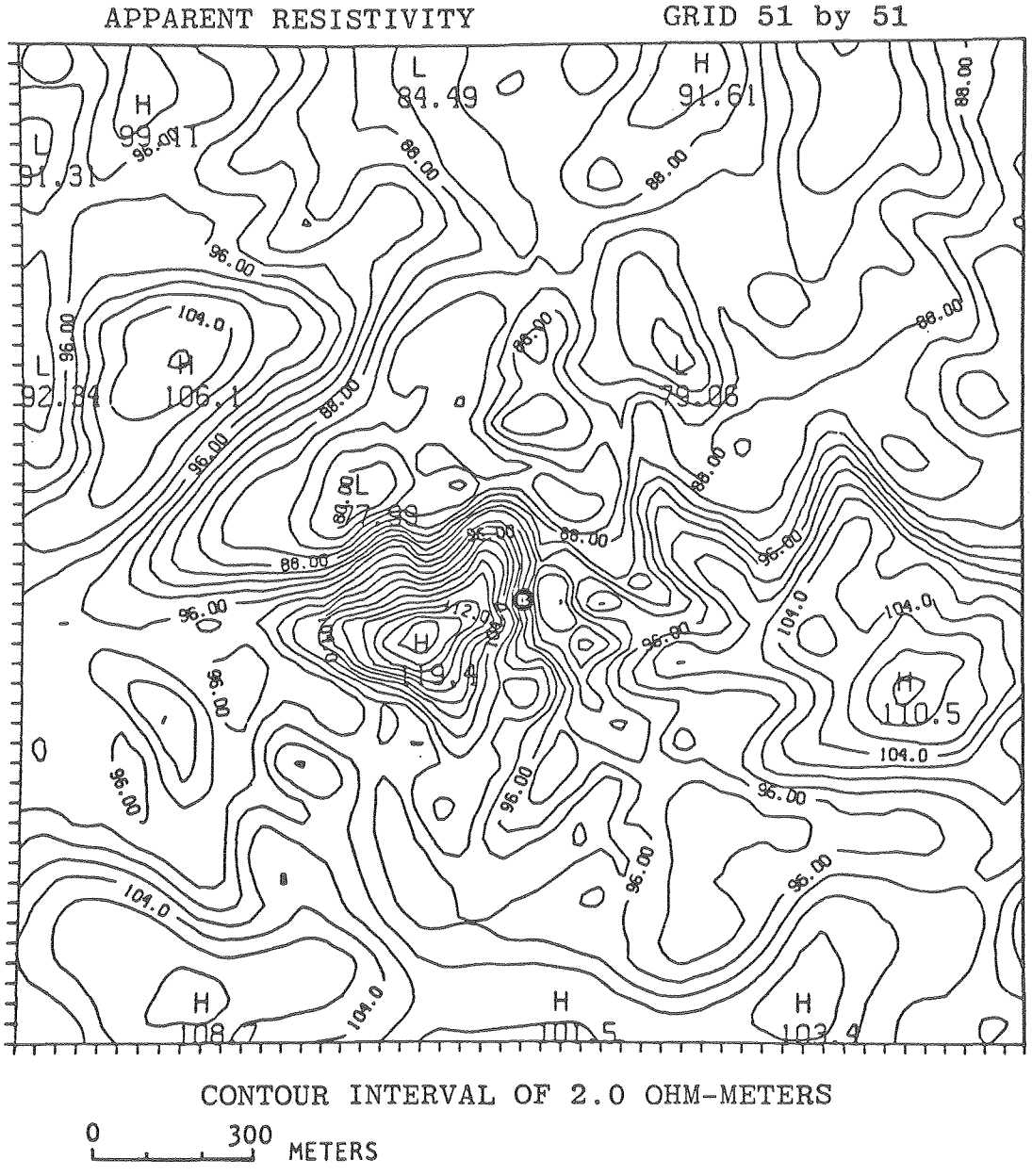

Figure 3-6-16. Model apparent resistivities computed from the total potential using flat earth geometric factors and straight line distances between electrodes. (51 x 51 element model surface).

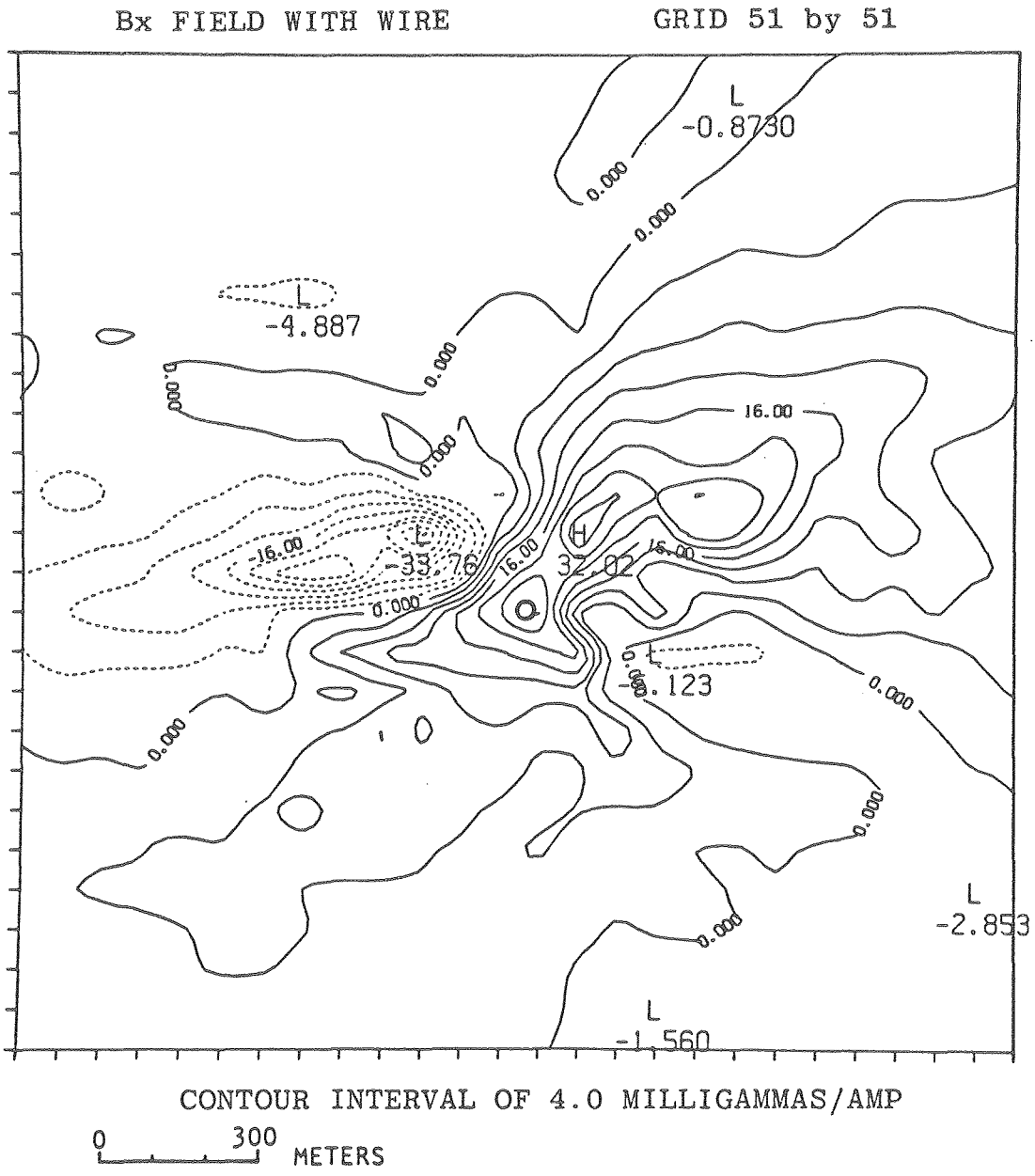

Figure 3-6-17. Magnetic field x component on the model surface due to current flow in the wires and in the earth. (51 x 51 element model surface).

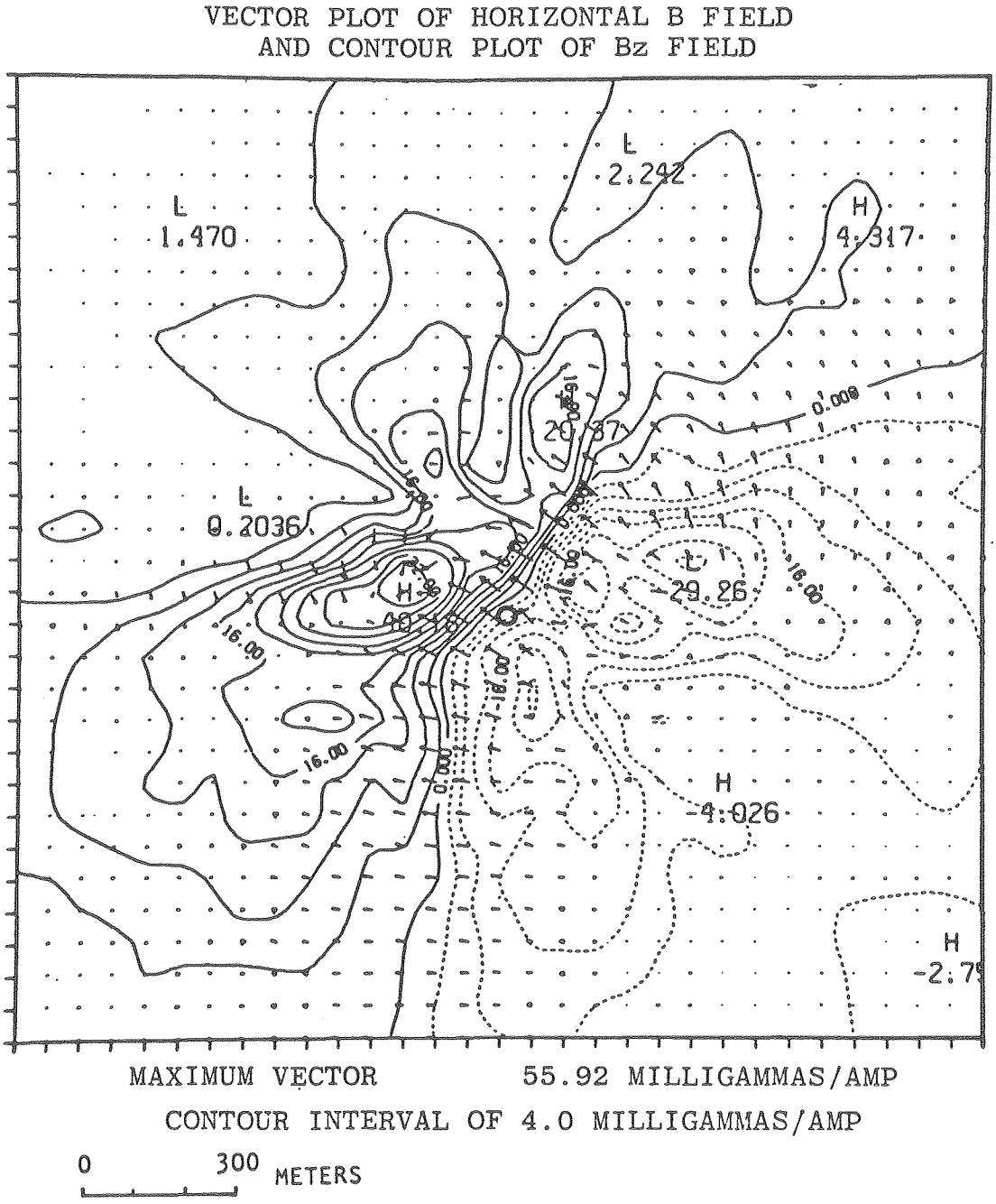

Figure 3-6-18. Combined plots of horizontal and vertical magnetic fields on the model surface due to current flow in the wires and in the earth. (61 x 61 element model surface).

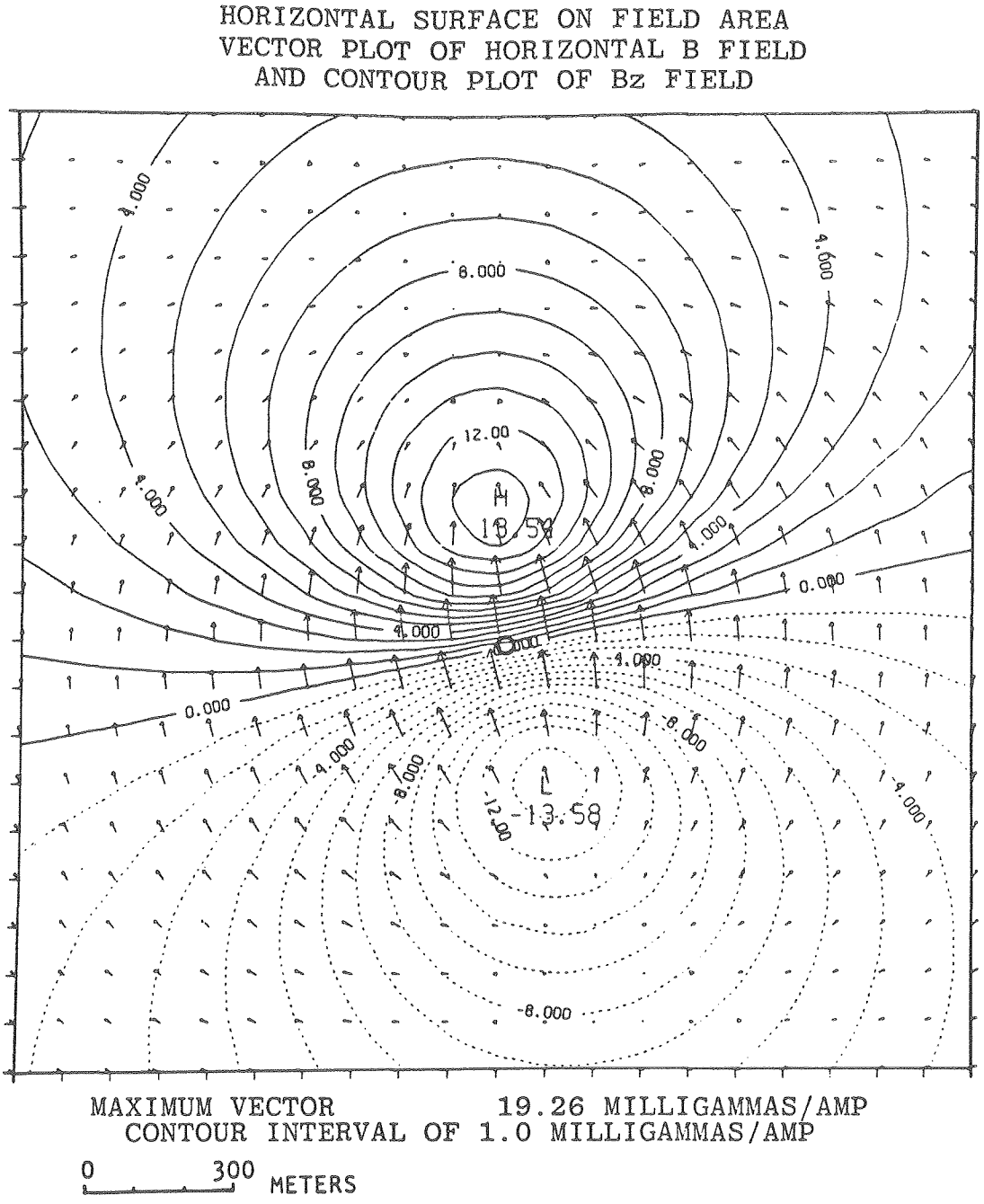

Figure 3-6-19. Combined plots of horizontal and vertical magnetic fields on the horizontal surface of a homogeneous earth model due to current flow in the wires and in the earth.

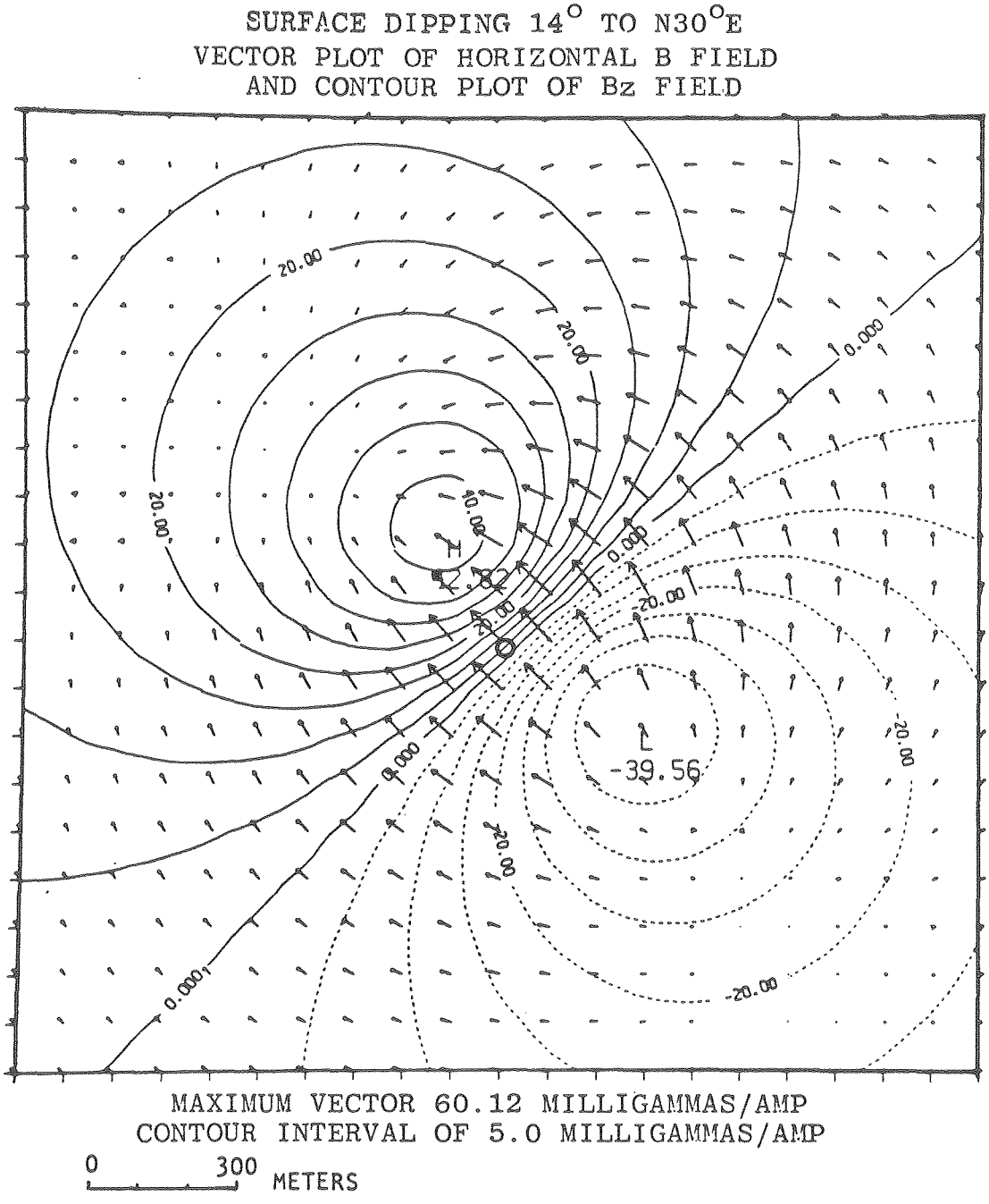

Figure 3-6-20. Combined plots of horizontal and vertical magnetic fields on the dipping (flat) surface of a homogeneous earth model due to current flow in the wires and in the earth.

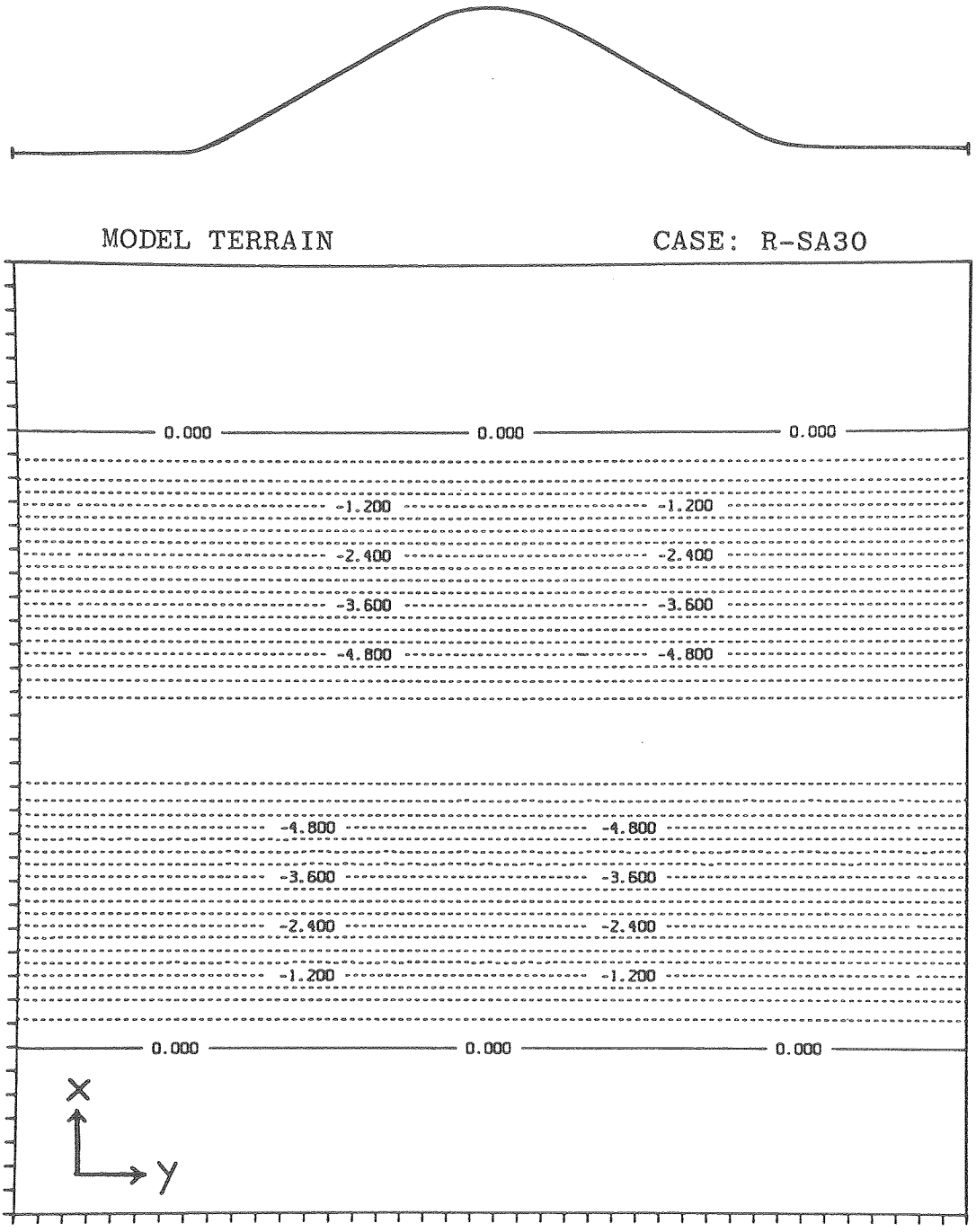

Figure 3-7-1. 2-D ridge with 30° slopes.

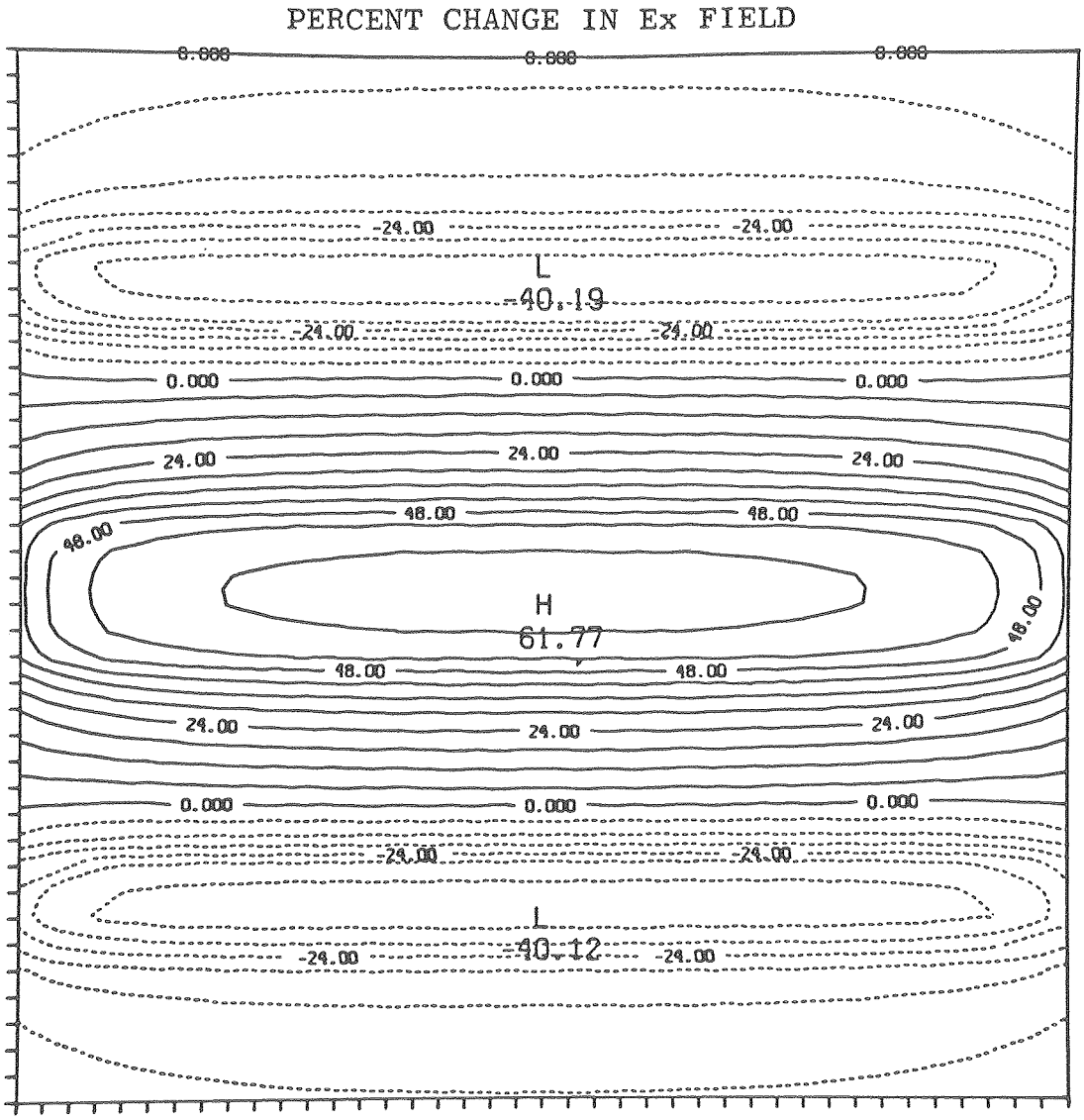

Figure 3-7-2. Percent surface electric field anomaly caused by a uniform electric field perpendicular to the strike of a 2-D ridge with 30° slopes. Negative values indicate an increase in electric field strength.

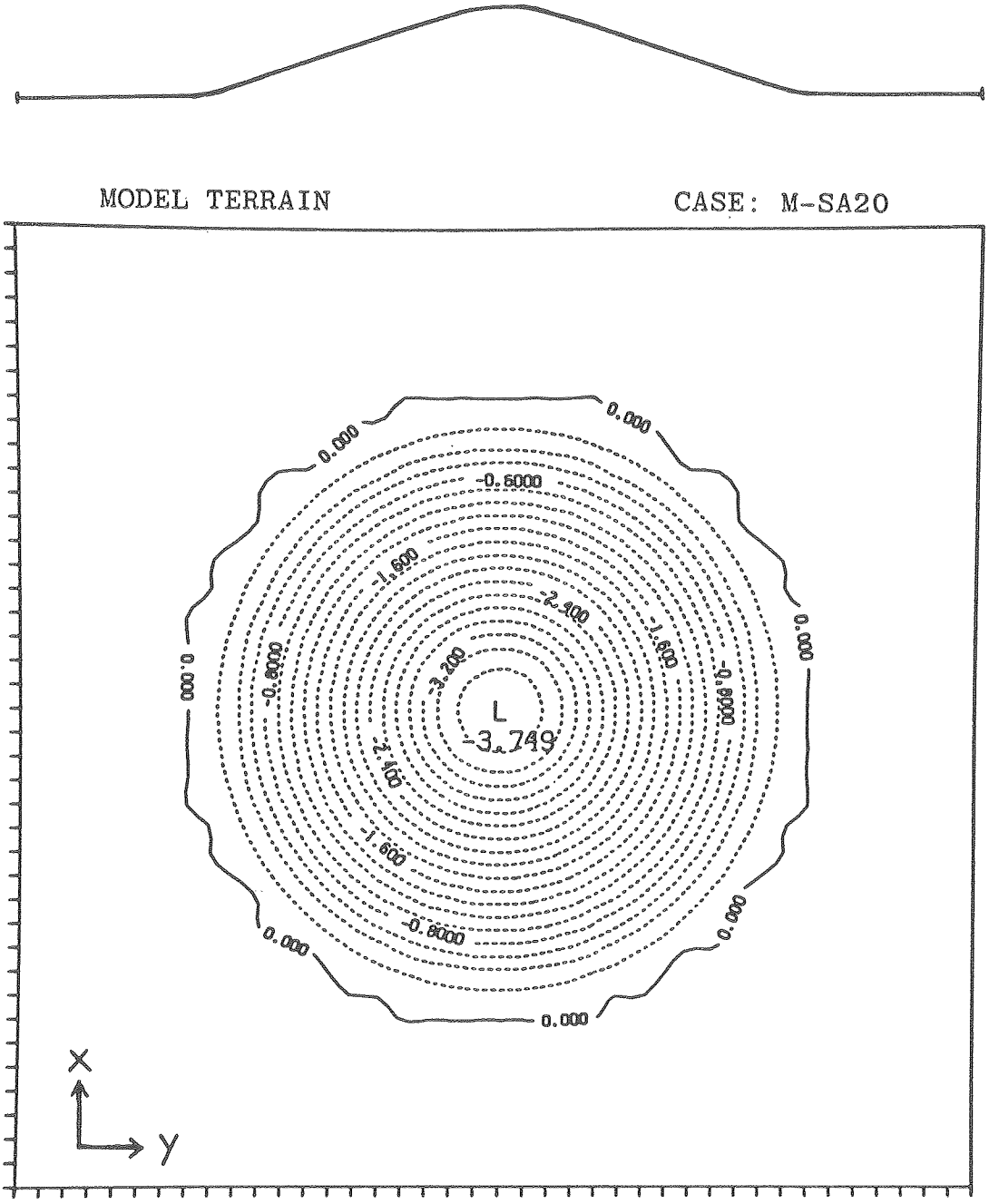

Figure 3-7-3. 3-D hill with 20° slopes.

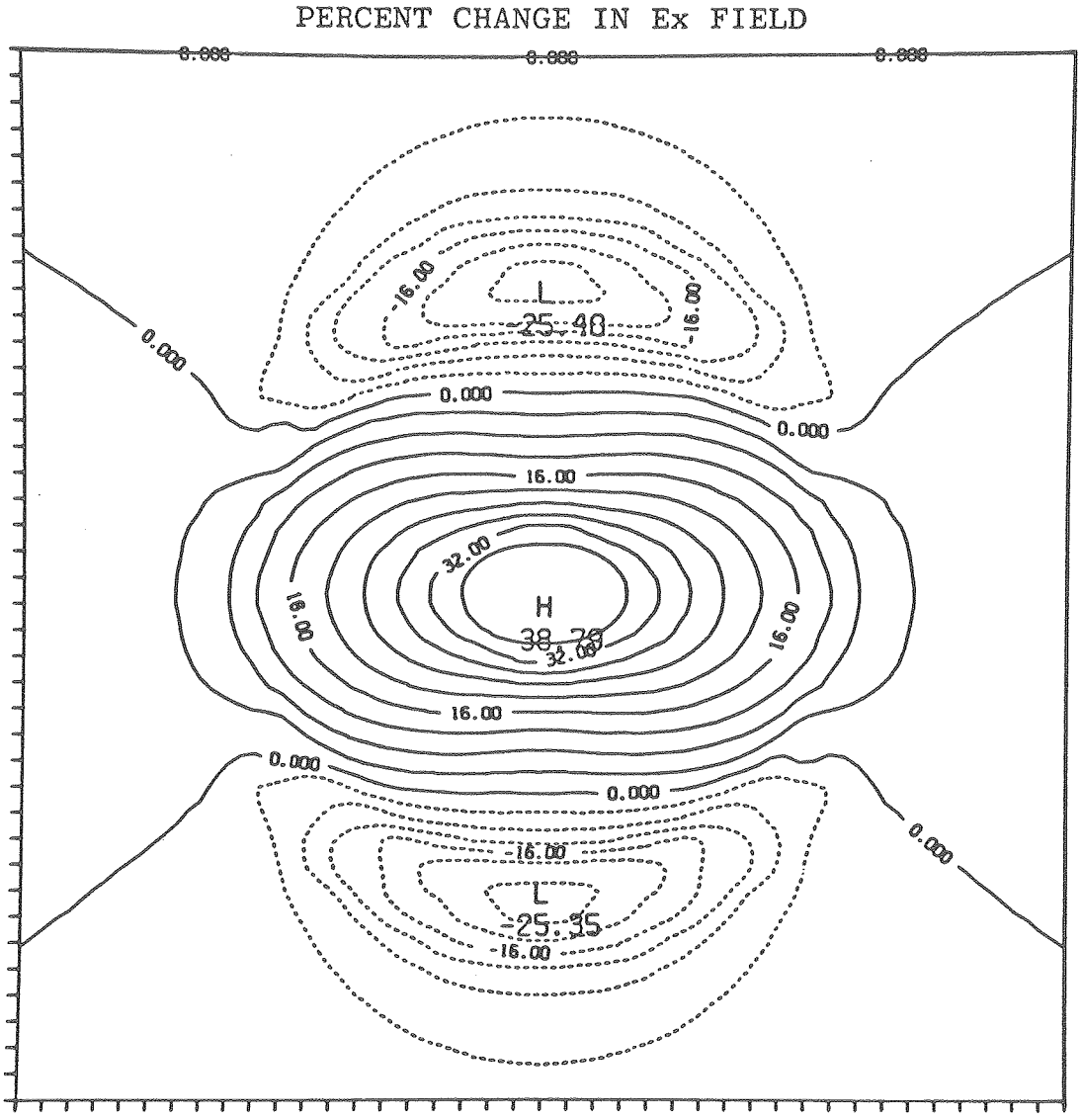

XBL 7911-12993

Figure 3-7-4. Percent surface electric field anomaly caused by a 3-D hill with 20° slopes in a uniform horizontal electric field. Negative values indicate an increase in electric field strength.

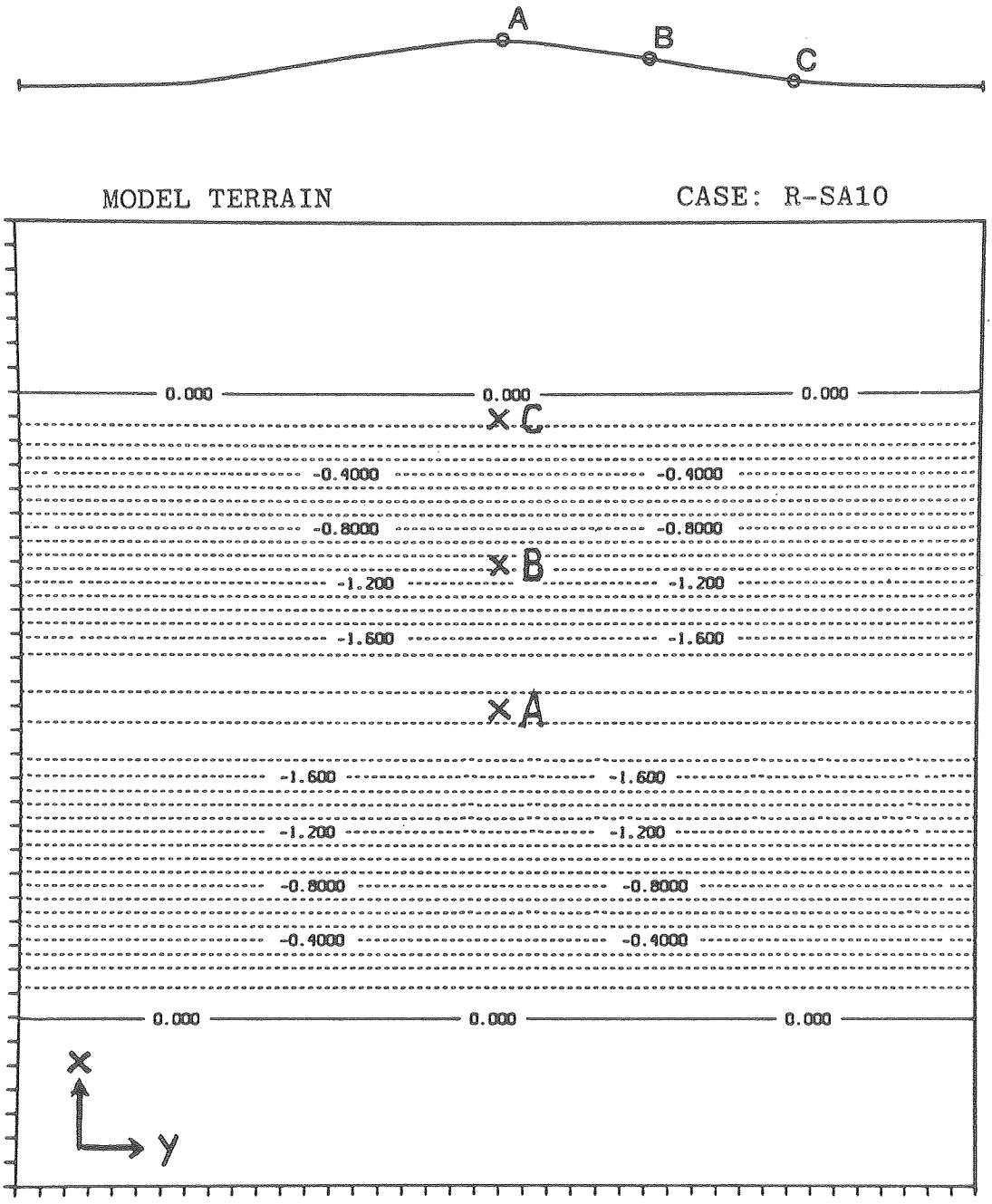

Figure 3-8-1. 2-D ridge model with 10° slopes. Current electrode locations at A, B, and C.

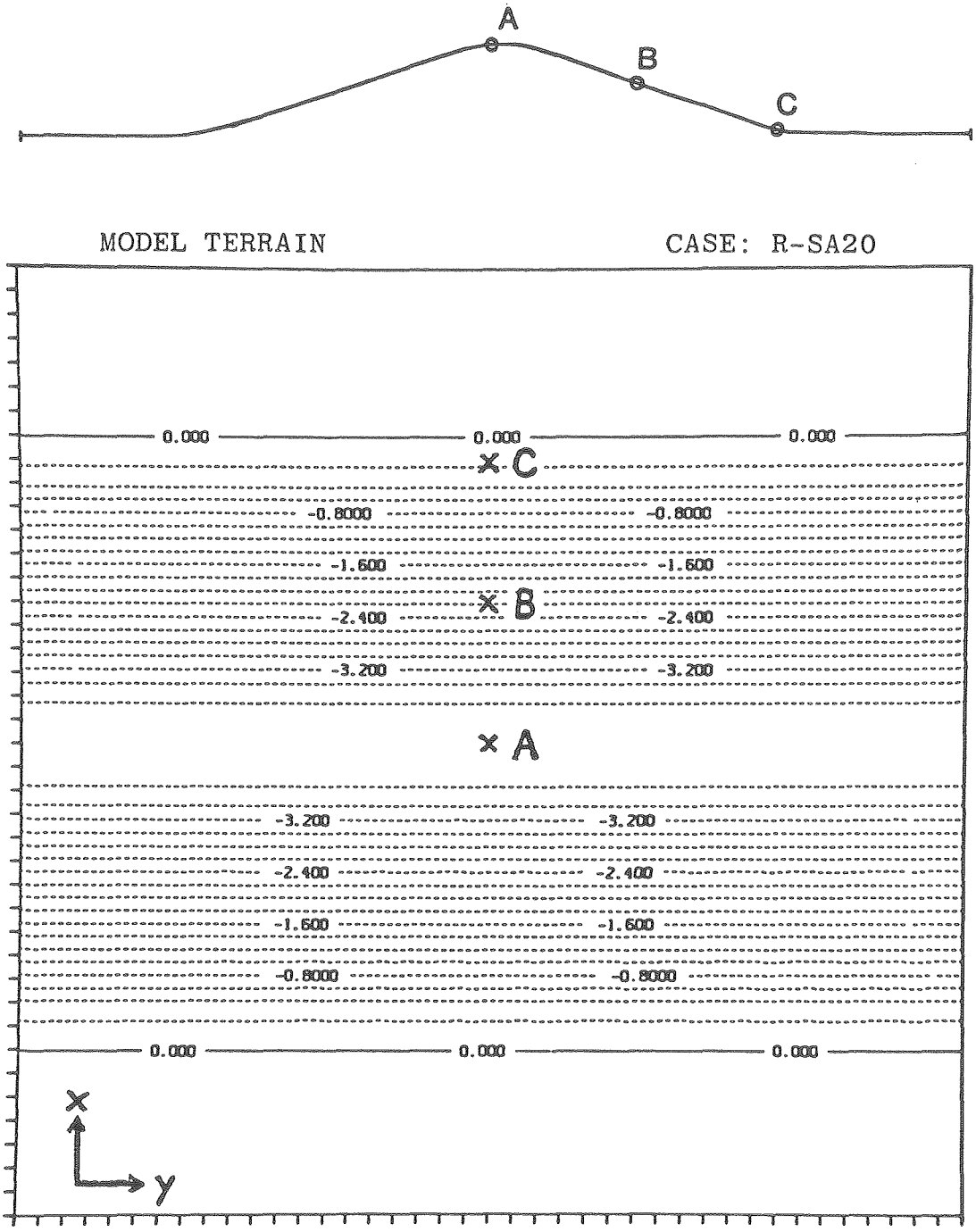

Figure 3-8-2. 2-D ridge model with 20° slopes. Current electrode locations at A, B, and C.

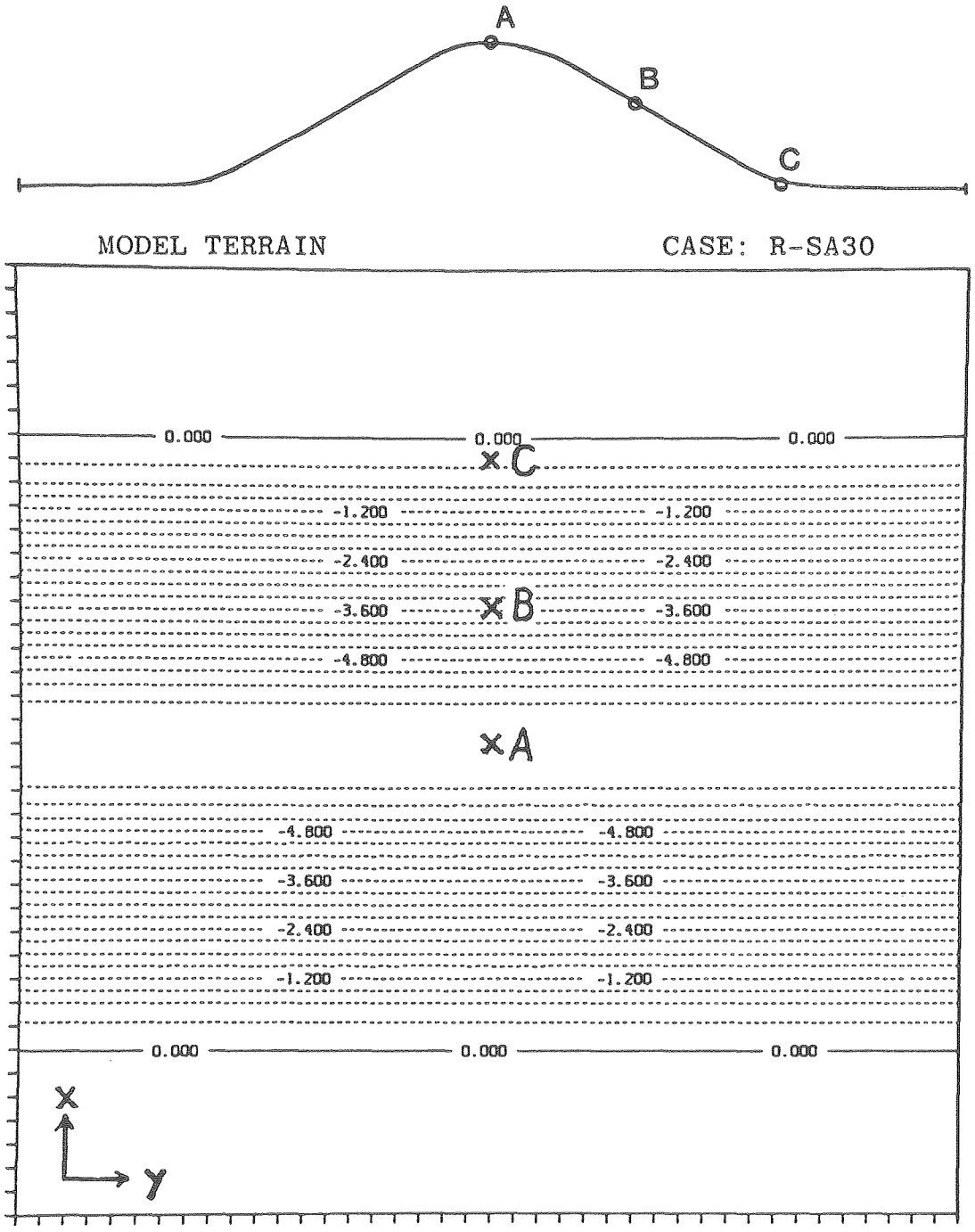

Figure 3-8-3. 2-D ridge model with 30° slopes. Current electrode locations at A, B, and C.

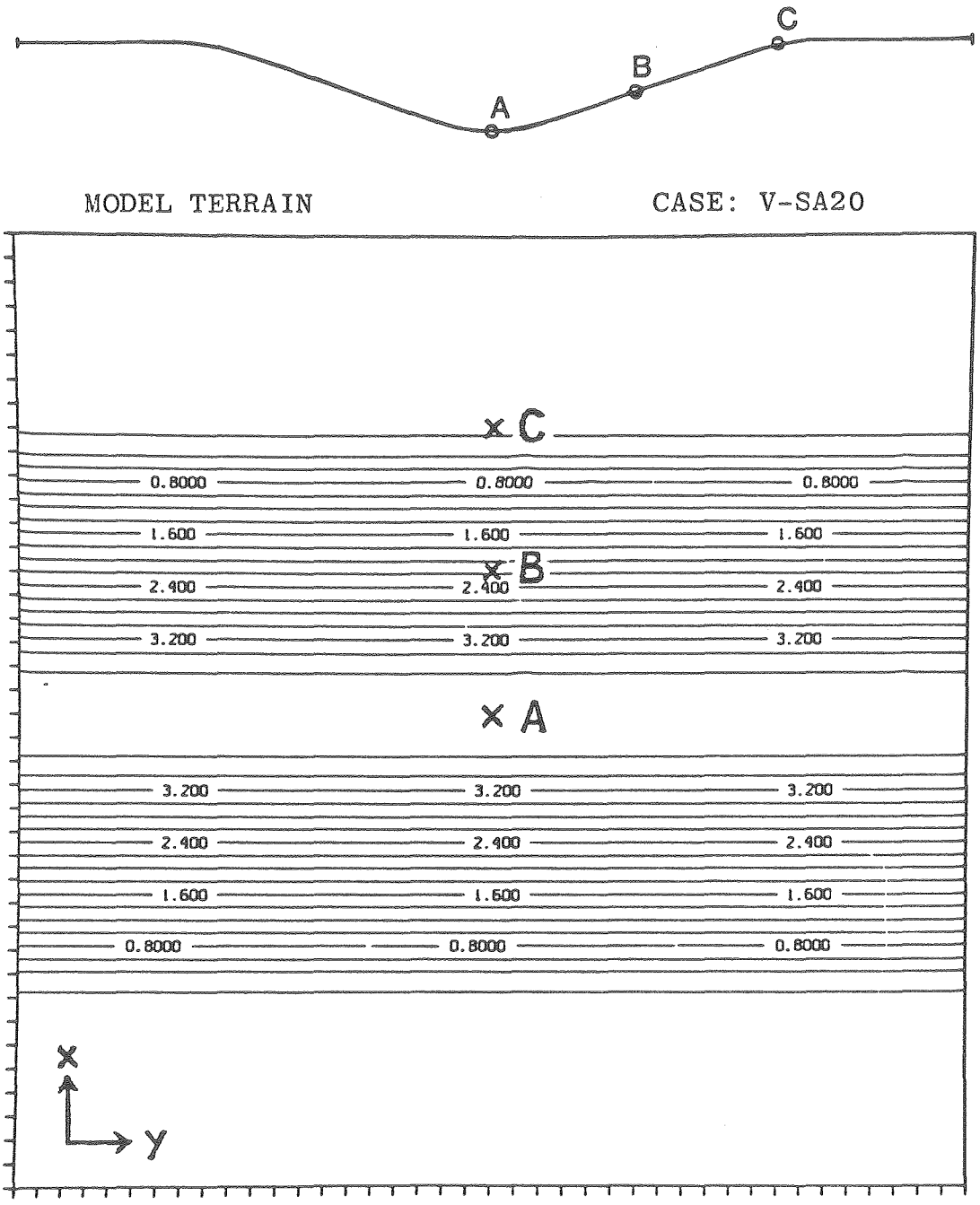

Figure 3-8-4. 2-D valley model with 20° slopes. Current electrode locations at A, B, and C.

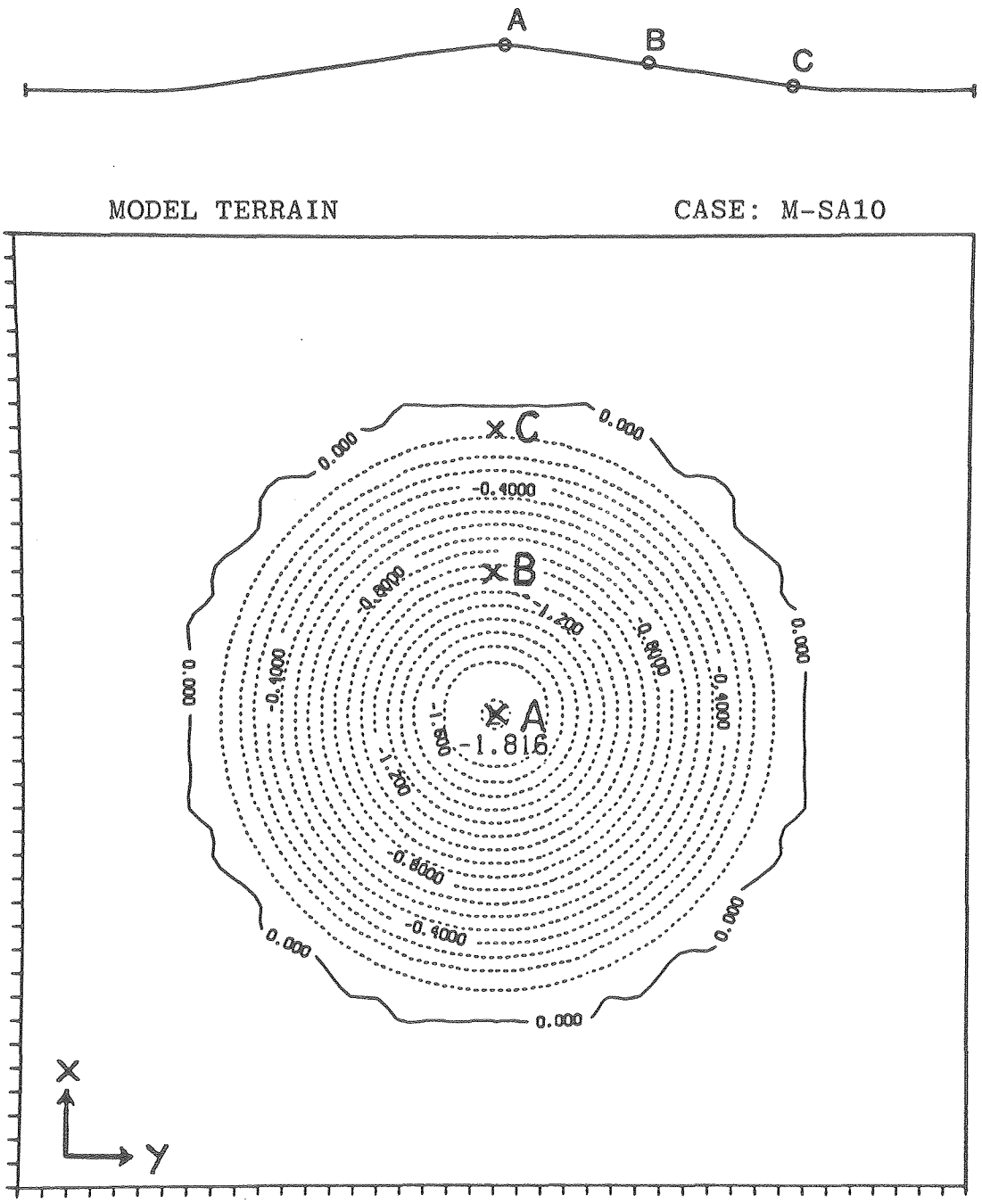

Figure 3-8-5. 3-D hill model with 10° slopes. Current electrode locations at A, B, and C.

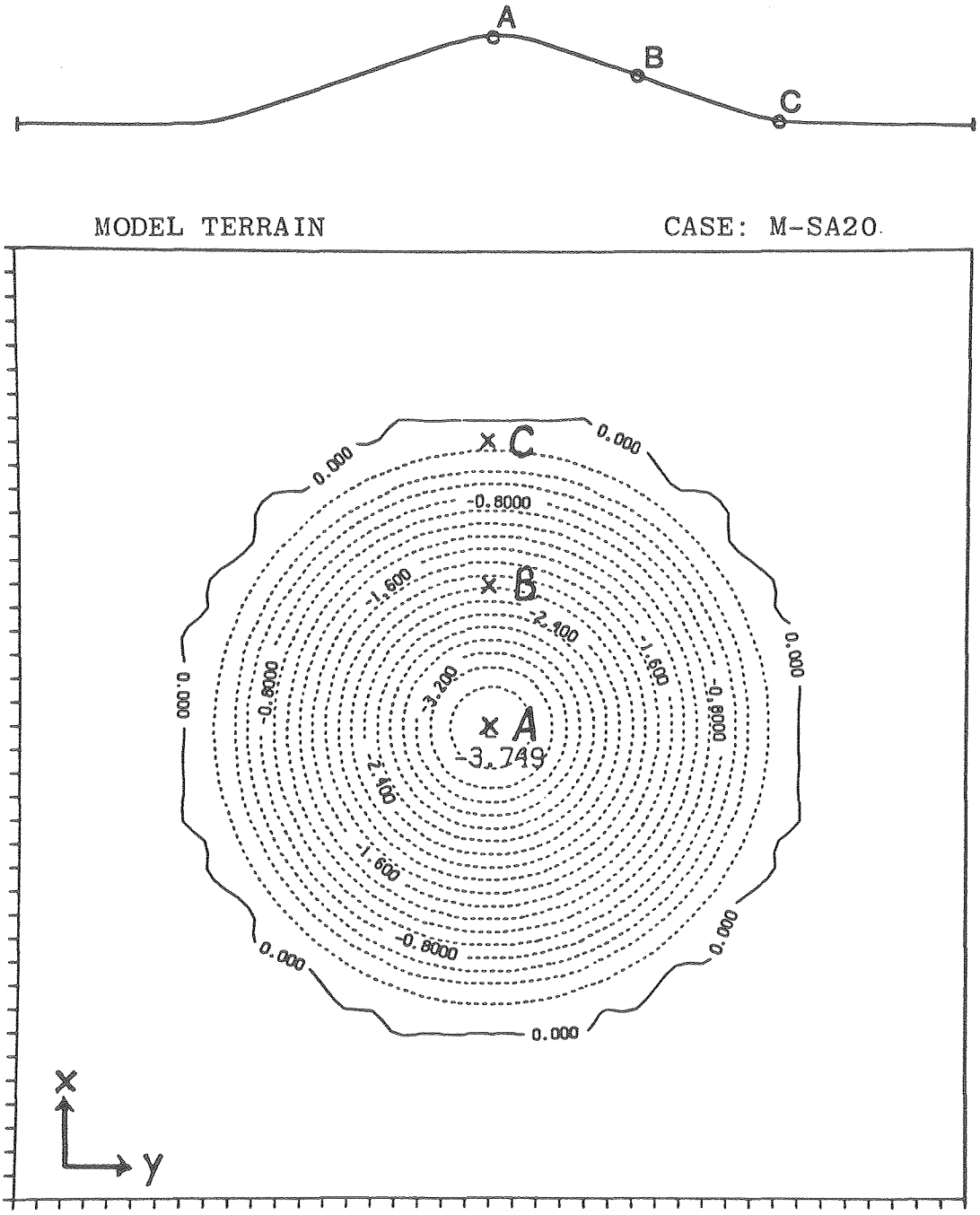

Figure 3-8-6. 3-D hill hodel with 20° slopes. Current electrode locations at A, B, and C.

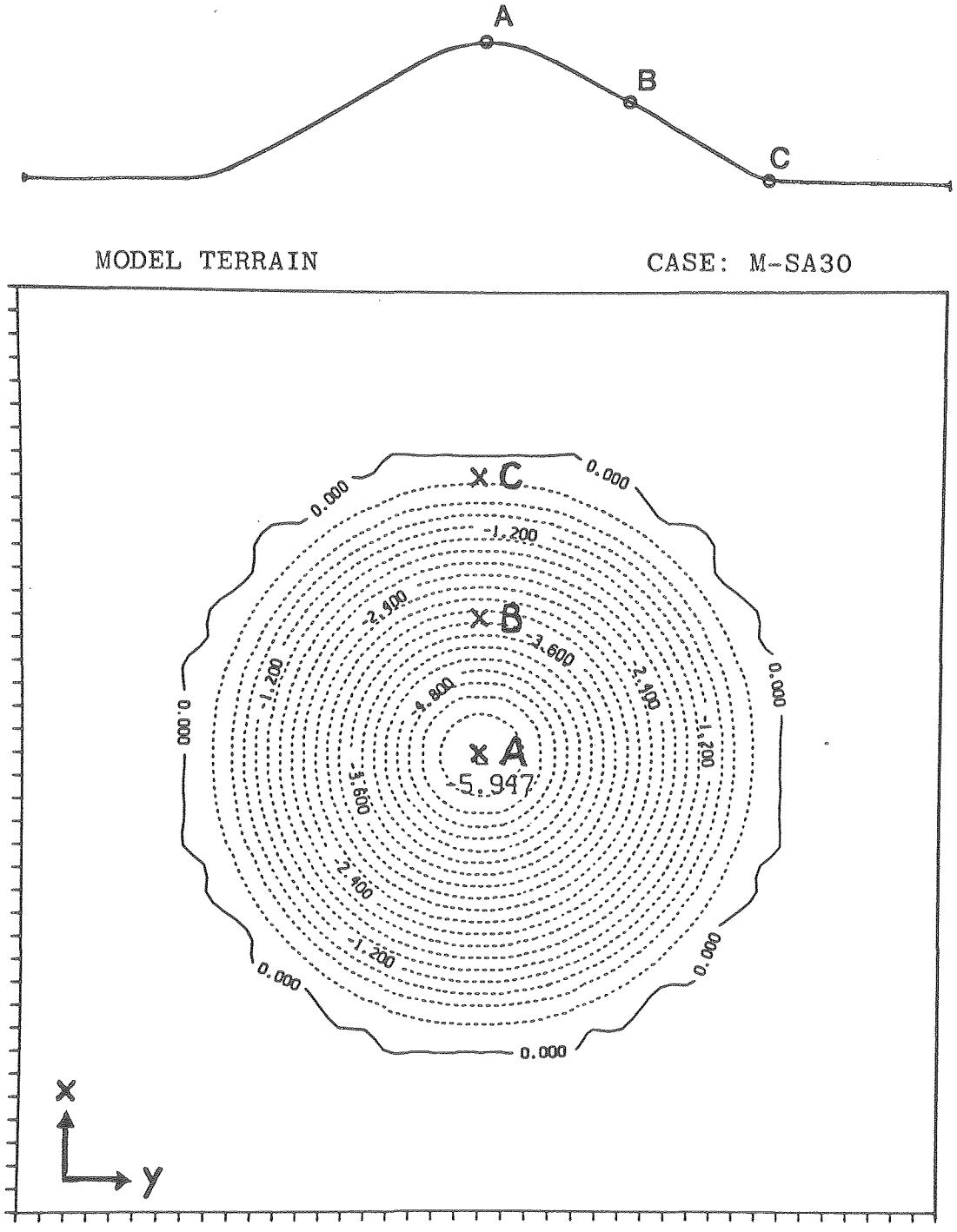

Figure 3-8-7. 3-D hill model with 30° slopes. Current electrode locations at A, B, and C.

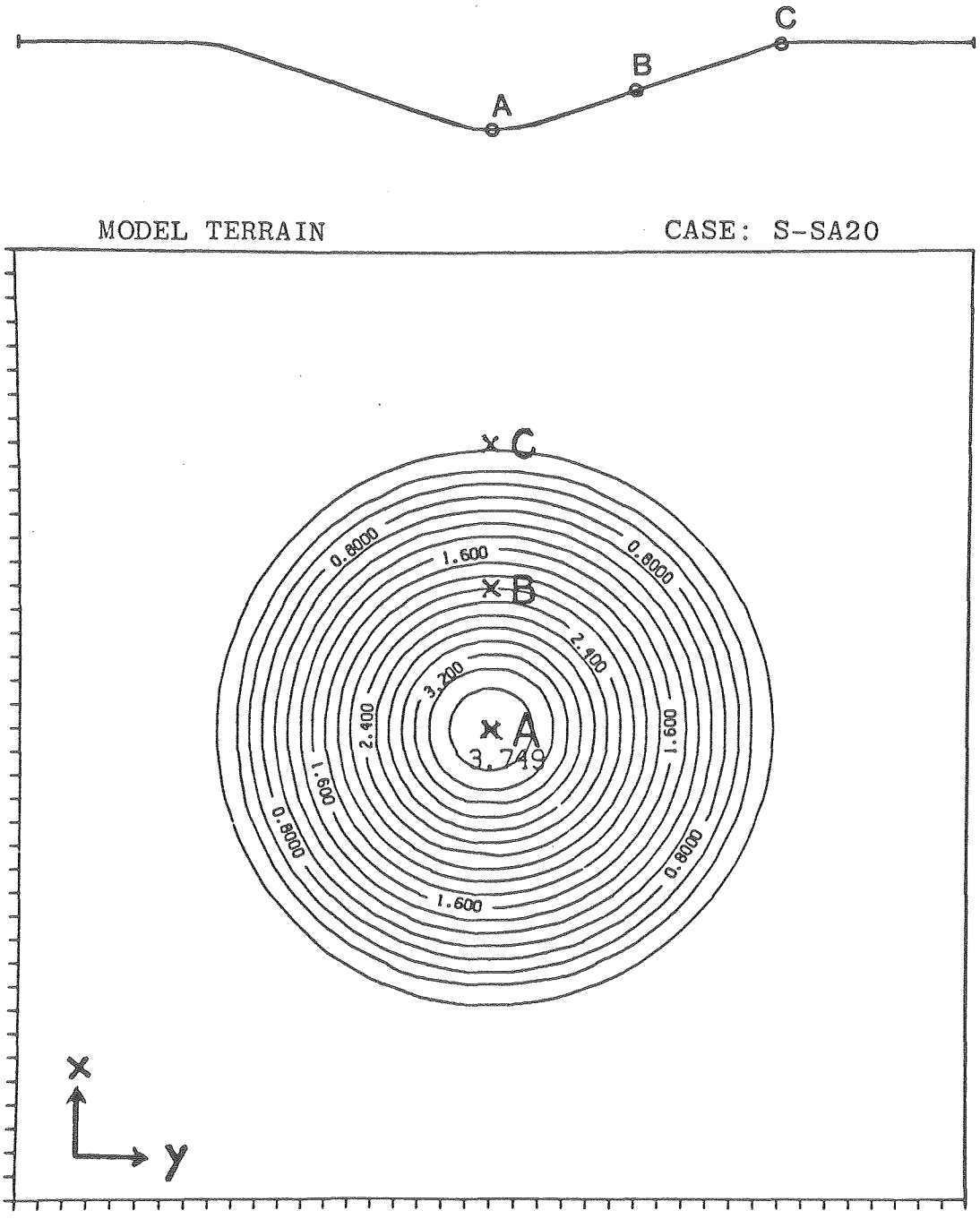

Figure 3-8-8. 3-D sink model with 20° slopes. Current electrode locations at A, B, and C.

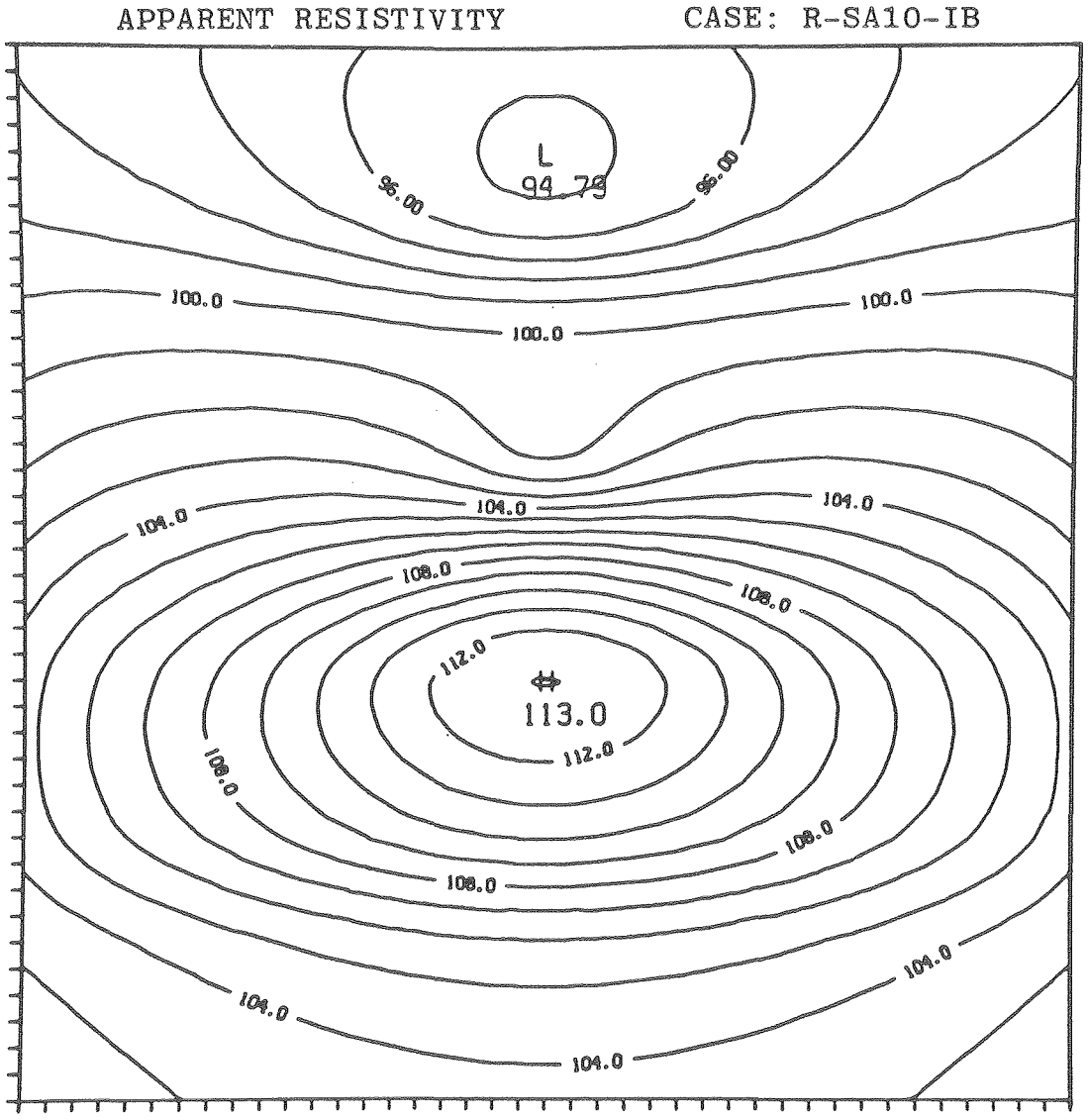

Figure 3-8-9.

XBL 7911-12925

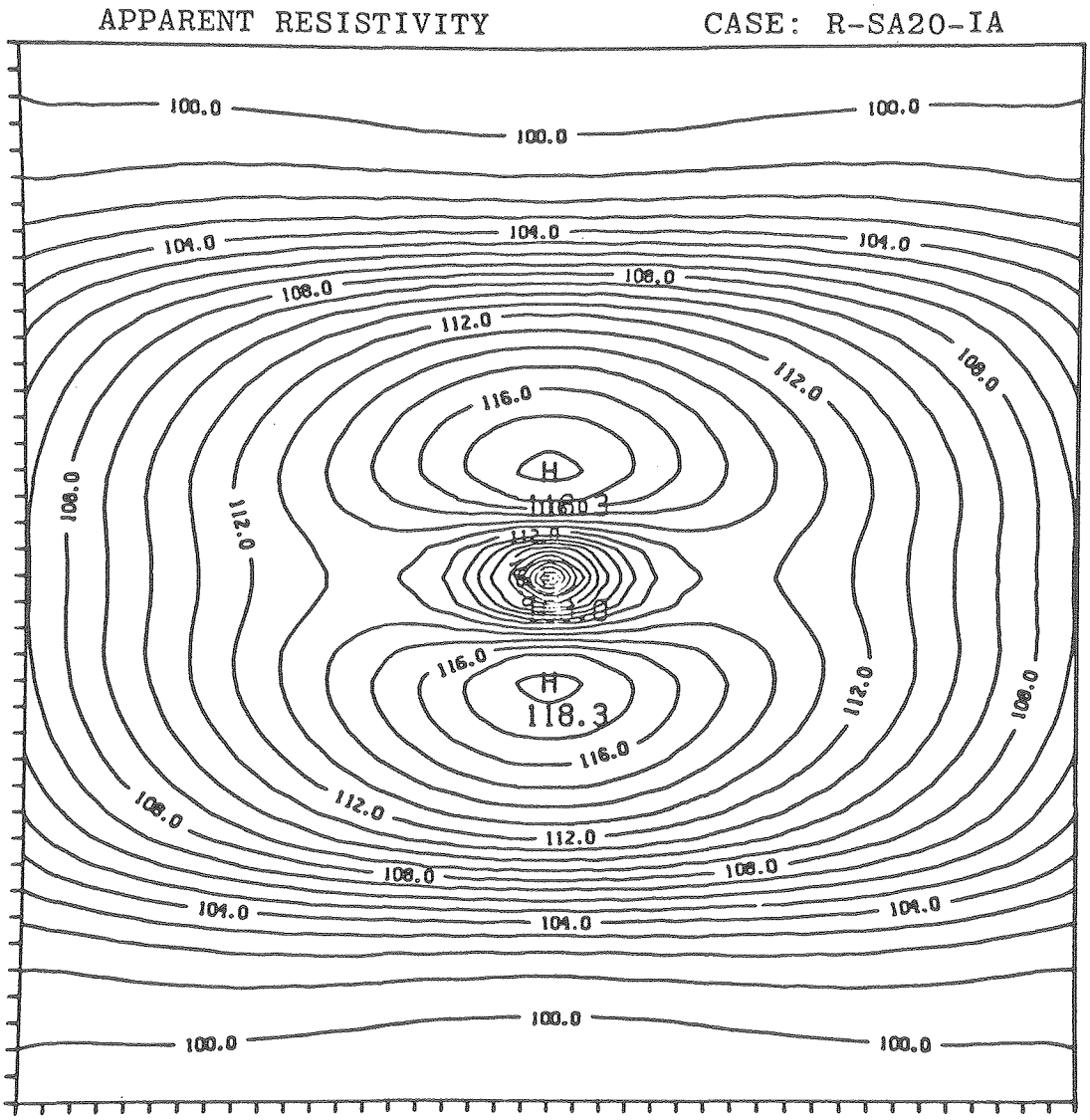

Figure 3-8-10.

XBL 7911-12884

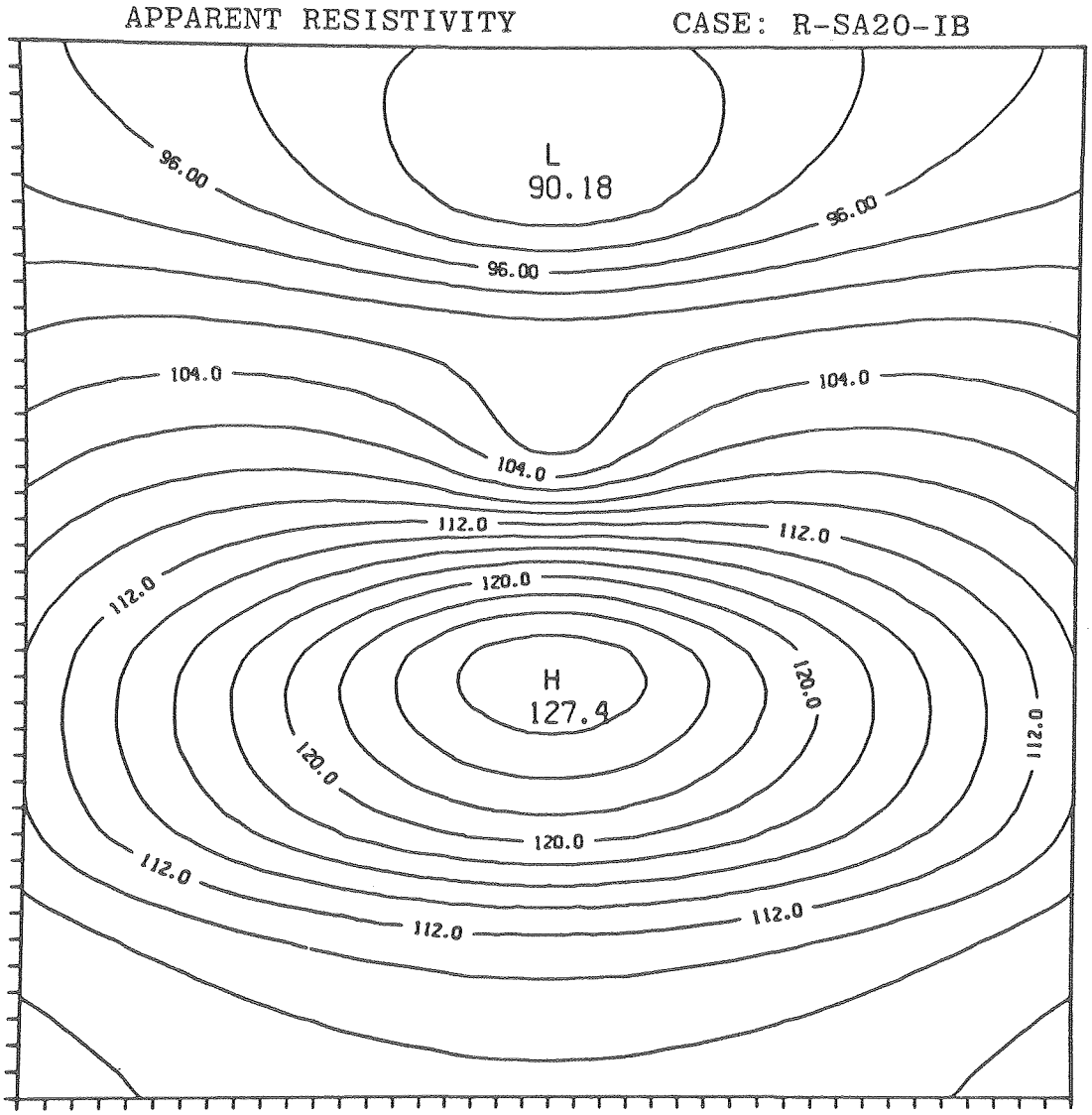

Figure 3-8-11.

XBL 7911-12929

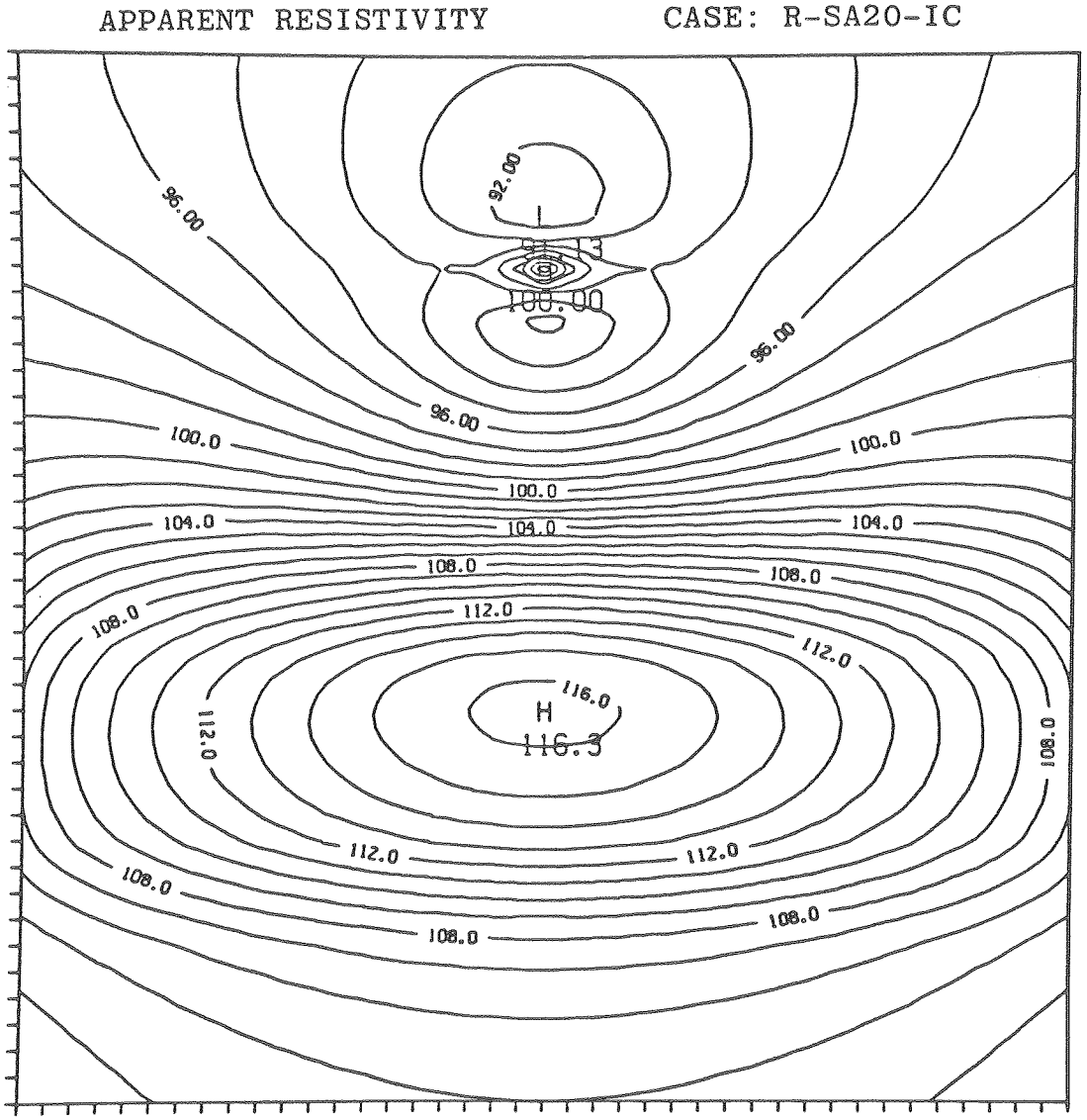

Figure 3-8-12.

XBL 7911-12932

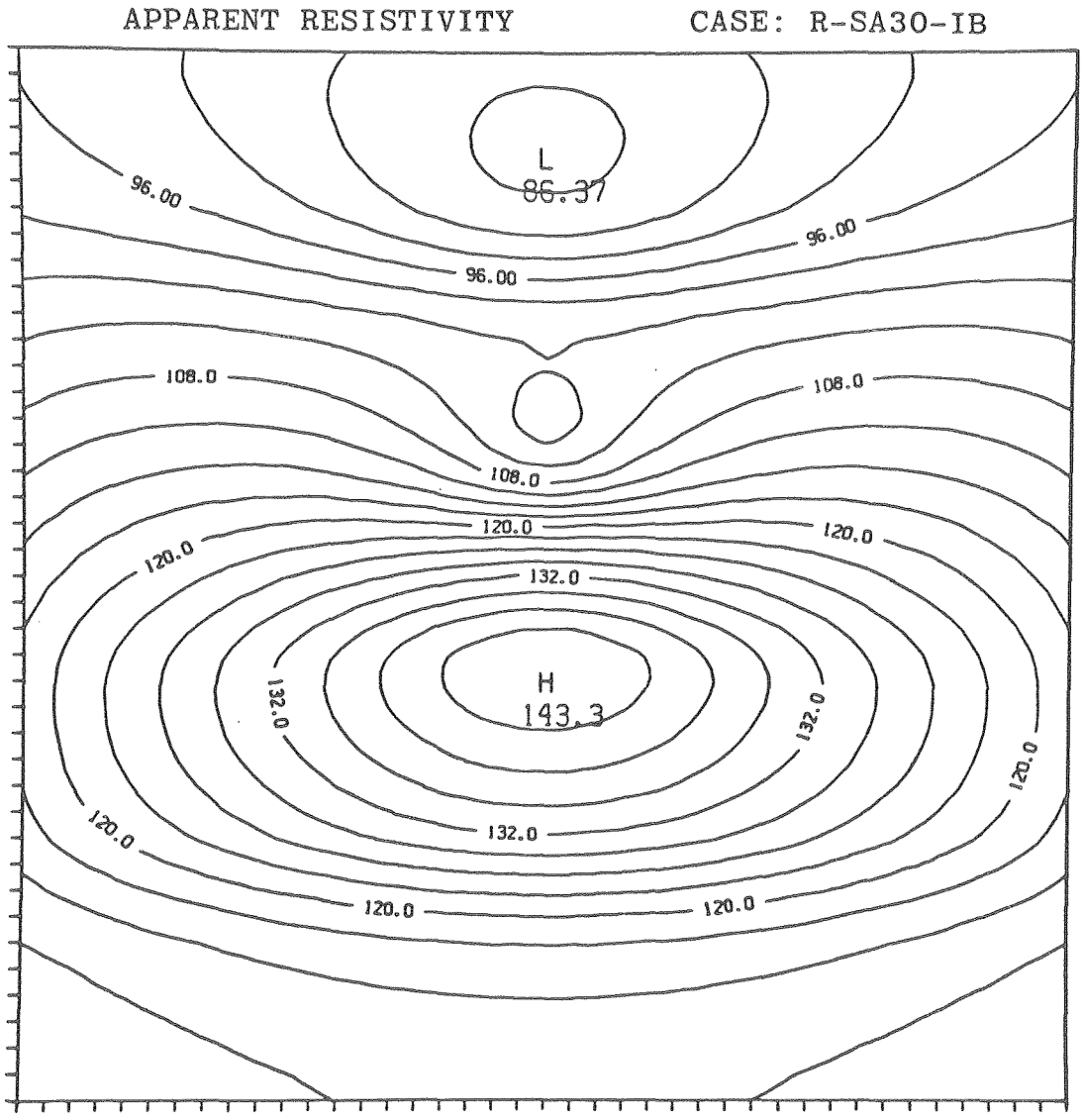

Figure 3-8-13.

XBL 7911-12936

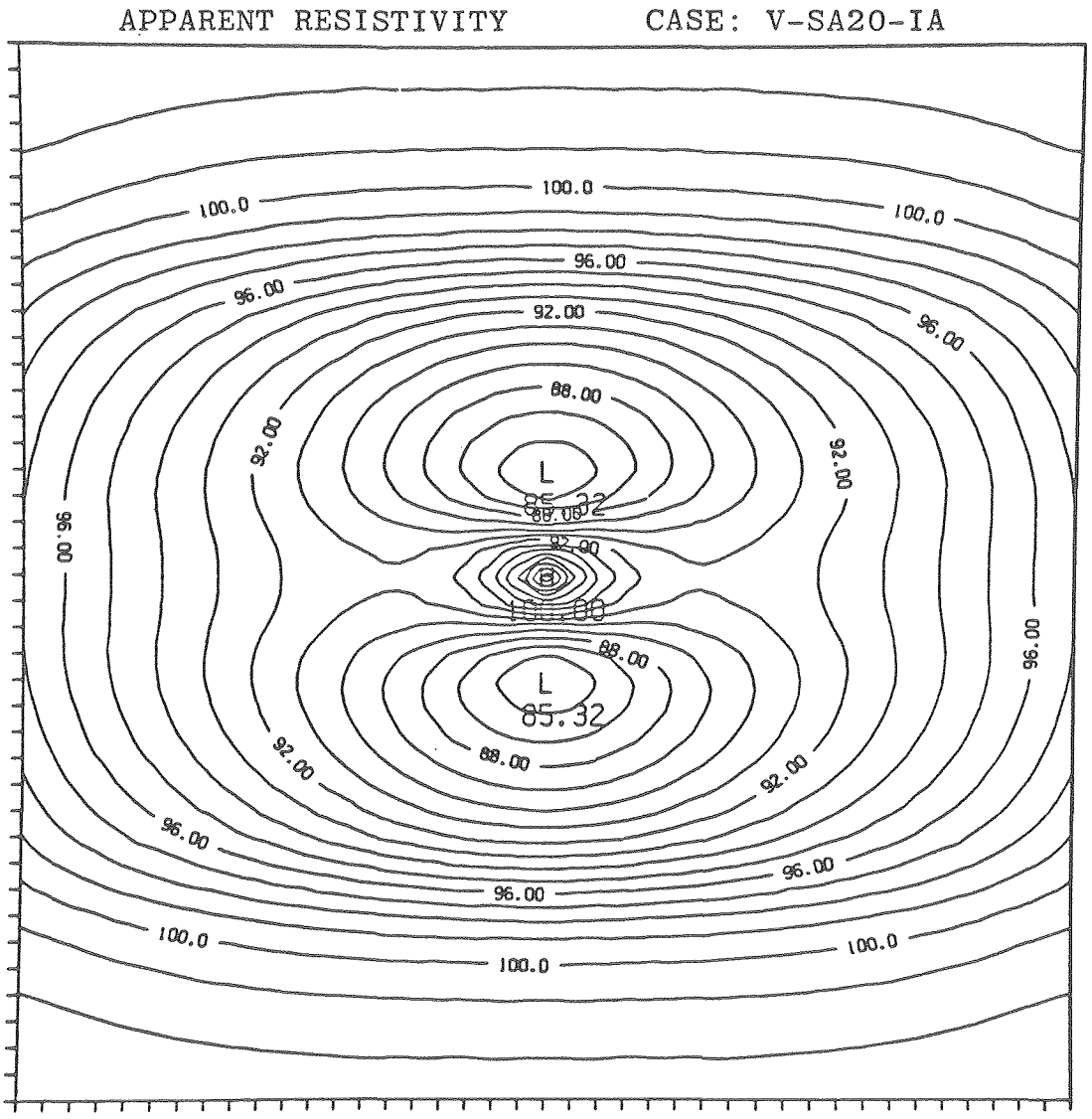

Figure 3-8-14.

XBL 7911-12940

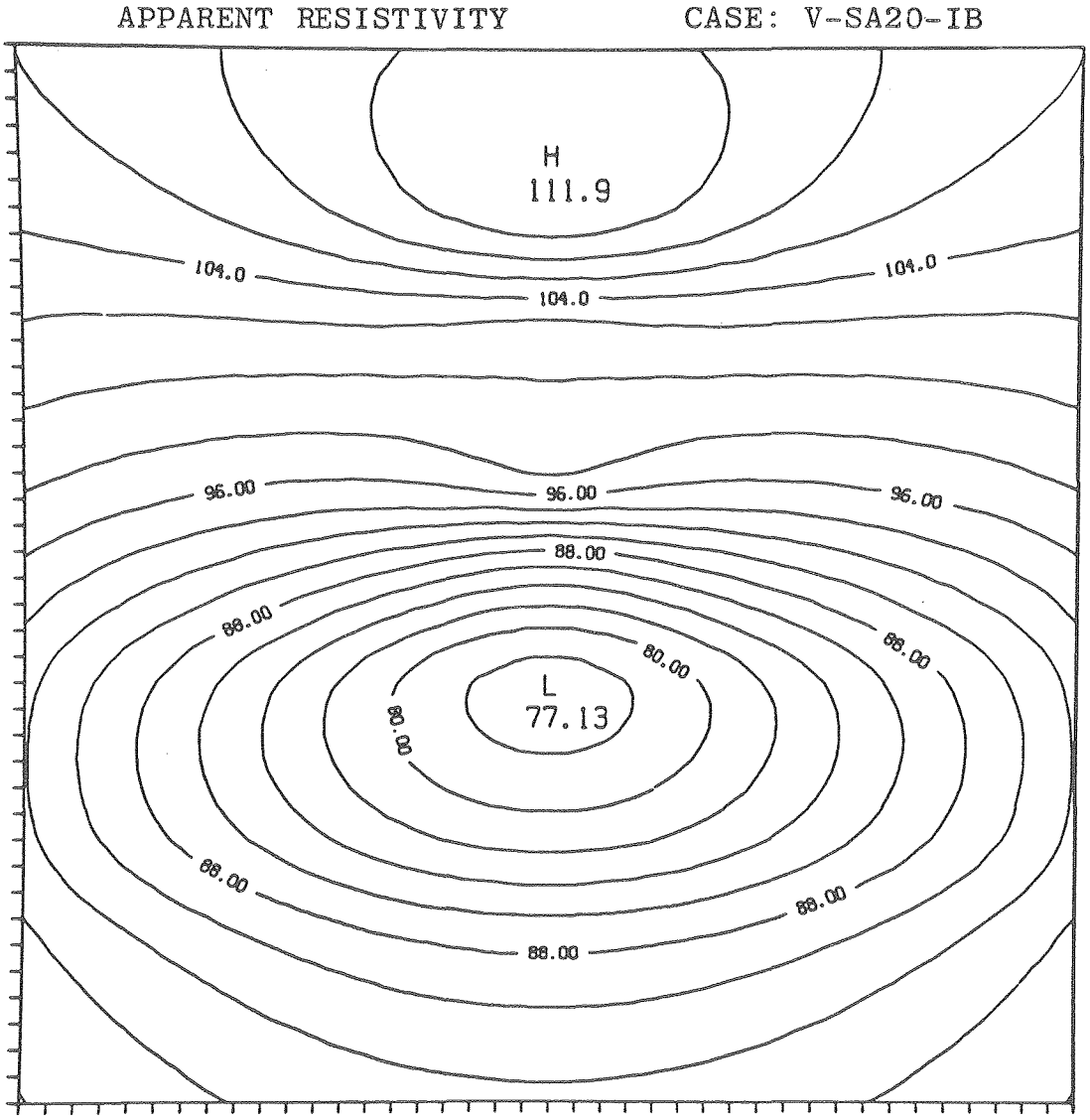

Figure 3-8-15.

XBL 7911-12944

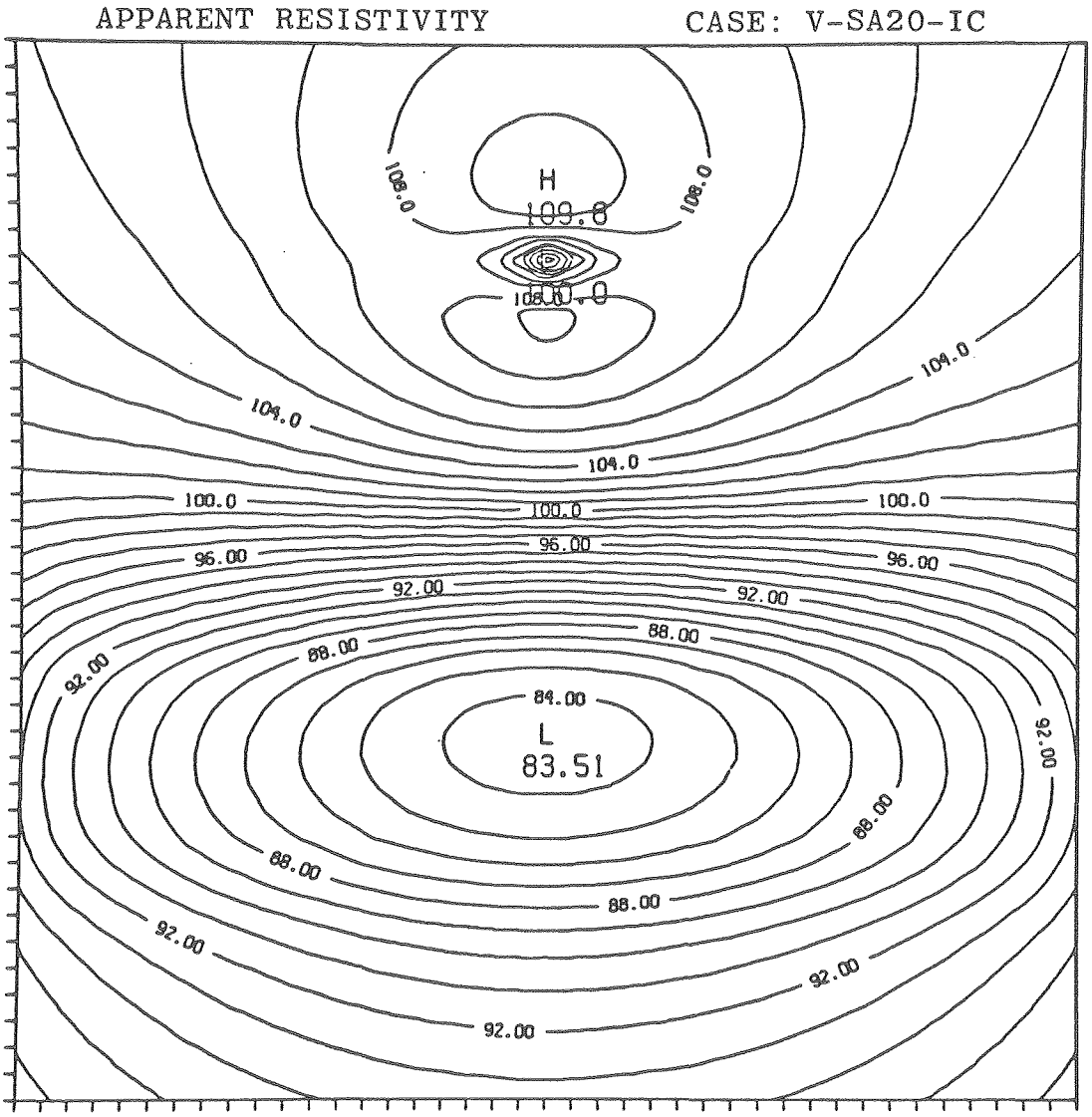

Figure 3-8-16

XBL 7911-12947

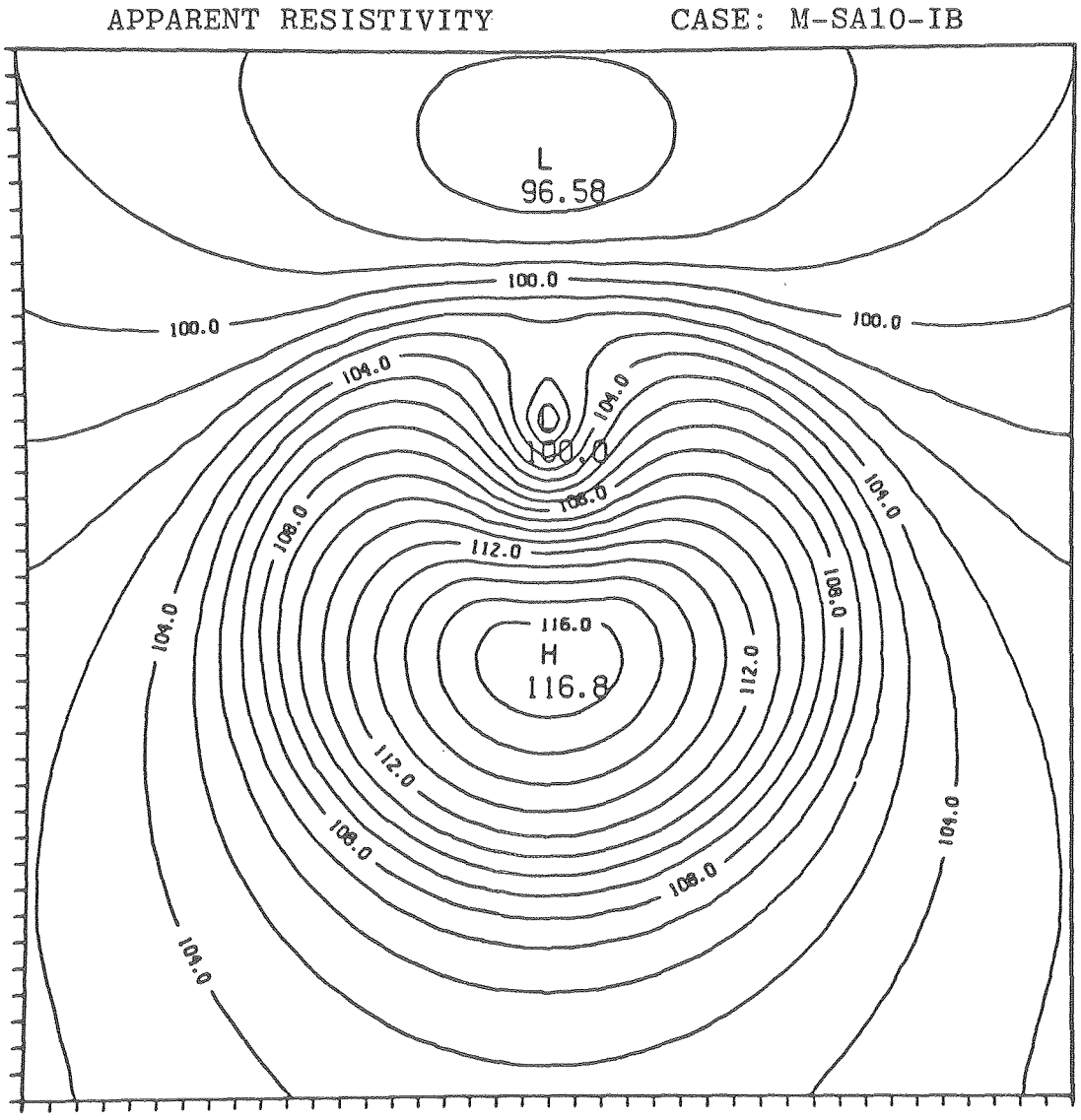

Figure 3-8-17.

XBL 7911-12951

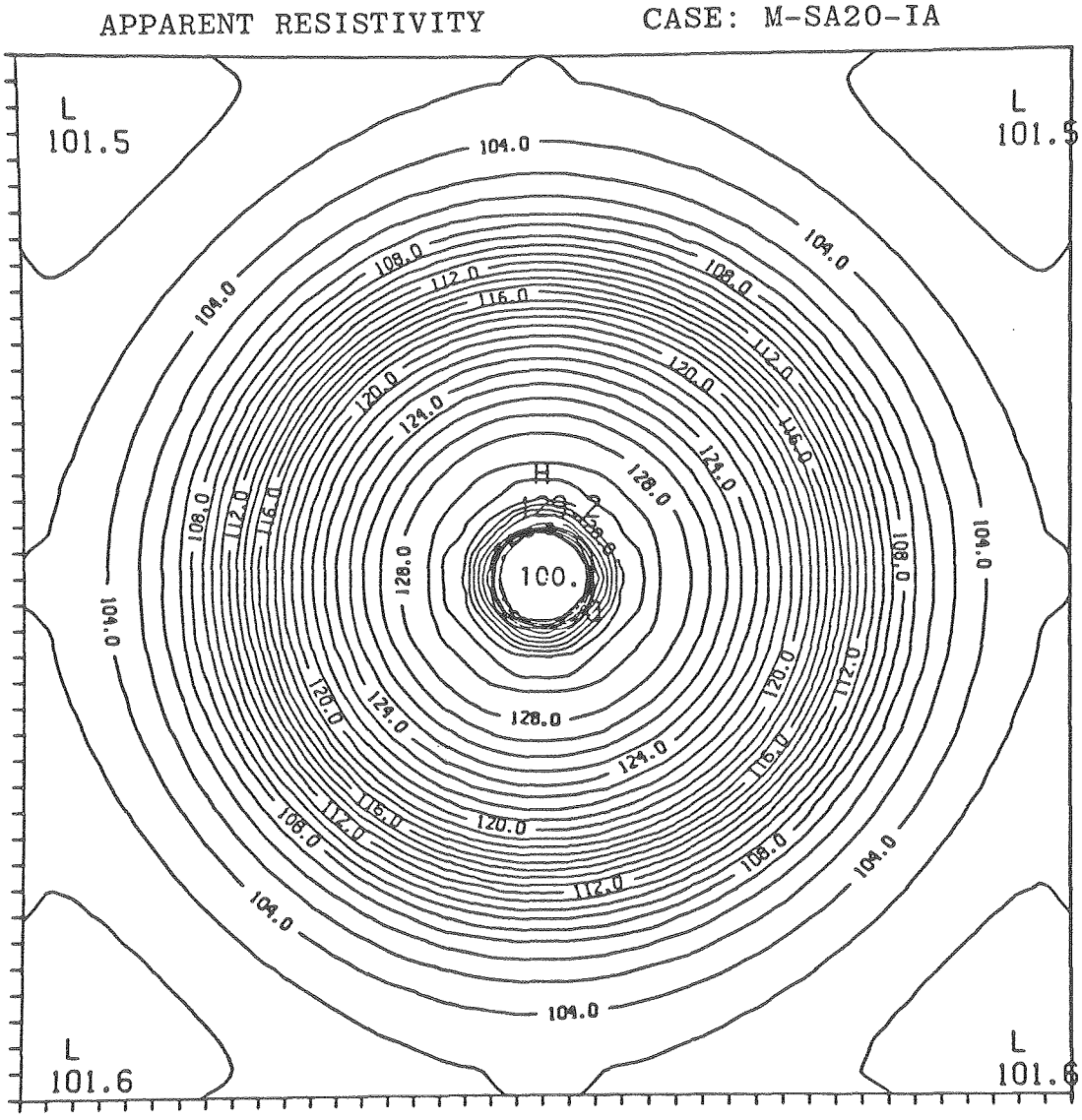
APPARENT RESISTIVITY
CASE: M-SA20-IA
L
101.5
L
101.5
L
101.6
L
101.6
H
100.
104.0
108.0
112.0
116.0
120.0
124.0
128.0

Figure 3-8-18.

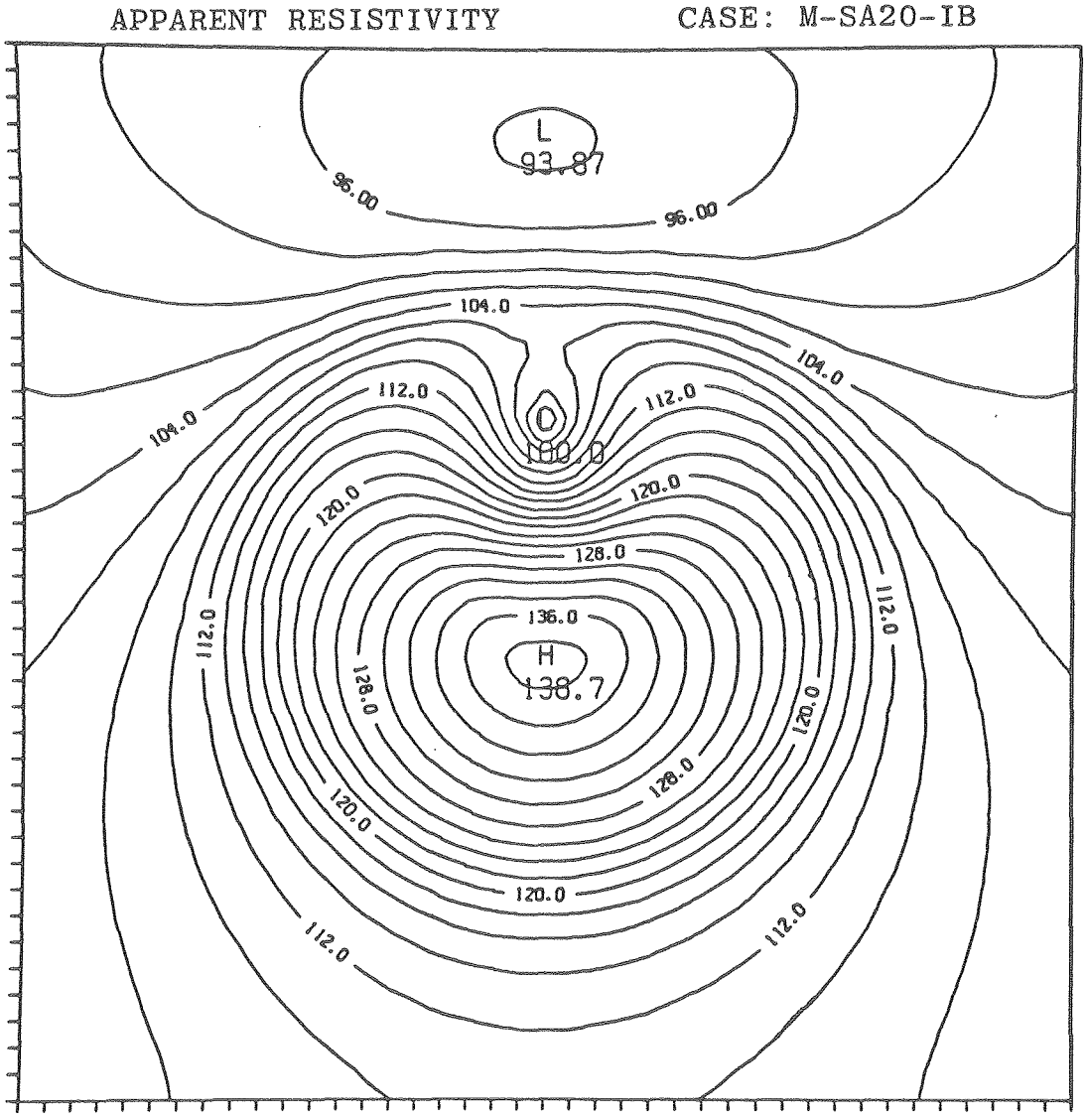

Figure 3-8-19.

XBL 7911-12959

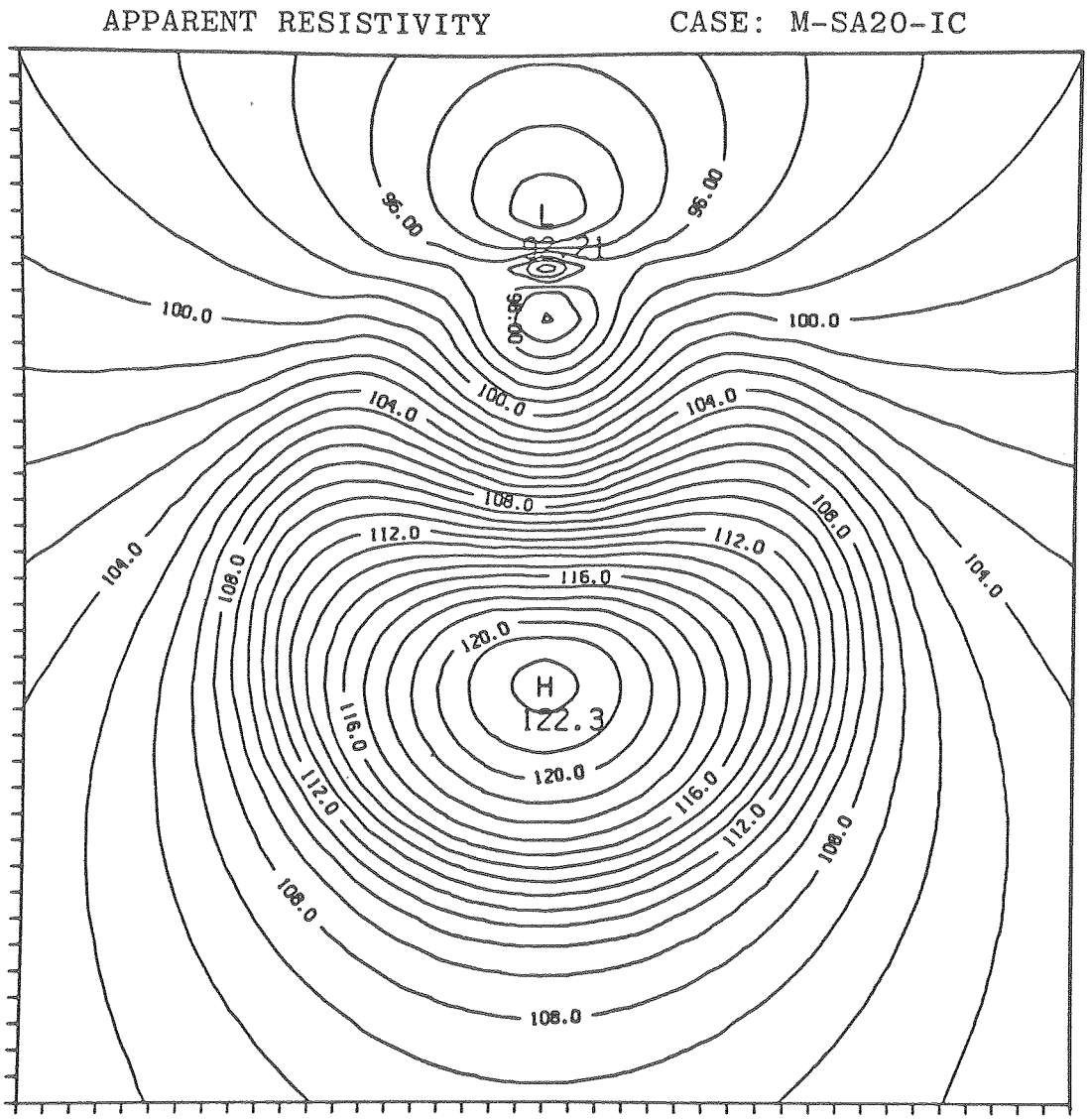

Figure 3-8-20.

XBL 7911-12963

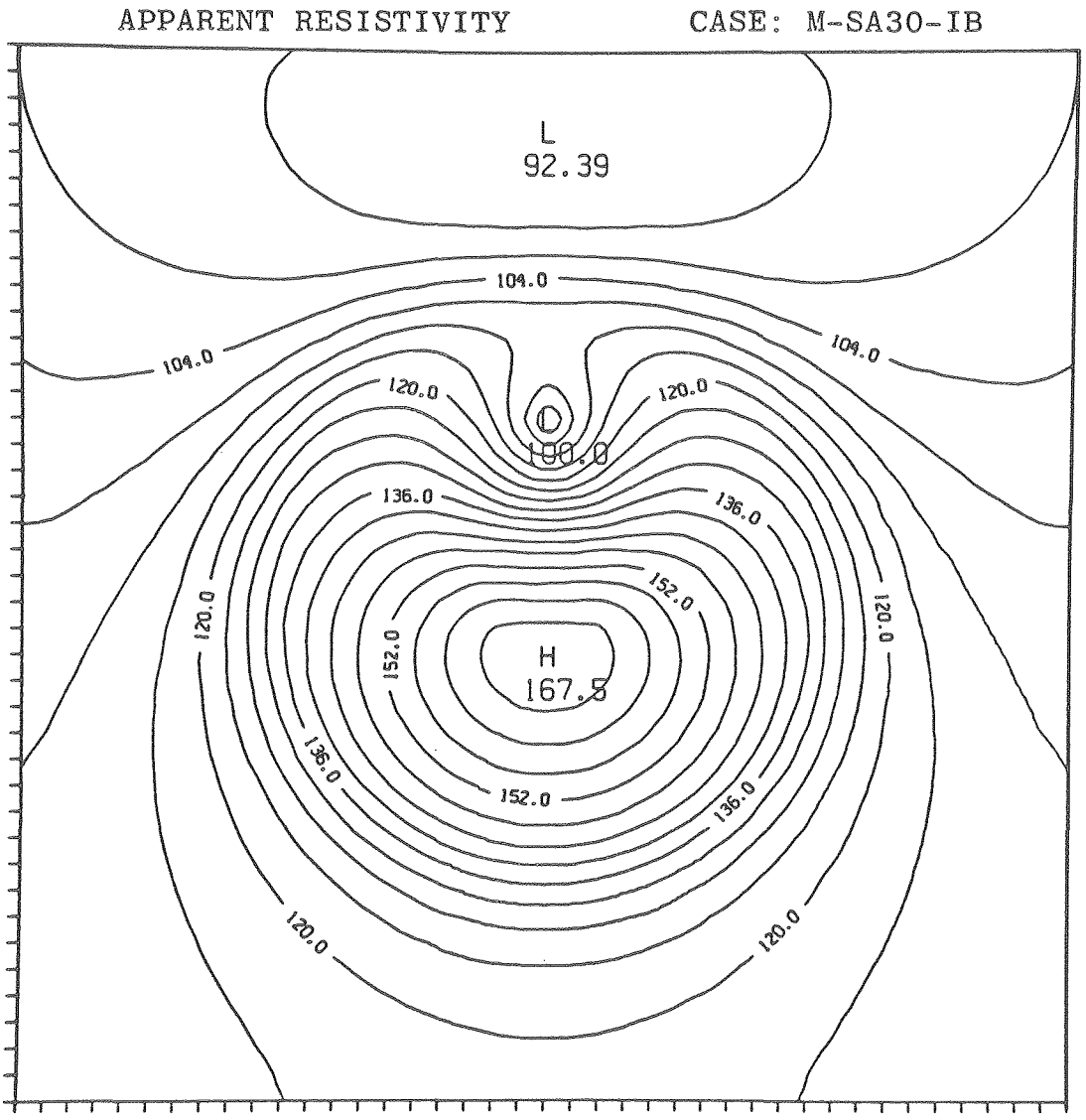

Figure 3-8-21.

XBL 7911-12967

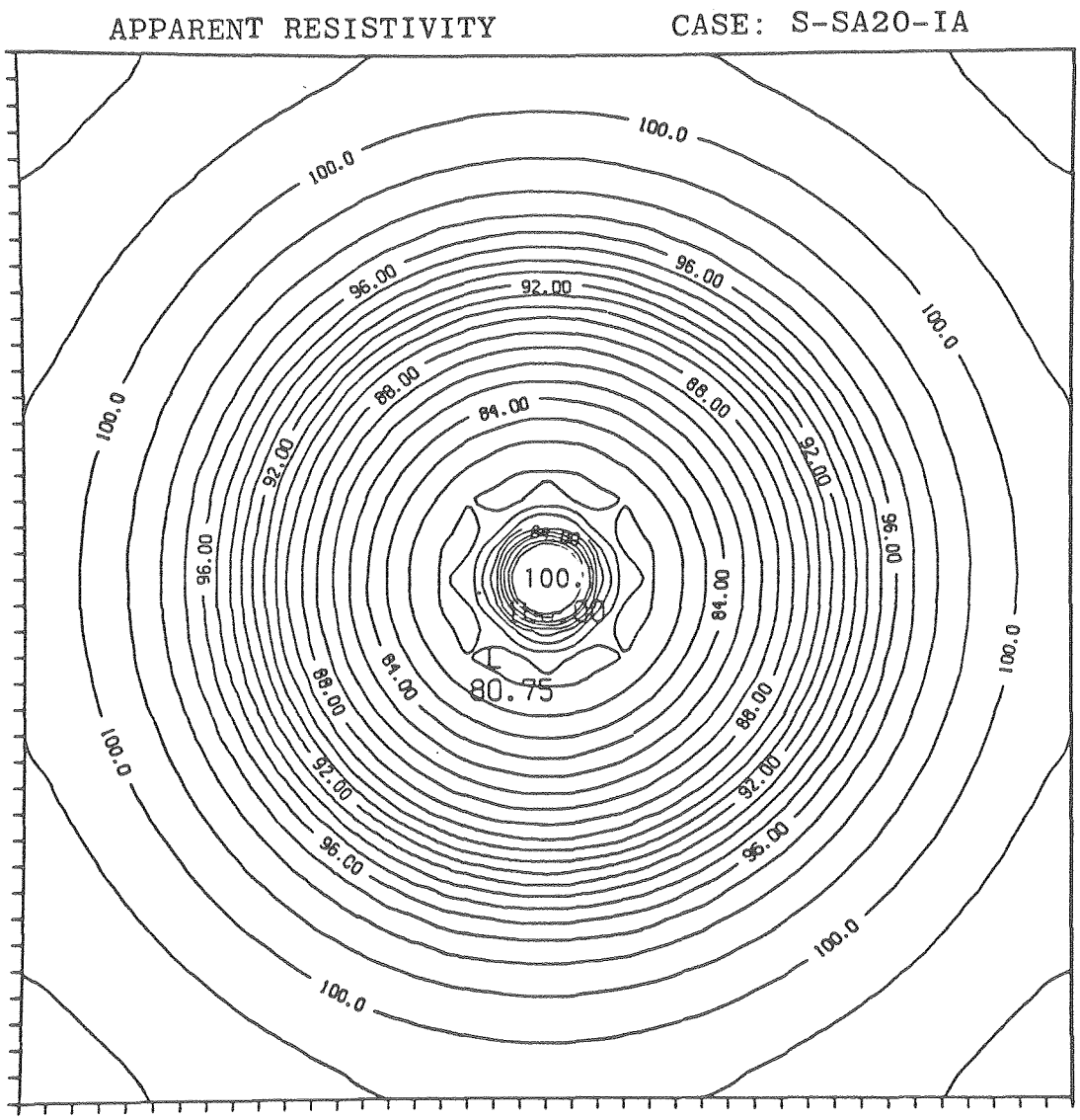
APPARENT RESISTIVITY
CASE: S-SA20-IA
100.0
96.00
92.00
88.00
84.00
80.75

Figure 3-8-22.

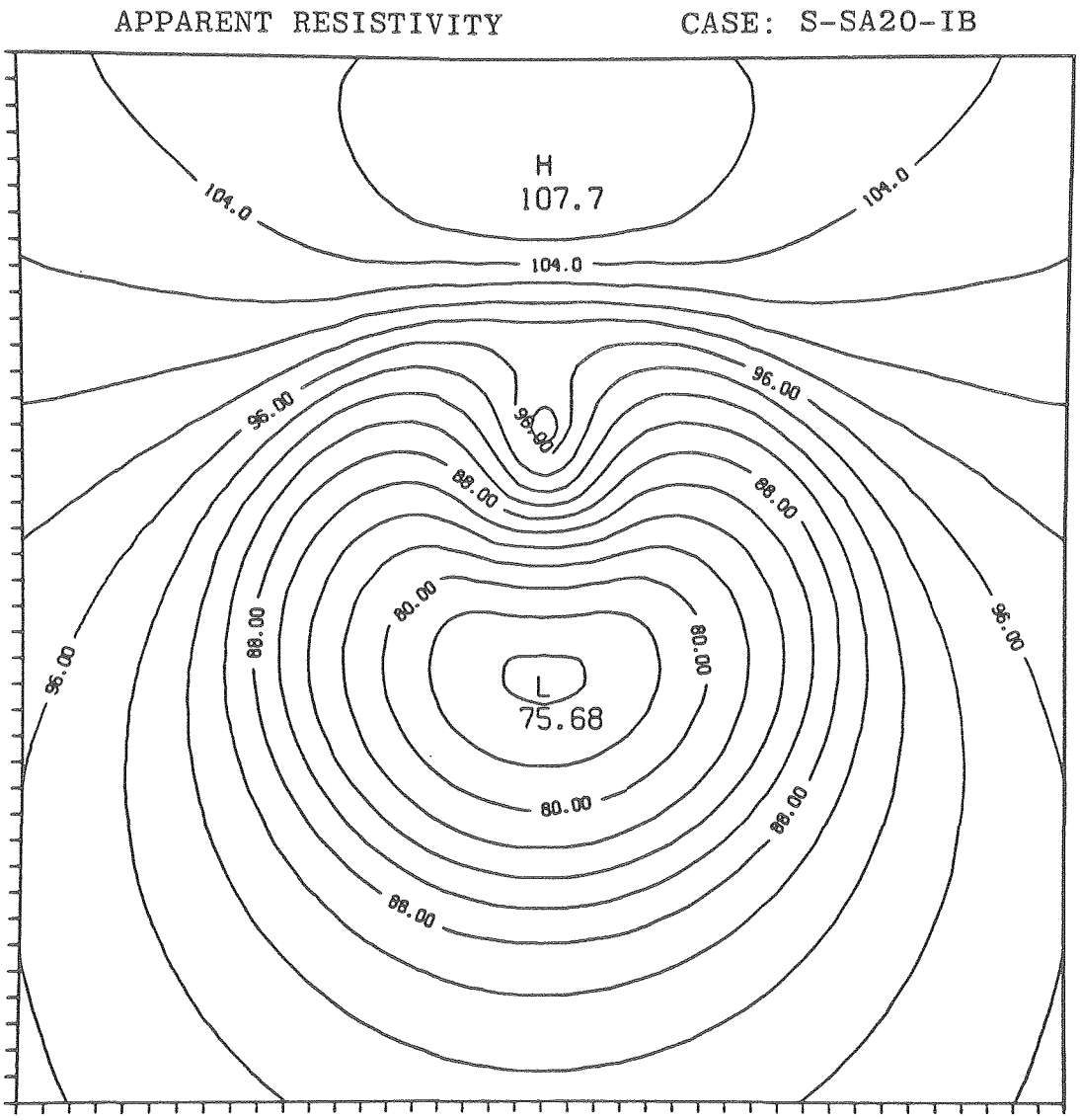

Figure 3-8-23.

XBL 7911-12975

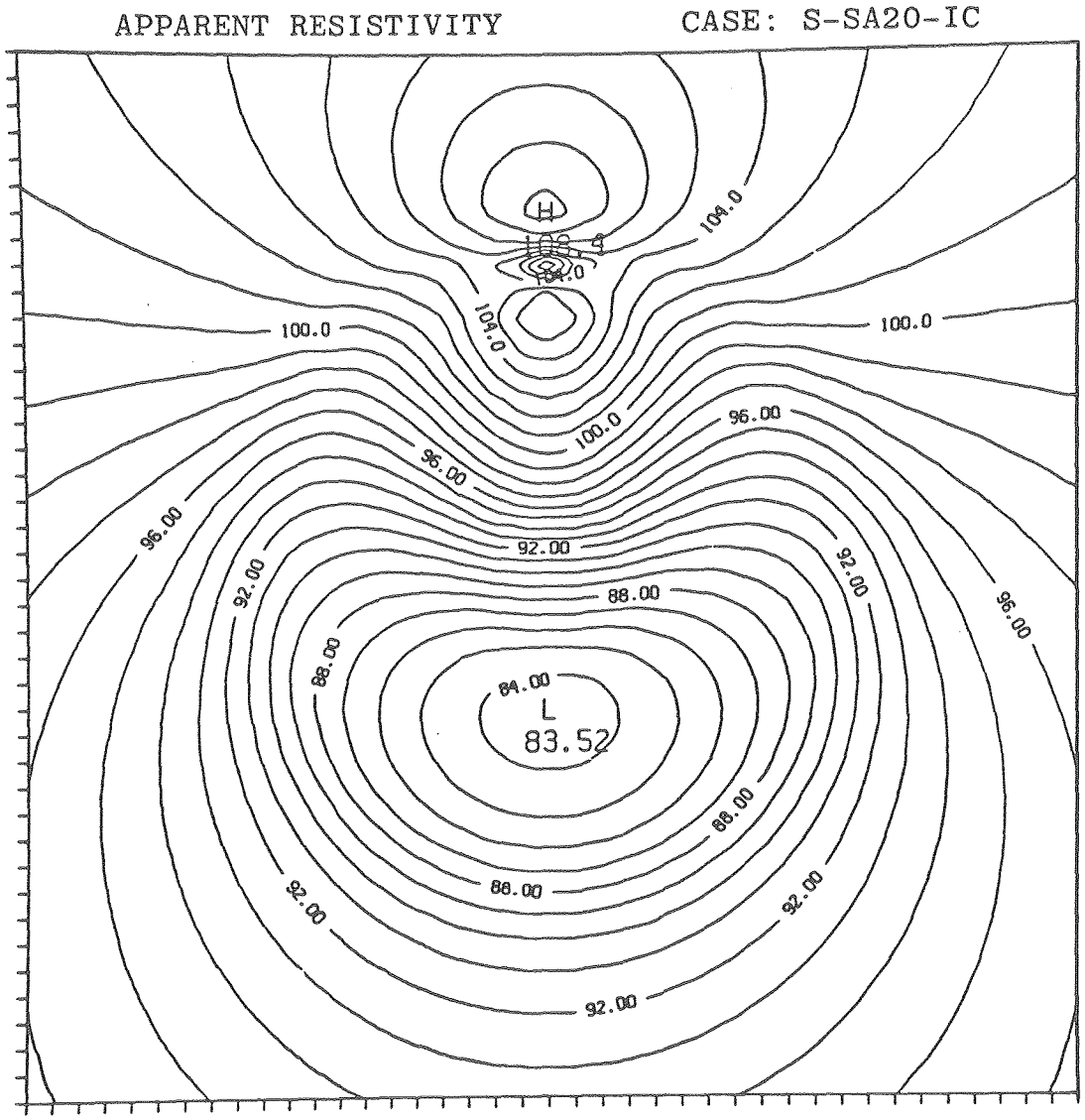

Figure 3-8-24.

XBL 7911-12979

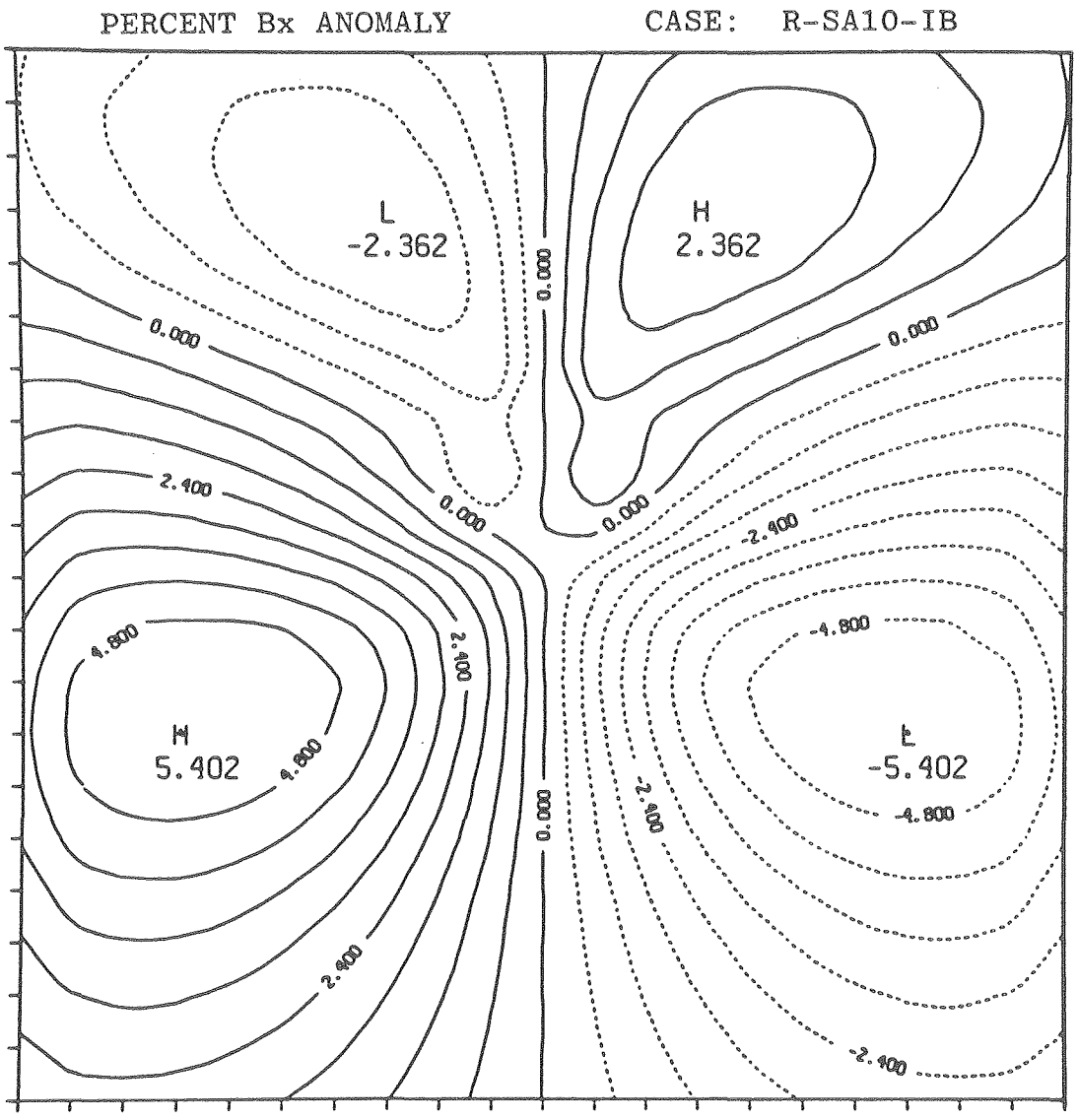

Figure 3-8-25.

XBL 7911-12926

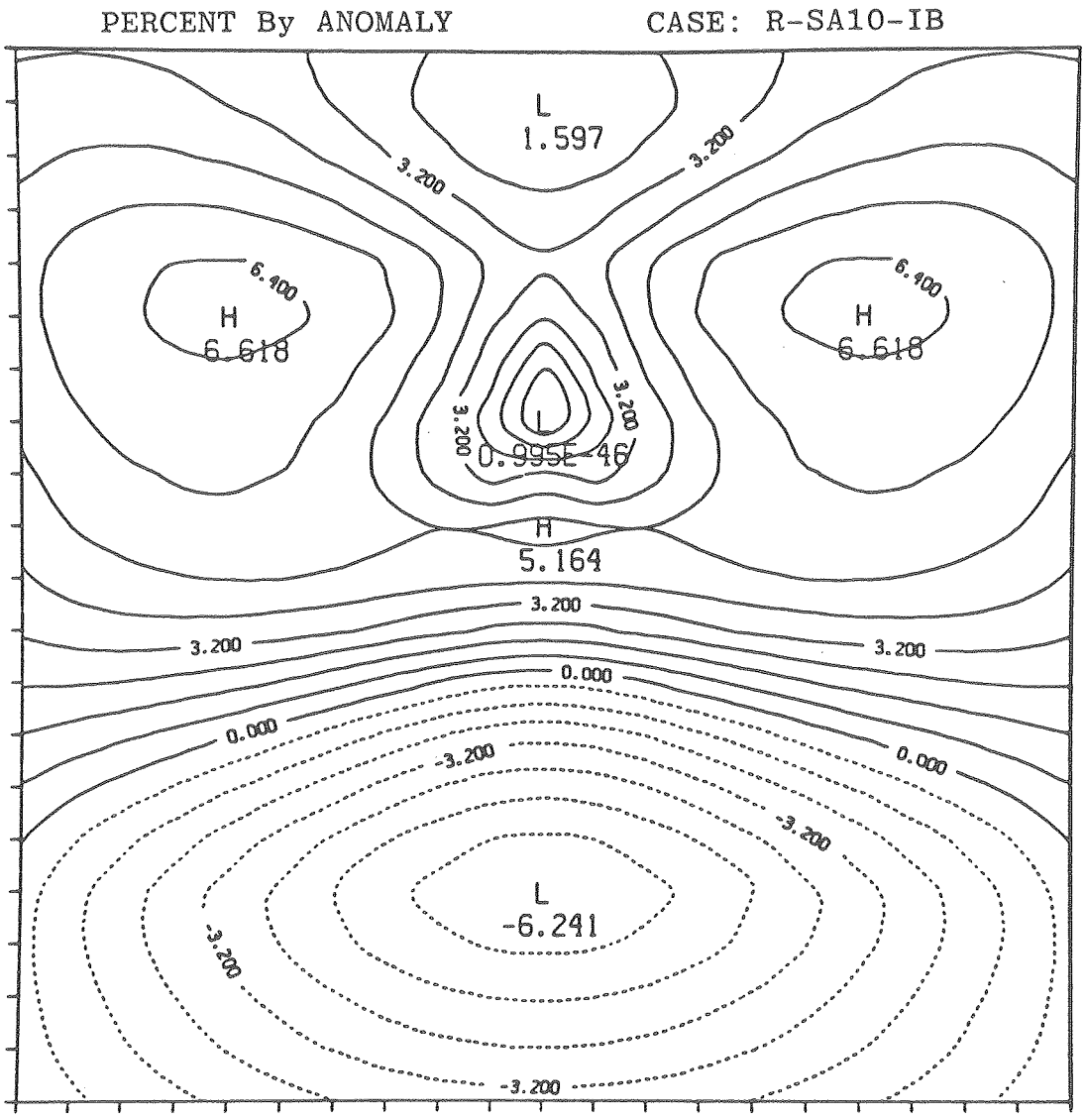

Figure 3-8-26.

XBL 7911-12927

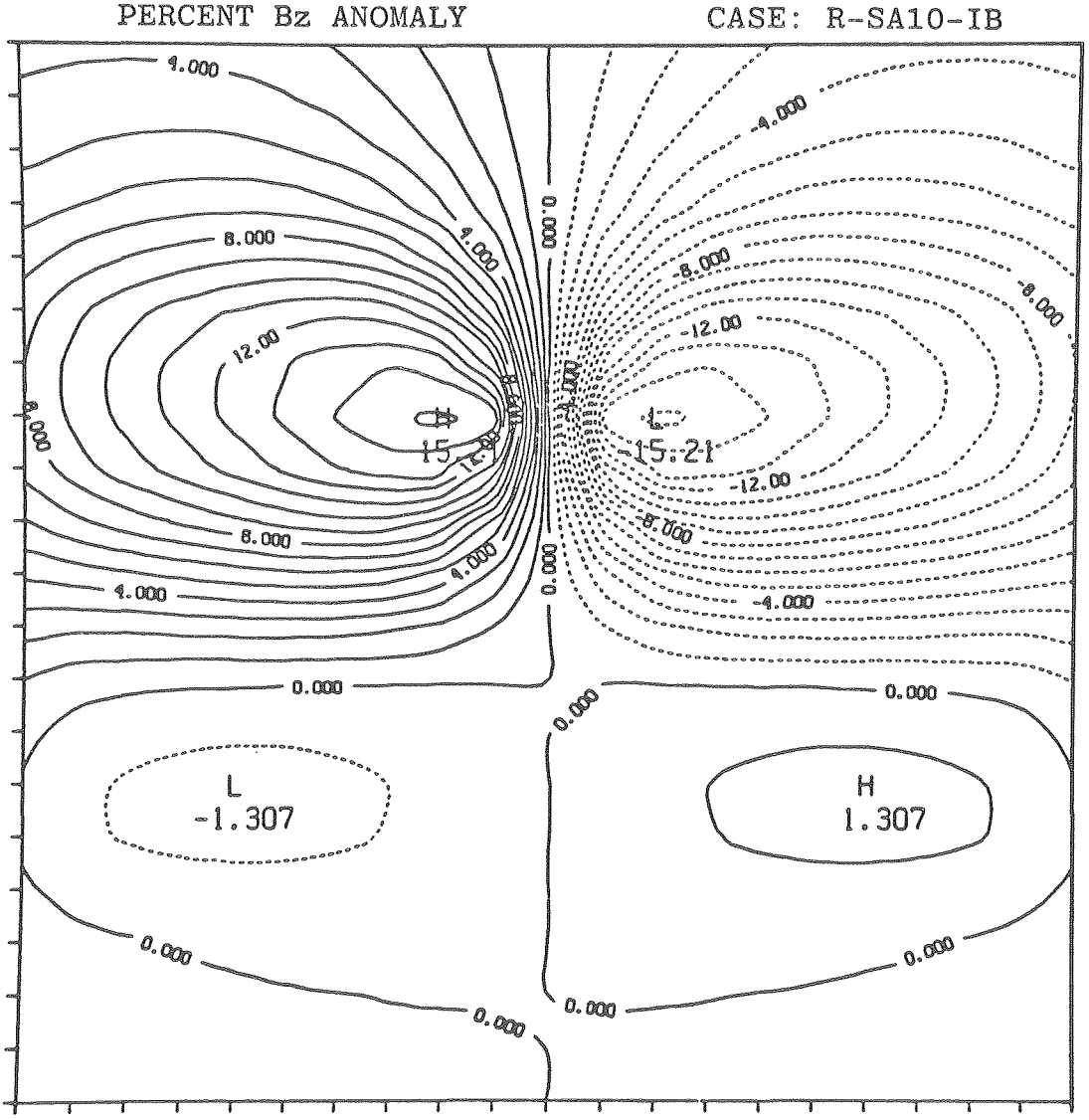

Figure 3-8-27.

XBL 7911-12928

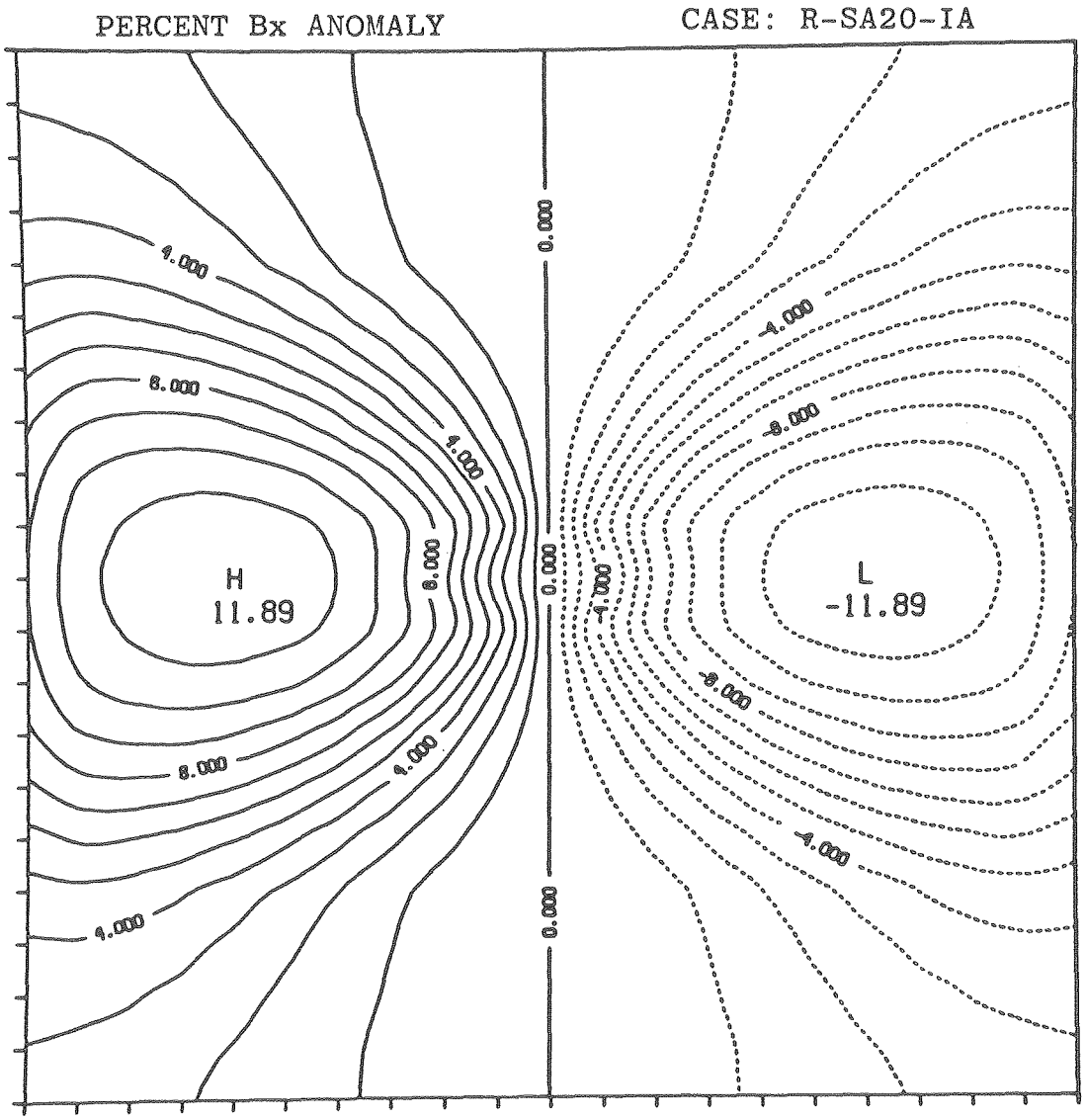

Figure 3-8-28.

XBL 7911-12885

PERCENT By ANOMALY CASE: R-SA20-IA

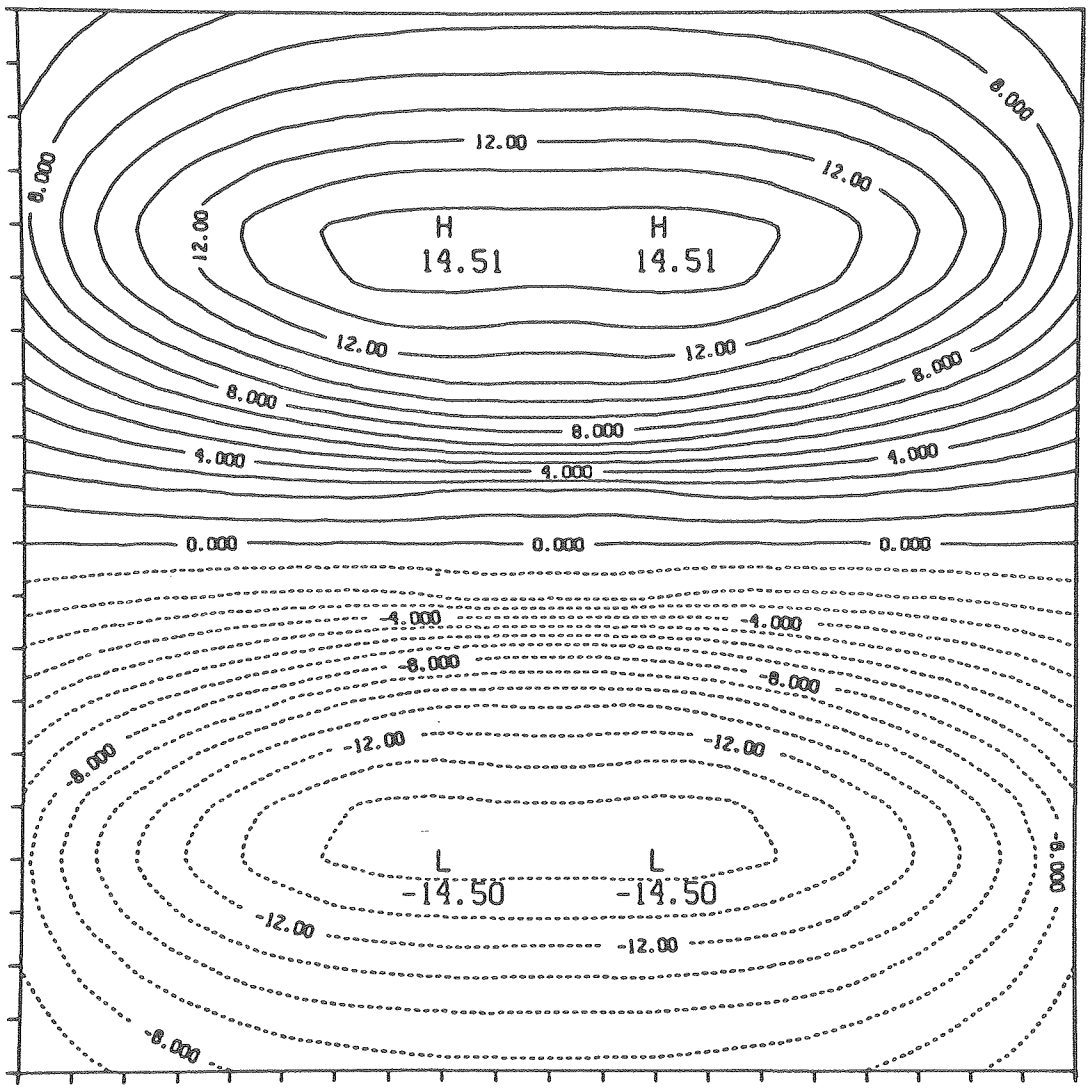

Figure 3-8-29.

XBL 7911-12886

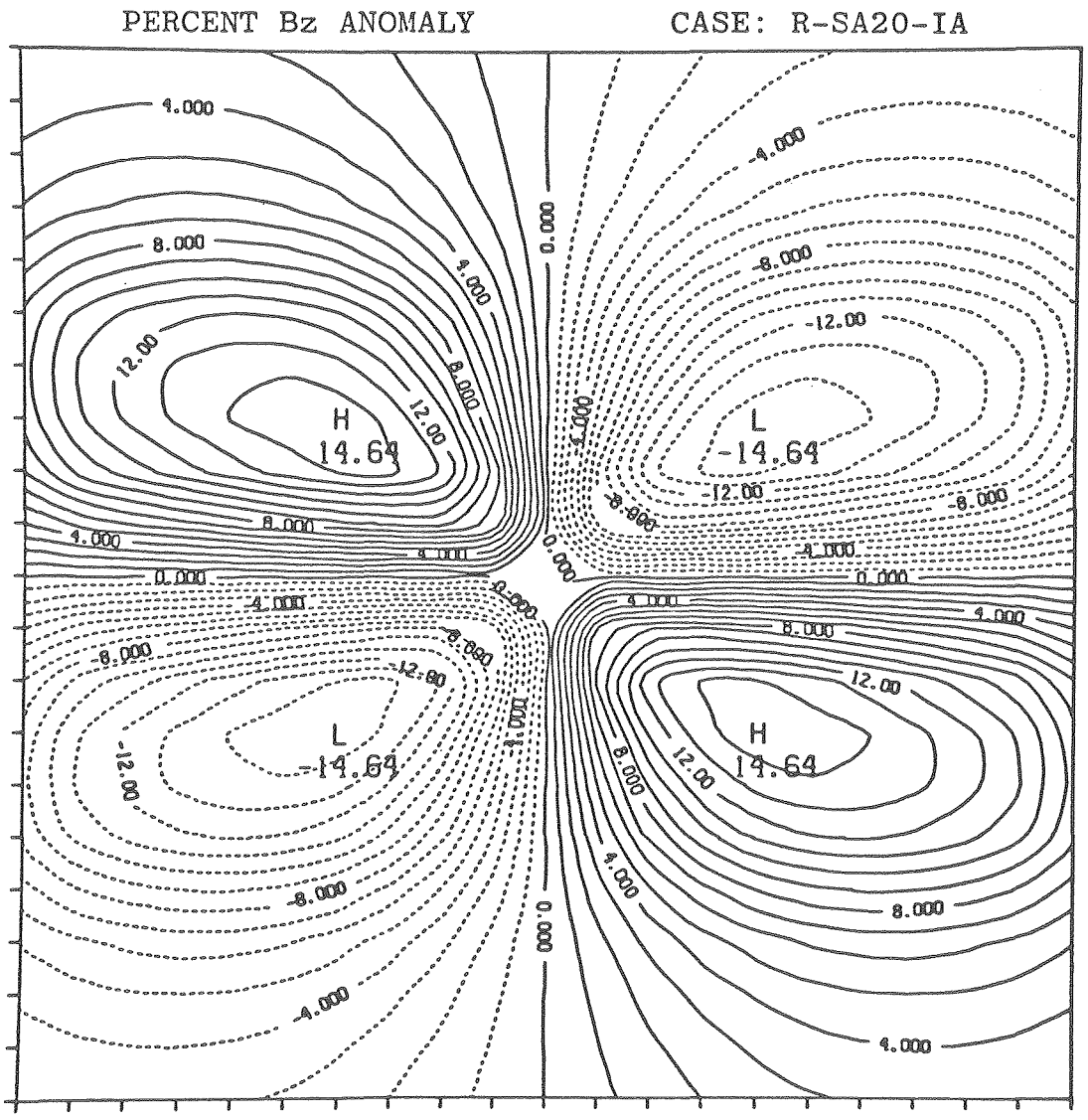

Figure 3-8-30

XBL 7911-12887

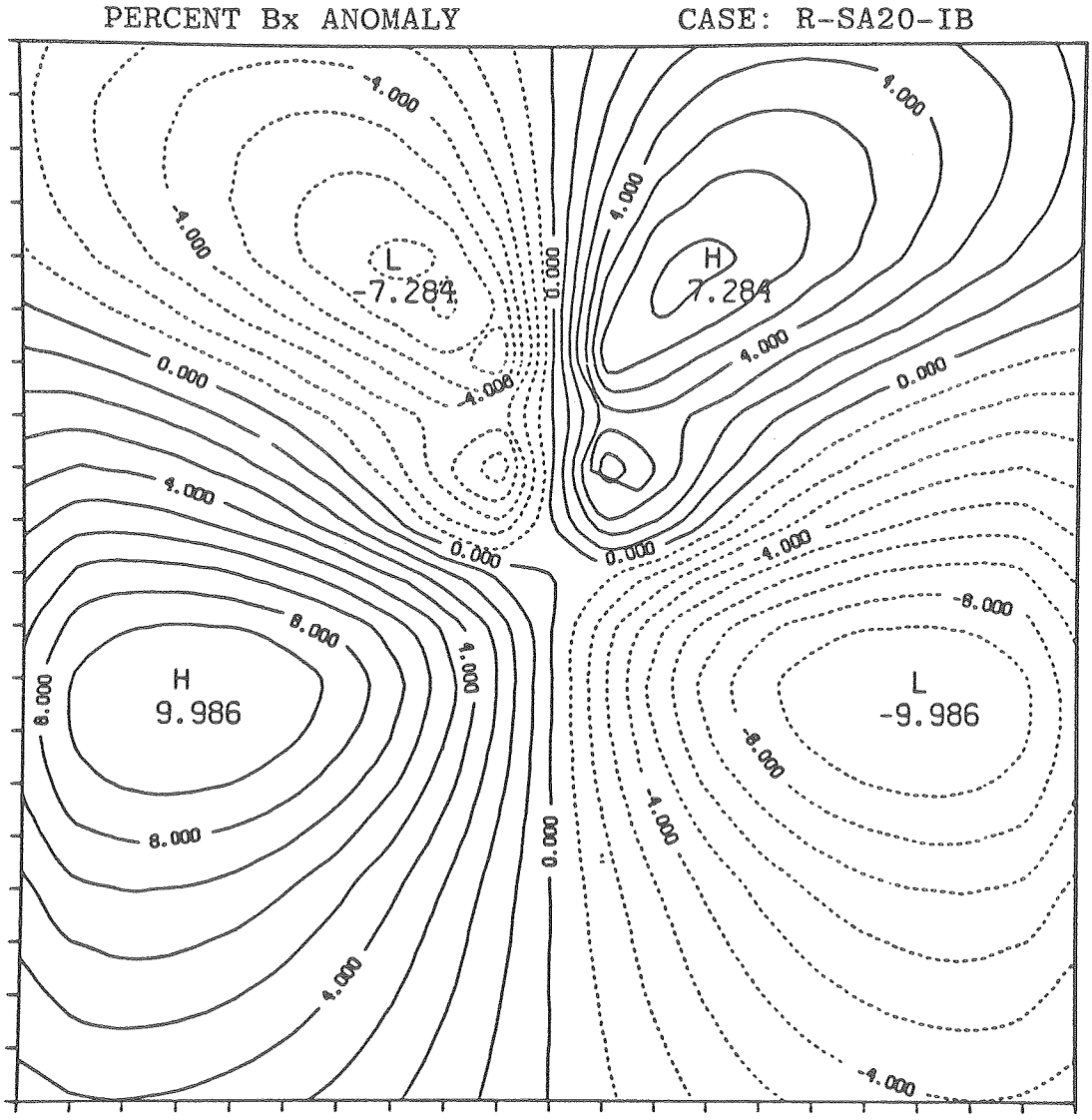

Figure 3-8-31.

XBL 7911-12930

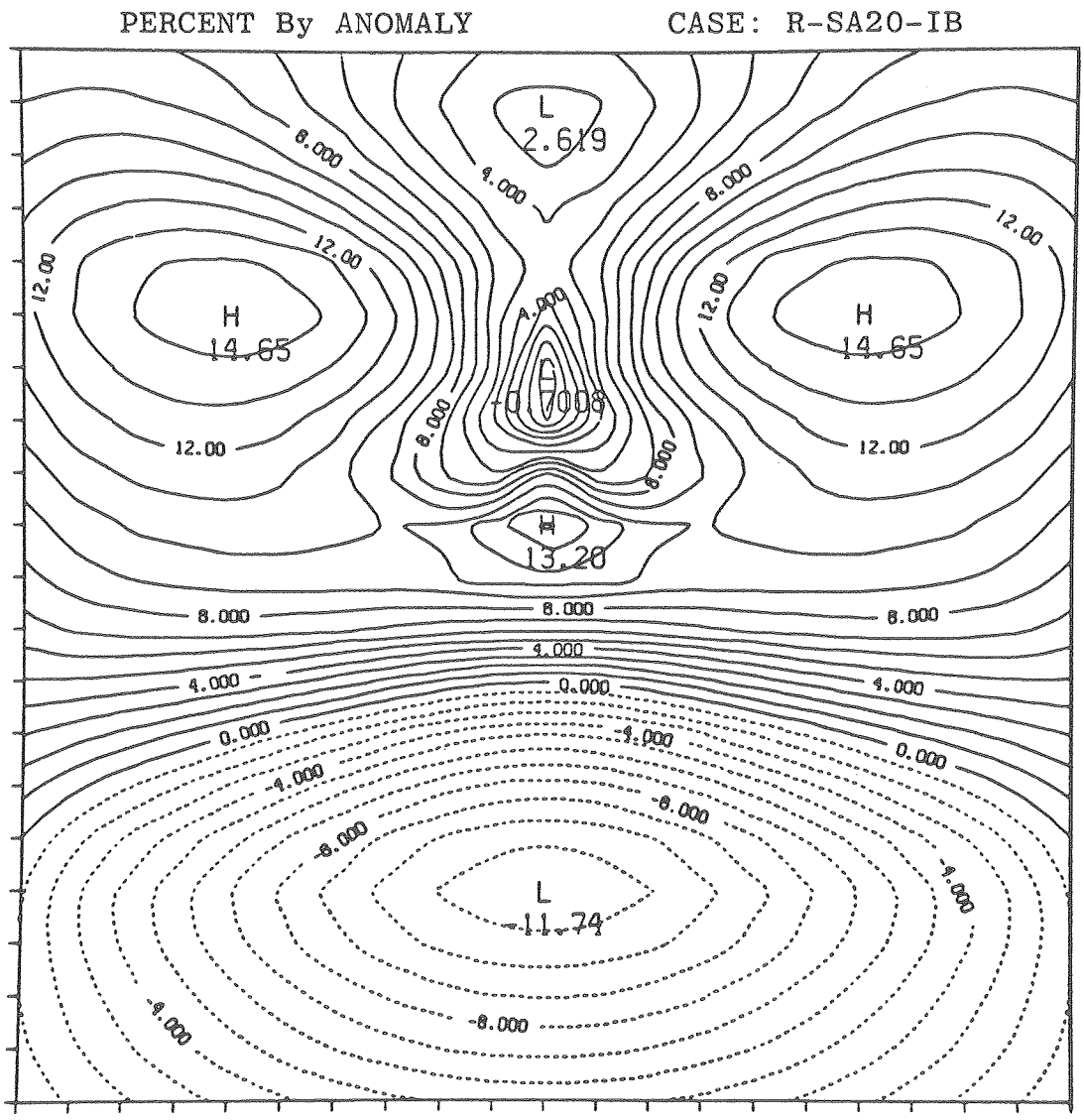

Figure 3-8-32.

XBL 7911-12931

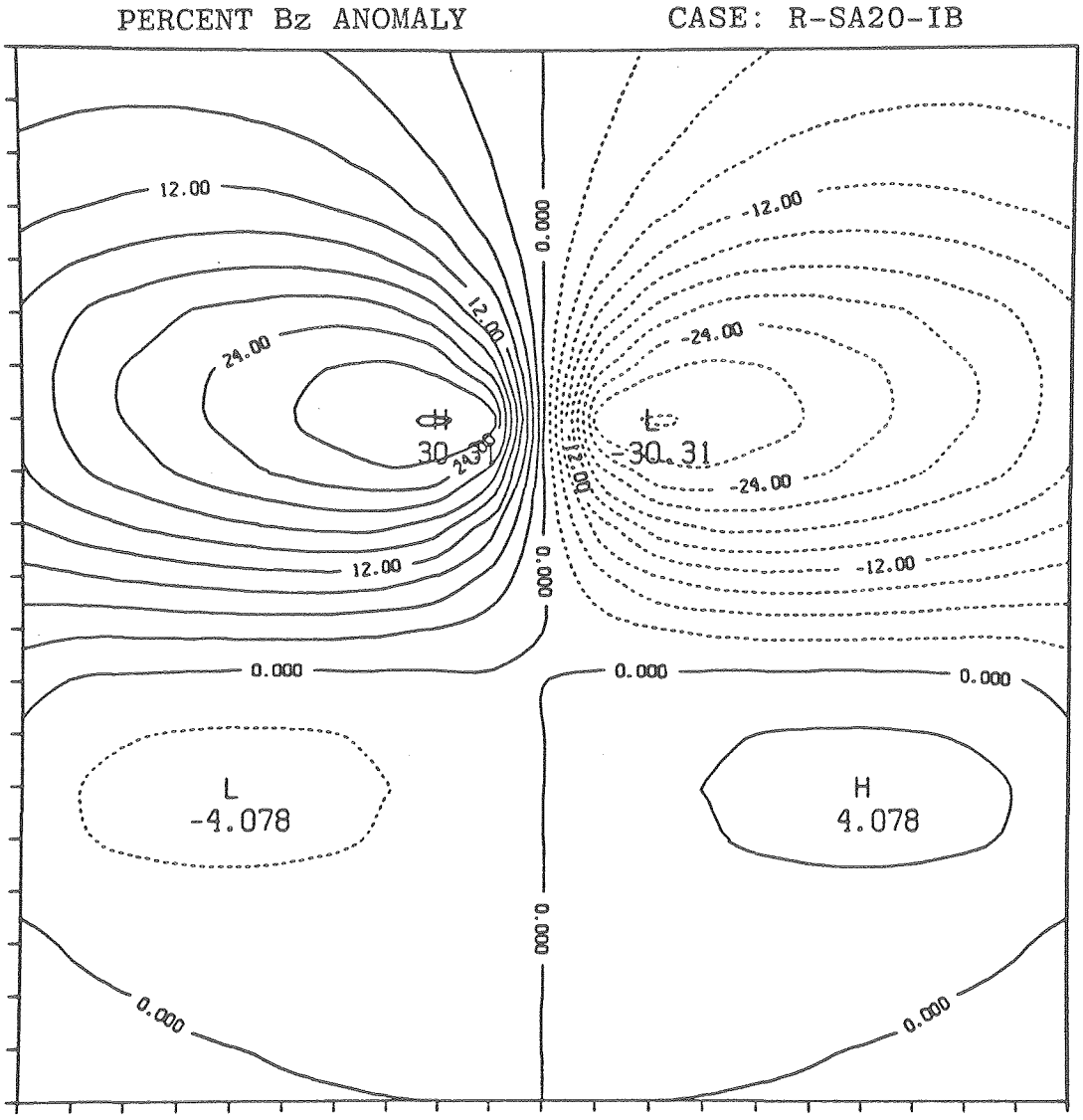

Figure 3-8-33.

XBL 7911-12883

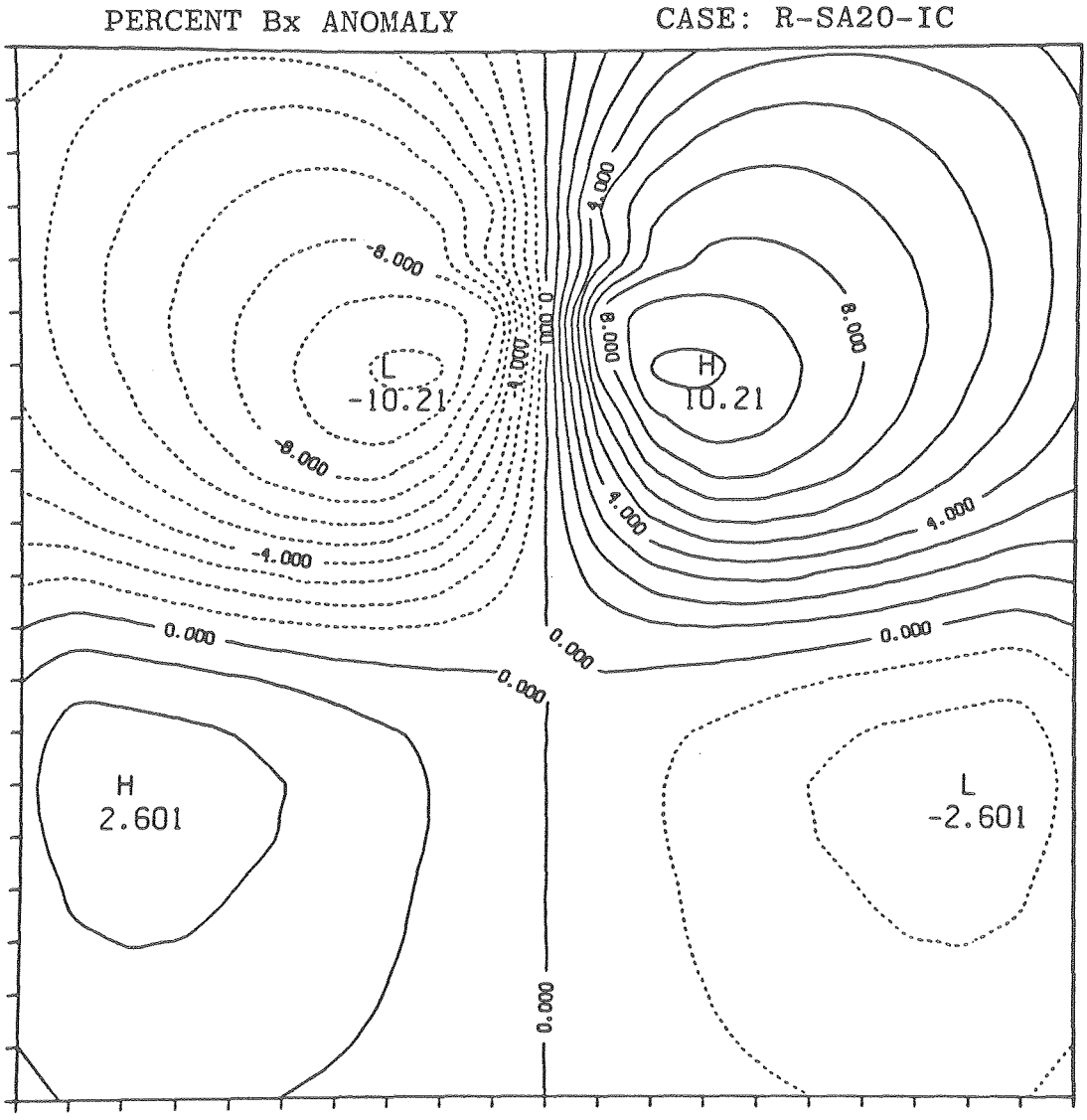

Figure 3-8-34.

XBL 7911-12933

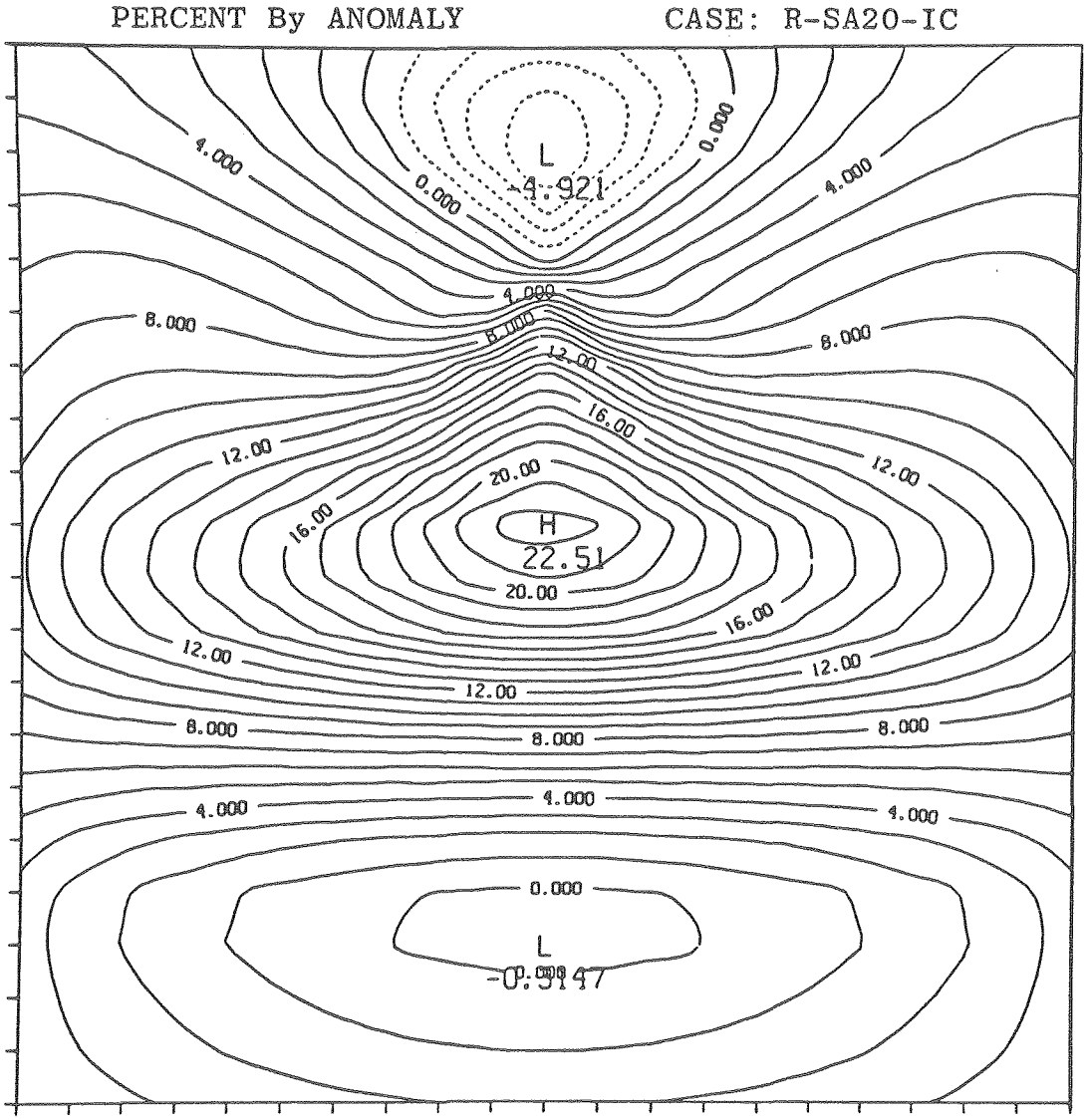

Figure 3-8-35.

XBL 7911-12934

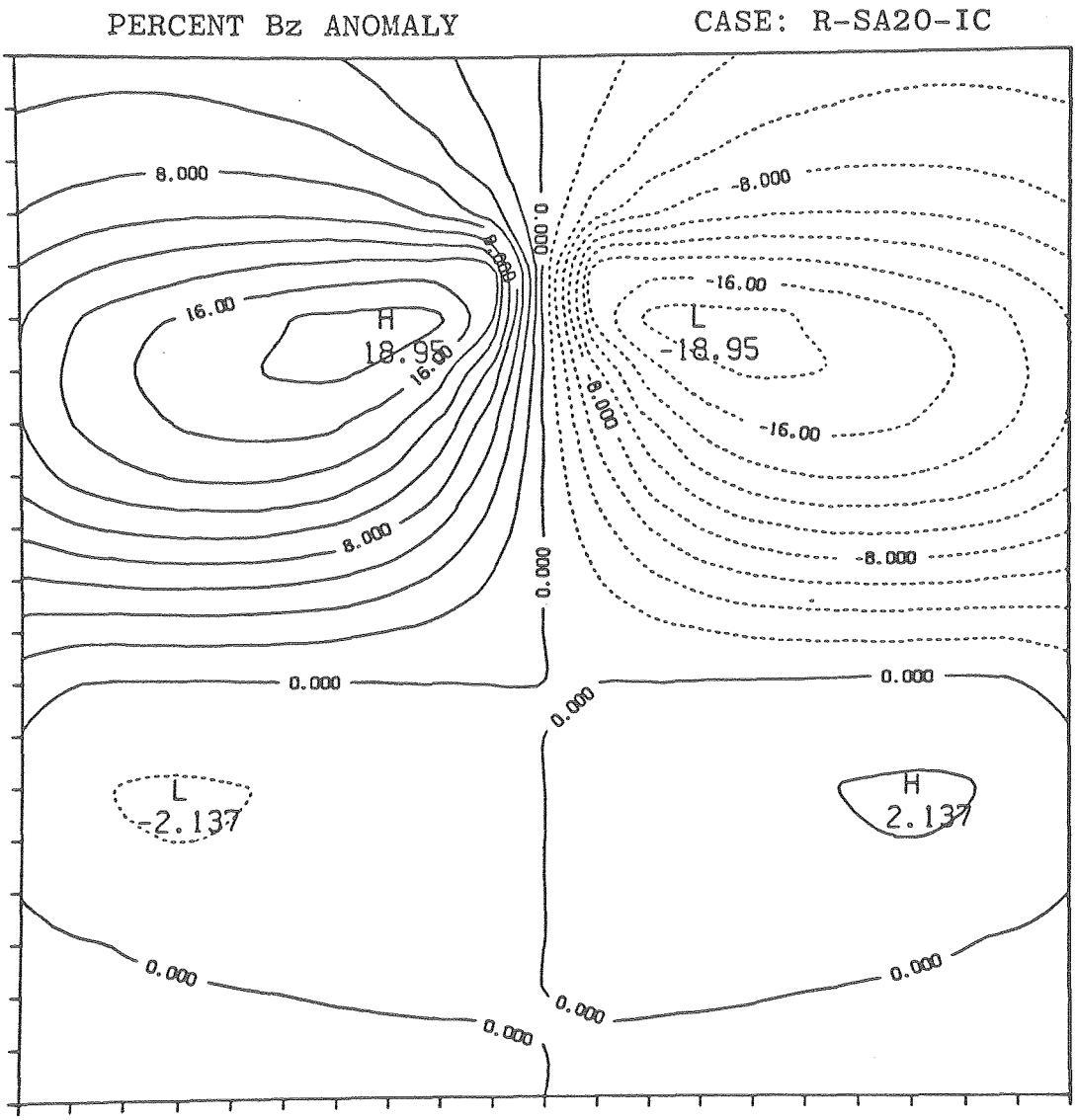

Figure 3-8-36.

XBL 7911-12935

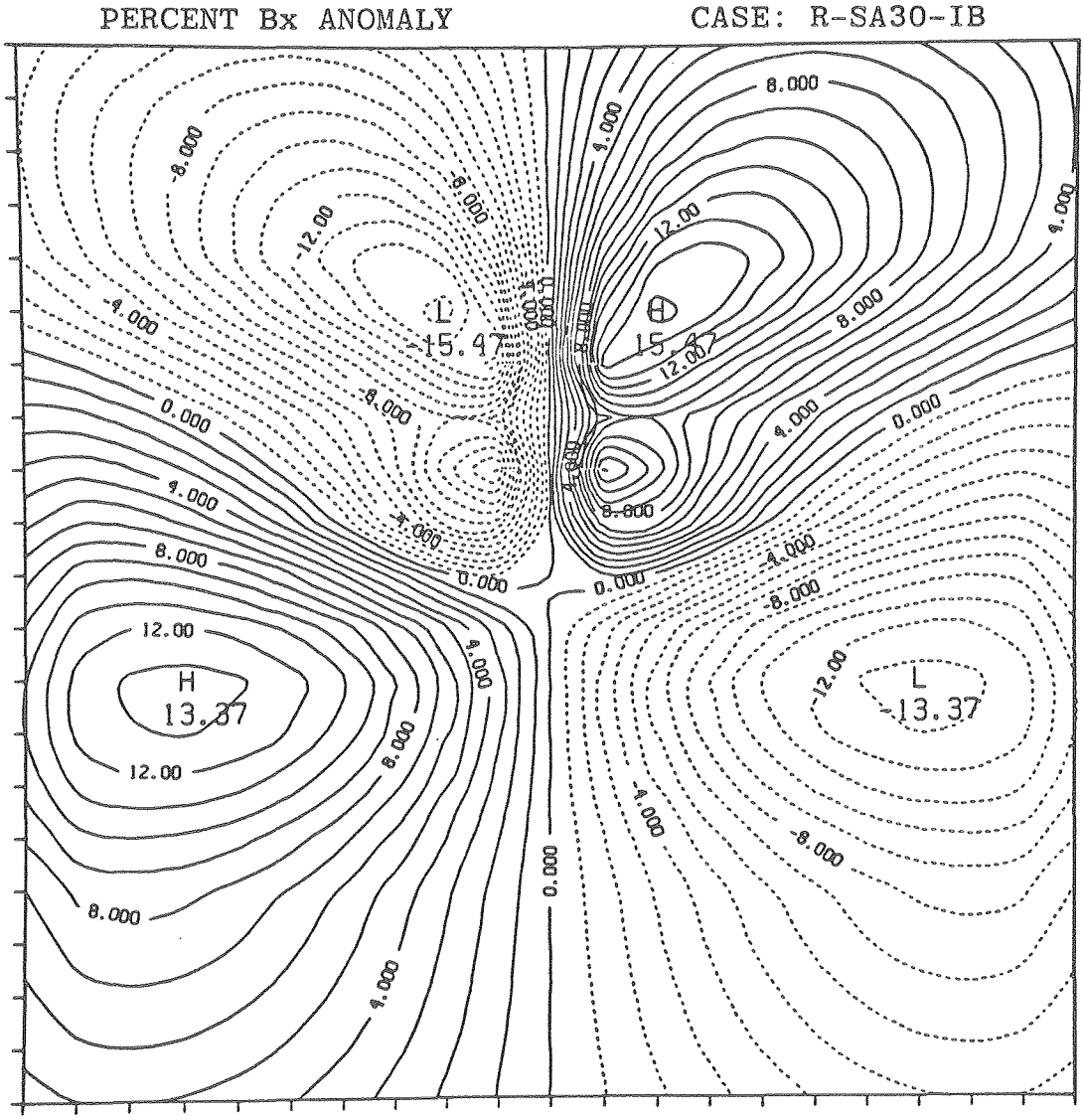

Figure 3-8-37.

XBL 7911-12937

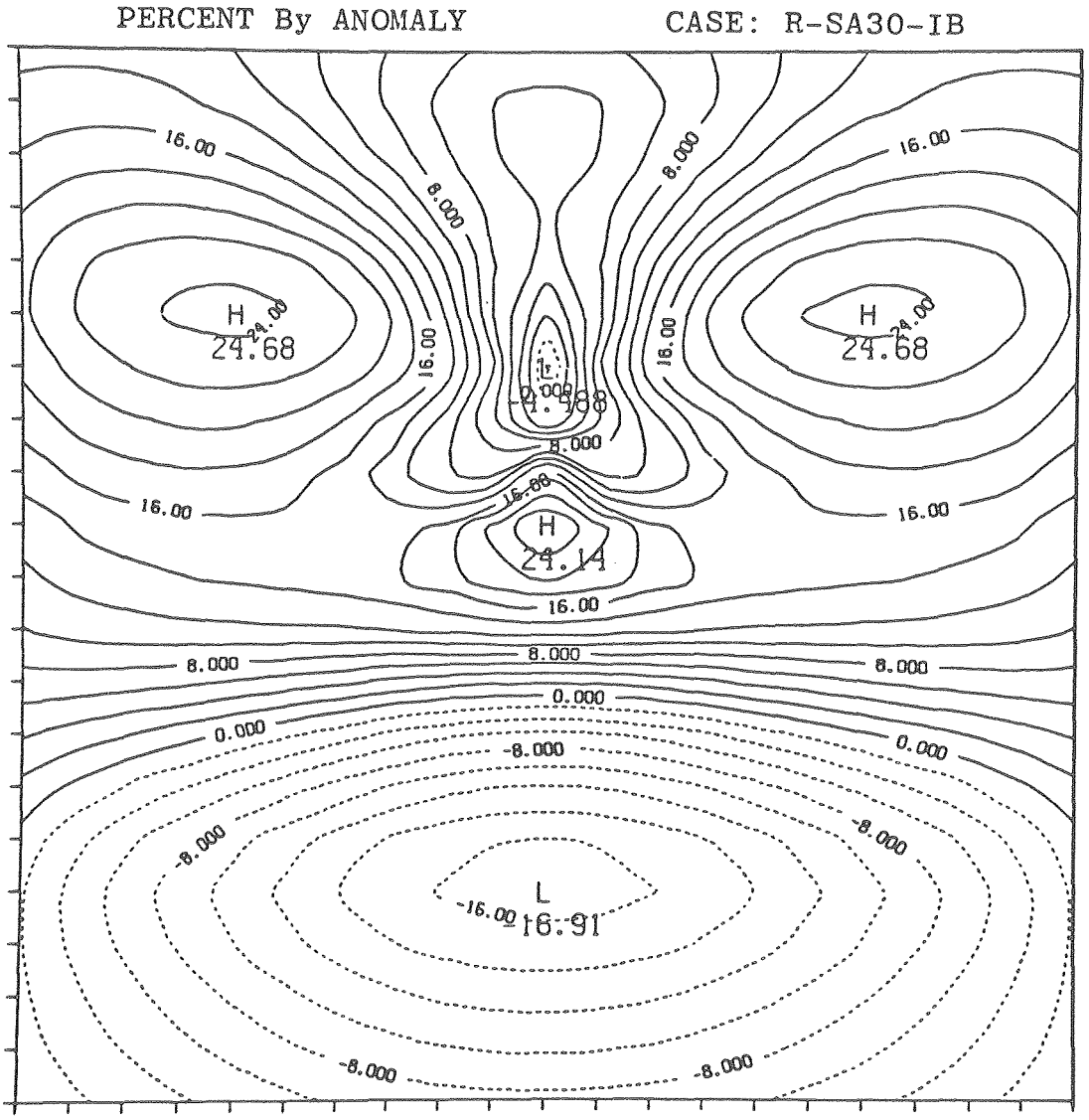

Figure 3-8-38.

XBL 7911-12938

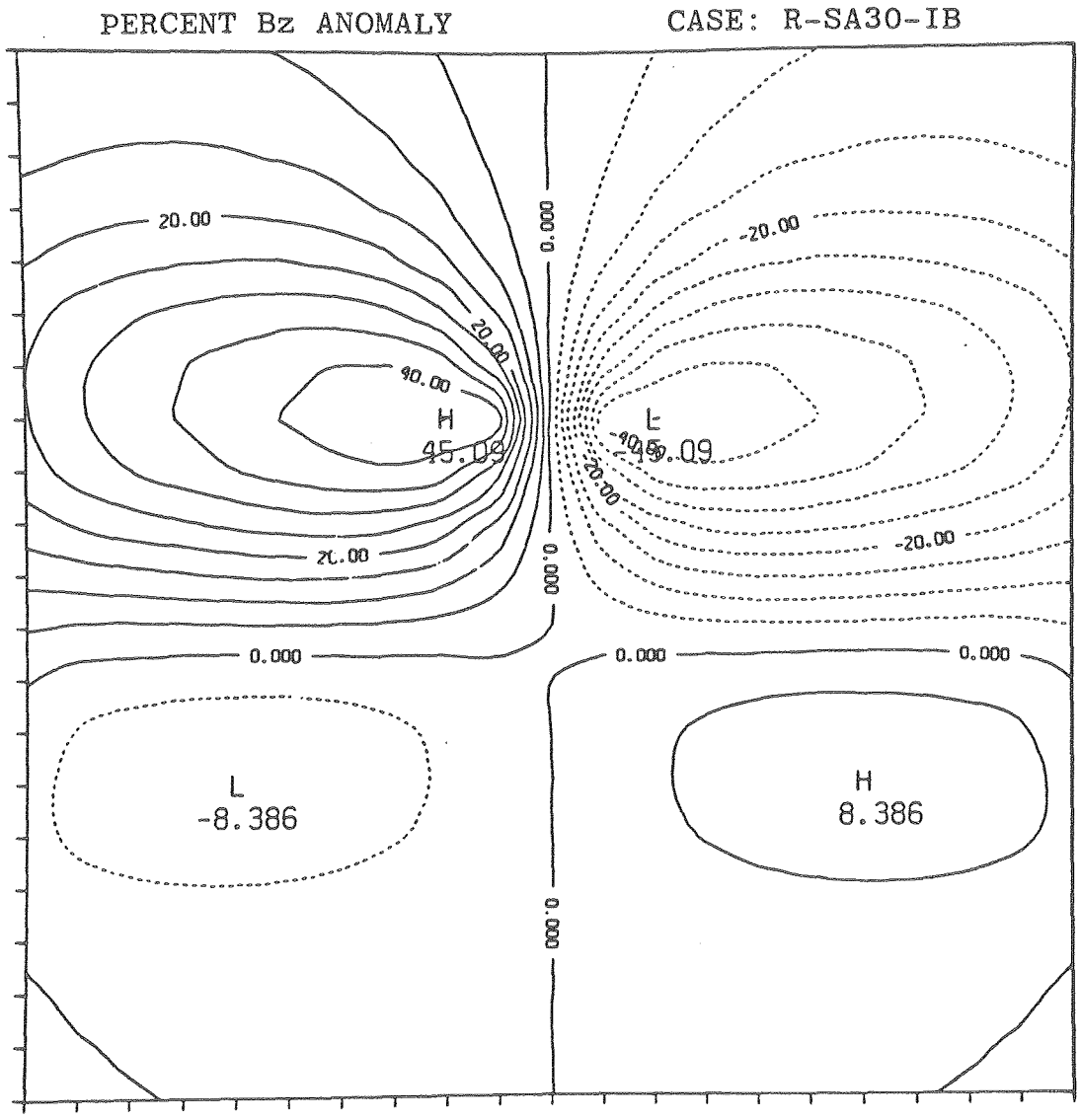

Figure 3-8-39.

XBL 7911-12939

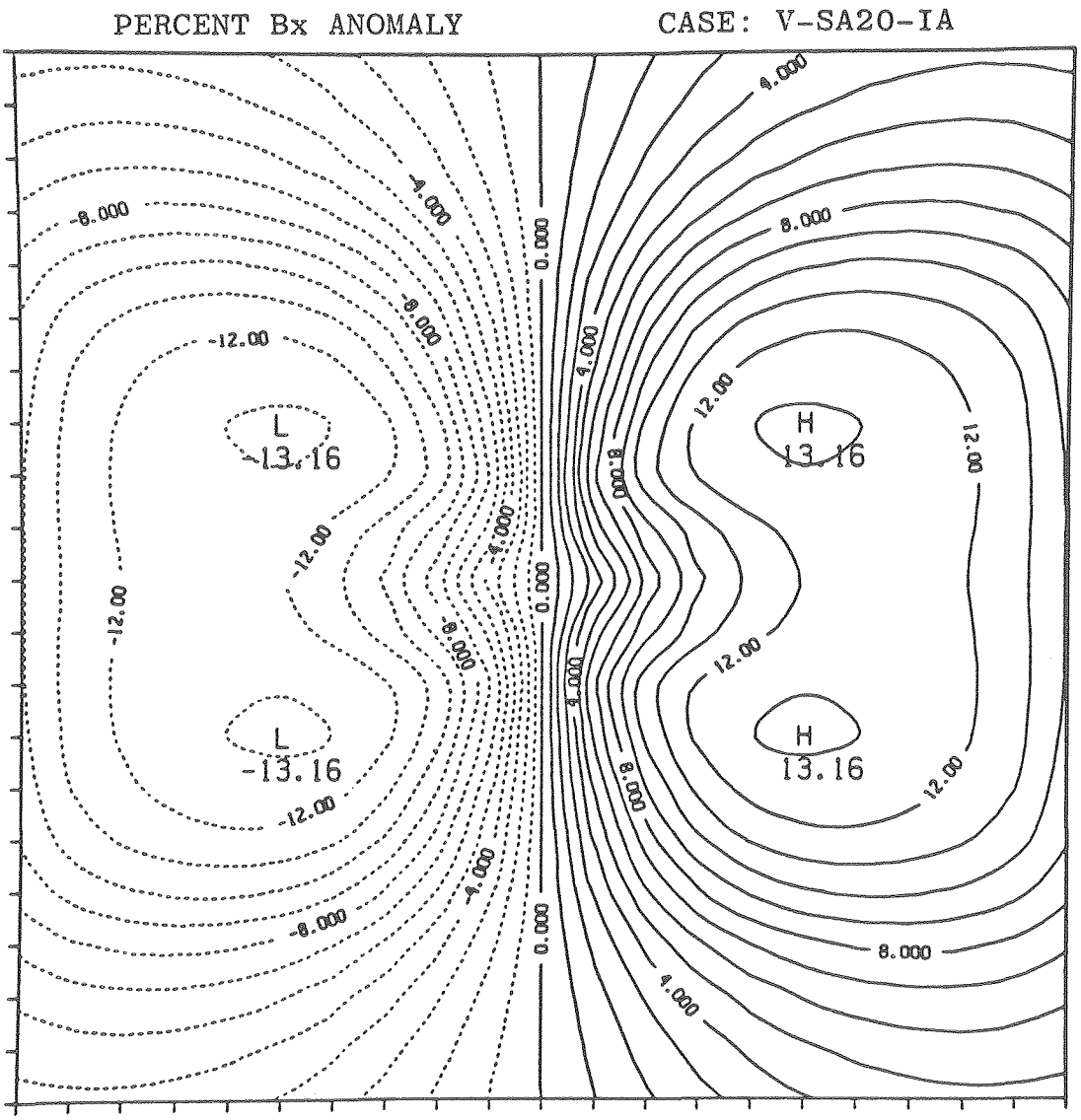

Figure 3-8-40.

XBL 7911-12941

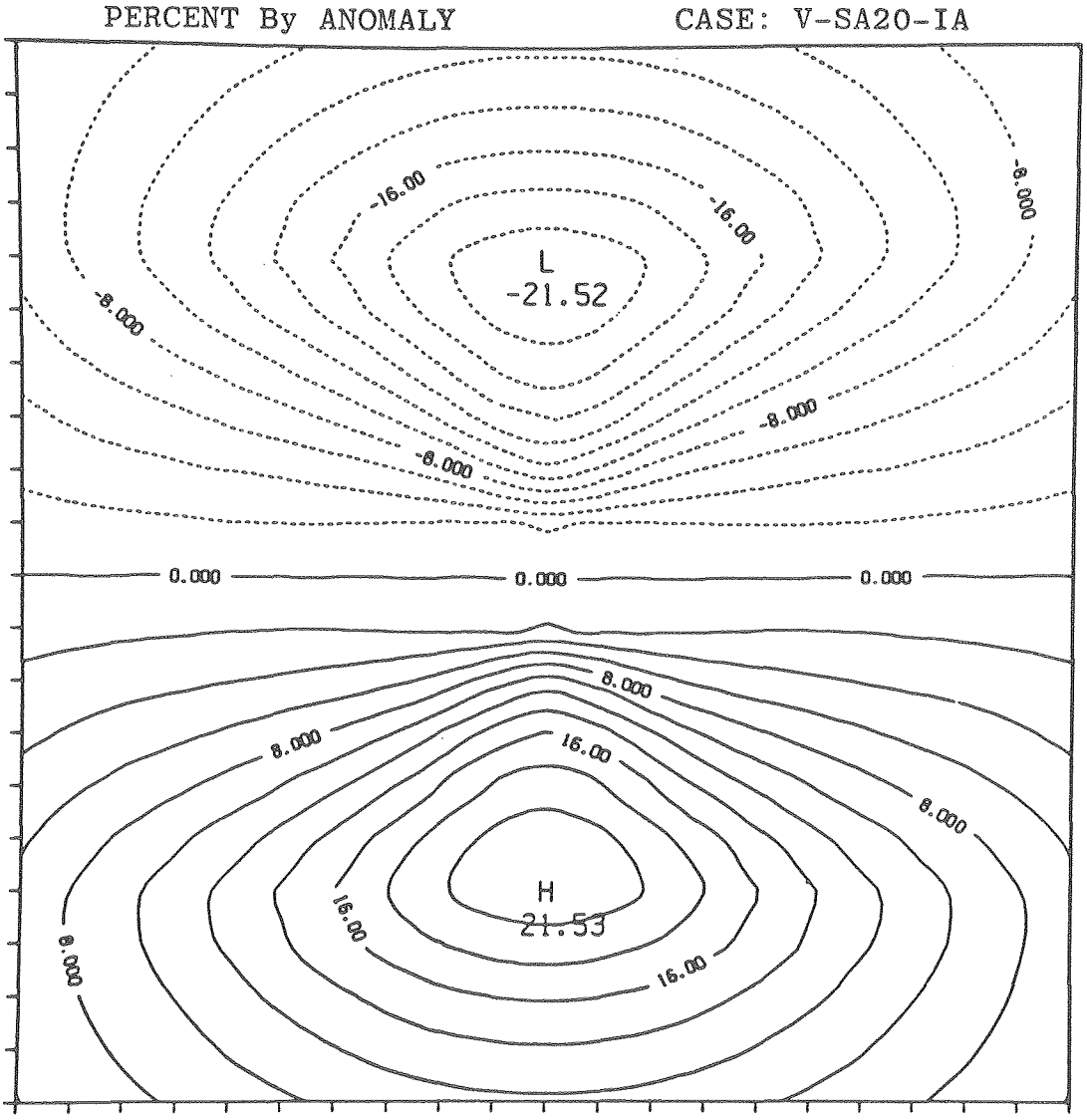

Figure 3-8-41.

XBL 7911-12942

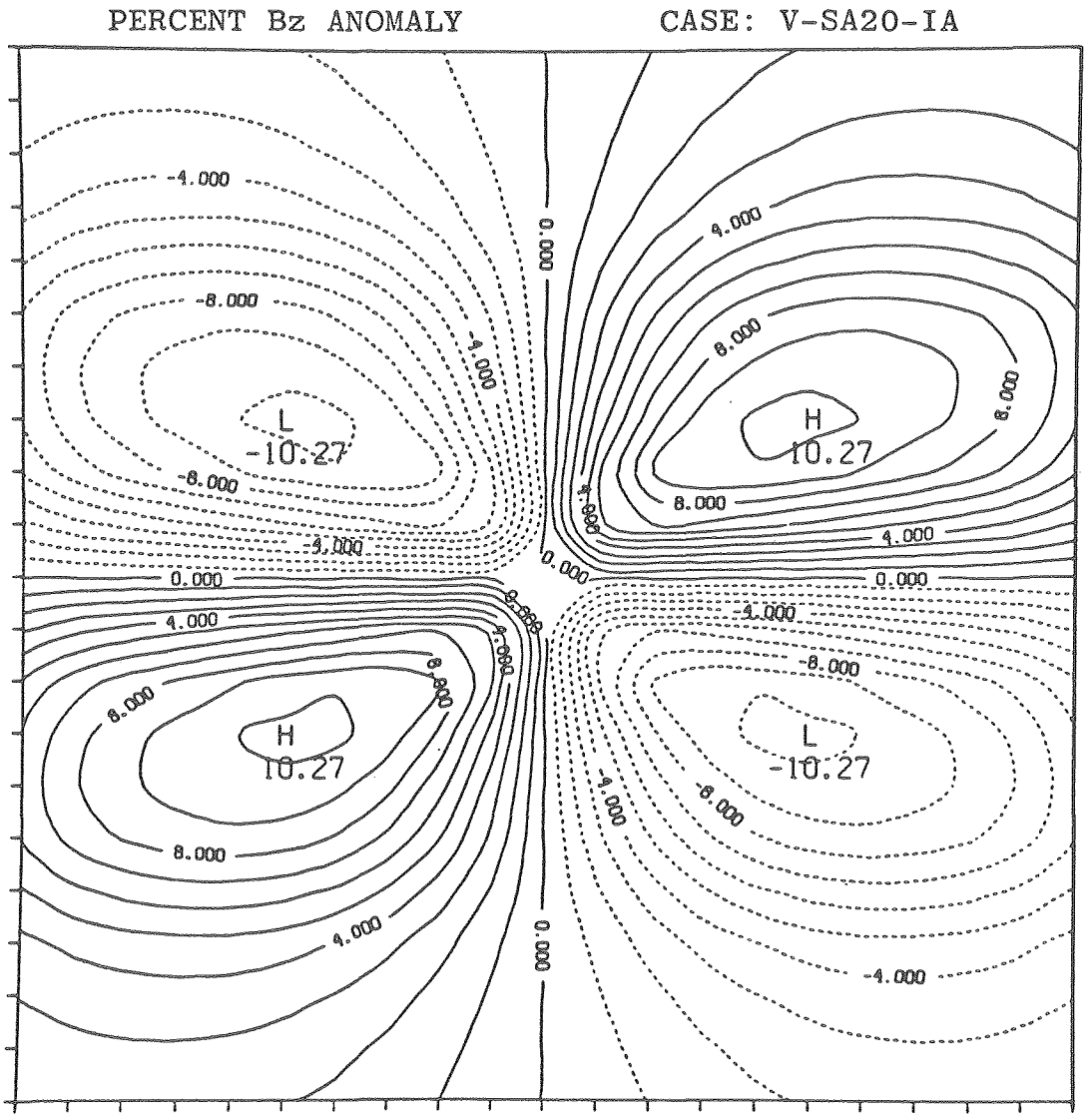

Figure 3-8-42.

XBL 7911-12943

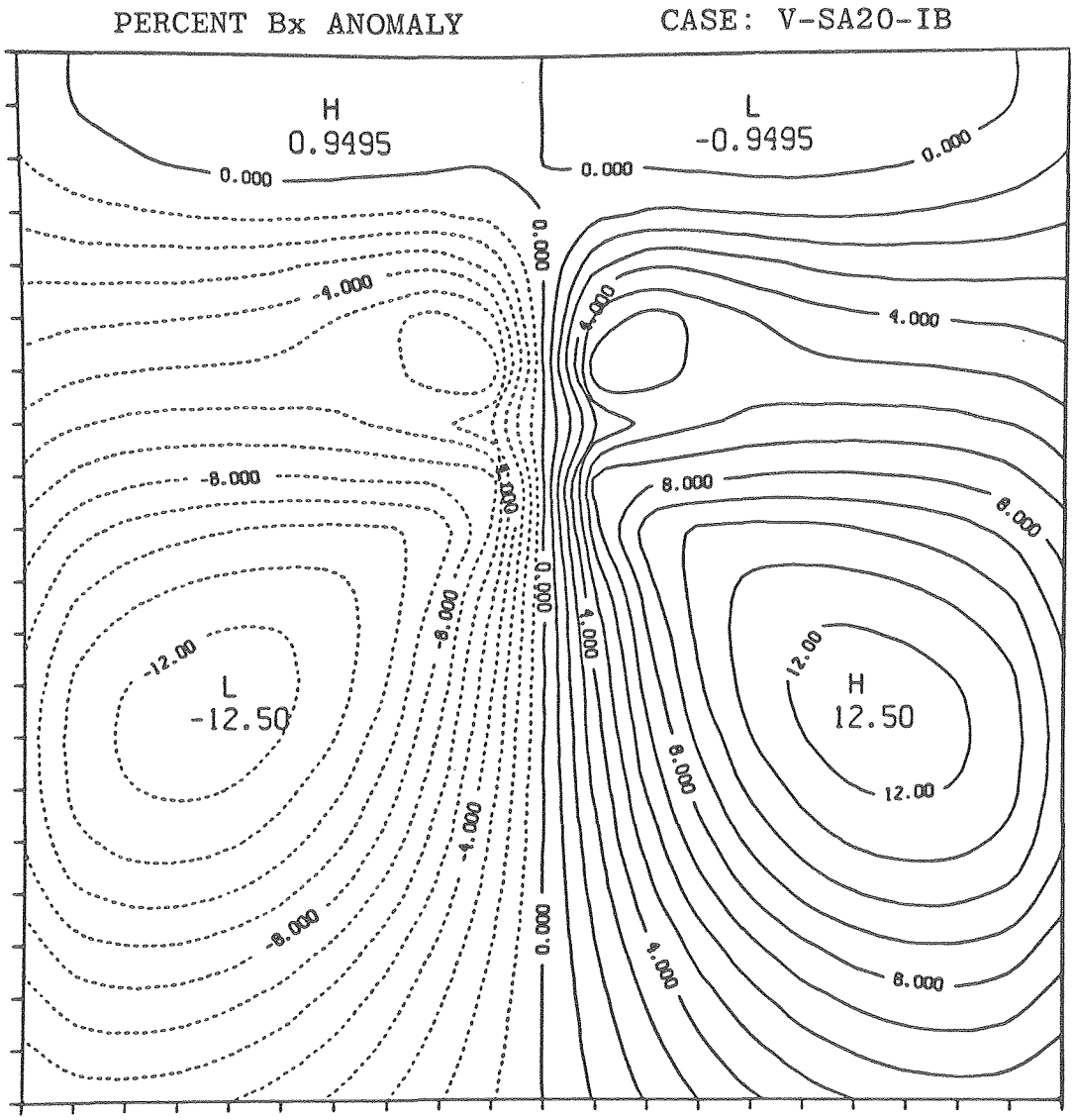

Figure 3-8-43.

XBL 7911-12945

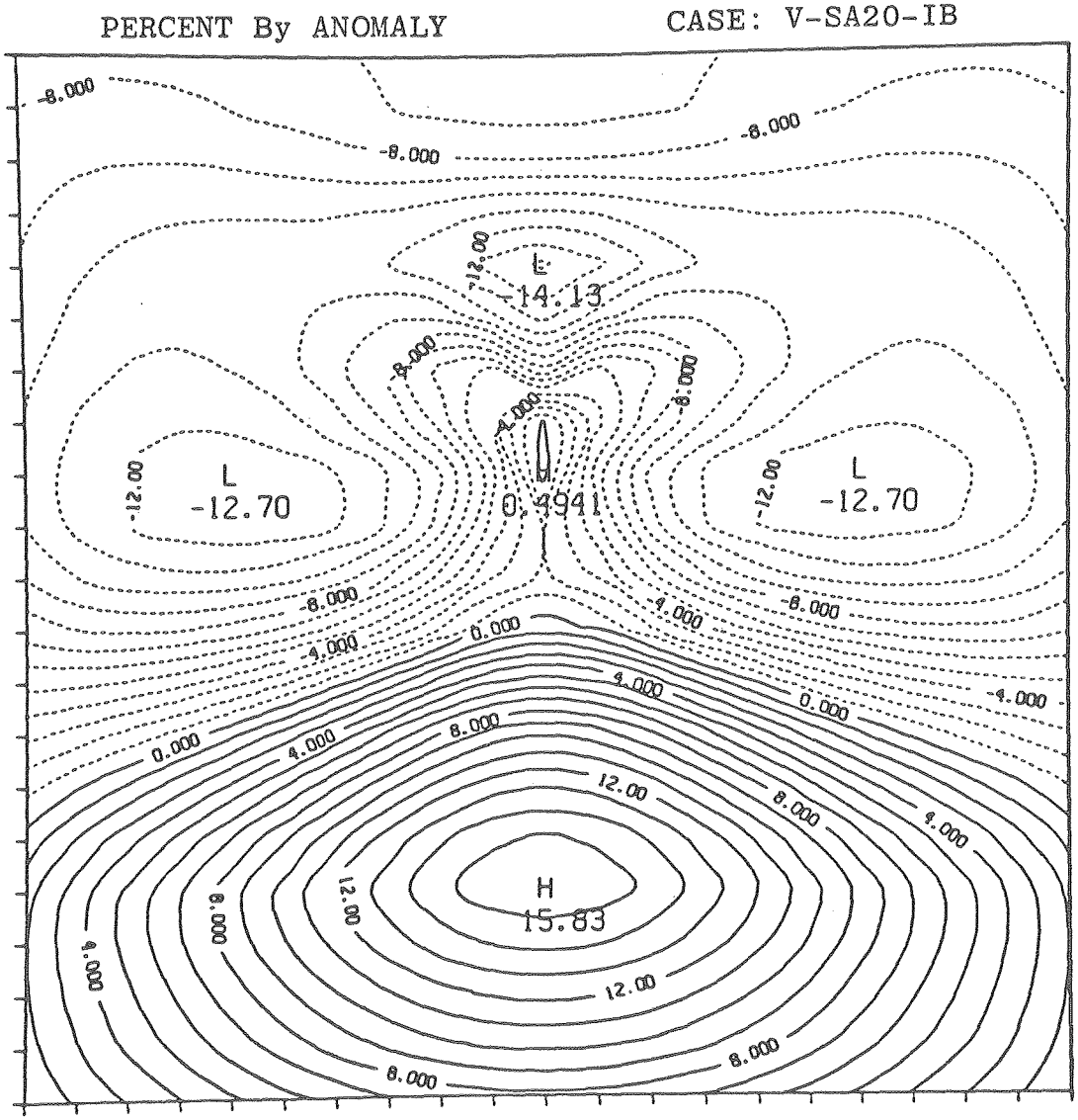

Figure 3-8-44.

XBL 7911-12946

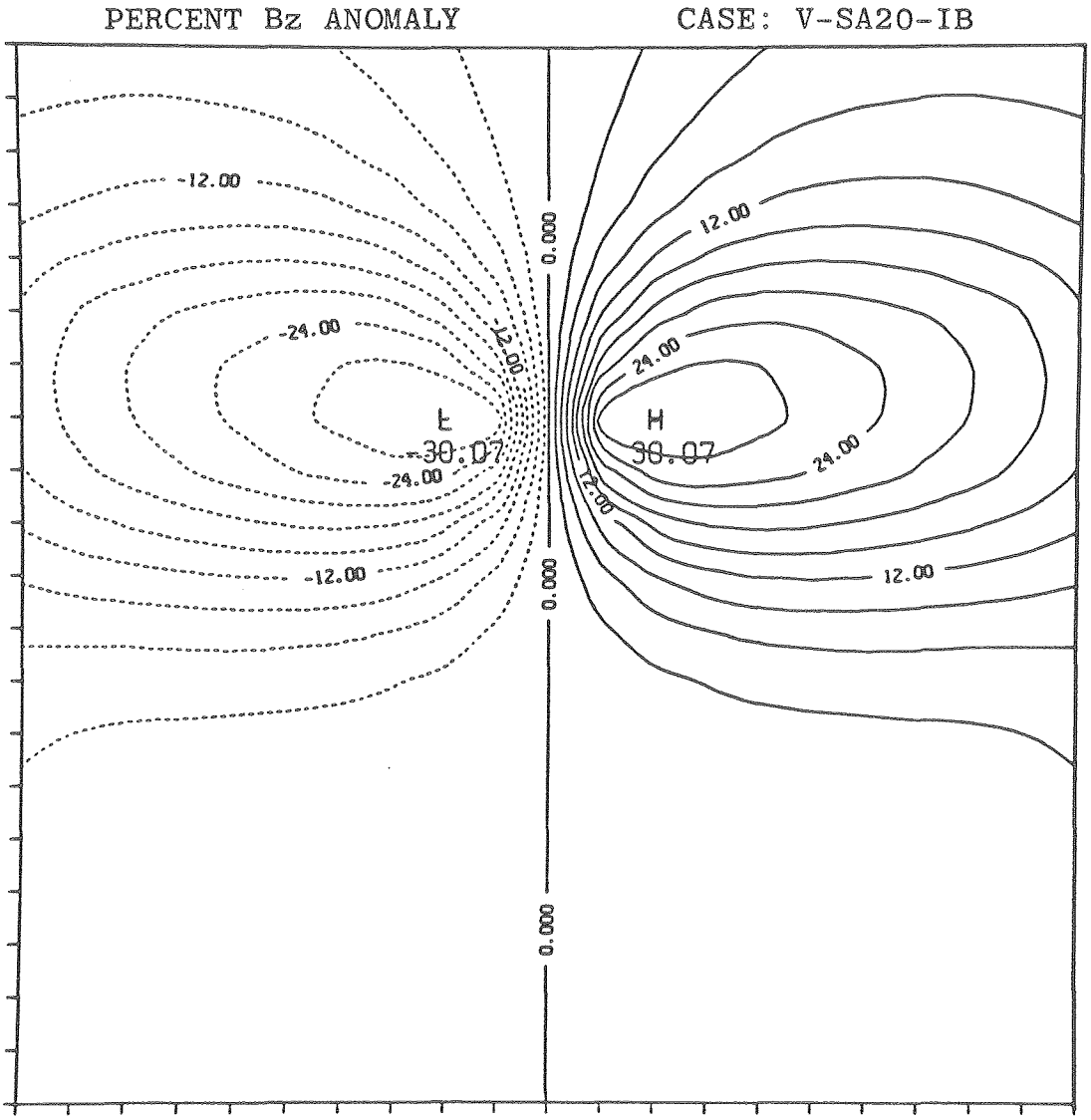

Figure 3-8-45.

XBL 7911-12882

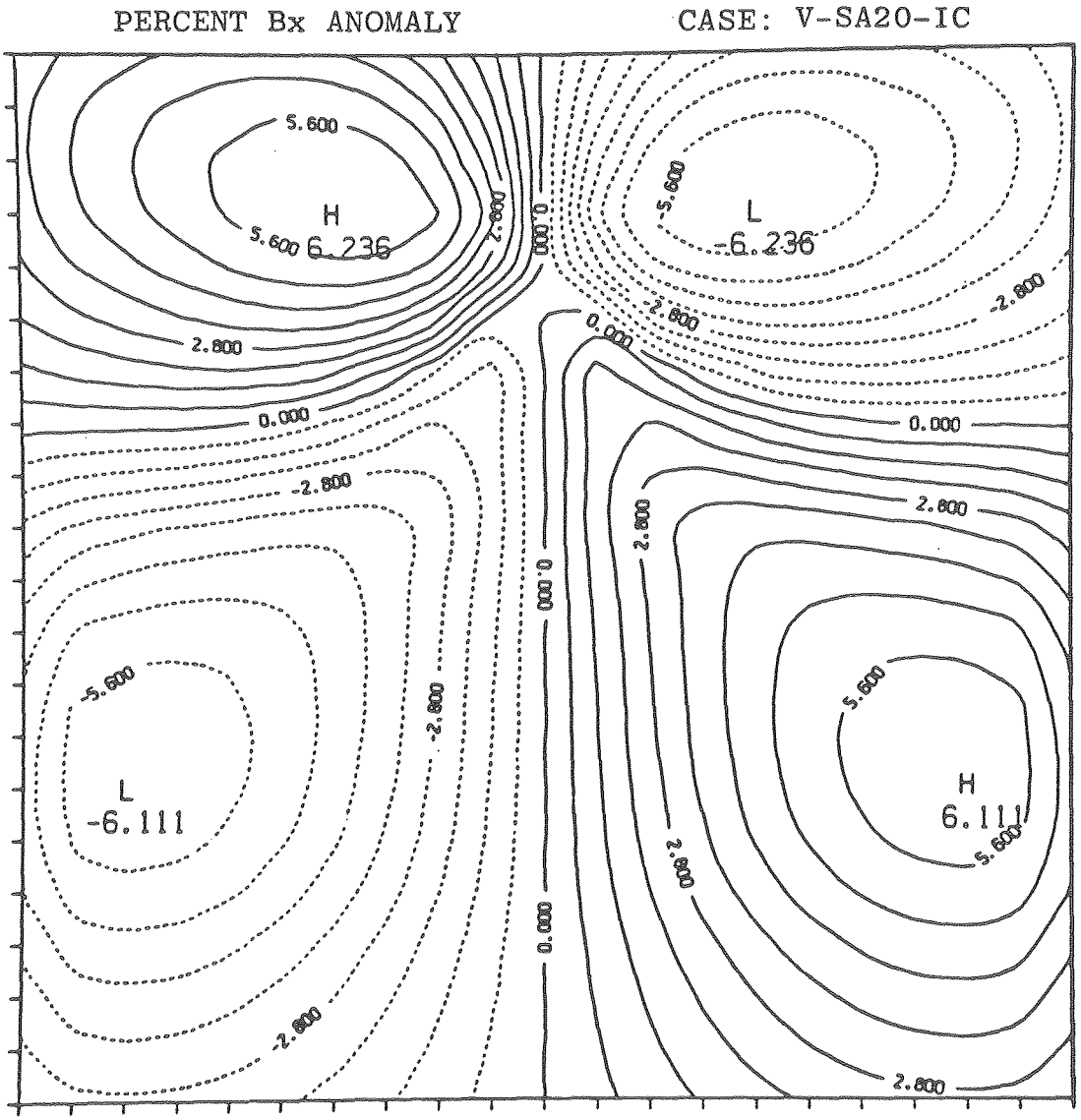

Figure 3-8-46.

XBL 7911-12948

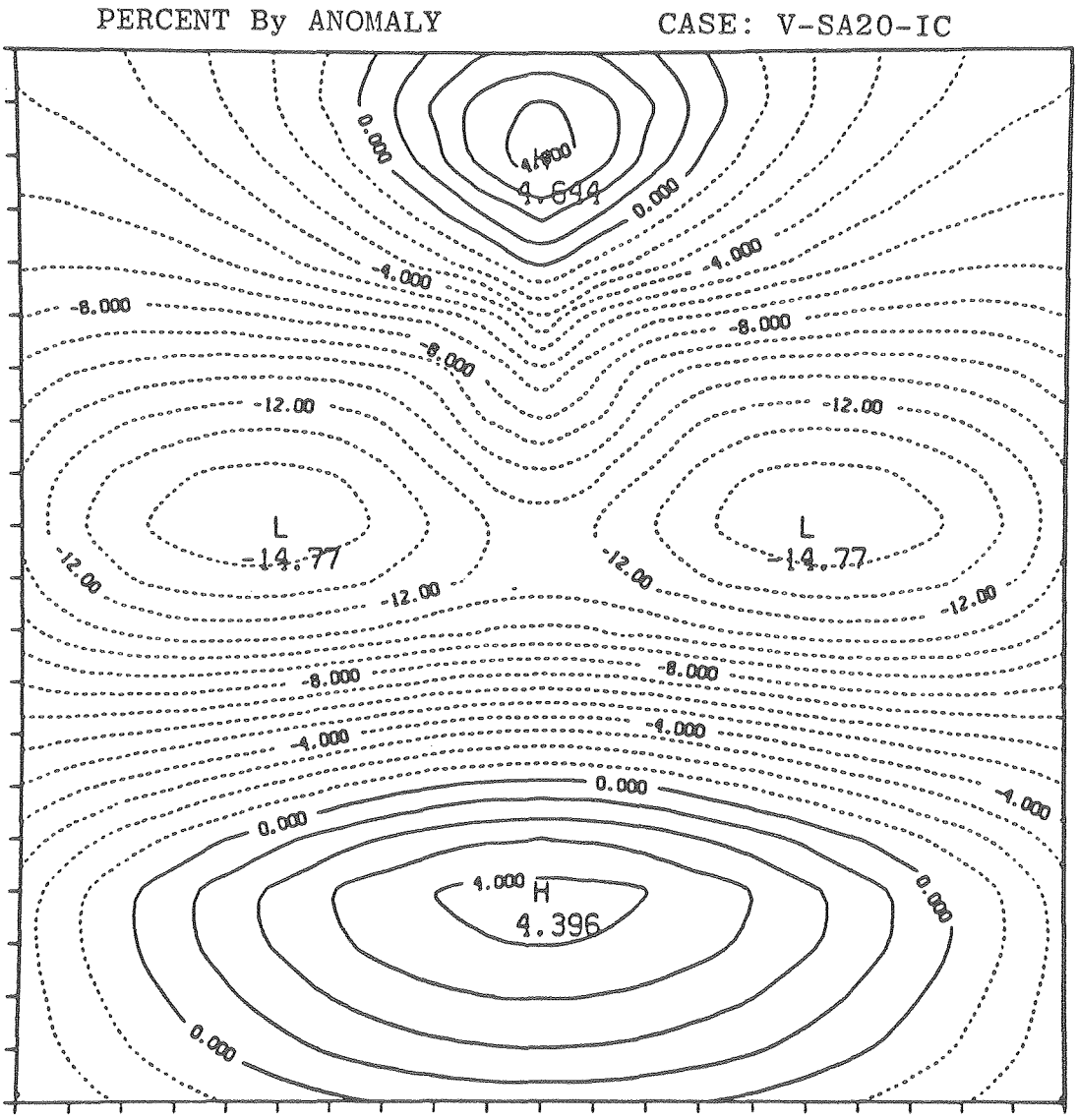

Figure 3-8-47.

XBL 7911-12949

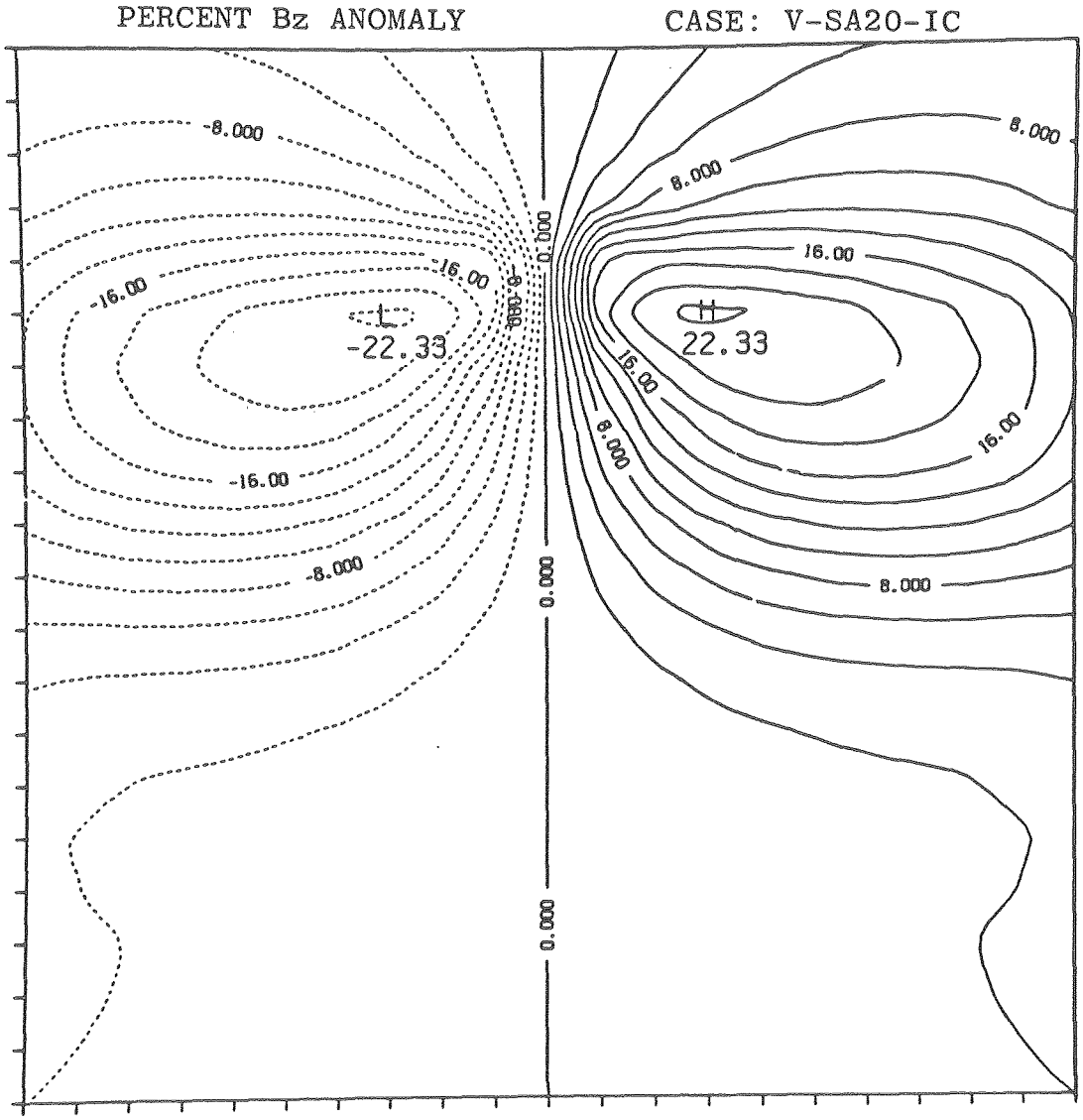

Figure 3-8-48.

XBL 7911-12950

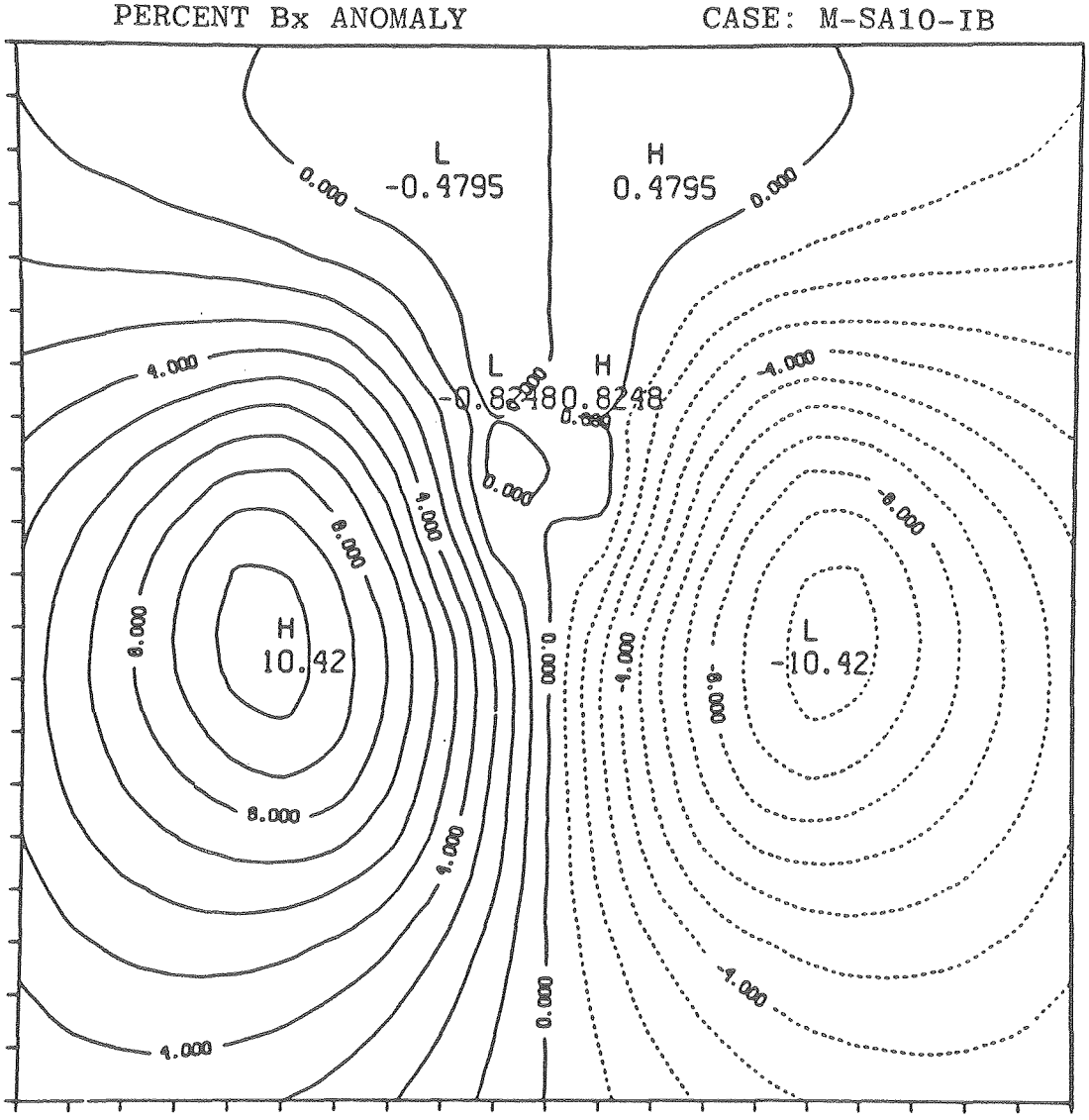

Figure 3-8-49.

XBL 7911-12952

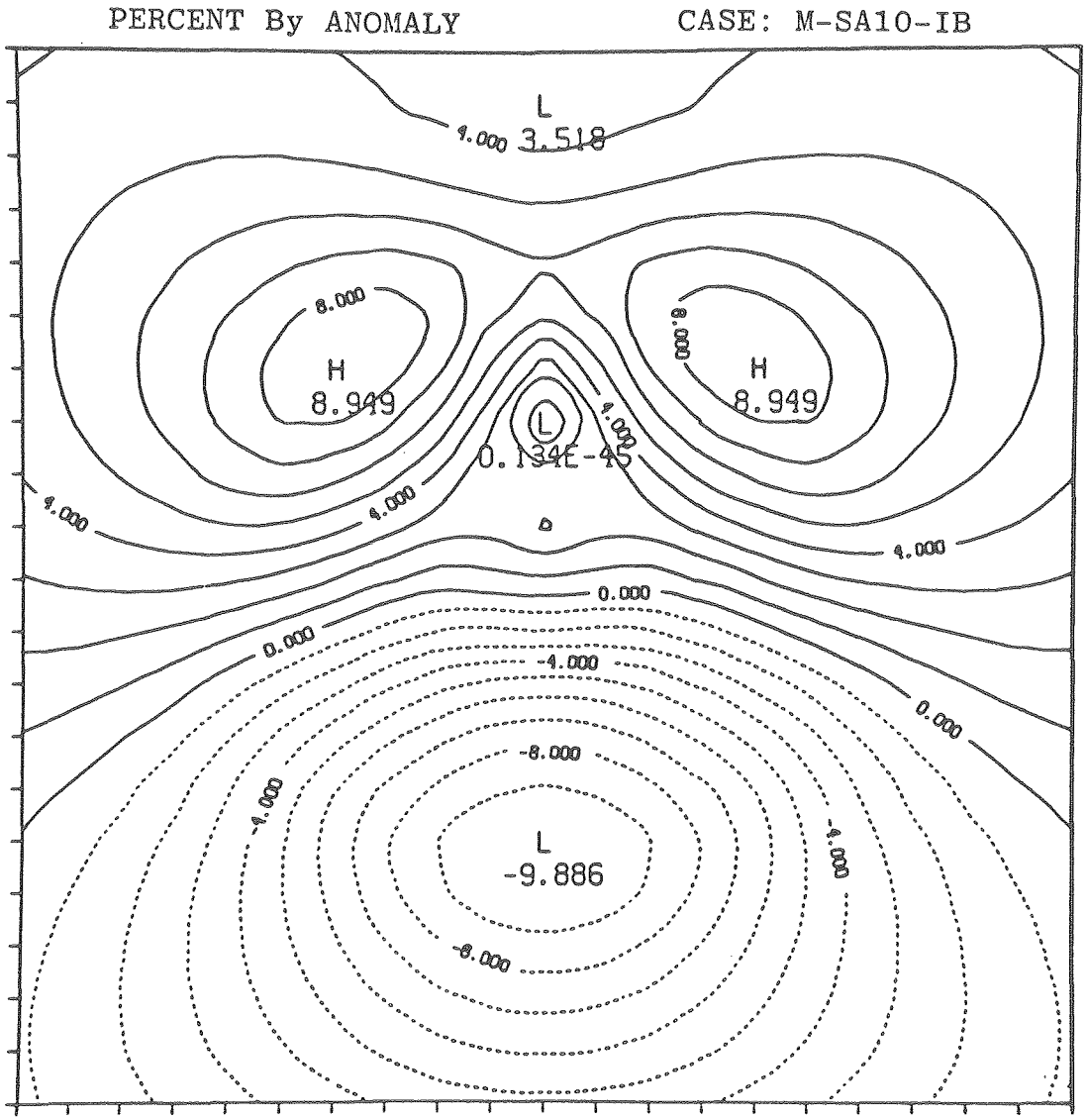

Figure 3-8-50.

XBL 7911-12953

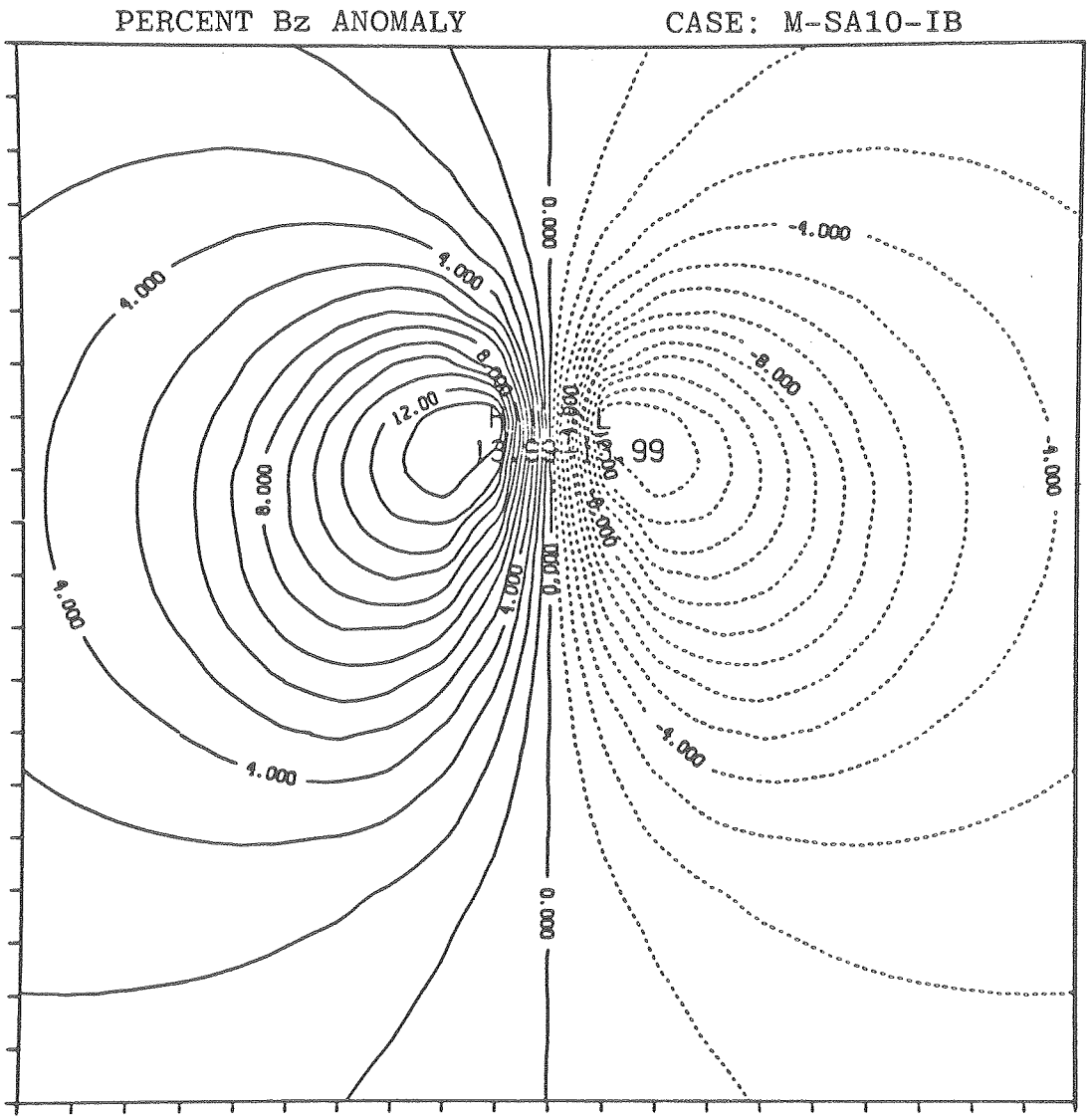

Figure 3-8-51.

XBL 7911-12954

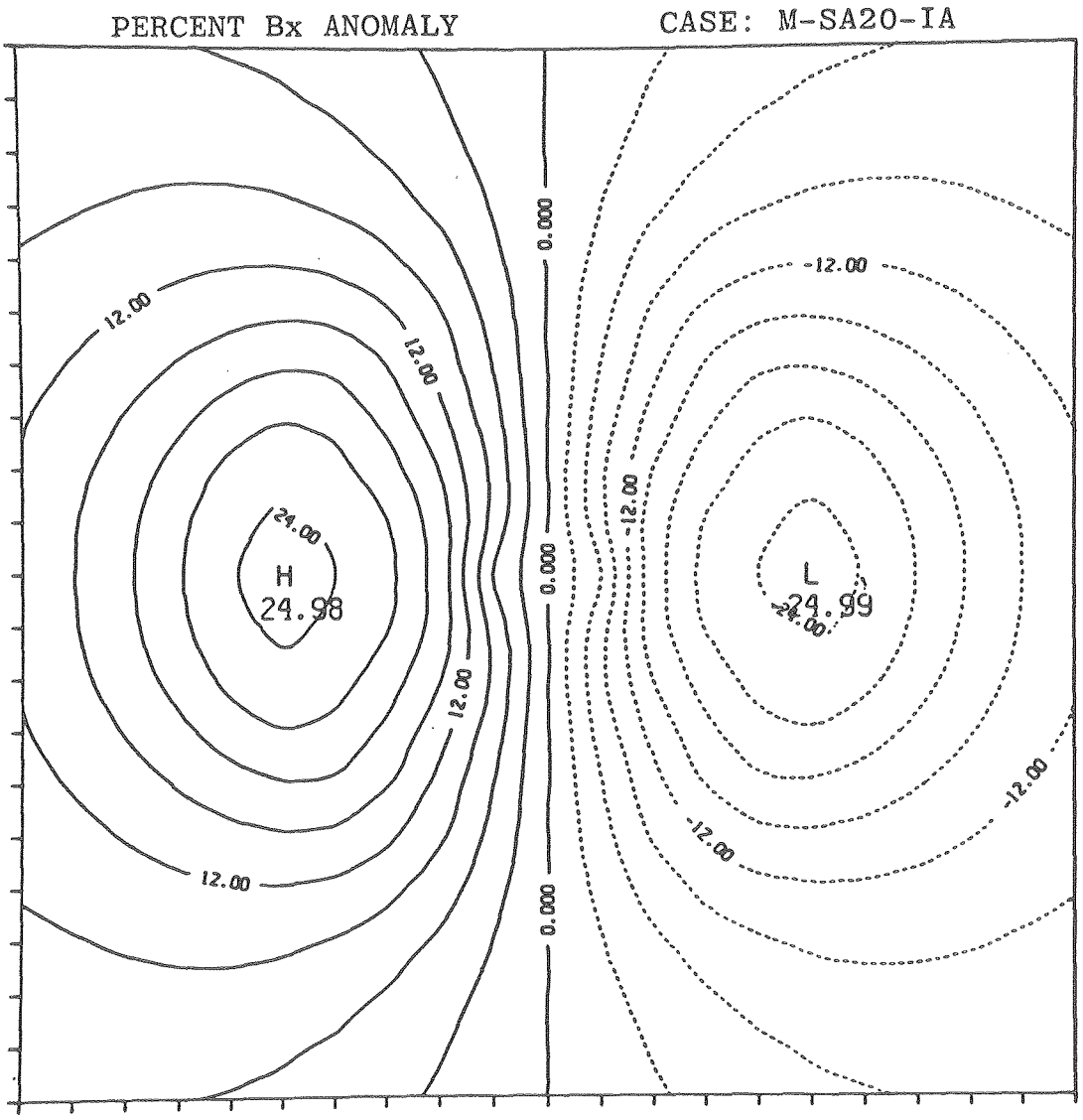

Figure 3-8-52.

XBL 7911-12956

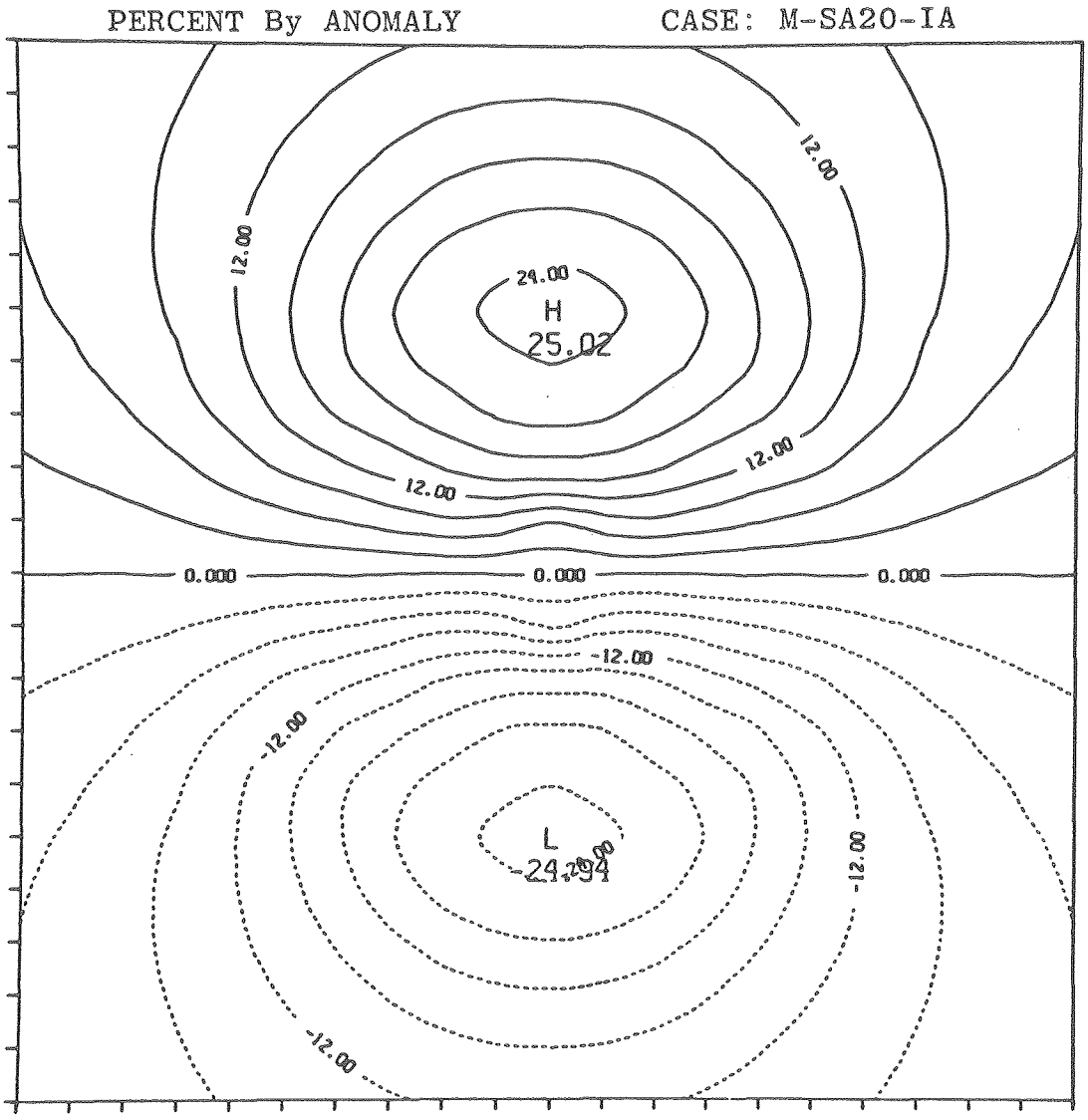

Figure 3-8-53.

XBL 7911-12957

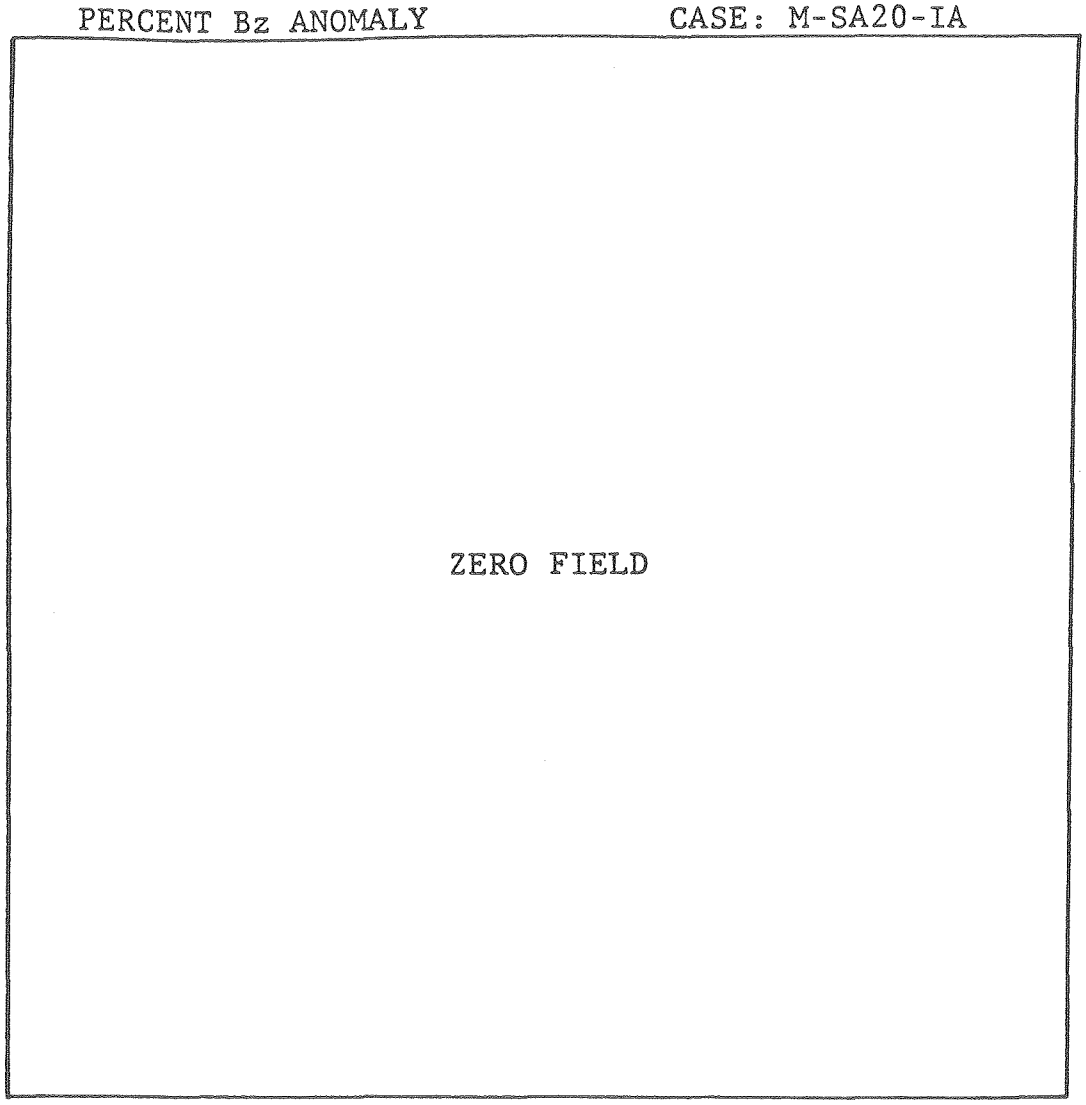

Figure 3-8-54.

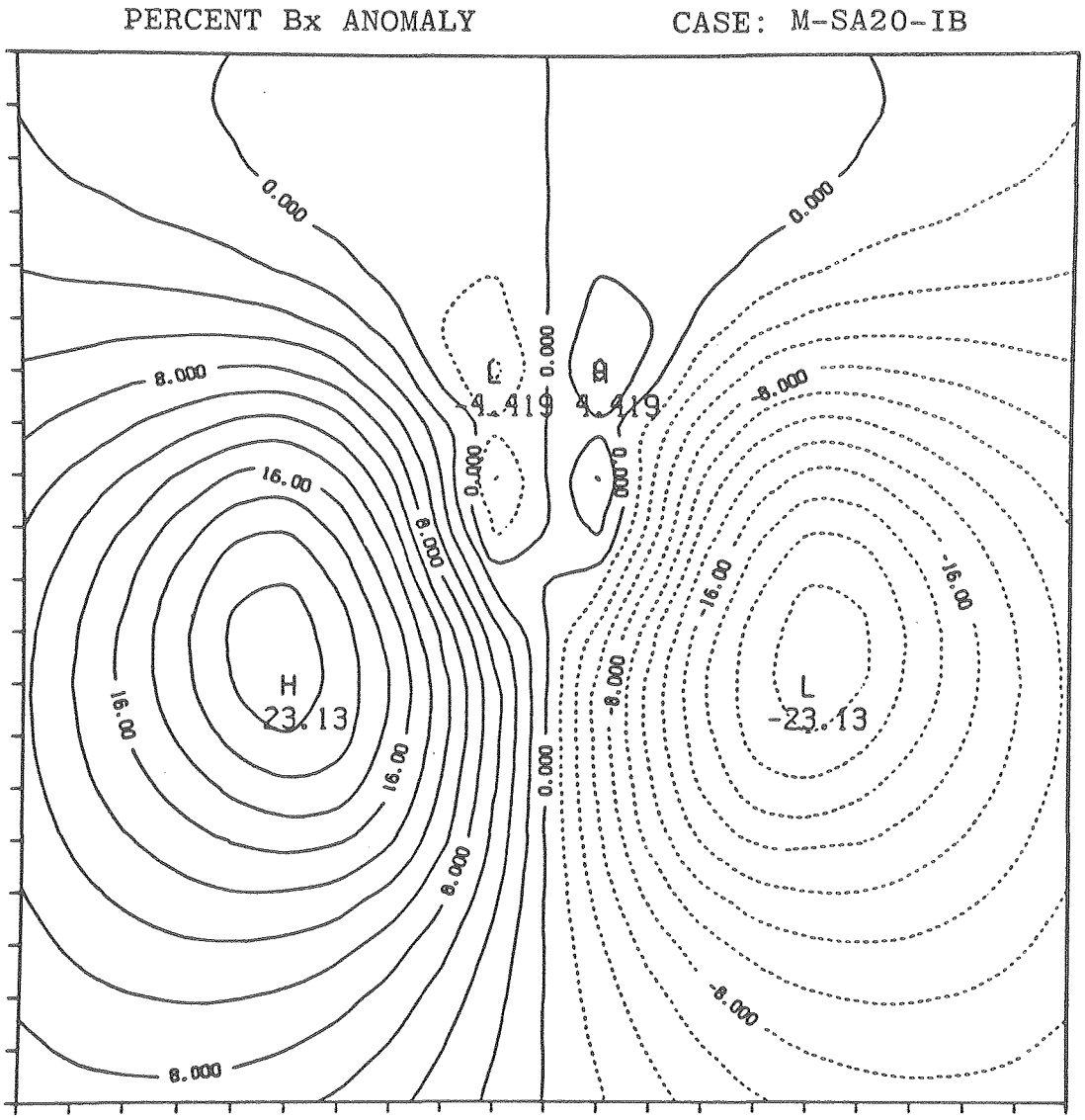

Figure 3-8-55.

XBL 7911-12960

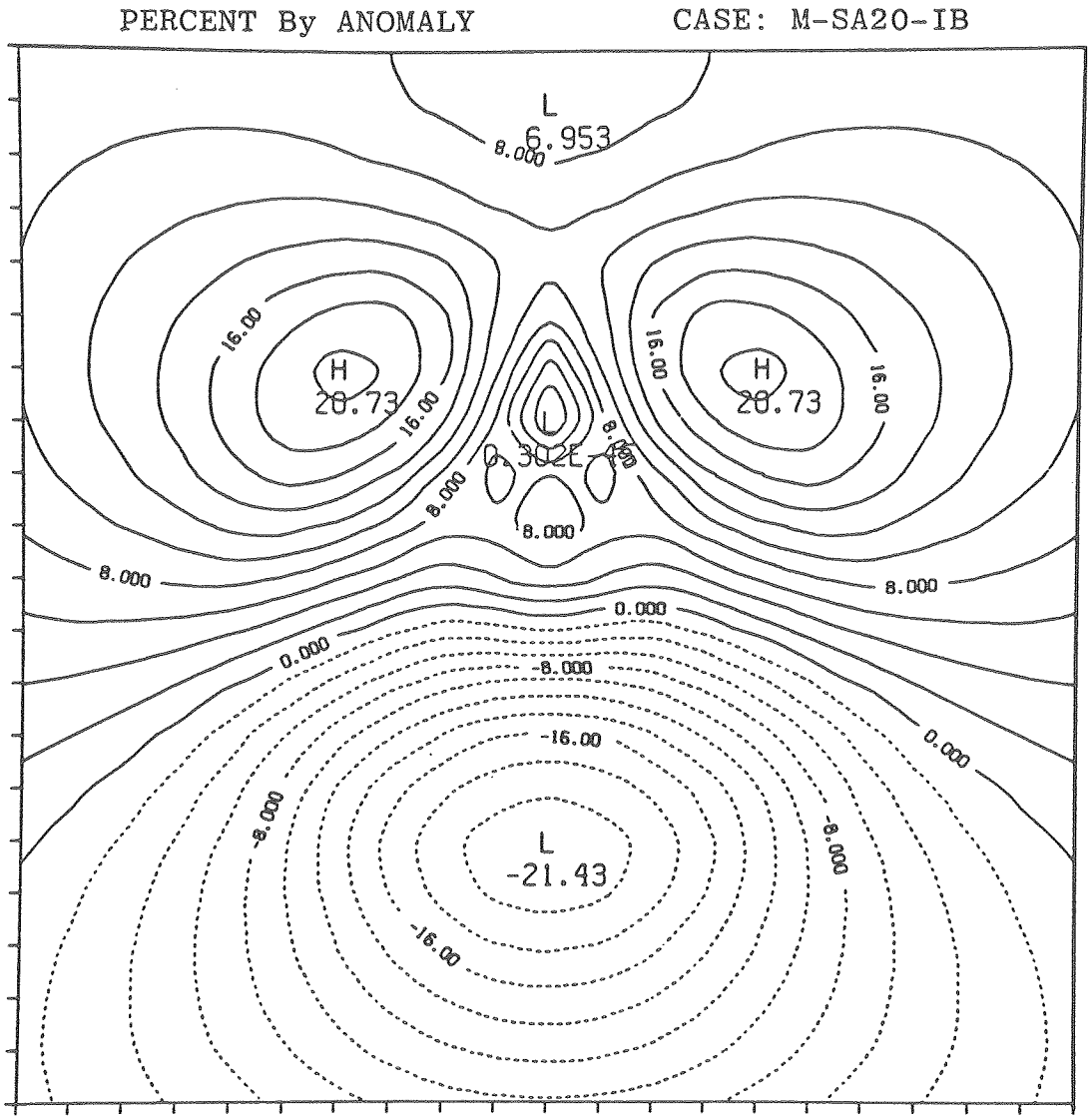

Figure 3-8-56.

XBL 7911-12961

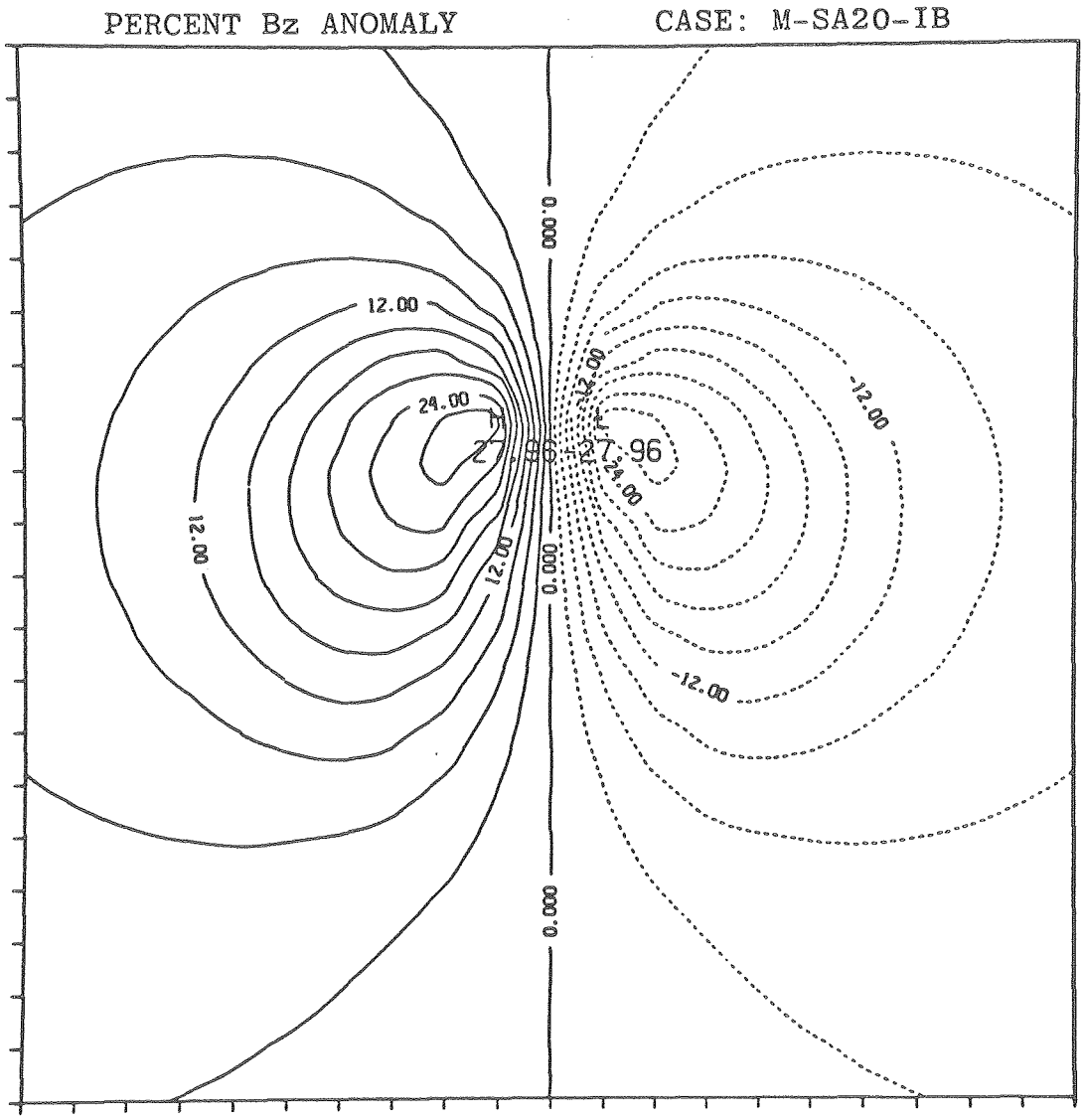

Figure 3-8-57.

XBL 7911-12962

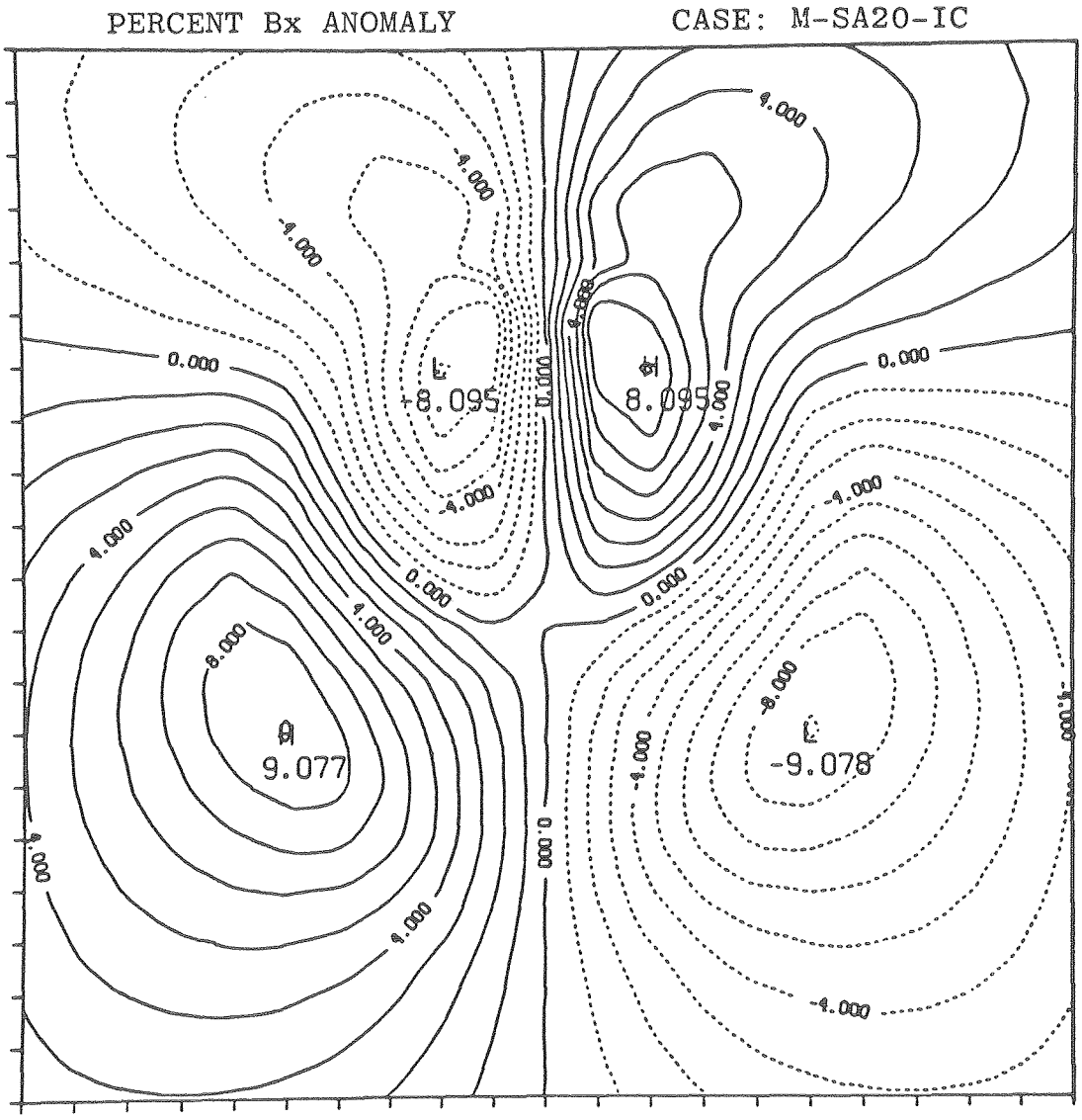

Figure 3-8-58.

XBL 7911-12964

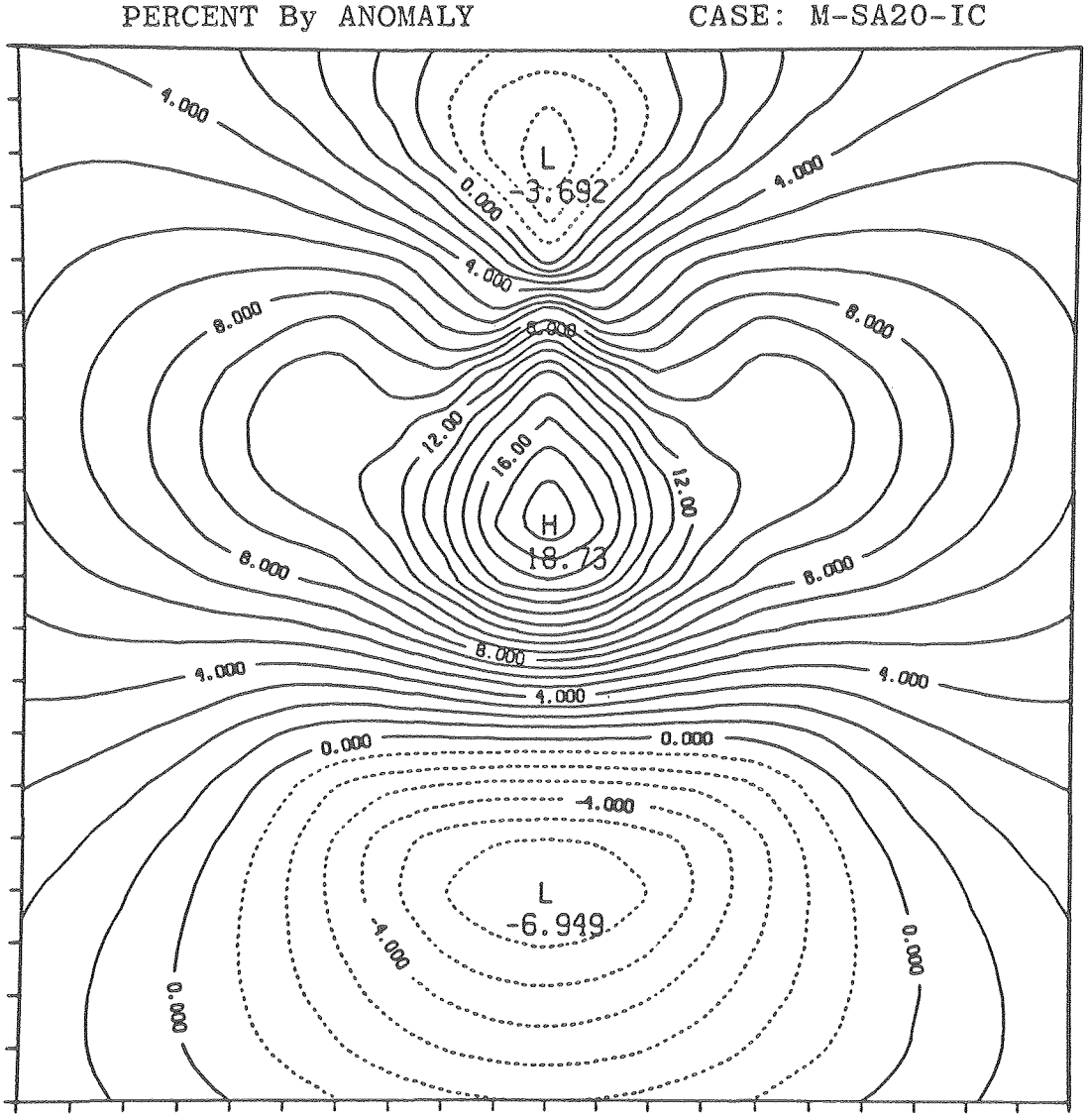

Figure 3-8-59.

XBL 7911-12965

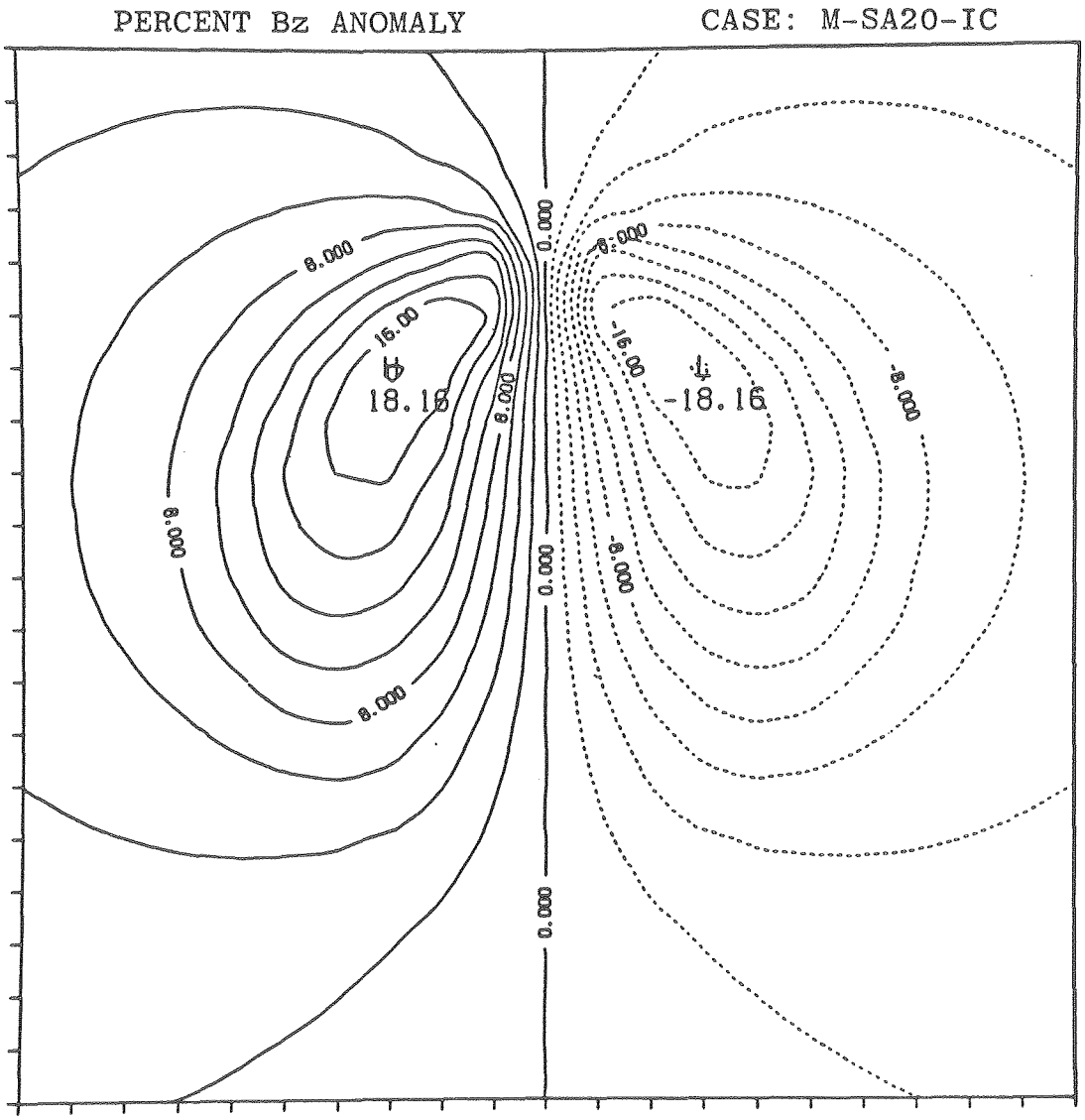

Figure 3-8-60.

XBL 7911-12966

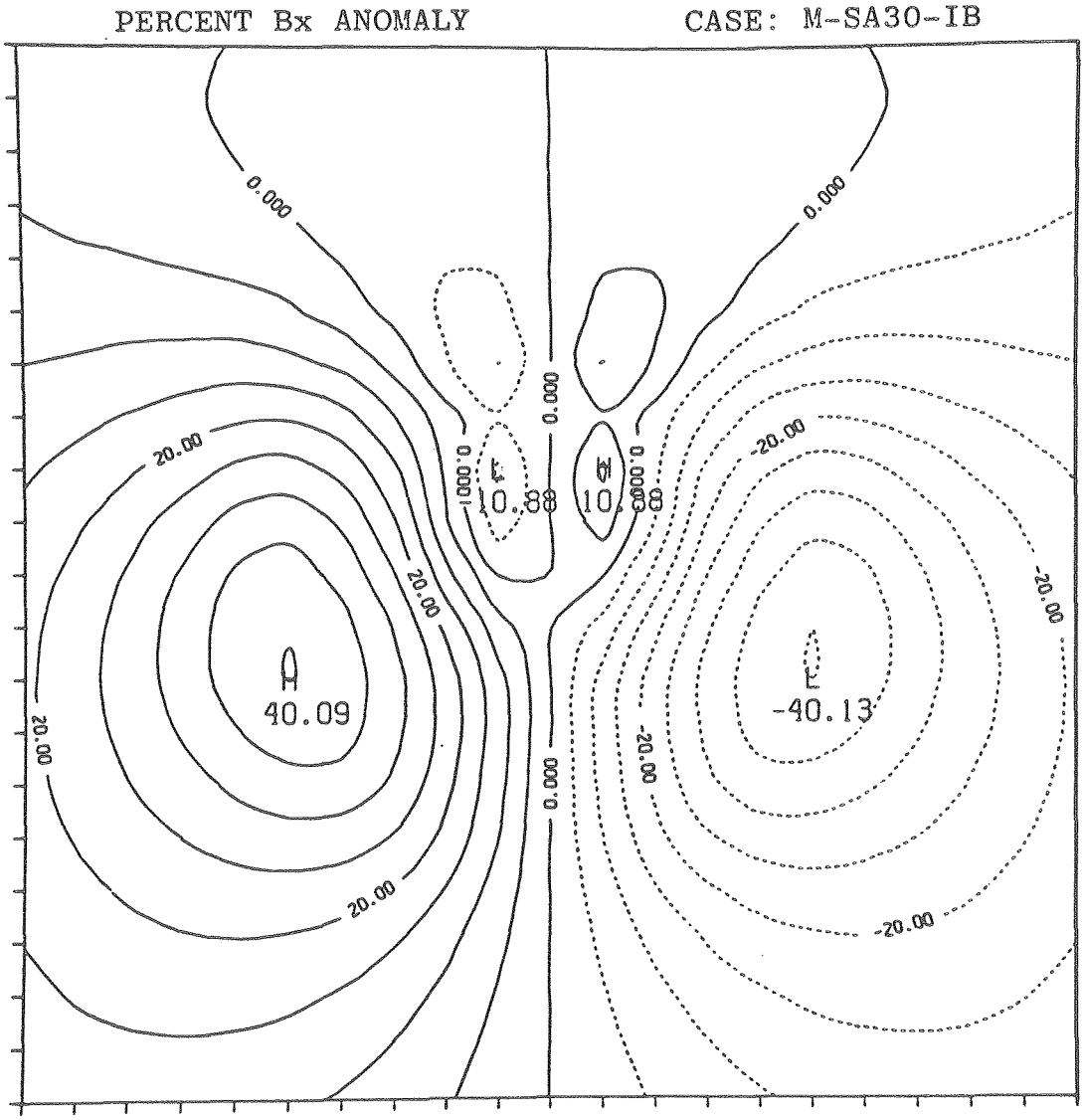

Figure 3-8-61.

XBL 7911-12968

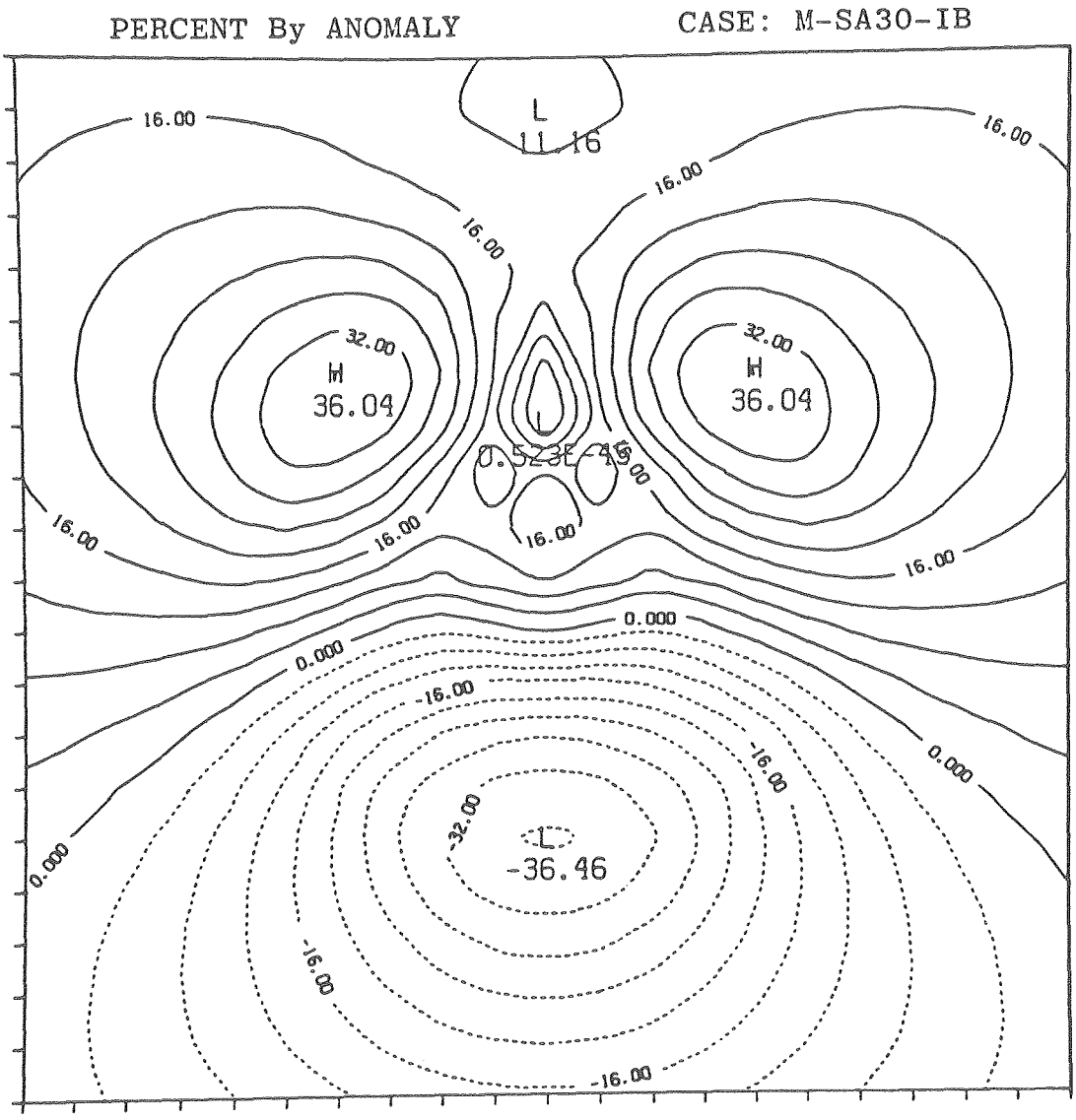

Figure 3-8-62.

XBL 7911-12969

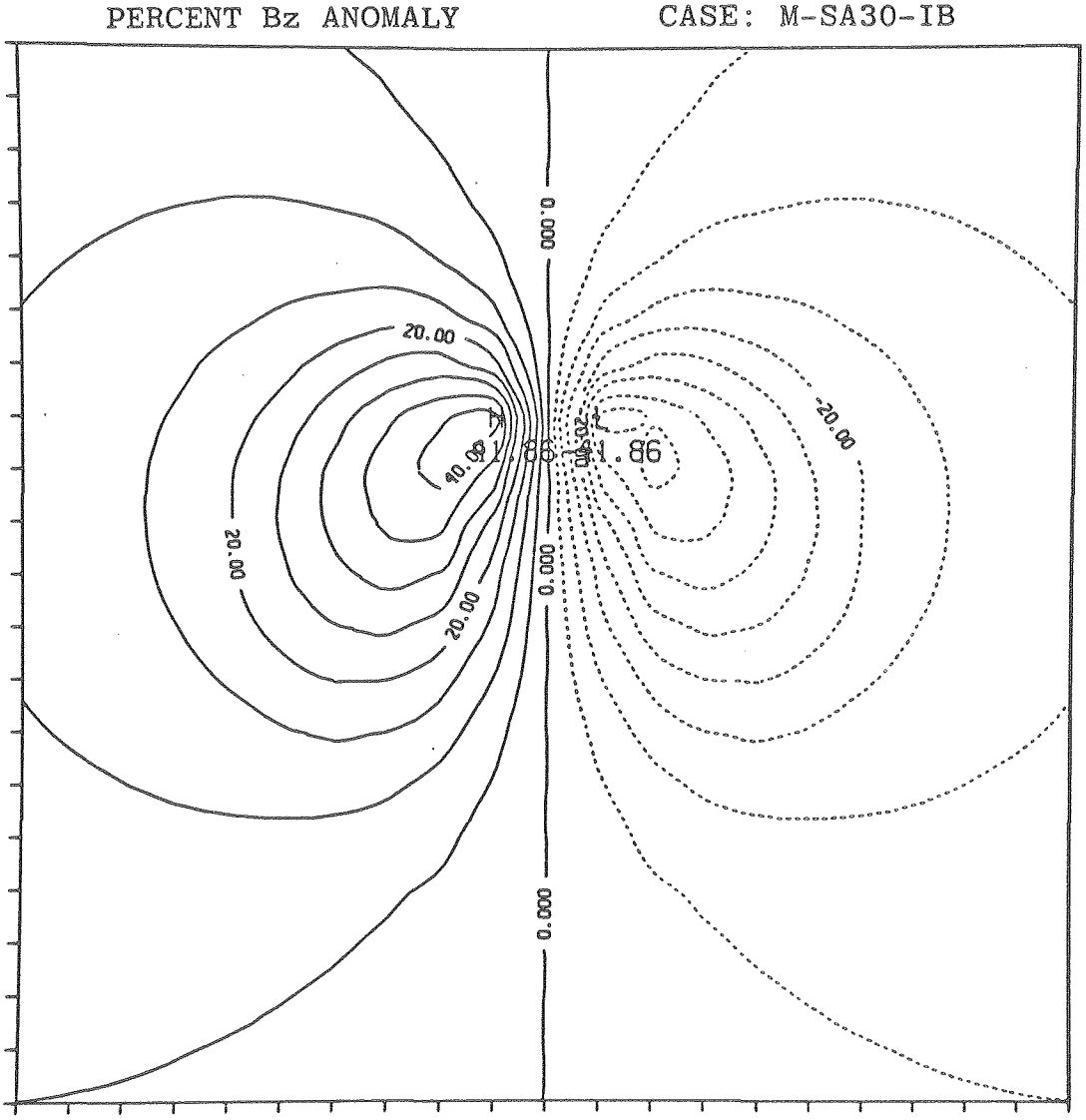

Figure 3-8-63.

XBL 7911-12970

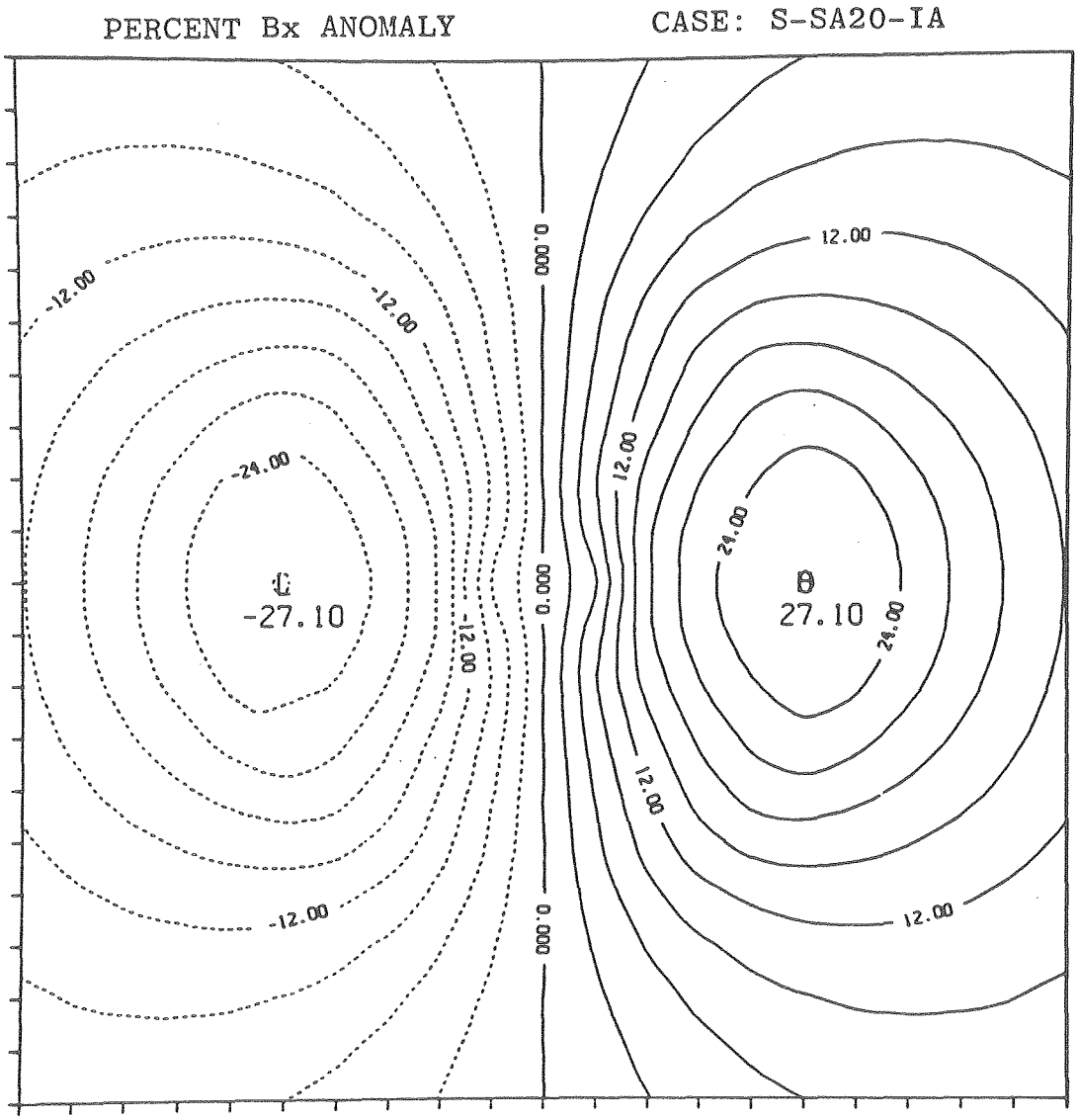

Figure 3-8-64.

XBL 7911-12972

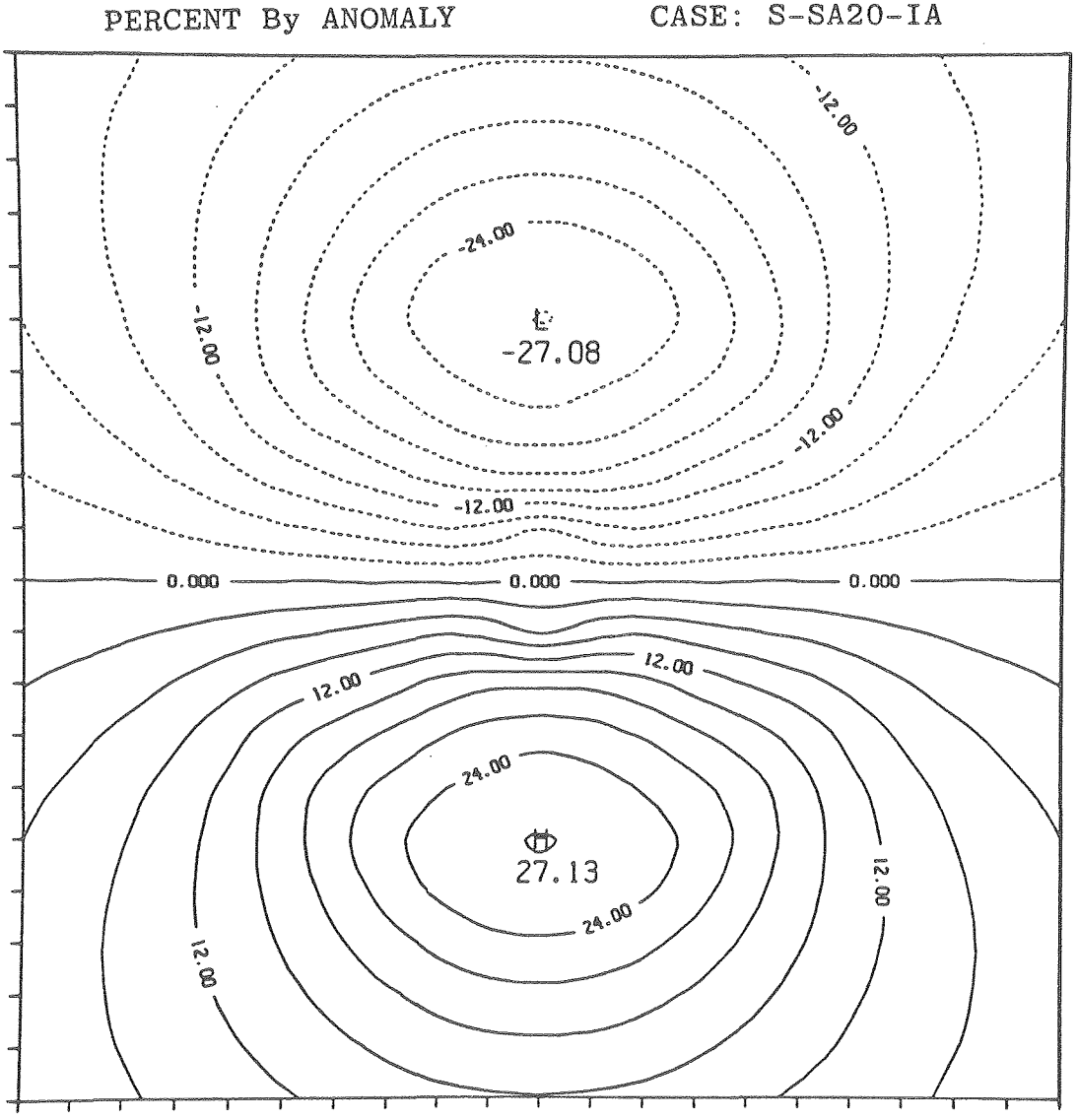

Figure 3-8-65.

XBL 7911-12973

PERCENT Bz ANOMALY CASE : S-SA20-IA

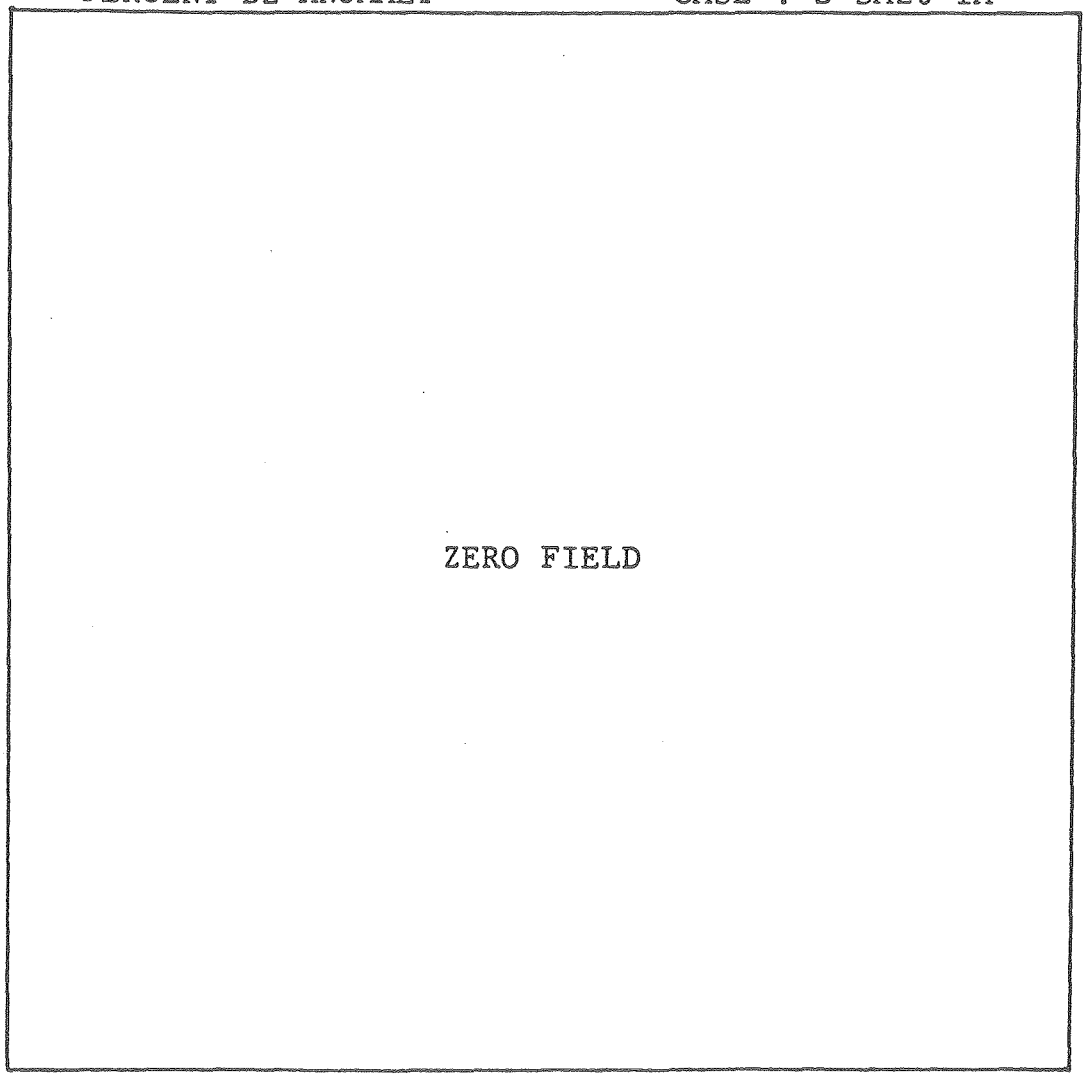

Figure 3-8-66.

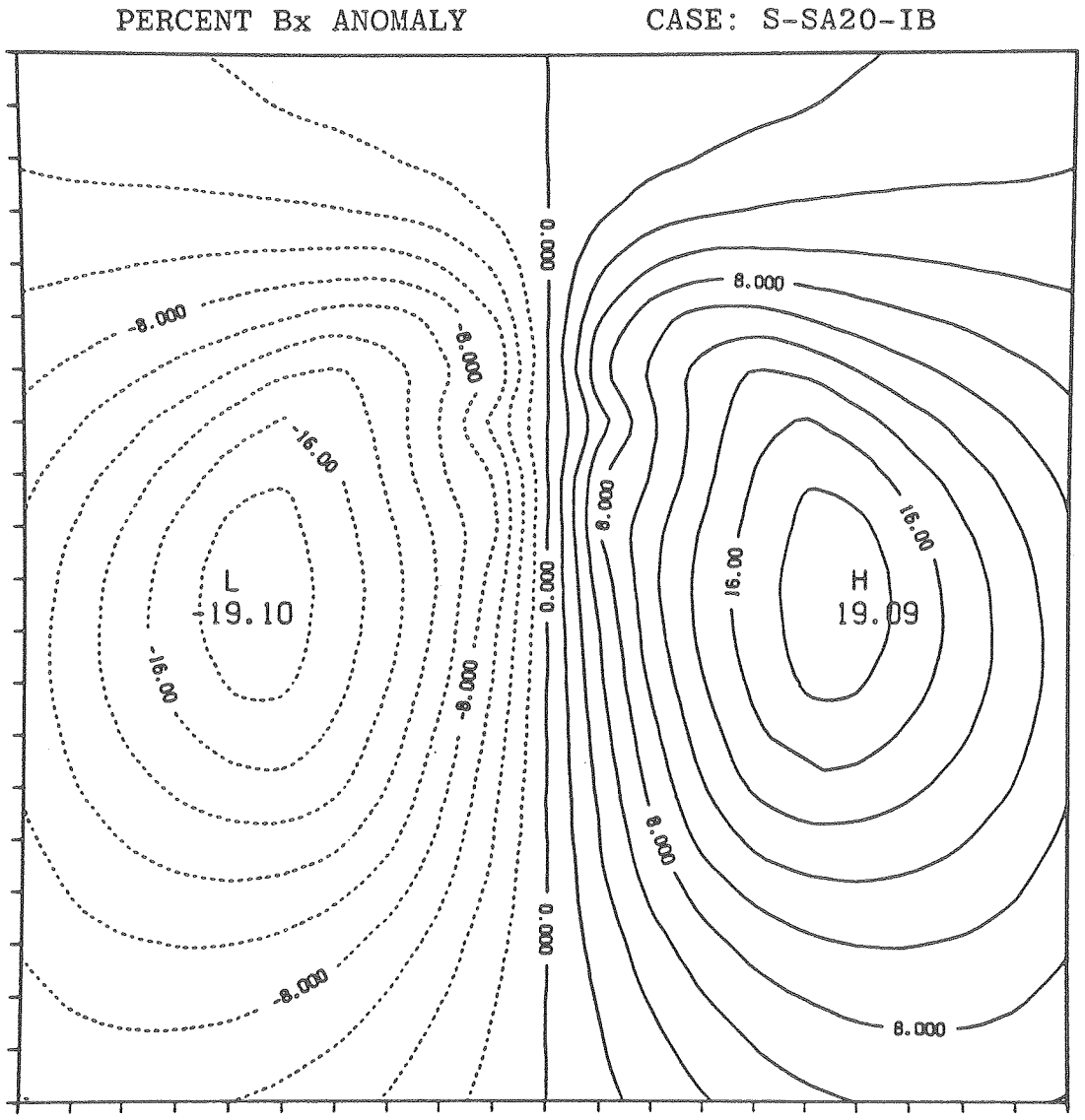

Figure 3-8-67.

XBL 7911-12976

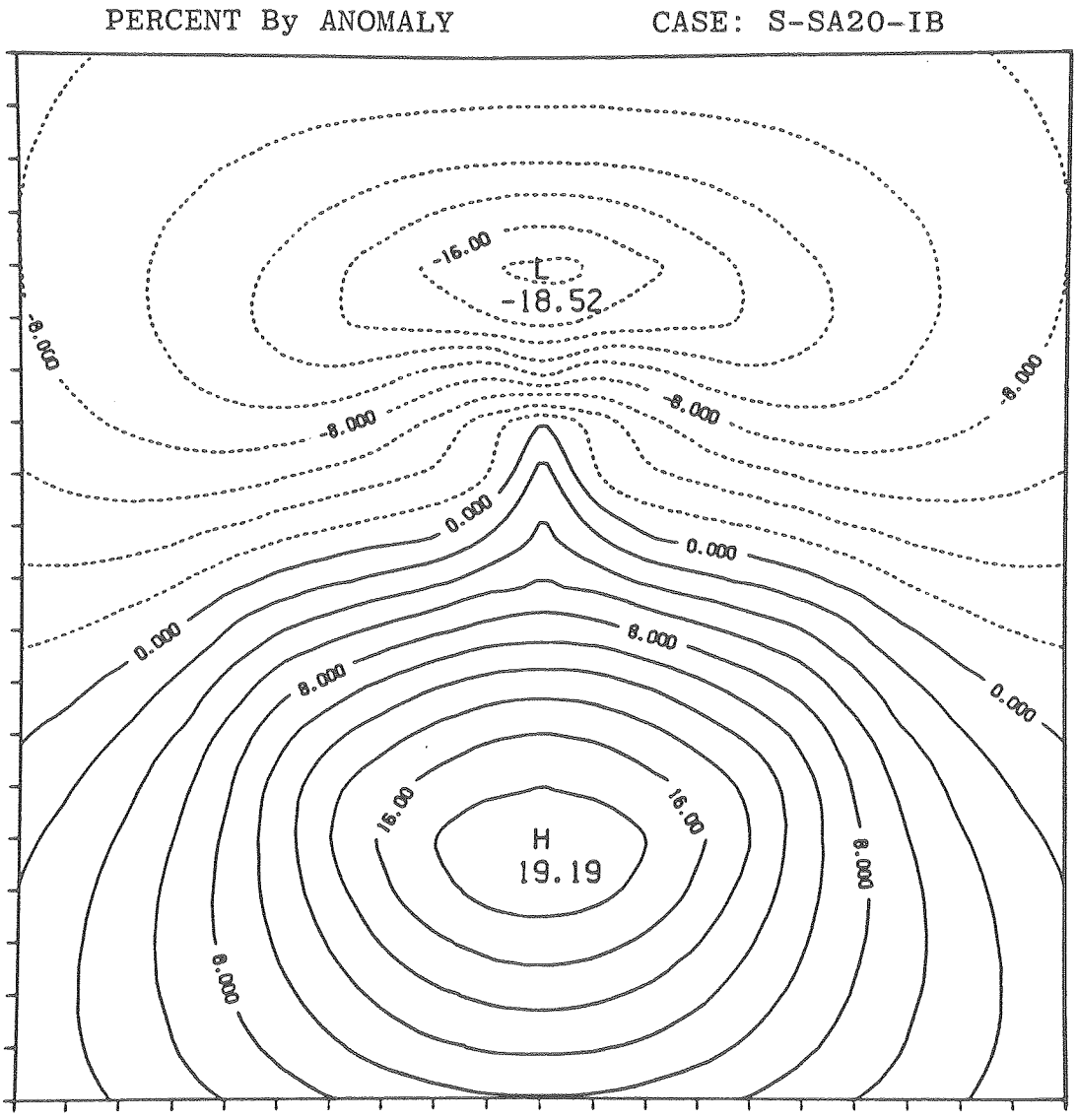

Figure 3-8-68

XBL 7911-12977

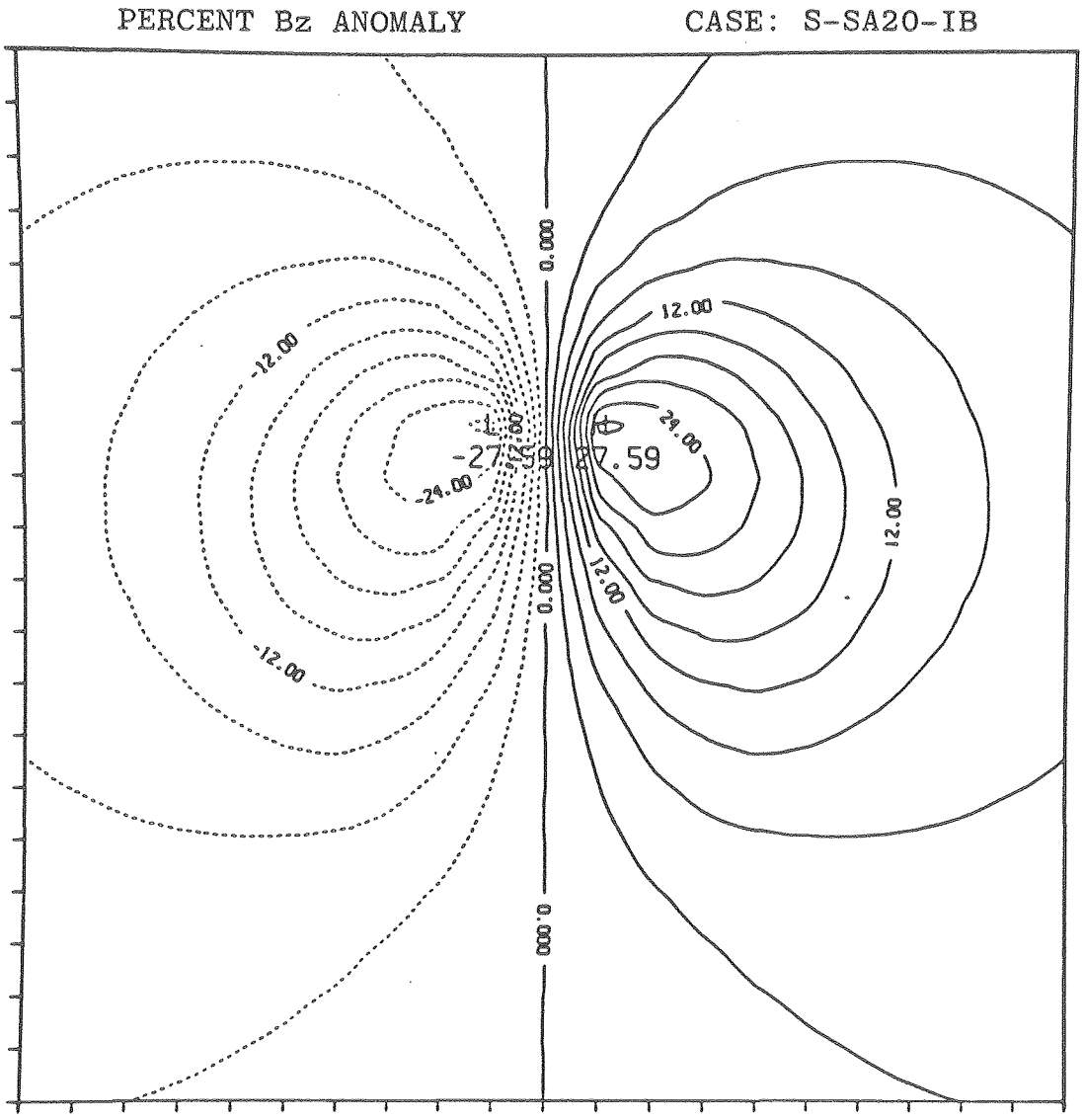

Figure 3-8-69.

XBL 7911-12978

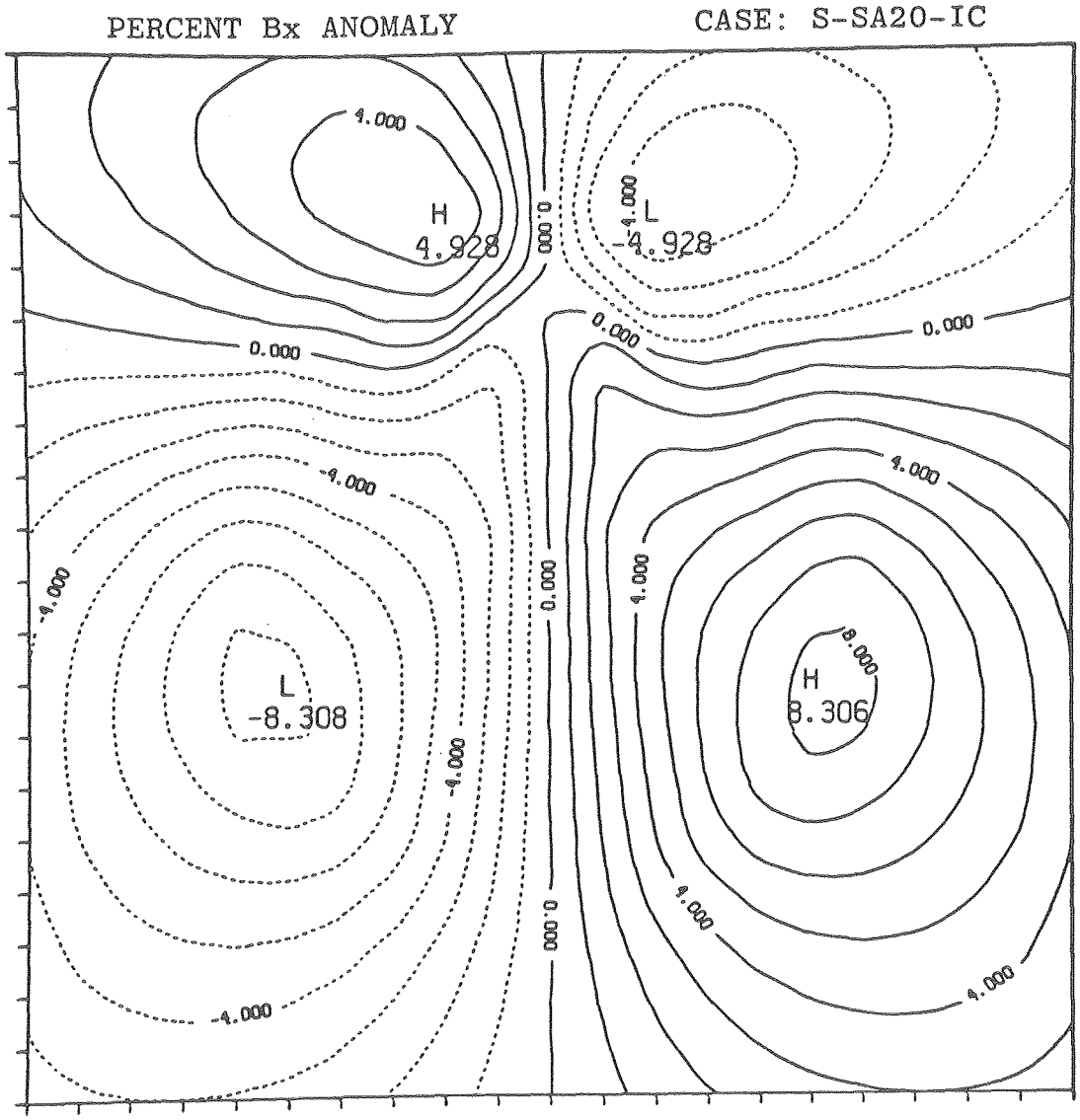

Figure 3-8-70.

XBL 7911-12980

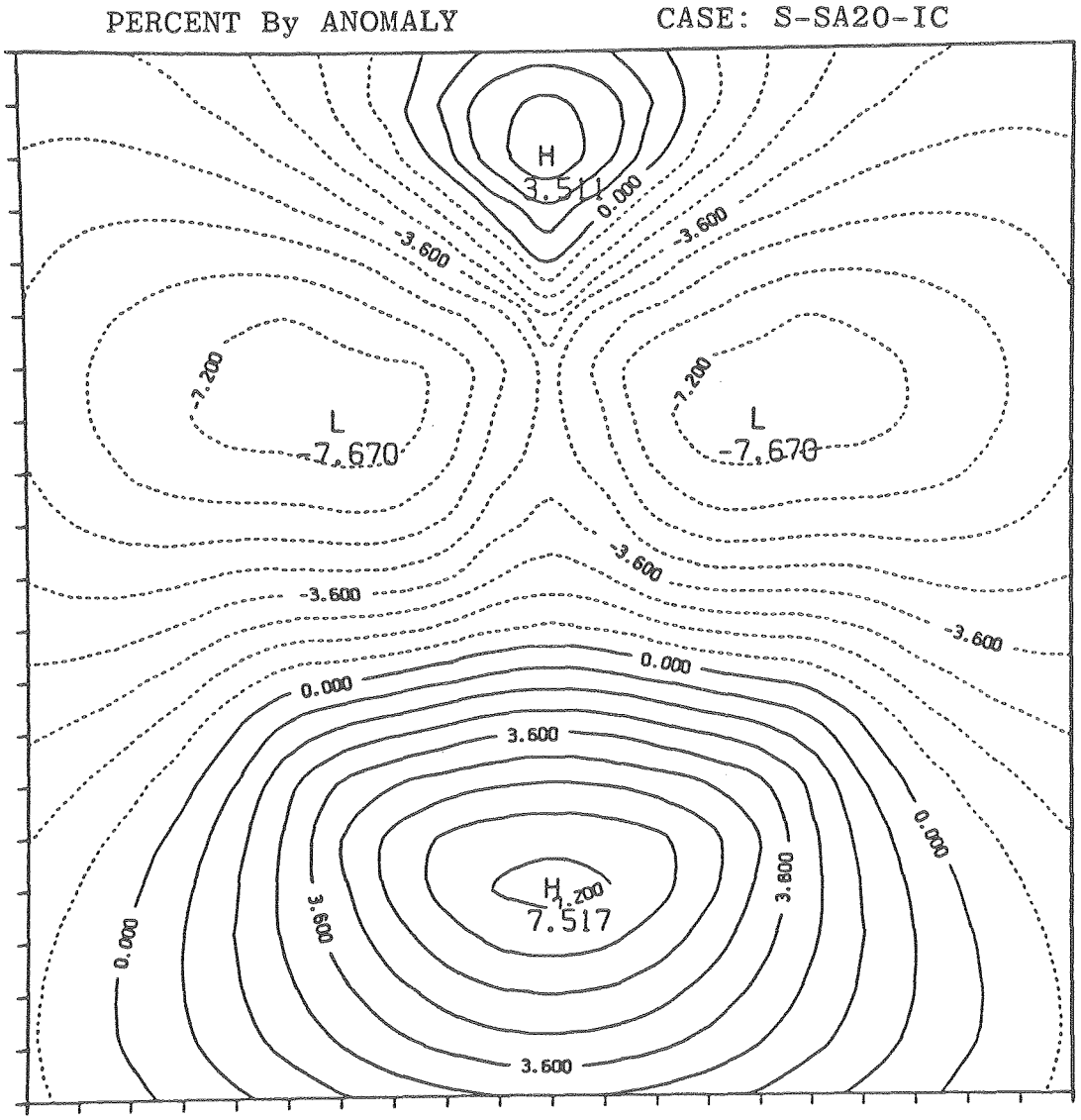

Figure 3-8-71.

XBL 7911-12981

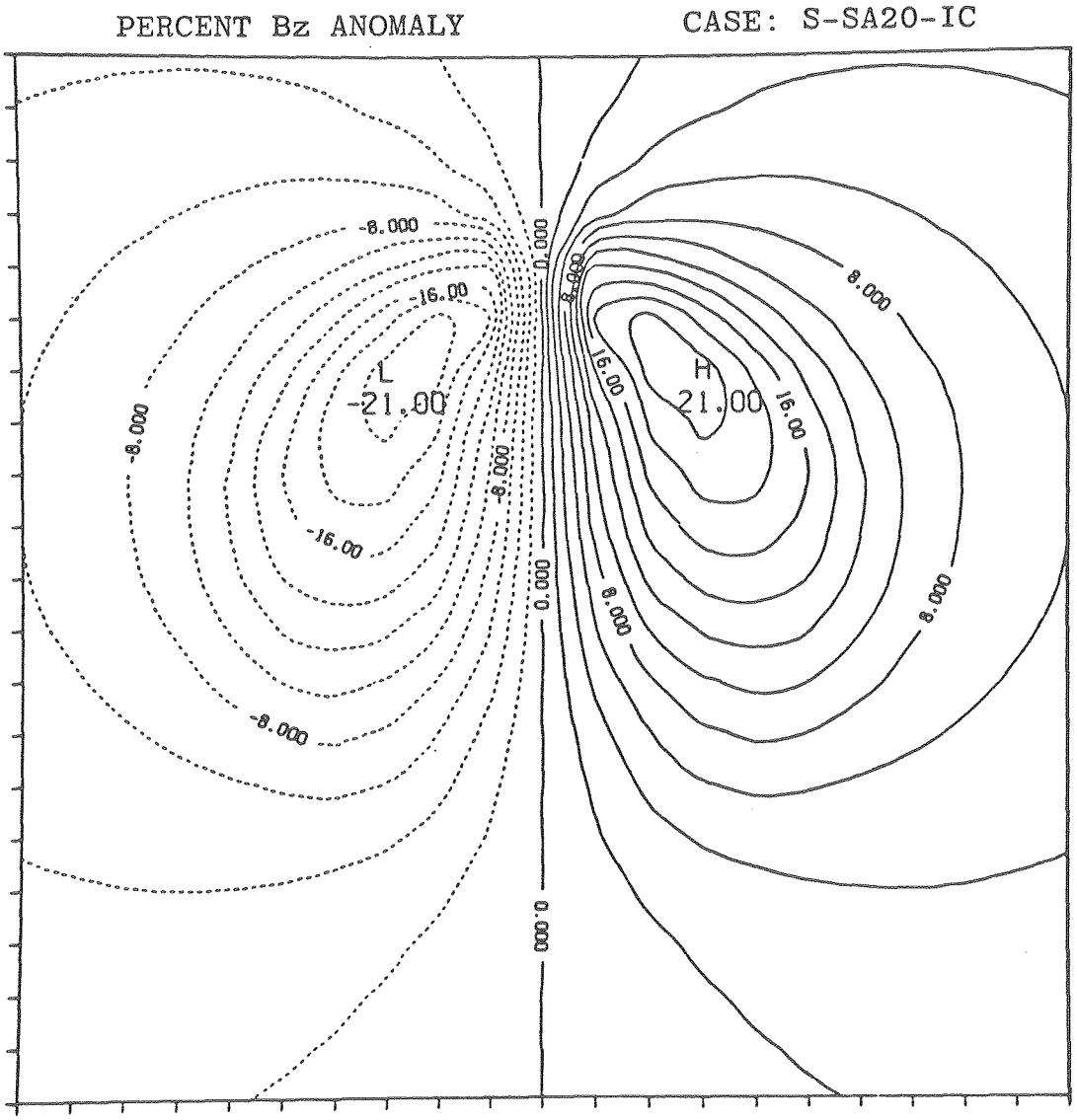

Figure 3-8-72.

XBL 7911-12982

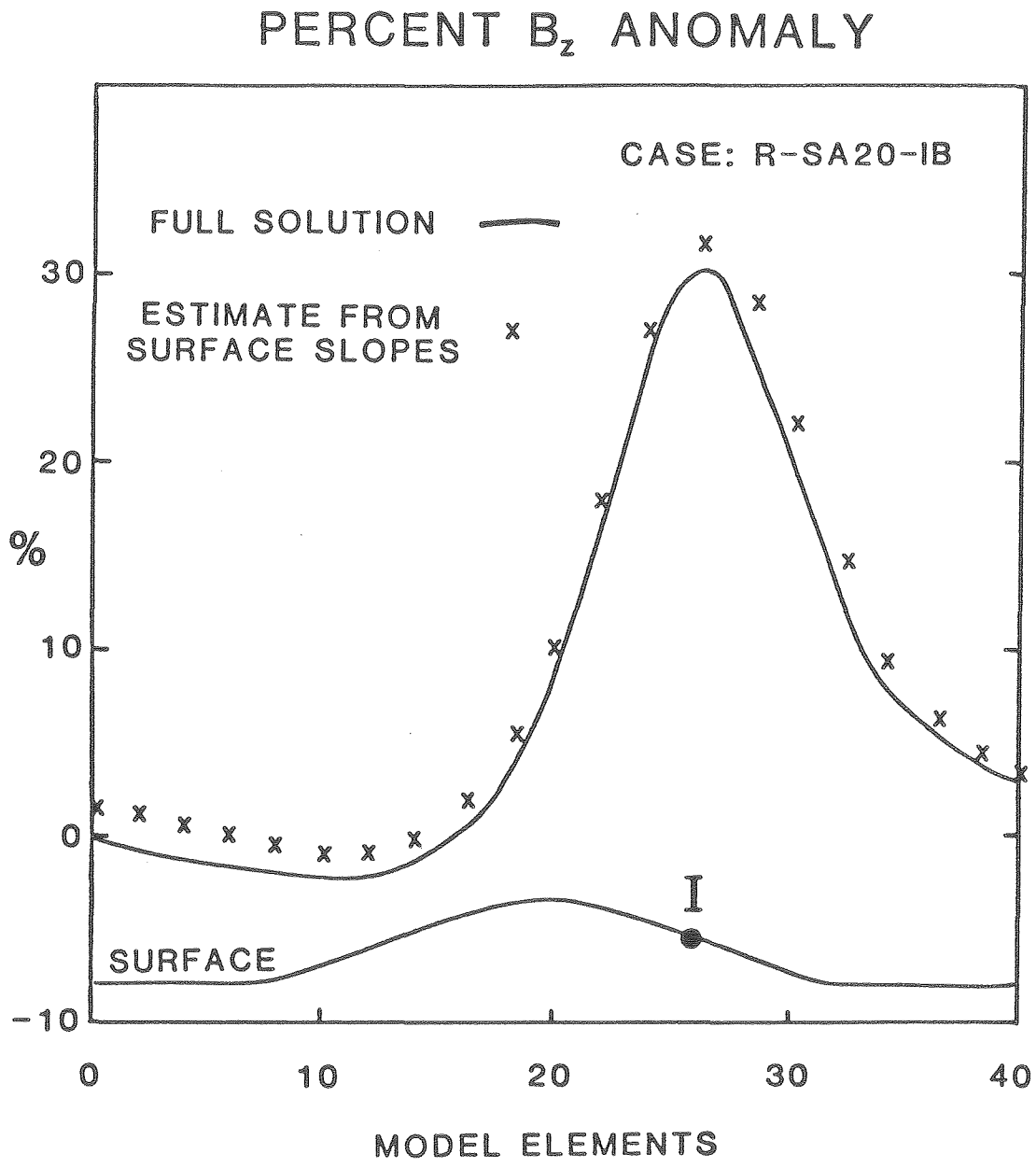

Figure 3-9-1. Comparison of vertical magnetic field anomalies calculated with the full numerical solution and with an approximate method using half-space electric fields and surface slopes.

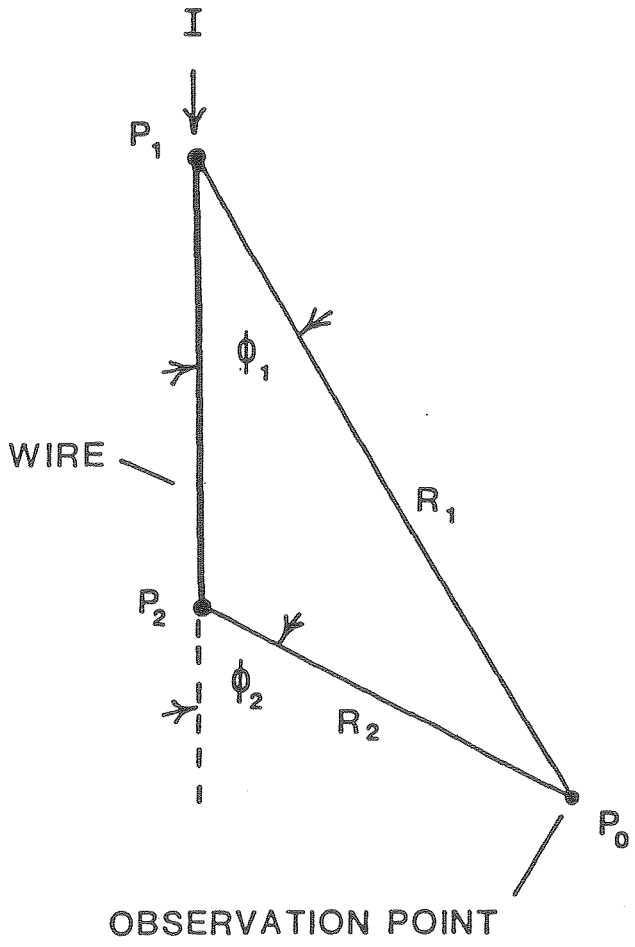

Figure II-1. Diagram defining the angles and distances used to determine the magnetic field due to current flow in a finite length straight wire segment.